PREDICTION OF DYNAMIC MUSCLE FORCES ACROSS THE ELBOW USING THREE-DIMENSIONAL VECTOR MODELLING

BY

KARYN M.A. WEISS-BUNDY

A Thesis
Submitted to the Faculty of Graduate Studies
in Partial Fulfillment of the Requirements
for the Degree of

MASTER OF SCIENCE

Department of Mechanical & Industrial Engineering
The University of Manitoba

THE UNIVERSITY OF MANITOBA

FACULTY OF GRADUATE STUDIES

*****

COPYRIGHT PERMISSION PAGE

PREDICTION OF DYNAMIC MUSCLE FORCES ACROSS THE ELBOW USING THREE-DIMENSIONAL VECTOR MODELLING

BY

KARYN M.A. WEISS-BUNDY

A Thesis/Practicum submitted to the Faculty of Graduate Studies of The University of Manitoba in partial fulfillment of the requirement of the degree of

MASTER OF SCIENCE

ABSTRACT

This thesis describes a new three-dimensional vector approach to the determination of muscle moment arms about the elbow joint. The vector approach is applied in conjunction with a muscle activation strategy to predict the force in the individual muscles. The determination of the individual muscle forces is made from the net joint moments calculated by a dynamic simulation of the motion of the upper limb, which is an independent work. From the instantaneous segment geometry of the human upper limb, net joint moments were resolved using body coordinate systems about the joint rotational axes. The contribution of the individual muscles to the net joint moments were analysed using the moment arms determined for the specific joint configuration and the relative muscle cross-sectional areas. The individual muscle forces were then calculated. The changes in muscle forces and lengths were used to determine the mechanical work done by each muscle, while the biological energy consumed in the muscle was determined using the force and time duration of the muscle activation. The relative risk of repetitive strain injury can then be estimated from the individual muscle forces and energies. In order to apply the three-dimensional vector technique to a human subject of any size, a scaling methodology was also developed. It was concluded that the three-dimensional vector approach developed for the calculation of individual muscle forces is valid. It was also shown that muscle forces associated with the dynamic component of motion are highly significant.

ACKNOWLEDGEMENTS

This thesis has been a long journey and were it not for the efforts of many people, would never have reached its conclusion.

First and foremost, I would like to express my deepest gratitude to my advisor, Dr. Alexander B. Thornton-Trump, for his seemingly endless patience, wisdom, and guidance; and especially for extending to me the privilege of working with him. Without his foresight, this thesis would never have been possible. Thank-you for being there to help me when I needed it most and keeping me focused on the task at hand.

Along with Dr. Thornton-Trump, special thanks to Dr. Ostap Hawaleshka and Dr. Zahra Moussavi for participating on my examining committee and for their careful review and comments regarding this thesis.

I would also like to thank Ms. Amy Chan for her tireless work and success in developing the dynamic model that is the backbone of the project.

Thank-you to the Worker's Compensation Board of Manitoba and NSERC for funding the research project.

A very special thanks to all my friends for the encouragement over the past two years and for giving me a good laugh and much needed distractions when I was about to lose my

sanity. To Tami, who as my roommate for a year and a half never once complained about the all night computer activity coming from my room. To Maria for never becoming upset when I fell asleep while on the phone with her during those late night marathon conversations. To Mark and Mike, my surrogate big brothers, for knowing exactly what I was going through and being so much fun while going through the same thing yourselves. Finally, to my best friend, my older sister Krysta, you've always been there for me and know me better than anyone else ever could.

I would like to thank my parents and grandparents for their constant love and support. I am especially grateful to my parents, Patricia and Clifford, for instilling in me the love of knowledge and the importance of education that has helped me get to where I am today. You always believed in me even when I didn't myself and were always proud of me.

TABLE OF CONTENTS

LIST OF FIGURES

LIST OF TABLES

CHAPTER 1

INTRODUCTION

The purpose of this thesis is to develop a technique that will predict the individual muscle forces from the joint moments. A dynamic simulation model of the human upper body motion calculates the net joint moments for the execution of a given task. These net joint moments include both the dynamic and static components. Once the muscle forces have been determined from the net moments, the relative risk of repetitive strain injuries from various human workstation tasks can be evaluated. A review of appropriate literature shows that the qualitative functional anatomy studies tend to lack the comprehensive information and methodology to determine muscle moment arms and additional quanitative data for the range of human sizes expected to use workstations.

Muscles contract and produce forces that are transmitted to the bones of the skeleton via tendons; movement then occurs as the bones rotate about the joints of the body. The moment arm is required to transform the translational forces developed by a muscle into rotational moments about the joint. Given the joint moment, to determine the force a muscle generates, it is essential to know the moment arm and line of action of the muscle as well as its physiological cross sectional area. A muscle control strategy is also necessary to distribute the total force exerted on the joint by the muscle group to its individual muscle force components. The control strategy is also necessary to establish the interrelation between the muscle forces of the agonist and antagonist groups. During movements, the orientations of the muscles and bones change with joint position, thus the

moment arms of the muscles spanning the joint will vary significantly with segment position. As a result of the moment arm variations, the capacity of a muscle to produce joint rotations can change with position even if muscle force remains constant throughout the joint range of motion.

1.1 Problems with Current Models

Although a great deal of valuable research has been done in the modelling of the upper limb, most of the focus has been on the highly complex shoulder joint. Current models of the elbow joint do not meet the needs of this thesis, in that they are rarely analysed in three-dimensions and seldom include dynamic components. These models tend to describe single joint configurations, rather than the full joint range of motion. In addition, they generally consider only one of the two joint degrees of freedom, either elbow joint flexion-extension or the self-rotation of the forearm. Thus it is currently very difficult to take the moment results from a dynamic simulation model of the upper limb and determine the force in each individual muscle contributing to the moment.

1.2 Significance of the Research

Currently in industry, poorly designed workstations can result in repetitive strain injuries to the workers. These repetitive injuries are dependent on the forces experienced in the muscles, the time spent doing the task, the number of repetitions of the task in a work session, and the limb geometry. These injuries can occur to the muscles, articular joint

surfaces, tendons, and other structures of a joint. Given that repetitive strain injuries result in high compensation costs and can lead to permanent physical damage to the joints and muscles, the ability to predict musculoskeletal injury potential is critical. In order to achieve injury risk predictions, the individual dynamic muscle forces experienced during a given task must be determined.

1.3 Goals of the Research

It is the goal of this thesis research to identify the forces in the significant muscles of the flexor and extensor groups crossing the elbow for the full range of joint motion. To accomplish this task, there are several main areas in which progress must be made. A method of determining the three-dimensional muscle origin and insertion points and the muscle lines of action is required. In addition, the bone anatomy must be made scalable so that the vector model can be applied to subjects of various sizes. The muscle moment arms in three-dimensional vector form must be resolved so that the net joint moment can be expressed and the total muscle force across the joint can be determined. A muscle activation strategy can then be used to determined individual muscle forces. This force identification will enable the net joint moments calculated by a dynamic model to be used in the determination of individual muscle forces at any point during the task cycle. Once this has been completed the task and workstation design can then be modified within the dynamic simulation and the changes in muscle forces analysed, enabling the task cycle with the lowest risk for repetitive strain injuries to be established.

The human upper limb is an exceptionally complex structure with seemingly limitless functionality, which makes possible the performance of a range of tasks in everyday work and life. This thesis will focus on the middle joint of the upper limb, the elbow. Motion of the elbow joint allows the height and orientation of the hand to be adjusted for effective placement. However, despite the commonality of the repetitive stress disorder of the wrist known as carpal tunnel syndrome, this joint was not included in this study due to the complexity of the mechanics of the human hand and wrist. To effectively analyse the linkage chain of the upper limb the individual muscle forces crossing the elbow joint need to be considered before those of the shoulder.

In the next chapter the available literature pertinent to this thesis has been reviewed. From this literature review the nature of the methodology that needs to be defined for the anatomical joint model can be developed and will be detailed in Chapter 3. Chapter 4 contains the results obtained from the analysis of the anatomical elbow model and a discussion of the validity of these results. Finally, the conclusions reached through this thesis and the recommendations for future work are presented in Chapter 5.

CHAPTER 2

LITERATURE SURVEY

2.1 Introduction

The research covered in this thesis falls under the area of biomechanical modeling of the human musculoskeletal system. The complete understanding of the human musculoskeletal system, including the manner in which it functions and is controlled, has long been the interest of anatomists, physiologists, neurophysiologists, ergonomists, engineers, and medical professionals among others. Possible applications cover everything from prosthesis design and surgical tendon transfers to robotic simulation, realistic computer animation, and injury prevention techniques. This type of research on humans has fascinated mankind for many centuries and has been actively researched from approximately 1860 to the present day.

The comprehension of the human musculoskeletal system requires knowledge of the anatomy and architecture of the bones and muscles, statics and dynamics of multi-link systems, and computer modeling techniques. The major problem associated with the modeling of the human musculoskeletal system is the inherent mechanical redundancy caused by the number of muscles crossing the joints of the body. While this redundancy gives the body versatility in its selection of muscles used to perform a given movement; when you add to this the large number of joint articulations in the human body and numerous degrees of freedom, the undertaking becomes more complex. Therefore, the

balance between simplifications to reduce the problem to a manageable size and maintenance of the key features of the human musculoskeletal system is sought. In this thesis, the biomechanical modeling of the human musculoskeletal system is focused on the human elbow joint. While a large portion of the research done to date has concentrated on the human lower limb, shoulder or wrist and hand; the elbow has not received sufficient attention to allow quantitative mechanical modeling. The techniques developed in modeling the elbow can be extended later to the other joints of the upper limb.

2.2 Optimization Models

In modeling the elbow joint, the relationship between the known external forces acting on the upper and forearm segments (weight, inertia, dynamic load, external load) and the unknown individual muscle forces crossing the elbow joint, is derived from force and moment equilibrium equations. However, since more muscles cross the joint than are necessary for movement, the number of unknown forces exceeds the number of equations available and a unique solution cannot be determined. Individual muscle forces can be determined or predicted either theoretically or experimentally. The theoretical approach consists of reducing the number of unknowns by using optimization theories and constraint equations, grouping muscles into functional units, or eliminating muscles from study. Experimentally, researchers have attempted to use direct force measurements from force transducers inserted into the muscle tissue or on the bone surface and from electromyography (EMG) to estimate individual muscle forces. However, direct

measurements have only been performed on animal subjects and EMG remains a controversial method for force determination. This has resulted in many researchers favoring the optimization approach, either linear or non-linear, in order to solve the indeterminate problem and calculate the muscle forces and joint torques of the elbow. Optimization methods are based on the assumptions that the load sharing between the muscles crossing a joint is unique and the neural control of the muscles is governed by physiological criterion that ensure efficient muscle activation. A review of the current force prediction models in the literature reveals a number of differing theories for muscle recruitment.

Amis et al. (1980) used the theory that the forces in muscles are shared in relation to their cross sectional areas and an equal muscle stress hypothesis for co-operating muscles. This hypothesis states that all muscles in a functional group are likely to have their fibers stressed equally as their maximum strength is approached. It is believed that this assumption will not hold true for lightly loaded situations, and may not be valid for predicting antagonist activity. Yeo (1976) investigated the hypothesis of minimizing the total muscular force using a linear optimization procedure and produced a solution that saw a single muscle activated to saturation before the next muscle became active. It was found that this theory produces a situation common to many linear optimizations in that they do not agree well with the documented EMG patterns of muscle activation by including little synergistic and antagonistic activity in the muscles. An et al. (1984a) found a similar solution in a muscle force prediction model by performing a linear optimization on the objective function to minimize muscle stress. The muscles were

recruited sequentially beginning with the 'cheapest' muscle being the only one active until its stress limit is reached, then the next 'cheapest' muscle becomes active and so on. In another study An et al. (1989) minimized muscle activation as the objective function in a linear optimization and added an additional inequality equation to define the upper bound of muscle force. The muscle length-tension relationship was incorporated in the model in an effort to obtain more physiologically accurate predictions. Kaufman et al. (1991a, 1991b) also attempted to minimize neuromuscular activation as the objective function in their linear optimization. It was found that the muscle force predictions were quite good including more realistic synergistic activity and more uniform recruitment of all the active muscles, which correlates well with known EMG patterns for the muscles.

Dul et al. (1984a) reviewed previous optimization theories and compared them using a model of the human lower limb. They found that while linear criteria recruit muscles in an orderly fashion, non-linear criterions are able to predict synergistic muscle activity. In addition, all criteria predicted that relatively more force was assigned to muscles with large moment arms and muscle size also plays an important role in force sharing between muscles. A non-linear optimization method used by Crowninshield and Brand (1981) minimized the summation of the cubed muscle stresses. This optimization would also maximize the endurance of the activity, as when muscle stress is low the potential for prolonged contractions is high. Synergistic activity was predicted that was in good agreement with the previous EMG activity found for the muscles. Dul et al (1984b) proposed a new criterion based on the hypothesis that muscular fatigue is minimized by the neuromuscular control during learned endurance activities, static and dynamic. The

objective function maximizes the endurance time of the activity such that muscular fatigue would be minimized. This optimization fit well with EMG data and also results in a prediction of the time for which the activity can be sustained. The most interesting feature of this approach is that the criterion is based on the maximum force and fiber composition of the muscle in question and is not dependent on the moment arm, however, the muscle force levels predicted with this model do depend on the moment arm of the muscle. The objective functions used in the studies are sometimes chosen more for simplicity and computational ease than for their relation to physiological criterion, and with no method available to test the validity of these force sharing hypotheses there is no way to determine which methods are correct and which are not.

In the doctoral thesis of Dowling, J.J. (1987) a different approach is taken to predict the forces in individual muscles crossing the elbow joint. The model includes the muscle activation determined via EMG, the force-velocity and length-tension relations of muscle, and series elastic components when multiplied by the moment arms and combined with the passive moment predicts the net elbow moment. Electromyography and kinematics during both static and dynamic tasks were used to run the model for predictions of the individual muscle forces. Both synergistic and antagonistic activity was present in the model and the results were in good agreement with the experimentally determined net moment. In the majority of the aforementioned studies the analysis was completed in isolated static joint configurations or encompassed a small portion of the range of motion, making any attempt to describe muscle recruitment over the full range of motion using these methods extremely complex.

2.3 Joint Anatomy

Before a model of the human elbow can be created to determine muscle forces, the functional anatomy of the elbow joint itself must be established. The elbow is classified as a *trochoginglymus* joint, possessing two degrees of freedom, flexion-extension and pronation-supination, which are mutually independent (Youm et al., 1979). There is also a third degree of freedom at the elbow, abduction-adduction, which is more commonly known as carrying angle (Morrey and Chao, 1976; Chao and Morrey, 1978; London, 1981; An et al., 1985). However, these studies have produced varying and sometimes contradictory results as to the relationships between carrying angle, flexion-extension, and pronation-supination, so it is generally not considered in models of the elbow joint. The flexion-extension motion of the elbow is defined as a rotation of the forearm about the humerus (Chao and Morrey, 1978; London, 1981). This rotation occurs about an axis that passes through the center of the trochlear sulcus and capitulum of the humerus (Morrey and Chao, 1976; Chao and Morrey, 1978; Youm et al., 1979; London, 1981; An et al., 1985; Veeger and Yu, 1996; Murray, 1997; Veeger et al., 1997a) and the instantaneous center of rotation for the flexion-extension of the elbow joint was found to lie in a fixed position at the center of the trochlear sulcus (Chao and Morrey, 1978; Youm et al., 1979). Pronation-supination is the rotation of the forearm about its longitudinal axis, which passes from the center of the radial head to the distal ulna (Morrey and Chao, 1976; Chao and Morrey, 1978; Youm et al., 1979; Veeger and Yu, 1996; Murray, 1997; Veeger et al., 1997a).

2.4 Muscle Architecture

Once the anatomy of the elbow joint has been established the architecture of the muscles crossing the joint can be considered. The architecture of a muscle consists of the attachment sites or origin and insertion points, moment arm, line of action, and physiological cross sectional area among other characteristics.

2.4.1 Origin and Insertion Locations

The origins and insertions of the muscles crossing the elbow joint have been determined qualitatively, in general anatomy texts, and quantitatively by anatomical studies. The qualitative aspects of a muscle origins and insertions simply determine the action of the muscle about the joints it crosses. The quantitative coordinates of the origins and insertions are needed to determine the lines of action of the muscle forces and moment arm of the muscle. Several researchers have investigated the coordinates of the muscles crossing the human elbow joint, but those of interest are the ones done in three dimensions. The works of Amis et al., 1979; An et al., 1981; Högfors et al., 1987; Seireg and Arvikar, 1989; Wood et al., 1989a & 1989b; and Veeger et al., 1997b; all provide three-dimensional coordinate data for the origins and insertions of the muscles crossing a human elbow joint. However, the data presented in these studies presents a challenge when trying to apply it to a computer model. The techniques used for the measurement of the data points vary between the studies and the coordinate systems they are measured in vary in both their orientation and location on the body including systems on the

humerus (both proximal and distal), ulna, radius, scapula, clavicle, and thorax. This lack of relative data hinders the effort to compile a complete set of coordinate data for the elbow from these studies as the coordinate transformations are complex and numerous. The doctoral dissertation written by W.M. Murray in 1997 solves some of these problems by presenting data on the origins and insertions of the muscle attachments and the bony landmarks along with the muscle architecture parameters for each specimen studied.

2.4.2 Moment Arms

To determine the force in muscles, the moment arm, which represents the mechanical advantage of a muscle, must be determined. Muscle moment arms have a significant effect on the estimations of individual muscle forces from joint moments, and it is essential to account for variations with both elbow and forearm position over the full range of motion. There are numerous techniques for measuring muscle moment arms, including: geometric measurement method, direct load measurement method, and tendon displacement method.

The geometric measurement method is based on the above definition for moment arm and requires the reconstruction of the location of the joint axis and the muscle paths or lines of action. Reconstructions can be created from bi-planar X-rays (Crowninshield and Brand, 1981), direct digitization during dissection (Amis et al., 1979), or serial cross sections (An et al., 1981). The geometric method can be used to measure moment arms *in vivo*, but the current techniques require the use of multiple X-rays, magnetic resonance

imaging (MRI), or computed topography (CT). In their research Amis et al. (1979) used the original moment arm derived from the digitization of an arm at a single joint position to estimate the moment arms at other positions. An et al. (1981) calculated the flexion-extension and pronation-supination moment arms of the muscles crossing the elbow in six different configurations. Unfortunately, the data may not be used to represent the variation of moment arms with elbow and forearm positions because each measurement was from a different specimen, and inter-individual variations could account for the apparent changes in moment arms.

The direct load measurement method is based the definition of moment arm as the ratio of the moment and force of a muscle (Gerbeaux et al., 1996). A load is applied to a muscle and the force and moment produced are measured, the moment arm is then calculated. This method cannot be used to estimate moment arms *in vivo*.

The tendon displacement method is based on a definition of moment arm as the derivative of tendon displacement versus joint angle (Murray, 1997; Murray et al., 2000). A constant weight is applied to the tendon of a muscle and the joint is rotated, from the tendon-displacement curve the moment arm in the plane of motion can be calculated. Once again this method cannot be used *in vivo,* but it is the easiest method with which to measure the variation in moment arms with joint position. Murray et al. (1995) used this method to determine muscle moment arms during elbow flexion from 0° to 130° and forearm supination from -70° to 90°. They found that the wrapping of muscles around

the radius during forearm rotation is very difficult to model and the small variations in the pronation-supination moment arms are hard to detect.

Some researchers have decided to simplify the task of muscle moment arm calculations by assuming that they are constant over the range of motion (Dul et al., 1984a & 1984b), while others have estimated moment arms using high order polynomials. The work of Pigeon et al. (1996) attempted to fit polynomial equations to previously reported data to determine moment arm variation with elbow flexion angle. Whereas Ettema et al. (1998) determined the muscle moment arms at the elbow by using a 3^{rd} order polynomial equation of muscle length and joint angle. Moment arms were calculated as both flexion-extension angle and pronation-supination angle varied, and for many of the muscles significant variations were found.

2.4.3 Line of Action

The line of action of muscle force is a crucial element in the determination of muscle forces. The simplest method to define the line of action is as a straight line from the muscle insertion to the origin (Yeo, 1976; van Zuylen et al., 1988; Soechting and Flanders, 1997). This introduces errors due to the lack of inclusion of deflections and wrapping around bones, muscle and other tissue. A modification to improve the straight-line approach is to include effector points in the line of action where muscles or tendons contact bones other than at their attachment sites (Gonzalez et al., 1996). This enables the line of action to be composed of multiple straight-line segments that better

approximates the actual path of the muscle force. Ettema et al. (1998) took the segmented straight-line approach one step further and included curved segments where large deviations from the straight path of the elbow muscles occurred. A more complex and intensive method to determine the line of action of muscle force is by the centroid technique. In this system the line of action is defined by connecting the digitized centroids of a series of muscle cross sectional areas (Amis et al., 1979; An et al., 1981; An et al., 1984b). The implied assumption with this method is that the actions of muscles are uniformly distributed across the muscle section. The centroid approach can produce accurate results for relaxed muscles in a single joint position, but to cover the full range of joint motion would require advanced imaging techniques, MRI or CT, and an extensive database for each subject. Jensen and Davy (1975) produced a study that compared the straight line and centroid approaches for determining muscle force line of action at the hip. They found that the centroid approach is more accurate to *in vivo* lines of action and also helps describe the action of a muscle on a joint, which can be lost with the straight-line method. Koolstra et al. (1989) developed a method of estimating three-dimensional muscle lines of action *in vivo* which uses MRI or CT image data. However, the technique requires complex data manipulation and regression analysis to achieve meaningful results.

2.4.4 Cross-Sectional Area

The physiological cross sectional area (PCSA) of a muscle is believed to be proportional to its force generating capacity. The method of determining the PCSA of a muscle varies

from study to study, but two main approaches can be identified. The first approach, used by Amis et al (1979) and Veeger et al. (1991), is to determine the PCSA by a cross section at the level of the largest apparent cross sectional area of the arm. The perimeter of the muscle is digitized and the contained area is calculated. However, this method carries large error potentials, as the location of the selected cross section is not necessarily that of the maximum cross section of a muscle and may not be perpendicular to the muscle fiber direction. The second approach calculates the PCSA as the muscle volume divided by length. Amis et al. (1980); and An et al. (1981) determined the muscle volume by water immersion and divided it by the mean fiber length to find values for the PCSA of the muscles crossing the elbow. Crowninshield and Brand (1981) also used water immersion to determine the muscle volume but chose to use muscle length in their calculations. More recently in the work of Murray (1997) and Murray et al. (2000), it has been suggested that for a more accurate calculation of PCSA, the muscle optimal fascicle length should be used instead of muscle fiber length while the muscle volume is calculated by muscle mass divided by density. Research by Dowling and Cardone (1994) revealed the benefits of using relative cross sectional area (RCSA) measurements in musculoskeletal models. The RCSA is defined as the unit-less ratio of the cross sectional area of the muscle under consideration to the total cross sectional area of all the muscles in the functional group (that is having the same action). This results in less error in the force predictions in the muscles. An added advantage of using a RCSA measurement is that there is no need to include a measurement of the specific tension of muscle (muscle force per PCSA), which has large variation in value in the literature. As with much of the data required to construct a muscle model, PCSA is determined from cadavers and is then

applied to living subjects, however Cutts and Seedholm (1993) found that the RCSA found using cadavers is similar to those found *in vivo*.

2.5 Anatomical Scaling

The muscle moment arms and lines of action are essential in the calculation of the muscle forces and are both geometrically related to the origin and insertion points of the individual muscles. Since the origin and insertion points of a muscle are directly related to the bone anatomy, and the dimensions of the bones vary with the height and weight of the subject, an anatomical scaling method is required. Previous studies in the literature that have measured elbow muscle moment arms or lines of action rarely measure the subject bone and body segment dimensions, not to mention the overall specimen size, which are all necessary to make the data applicable to a scaling technique.

An et al. (1981) measured several muscle anatomical parameters and normalized their data based on the ratio of the square root of the muscle cross-sectional area to facilitate the comparison between the different sized specimens. Murray (1997) proposed to quantify the amount of variation in the elbow muscle moment arms across specimens of different sizes and evaluate the relationships between the elbow muscle moment arms and the anthropometric dimensions of the upper extremity. This study attempted to predict the muscle moment arms based on linear regression equations and normalized elbow muscle moment arm curves. It was found that a subject specific musculoskeletal model could be developed but advanced medical imaging techniques would be required to create

a three-dimensional reconstruction for use with this particular analysis method. However, Murray (1997) contained a small data set of ten subjects that consisted of the vector points of the elbow muscle origins and insertions and the bone surface geometry coordinates along with various anthropometric segment dimensions. Yet, the lack of relation to the overall dimensions of the specimens used still makes the data insufficient to allow scaling to the general population size distribution. Diffrient et al. (1974) contains data on various segment dimensions in relation to the height, weight, and gender of the subject and some measurements are given for the standard population distributions (2.5, 50, and 97.5 percentiles). In combination, the data supplied by Murray (1997) and Diffrient et al. (1974) can be used to arrive at an initial series of scaling functions to help provide more accurate muscle force predictions for various sizes of subjects.

CHAPTER 3

METHODOLOGY

3.1 Introduction

This chapter details the methodology used to develop the equations for the three-dimensional vector model of the elbow joint musculature. The function of the dynamic simulation program and the anatomical elbow model are described in Section 3.2. Section 3.3 provides the rationale behind the selection of muscles for inclusion in the elbow model. The method used to scale the body segment parameters along with the bone and muscle anatomy to subject size is outlined in Section 3.4. Following this, the detailed methodology for the elbow model is presented. The determination of the three-dimensional muscle moment arms is developed in Section 3.5. In Section 3.6, the procedure for determining the individual muscle forces from the net joint moment is detailed. The equations for determining the muscle energies, both mechanical and biological, are developed in Section 3.7. Finally, the assumptions and limitations of the elbow model are discussed in Section 3.8.

3.2 Programs

The following sections explain the functions of the dynamic simulation program and the anatomical elbow model. It should be noted that the description of the dynamic

simulation program is presented in more detail than that of the elbow model, as the later sections of this chapter concern themselves solely with the anatomical model.

3.2.1 Dynamic Simulation Program Function

In order to calculate the muscle forces across the joint, a net joint moment is required. For this work the program to determine these net moments, which include both the static and dynamic components, was developed by Dr. A.B Thornton-Trump and Ms. A. Chan as part of a research grant from the Workers Compensation Board of the province of Manitoba (Thornton-Trump, A.B., 2002). The details of the program are beyond the scope of this thesis and as such only a very brief description of the program and a generic flow chart are presented here. This outline of the dynamic simulation program allows the reader to confirm that the dynamics are three-dimensional and included in the simulations run to confirm the individual muscle force calculations.

The dynamic simulation program was developed to describe the upper body motion in three-dimensional space and produce output that allows the assessment of the risk of repetitive strain injuries through the required joint moments while a worker performs a task. The flow chart of the master program is presented in Figure 3.1, beginning on page 23. The dynamic simulation model was designed to calculate the joint forces and moments from the accelerations of the upper body segments and a work object in three-dimensional space. Forces and moments of simplified spinal segments, representing the thoracic and lumbar vertebrae, were also included in the dynamic program. This

inclusion allows the model to more closely approximate the actual movement of a human subject where the torso rarely remains fixed in space.

In order to start the analysis of the motion, the program requires set-up information from the user. The size and location of the workstation must be specified, along with the size and weight of the work piece. Initial and target positions of the work piece are then defined using a graphical interface program. Finally, the operator parameters of gender, height, and weight are identified as well as the task cycle time and the desired acceleration profile for the task. The program will then calculate the body segment parameters, as described in section 3.4.1, and determine the optimal operator position relative to the workstation and the work piece placement.

After all the necessary information has been input to the program, the dynamic simulation program will design the path of the work piece moving from the initial location to its target location according to the time and acceleration profile. The path is assumed to be of parabolic shape in three-dimensional space. The position of the object in the global coordinate system during a single task cycle is calculated using a six-degree polynomial equation.

The upper body, which includes the upper and lower back, upper arm, forearm, and hand segments, is modeled as a chain of rigid bodies interconnected by revolute joints. An Eulerian angle system is used and local coordinate systems are assigned for each segment at the joint. The kinematic relationship between each of the segments is then developed

using its transformation matrix. Then the orientation and position for each of the upper body segments can be calculated using the inverse kinematic relationships.

Since the orientation and position of each upper body segment is known, the angular velocity and angular acceleration can be calculated by differentiating each angle rotation across the time profile. These angular velocities and accelerations and the linear acceleration of each segment, are presented with respect to each local coordinate system and the global system, and used in the development of the dynamic model of the upper body. The indirect dynamic model of the upper body for the task is expressed using the Eulerian equation, which consists of Newton's second law of motion and the equations of angular motion. Reaction moments and forces of each segment are determined from the dynamic model and then used later by anatomical models in the calculation of the muscle forces and energies. The dynamic simulation computer program was structured in such a way that further anatomical joint models can be easily accommodated as they are developed.

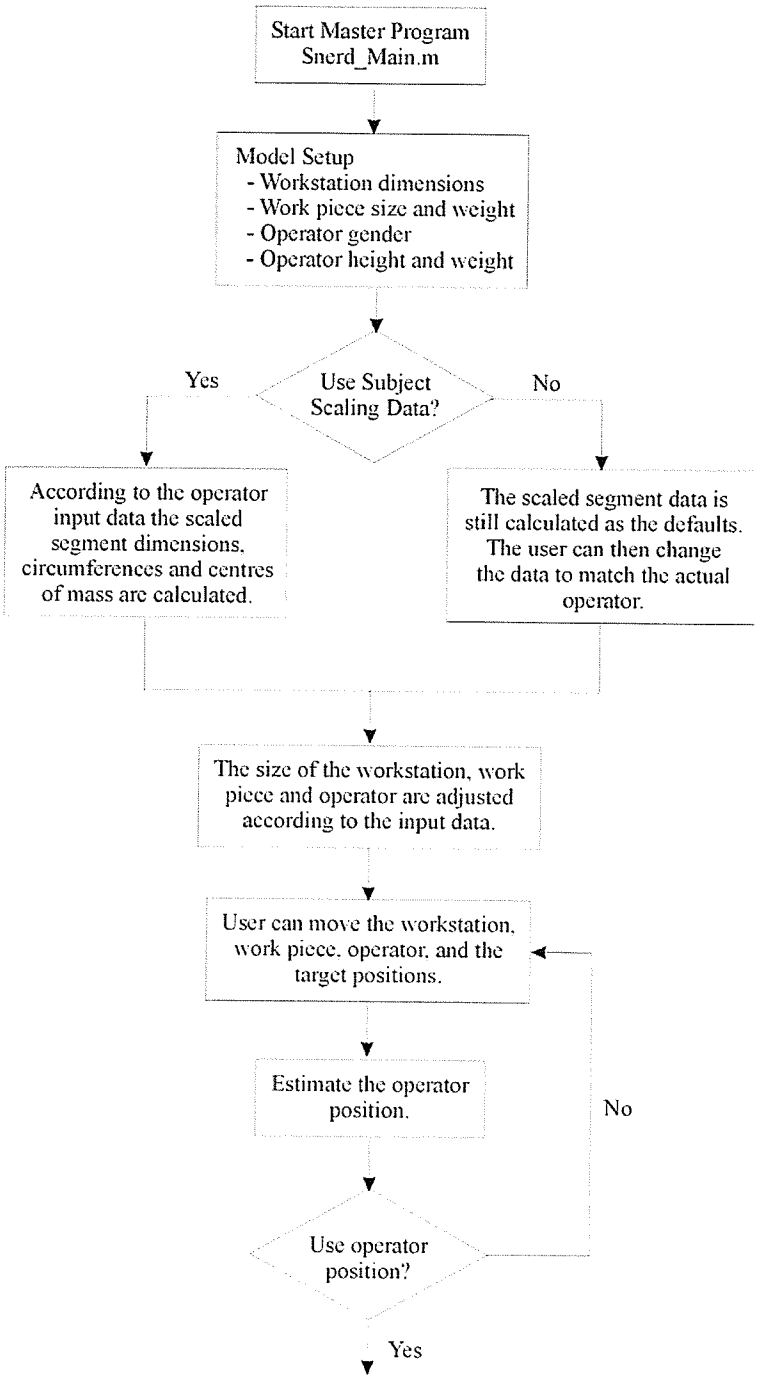

Figure 3.1 Dynamic Simulation Program Flow Chart

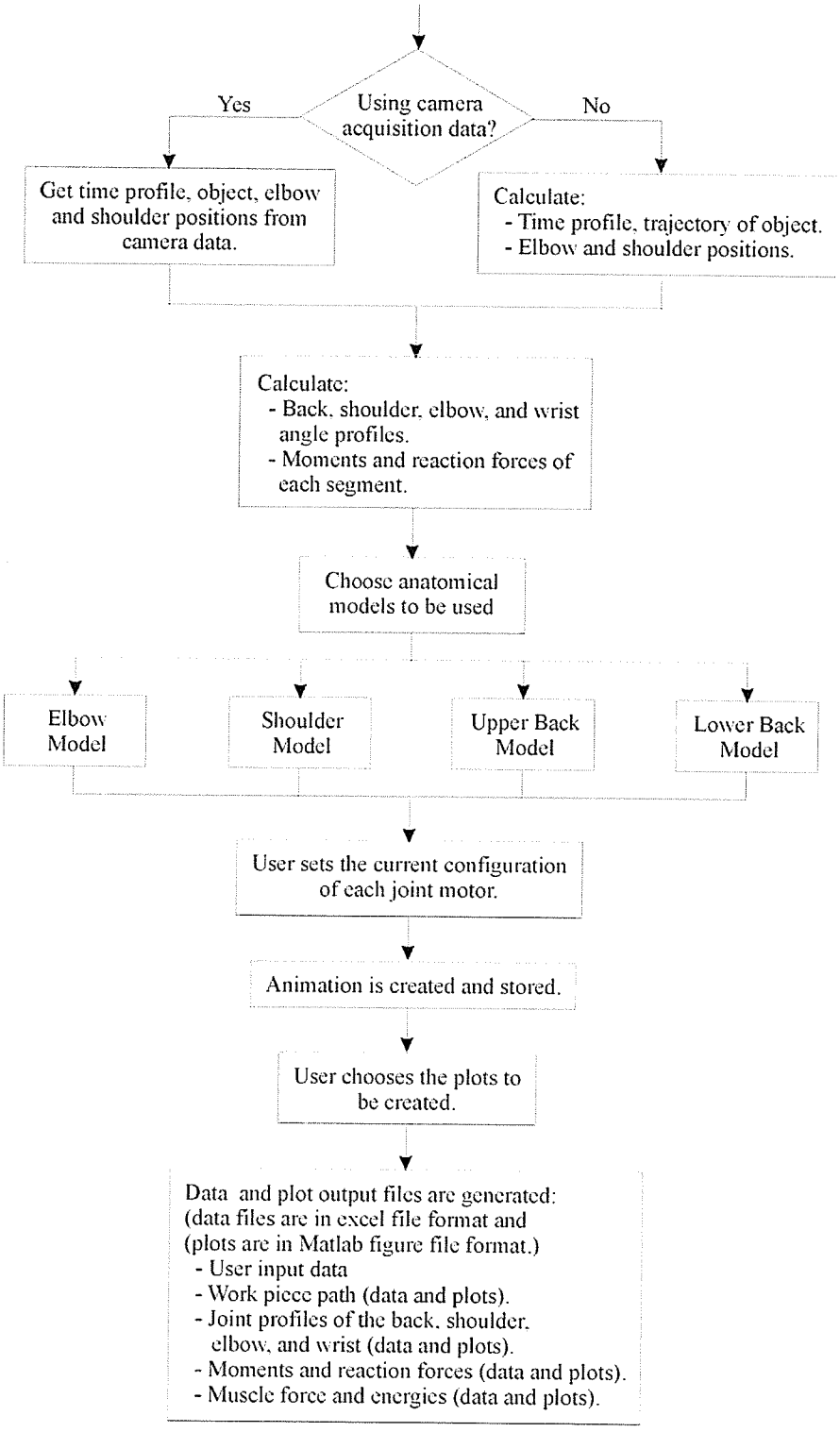

Figure 3.1 Dynamic Simulation Program Flow Chart

3.2.2 Anatomical Elbow Model Function

The following description of the three-dimensional vector model of the elbow joint musculature consists of original work developed by the author. The anatomical elbow model was developed to quantify the forces in the individual muscles crossing the human elbow joint during a task cycle and to identify the relative risk for repetitive strain injuries. Figure 3.2, on page 27, presents the flow chart of the elbow model that runs with the dynamic simulation program. This anatomical model contains only six muscles at this point and employs simplifying assumptions to allow for the estimation of the individual muscle forces and energies from the joint moments determined by the dynamic model.

In order to calculate the muscle forces and energies the model requires various inputs. The user specifications of the operator gender, height, and weight, along with the body segment parameters determined earlier in the dynamic simulation program are transferred to the elbow model. In addition, the dynamic model supplies the task cycle time, three-dimensional net elbow joint moment, and the flexion-extension and pronation-supination angles of the elbow. The muscle origin and insertion points are then calculated based on the given operator physical attributes and the results of the body segment parameter scaling equations, as described in section 3.4.2.

After the inputs are received, the anatomical elbow model calculates the muscle moment arms at each joint position along the task path. The moment arms are determined based

on the location of the origin and insertion points in space and a straight line of action for the muscle force. The moment arms are calculated using a three-dimensional vector approach. The components of the elbow joint moment produced by the dynamic model are transformed relative to the anatomical axes of rotation for flexion-extension and pronation-supination. Now the forces in each muscle crossing the elbow joint can be calculated from the dynamic moment using another set of vector relationships. Finally, the mechanical and biological energies expended and consumed, respectively, by each muscle are determined over the full task cycle. The individual muscle forces and energies are then output from the anatomical model back to the master program for data file storage and graphical display. The program listing of the anatomical elbow model can be seen in Appendix A.

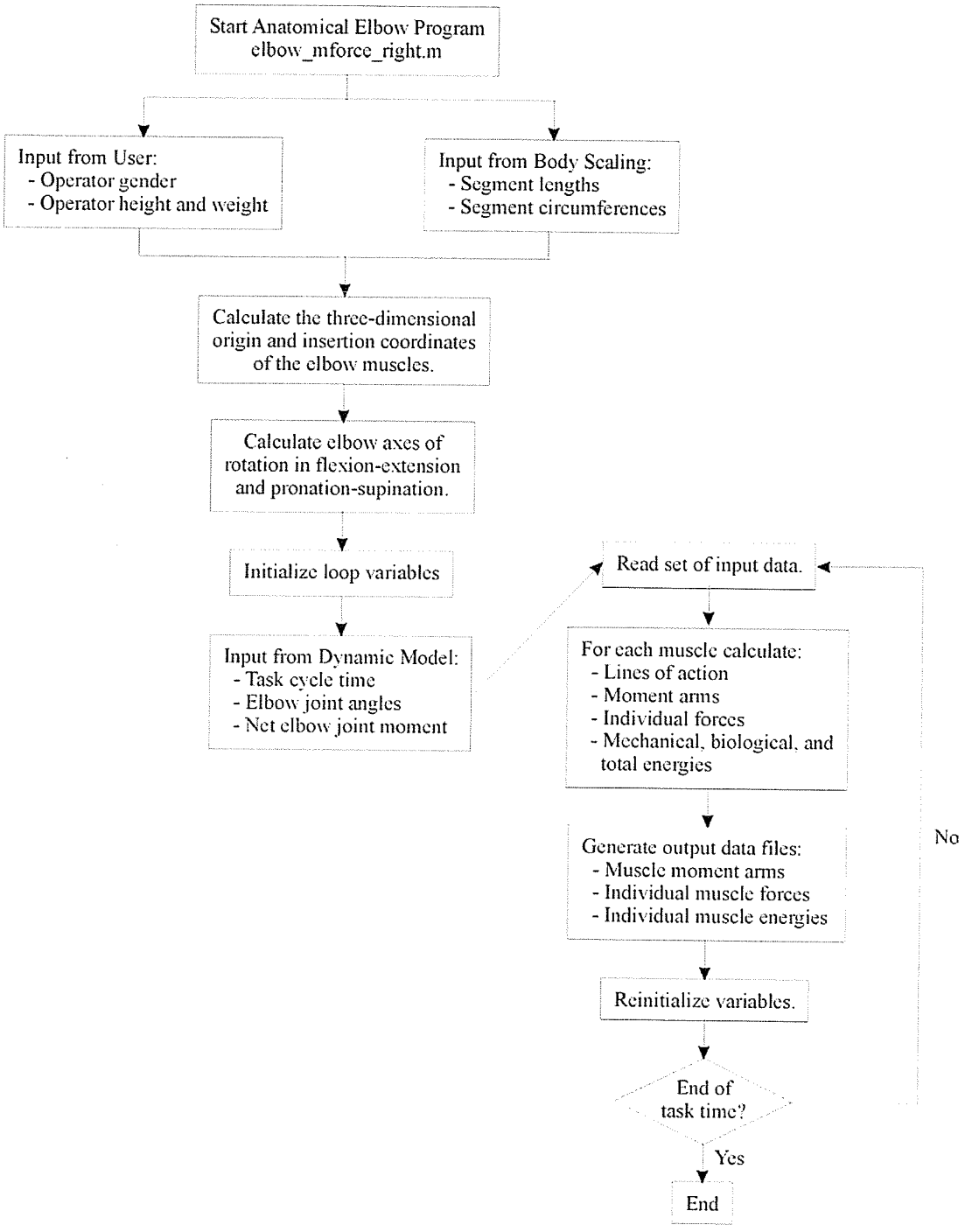

Figure 3.2 Anatomical Elbow Model Flow Chart

3.3 Muscle Selection

Before the three-dimensional modeling of the elbow musculature can begin it must be decided which of the twenty-four muscles that cross the joint will be considered. The number of muscles being modeled must be reduced, as a model that included them all would be extremely complex and would require an excessive amount of processing capacity and time. In addition, some of the muscles crossing the joint do not, as their primary functions, create movements about the elbow but rather movements of the wrist and/or fingers. Electromyographical studies have attempted to identify the active muscles during specified elbow movements, and will be used in this thesis to determine the significant muscles to be used in the model.

Basmajian (1969), Basmajian and DeLuca (1985), Basmajian and Latif (1957), de Sousa et al. (1961), and Pauly et al. (1967) all found that the Biceps Brachii, Brachialis, and Brachioradialis muscles were the prime movers during flexion of the elbow. Biceps Brachii is active during elbow flexion when the forearm is in both the supinated and neutral positions. However, due to the muscle insertion on the radial tuberosity it is mostly inactive in flexion, while maintaining a flexed position, and in antagonistic capacity when the forearm is in a prone position. The two heads of Biceps have been shown to be far more active in flexion when resistance is applied to the movement. The Brachialis muscle is an active flexor of the elbow in all forearm positions no matter if the movement is slow, fast, or simply maintenance of a flexed position. Brachioradialis is found to be mainly active when performing fast elbow flexion and when there is a weight

in the hand or there is resistance to movement. In addition, the Pronator Teres muscle is being included as a flexor as it also shows activity when there is resistance to the movement (Basmajian and Travill, 1961). Although not usually examined as an elbow flexor in electromyographical studies to date, the Extensor Carpi Radialis Longus muscle has demonstrated a potential for elbow flexion due to its moment arm length and cross-sectional area (Amis et al., 1979; An et al., 1981).

Two muscles have been found to display significant electromyographical activity during elbow extension: Triceps Brachii and Anconeus (Basmajian and Griffin, 1972; Pauly et al., 1967; Travill, 1962). These studies have shown that the three heads of the Triceps Brachii muscle (long, medial, and lateral) function in extension in much the same manner as the Biceps and Brachialis in flexion. That is, the medial head of Triceps is found to be active in all situations of elbow extension, while the long and lateral heads are more active when the motion is resisted. The Anconeus muscle has been found active during elbow extension, especially during slow movements, but its definitive role is still the subject of great debate. Thus, due to its small moment arm and cross-sectional size its potential contribution to elbow extension is relatively small compared to that of Triceps (Amis et al., 1979; An et al., 1981) and it will be excluded from this model.

Unfortunately, there are very few studies that have examined the roles of upper limb muscles during pronation and supination of the forearm. Basmajian and Travill (1961) did a small electromyographical investigation of forearm movement and found that Pronator Quadratus is the prime mover, while Pronator Teres becomes active when

pronation is rapid or against resistance. The activity in both muscles does not change with the position of the elbow joint. In the case of supination, Basmajian and Travill (1961) found that the Supinator muscle was active by itself during slow unresisted movement in any elbow configuration and during fast supination with the elbow extended. When rapid unresisted supination in a flexed elbow position or any supination against resistance is required, Biceps Brachii becomes active to supplement the Supinator activity. However, of the four muscles only Pronator Teres and Biceps Brachii will be considered in the current model due to the lack of the appropriate anatomical information on Pronator Quadratus and Supinator. Commonly viewed in most gross anatomy texts as a pronator from the supine forearm position and a supinator from the prone forearm position, Brachioradialis was found to be an auxiliary muscle in these movements when additional strength is required (Basmajian and Latif, 1957). In summary, the anatomical elbow model will include the primary moment generating muscles of the flexor and extensor functional groups. Thus the Biceps Brachii, Brachialis, Brachioradialis, Extensor Carpi Radialis Longus, and Pronator Teres muscles will represent the flexor muscles, while the Triceps Brachii muscle will represent the extensor muscles.

3.4 Anatomical Scaling

The development of the anatomical scaling methodology will be presented before that of the vector model to maintain the data input order used in the anatomical elbow model program code. The author has developed all of the correlation equations that are presented here in the anatomical scaling methodology and in Appendix B. This work

was undertaken to allow the model to be applicable in a general manner, in other words to any size of subject, rather than to a specific subject. In order to generate reasonable estimations of the individual muscle forces, the anatomical parameters used by the elbow model must be scaled based on the size of the subject being analyzed. It is necessary to adjust the anatomical measurements used by both the dynamic simulation program and the elbow model, as there is a large variability between human subjects. Given the height and weight of the subject, the body segment parameters, such as segment length, circumference, and centre of mass position are calculated. From these body segment parameters the bone and muscle parameters, which determine the bone lengths and the muscle origin and insertion points respectively, are then computed. The program listing of the scaling model can be seen in Appendix C.

3.4.1 Body Segment Parameters

The dynamics and graphics portions of the dynamic simulation program use the body segment parameters to compute the dynamic reaction forces and net moments at the various joints and to establish the size of the worker relative to the workstation, respectively. Formulae are needed to calculate the segment depths, widths, circumferences, lengths, and the longitudinal locus of the segment centres of mass from the height and weight of the subject being analysed. Raw data from Diffrient et al. (1974) was used to determine a set of mathematical equations for estimating the majority of the body segment parameters, with the exception of the centres of mass and the trunk segment lengths, which used data from deLeva (1996).

The full set of equations developed for the body segment parameter calculations are presented in Table B.1 of Appendix B. When possible, correlation equations were calculated from the data to compute the segment parameters based on the subject's height, however this was not always possible. In the case of the head width and length, the dimensions take only two values over the lower subject height ranges before correlations can be found. The segment circumferences, chest depth and hip depth relations are based on the 2.5, 50, and 97.5 percentile male and female data. The lengths of the three torso segments: upper, mid, and lower, are determined as ratios of the full torso length.

The body segment measurements are graphically depicted in Figures 3.3 and 3.4, on pages 34 and 35. The length of the head is measured from the crown to the bottom of the chin, the width at the level of the temples, and the circumference slightly superior to the eyebrows. About the chest, the measurements are taken at the level of the nipples for a male subject and at the axillae for a female subject at the end of a quiet exhale. The full length of the torso is divided into three segments: the upper torso, from the base of the neck to the level of the xyphoid process; the mid torso, from the xyphoid process to the level of the omphalion; and the lower torso, from the omphalion to the hip joint centre. The upper and middle torso segments are combined to correspond to the upper back segment of the dynamic model, where the rotational joint is located at the level of the twelfth thoracic vertebra. Whereas the lower back segment, with the rotational joint at the level of the fifth lumbar vertebra, is represented in the anatomical scaling as the lower

torso segment. The length of the lower body measures from the hip joint centre to the floor. For the upper arm, the length is measured from the shoulder joint centre to the elbow joint centre, while the circumference is taken at the level of the axilla. The circumference of the elbow is measured with the elbow flexed to ninety degrees at the posterior tip of the olecranon process and the crease of the elbow, while the wrist circumference is measured over the protrusions of the radius and ulna. Around the forearm, the circumference is measured at the maximum point and the length of the segment is from the elbow joint centre to the wrist joint centre. The circumference of the hand is measured around the palm at the base of the fingers excluding the thumb and its length from the wrist crease to the tip of the middle finger. The centres of mass for the torso segments are calculated longitudinally from the hip joint centres, and the centre of mass fro the upper arm, forearm, and hand are determined longitudinally from the shoulder, elbow and wrist joints respectively.

The mathematical relations for the body segment parameters were set up using data representing the "average", or 50^{th} percentile, male and female specimens. Thus, once the segment parameters have been calculated from the height of the subject, their weight is used to modify the applicable measurements, specifically, the segment circumferences, chest depth and width, and hip depth and width. This correction is made by calculating the body mass index (*bmi*) for the subject as follows:

$$bmi = \frac{weight}{(height)^2} \tag{3.1}$$

where weight is measured in kilograms and height in meters. For a *bmi* between 20 and 25, the subject is considered to have the standard body type and no adjustment is made to

the segment parameters. If the subject's *bmi* is less than 20, the subject has an ectomorphic body type and the adapted parameters are assumed to be 90% of the standard measurements. A *bmi* between 25 and 27 indicates the subject is slightly endomorphic and the measurements are taken as 110% of the standard ones. Finally, if the *bmi* is over 27 the subject is endomorphic and the correction to the standard parameters is 120%.

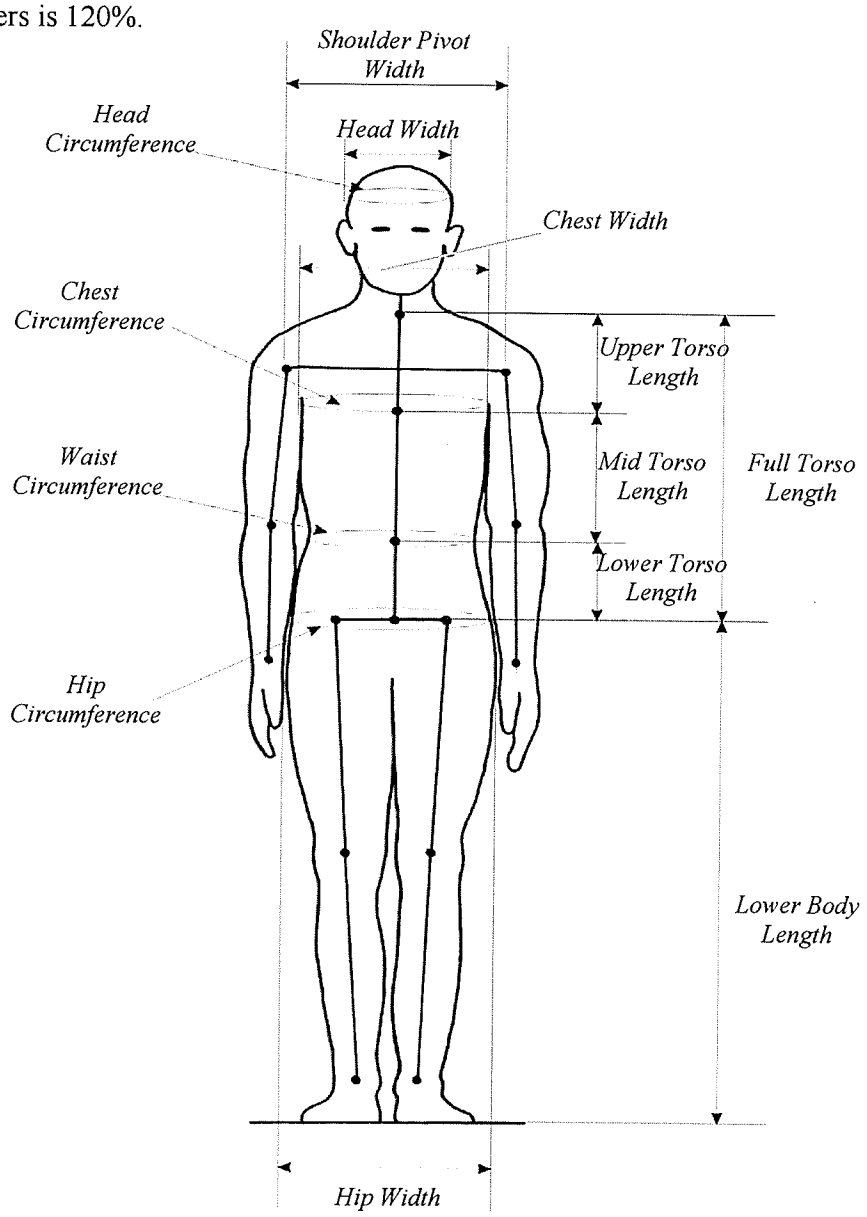

Figure 3.3 Front View of Body Segment Parameters

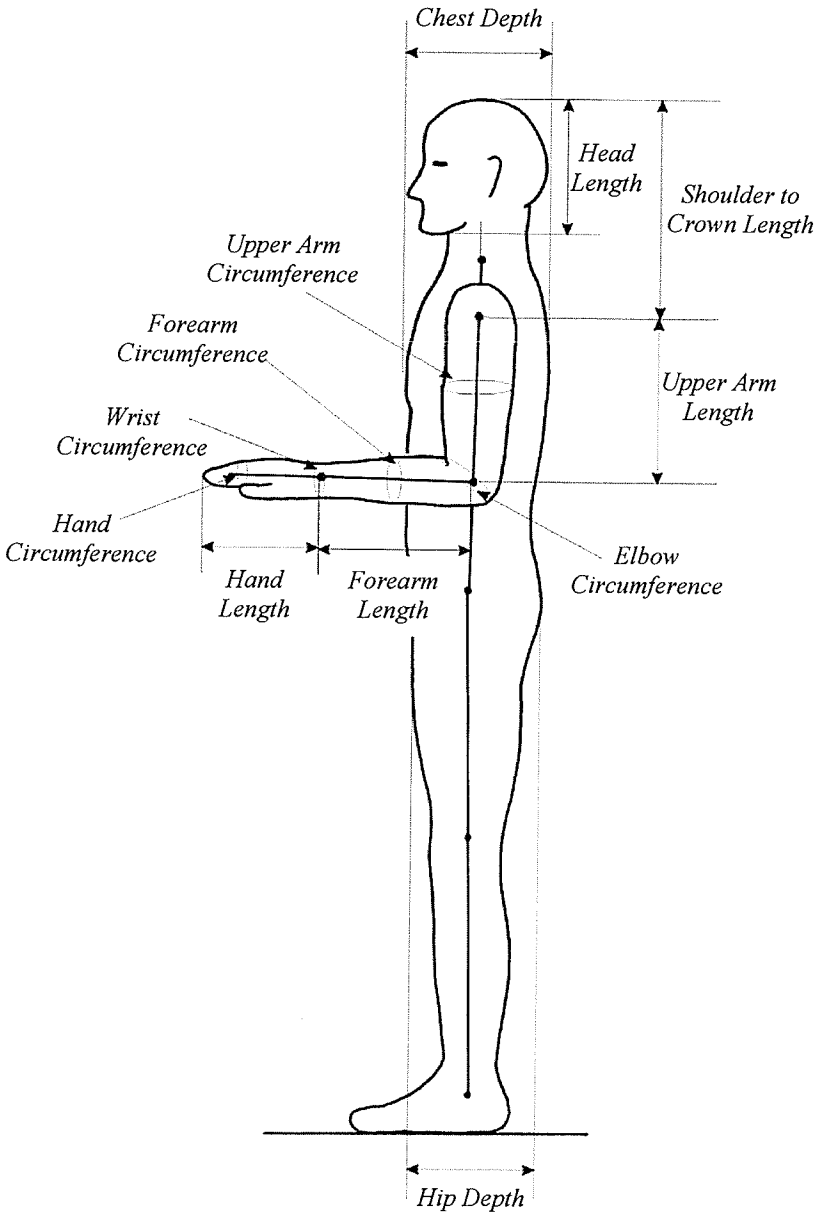

Figure 3.4 Side View of Body Segment Parameters

3.4.2 Bone and Muscle Parameters

In order to correctly apply the vector techniques necessary for the calculation of the muscle forces to an individual subject, the muscle geometry had to be determined. From the external measurements of the segment parameters, the underlying bone dimensions can be calculated. With the detailed bone measurements, the three-dimensional muscle origin and insertion locations can be computed. Unfortunately, this task was much more difficult than anticipated as very few studies that provide information on the bone and/or muscle measurements, include the height, weight, or segment dimensions of the subject.

The doctoral thesis by Murray (1997) contains data on the external segment and bone dimensions, along with the measurements of the three-dimensional muscle origin and insertion points. The data from Murray (1997) was related to the Euler and Cartesian coordinate systems used in the dynamic simulation program and the elbow model, respectively. Relationships were then calculated to scale the coordinate data of the bones and muscles to the segment dimensions. However, only ten specimens were examined in the Murray study and with such limited data, correlation equations were not always found for the desired parameters. As a result any correlations found, carry with them a large amount of uncertainty.

Table B.2 in Appendix B contains the equations developed to calculate the bone parameters from the segment measurements. Correlation equations were found to determine the humerus, radius, and ulna bone lengths from the lengths of the upper arm

and forearm segments. In addition, a linear correlation was obtained for the transepicondylar width of the humerus from the circumference of the elbow. The distal radial-ulna width equation was found as a ratio of the wrist circumference, the equation for calculation of the humeral shaft radius as a ratio of the transepicondylar width, and finally the humeral head radius was found to be best represented by a constant value for male and female subjects independently. Coordinates for the centre of the trochlear sulcus and centre of the capitulum of the humerus are needed to calculate the axis of rotation for flexion-extension of the elbow joint. The location of the centre of the trochlear sulcus is already known, as it is the centre point of the coordinate system being used. The x-coordinate of the centre of the capitulum is calculated by a ratio of the humeral length, while the y- and z-coordinates are found proportional to the elbow circumference. Locations of the centre of the head of the radius and the centre of the distal ulna are used to calculate the axis of rotation for the pronation-supination of the forearm. The x-coordinate of the centre of the radial head is relative to the length of the radius, and the y- and z-coordinates are ratios of the forearm circumference. The location of the y- and z-coordinates of the distal ulna are percentages of the circumference of the wrist, while the x-coordinate was found as a logarithmic correlation of the ulna length.

The mathematical relations for calculating the three-dimensional locations of the muscle origins and insertions, as described in section 3.5.2, are presented in Table B.3 of Appendix B. The majority of the coordinate locations of the muscle bony attachments could not be found using correlation equations and were determined as proportions of the bone parameters. The Biceps Brachii muscle origin x-coordinate was found as a

logarithmic correlation to the length of the humerus and the y- and z-coordinates as ratios of the radius of the humeral ball. Its insertion coordinates were found by three linear correlations of the radius length in the x-direction and the centre of the radial head in the remaining two directions. For the Brachialis origin the x-coordinate is determined as a percentage of the humerus bone length, the y- and z-coordinates are calculated as ratios of the humeral shaft radius. The insertion coordinates of Brachialis are found relative to the ulna length and transepicondylar width. Brachioradialis origin x-coordinate is exponentially correlated to the humerus length, while the other two coordinates are ratios of the humeral shaft radius. A linear correlation to the length of the radius was found for the x-coordinate of the Brachioradialis insertion, and proportions of the distal radius-ulna length establish the y- and z-coordinates. The Extensor Carpi Radialis muscle origin coordinates are located using ratios of the humerus length in the x-direction and the radius of the humeral shaft in the other two directions. For its insertion point the x-coordinate has a linear correlation to the radius length, while the y- and z-coordinates are percentages of the distal radius-ulna width. The Pronator Teres muscle origin coordinates are found as percentages of the humerus length in the x-direction, the humeral shaft radius in the y-direction, and the transepicondylar width in the z-direction. The x-coordinate of the insertion of Pronator Teres is determined as a ratio of the length of the radius and the remaining two coordinates are found proportions of the distal radius-ulna width. Finally, the Triceps Brachii origin coordinates are found relative to the humerus bone length and the humeral shaft radius. Its insertion x-coordinate is located using a portion of the length of the ulna, while the y- and z-coordinates are ratios of the transepicondylar width.

3.5 Muscle Moment Arm Determination

The theory presented for the calculation of the muscle moment arms, while just an application of vector mathematics, is an approach developed by the author. The potential for a muscle to generate a moment about a specified joint is directly related to its moment arm. By definition, the moment arm is the perpendicular distance from the joint axis of rotation to the line of action of the muscle force. Due to the significant effect the muscle moment arms have on the estimation of the individual muscle forces, it is essential to account for variations of both the elbow and forearm positions over the full joint range of motion. The basic vector equation for the moment-force relation is shown below along with the accompanying schematic.

$$\bar{M} = \bar{r} \times \bar{F} \tag{3.2}$$

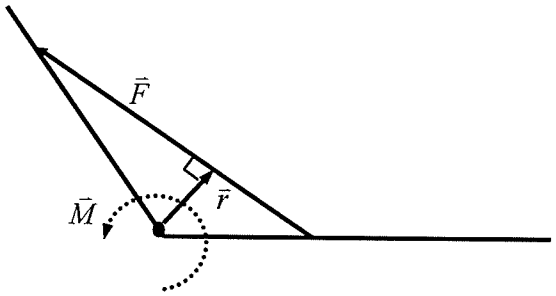

Figure 3.5 Basic Moment Schematic

where $\bar{M}$ is the moment vector about the centre of rotation, $\bar{r}$ is the moment arm vector, and $\bar{F}$ is the force vector.

In order to calculate the individual muscle moment arms the three-dimensional coordinate system must first be established, then the coordinate points of the muscle origins and insertions determined. From the origins and insertions the muscle lines of action are established and then the moment arms for each muscle are calculated.

3.5.1 Coordinate System Orientation

The elbow will be modelled as a two degree of freedom joint. One degree of freedom is the flexion-extension movement, which occurs at the elbow joint proper, while the second movement is the self-rotation of the forearm, or pronation-supination. As established by the previous studies examined in the literature review, the axis of rotation for the flexion-extension of the elbow passes through the centre of the trochlear sulcus and capitulum of the humerus, and the instantaneous centre of rotation lies at the centre of the trochlear sulcus. In addition, the axis of rotation for the pronation-supination of the forearm was found to pass from the centre of the radial head to the centre of the head of the ulna. The data being used for the initial set-up of the elbow muscle model, from Murray (1997), is described in relation to a coordinate system located at the centre of the humeral head. However, it is desired to have the coordinate system for the elbow model located at the centre of the trochlear sulcus. Thus, the local coordinate system is fixed to the humerus and rotates with the upper arm such that the positive x-axis points superiorly, from the elbow towards the shoulder, along the length of the humerus; the positive y-axis points posteriorly and the positive z-axis points laterally away from the body. In order to accomplish this, the coordinate system used by Murray (1997) must be

translated to the new location at the distal end of the humerus via a vector joining the centre of the humeral head and the centre of the trochlear sulcus. These coordinate systems at the proximal and distal humerus along with the translation vector are illustrated in Figure 3.6.

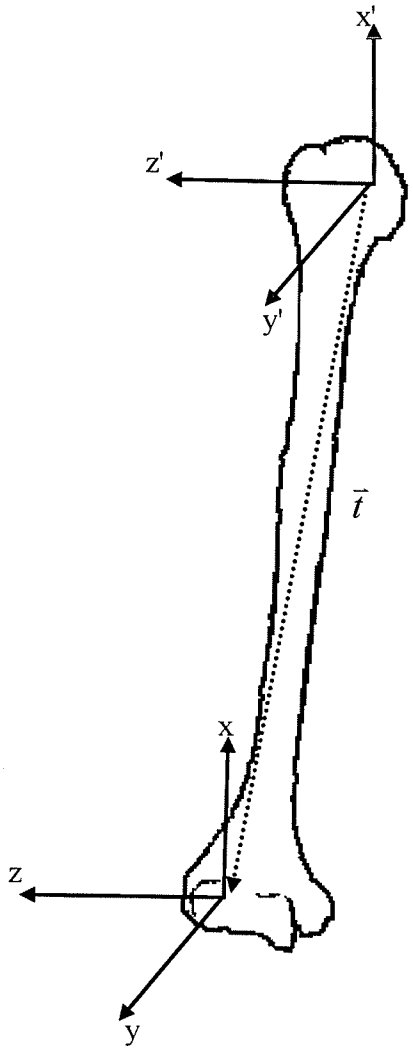

Figure 3.6 Coordinate System Translation

The following matrix operation is used to translate the coordinate system and muscle origin and insertion coordinate points from the centre of the humeral head to the trochlear sulcus:

$$\begin{bmatrix} x_1 \\ y_1 \\ z_1 \\ 1 \end{bmatrix} = \begin{bmatrix} 1 & 0 & 0 & t_x \\ 0 & 1 & 0 & t_y \\ 0 & 0 & 1 & t_z \\ 0 & 0 & 0 & 1 \end{bmatrix}^{-1} \cdot \begin{bmatrix} x \\ y \\ z \\ 1 \end{bmatrix} \tag{3.3}$$

where the translation vector $\bar{t} = (t_x, t_y, t_z)$, the coordinates based on the centre of the trochlear sulcus are (x_1, y_1, z_1) and the coordinates based on the centre of the humeral head are (x, y, z).

3.5.2 Muscle Origins and Insertions

The following descriptions were adapted from information found in Moore and Dalley (1999) and Norkin and Levangie (1992) and are not the results of anatomical dissections by the author. The origin and insertion points for the six muscles being considered in the elbow model must be defined before further calculations towards the muscle moment arms can be done. The Biceps Brachii has two distinct muscle heads; the long head originates on the supraglenoid tubercle of the scapula while the short head originates on the coracoid process of the scapula, as shown in Figure 3.7. As the scapula is not included in the elbow model, an effective origin must be used. The tendon of the muscle's long head is held in the intertubercular groove at the proximal end of the

humerus by a ligament and this point is used as the origin for both heads. The two heads of Biceps fuse into a single tendon that inserts on the radial tuberosity.

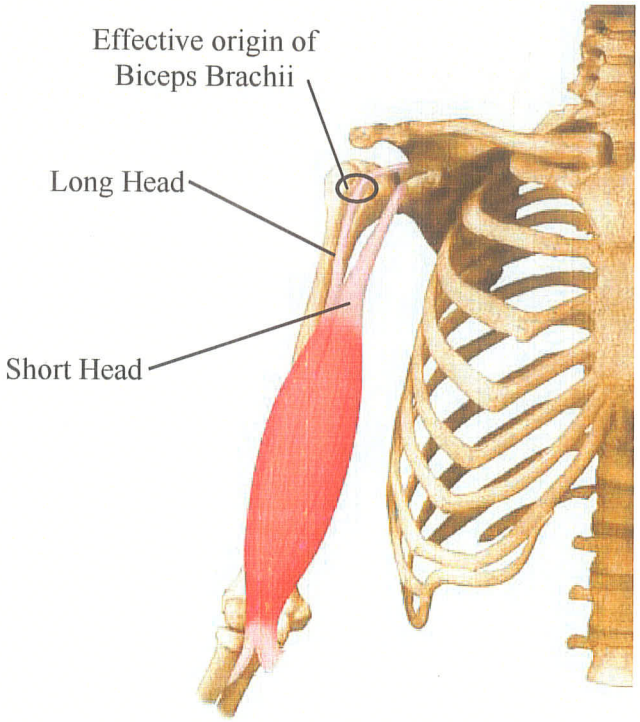

Figure 3.7 The Biceps Brachii Muscle (adapted from Teitz and Graney)

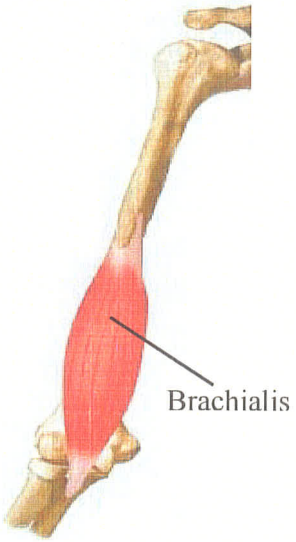

Figure 3.8 The Brachialis Muscle (adapted from Teitz and Graney)

Brachialis, shown in Figure 3.8, has its origin on the distal half of the anterior aspect of the humerus and inserts on the tuberosity and coronoid process of the ulna.

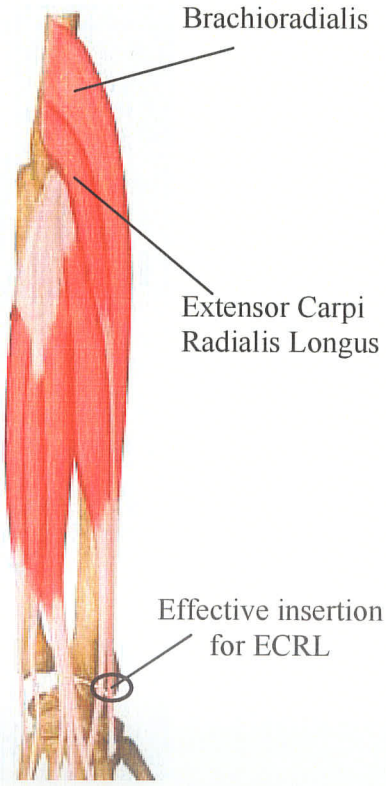

Figure 3.9 Brachioradialis and ECRL Muscles (adapted from Teitz and Graney)

The Brachioradialis muscle derives its origin from the lateral supracondylar ridge of the humerus and its insertion on the base of the radial styloid process. Extensor Carpi Radialis Longus, or ECRL, originates on the lateral epicondyle and lower third of the lateral supracondylar ridge. It inserts on the posterior aspect of the base of the second metacarpal, but since the bones of the wrist and hand are not included, the insertion was defined as the styloid process of the radius. The Brachioradialis and Extensor Carpi Radialis Longus muscles are pictured in Figure 3.9.

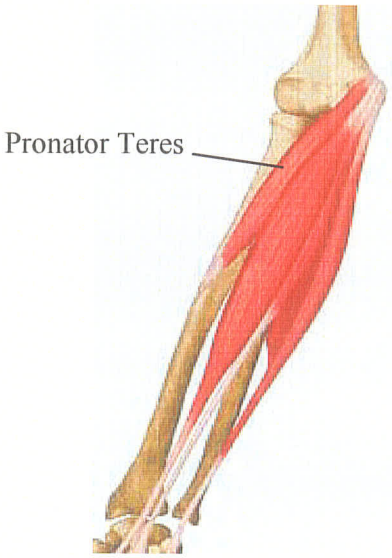

Figure 3.10 The Pronator Teres Muscle
(adapted from Teitz and Graney)

The Pronator Teres muscle, as shown in Figure 3.10, originates on the medial epicondyle of the humerus and medial aspect of the coronoid process of the ulna, although for the elbow model only the origin on the humerus will be used. Its insertion is located on the middle third of the lateral aspect of the radius.

Triceps Brachii is divided into three heads: the long head origin is on the infraglenoid tubercle of the scapula, the lateral head on the superior half of the posterior-lateral aspect of the humerus distally to the greater tubercle, and the medial head on the inferior two-thirds of the posterior humerus inferior to the radial groove. Once again because the scapula was not included in the elbow model, the origin of all three heads of Triceps was taken as that of the lateral head. Like Biceps, the multiple heads of the Triceps muscle fuse into a single tendon, which then inserts onto the olecranon process of the ulna. The Triceps Brachii muscle is pictured in Figure 3.11.

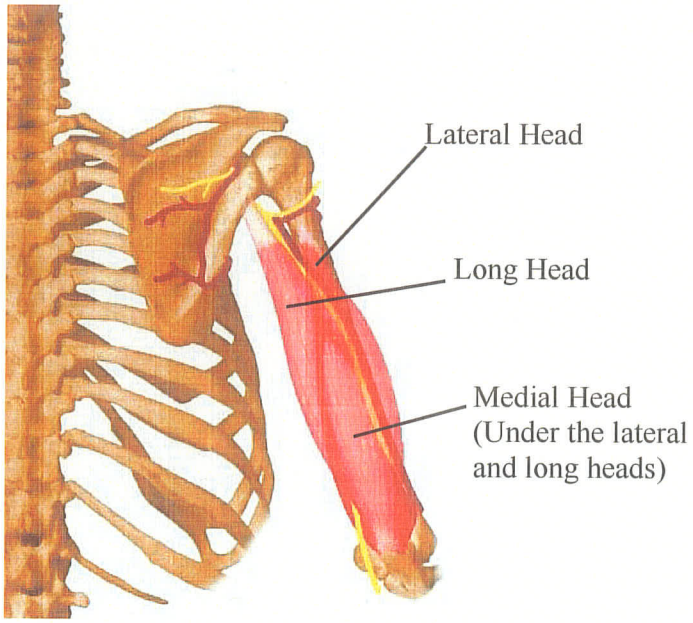

Figure 3.11 The Triceps Brachii Muscle (adapted from Teitz and Graney)

In Murray (1997), the muscle attachments that covered a surface area on the bone were digitized; the centroid of the area was estimated and used as the point of attachment for the muscle. Other attachment sites were estimated by a curve or line, digitized, and the midpoint used for the origin or insertion. These three-dimensional origin and insertion data points, once adjusted to the origin at the centre of the trochlear sulcus, are used to calculate the muscle lines of action and in the calculation of the scaling relationships.

3.5.3 Muscle Line of Action

The muscle line of action represents the effective line of pull of the muscle force from its insertion to origin point. As the elbow model is being developed in three-dimensions, the straight-line approximation will be used which avoids the problems caused by the joint

centre of rotation lying within the bone rather than on its surface. In two-dimensions this approximation results in the moment arm magnitudes becoming zero magnitude when the elbow joint is fully extended, whereas, in three-dimensions it does not. A curvilinear approximation of the line of action could be used in the model, however it was not implemented at this time due to a lack of anatomical data pertaining to muscle belly volume in the literature. The calculation of the muscle line of action is as follows:

$$\vec{la} = \vec{o} - \vec{i} = (o_x - i_x)_{\hat{i}} + (o_y - i_y)_{\hat{j}} + (o_z - i_z)_{\hat{k}} \qquad (3.4)$$

where $\vec{la} = (la_x, la_y, la_z)$ is the individual muscle line of action, $\vec{o} = (o_x, o_y, o_z)$ are the individual muscle origin coordinates, and $\vec{i} = (i_x, i_y, i_z)$ are the individual muscle insertion coordinates.

3.5.4 Muscle Moment Arm

The three-dimensional vector method of determining moment arm for each muscle has been developed by the author and has not been previously reported in the literature. Now that the muscle origin and insertion coordinates have been defined and the muscle line of action procedure determined, it is possible to calculate the muscle moment arms. The first step is to perform the forearm and elbow rotations from the initial positions to the desired angles of pronation-supination and flexion-extension on the muscle insertion vectors. The initial position of the elbow joint is full extension with the elbow angle equal to 0°, while the forearm is in the neutral or semi-prone position with supination being a negative angle and pronation a positive one.

The pronation-supination rotation is performed before the flexion-extension. Since only muscles that attach to the radius will be affected by the rotation of the forearm, both the Brachialis and Triceps will remain unchanged. During pronation-supination, the head of the radius spins about its long axis at the proximal end of the forearm, while at the distal end the radius crosses over the ulna. Accordingly, because their insertions are on the distal portion of the radius, the movements of the insertion vectors for Brachioradialis, Extensor Carpi Radialis Longus, and Pronator Teres are simply rotations about the long axis of the forearm. This is performed via the following matrix operation:

$$\vec{i}_{p/s} = \begin{bmatrix} 1 & 0 & 0 & 0 \\ 0 & \cos(\beta) & -\sin(\beta) & 0 \\ 0 & \sin(\beta) & \cos(\beta) & 0 \\ 0 & 0 & 0 & 1 \end{bmatrix} \cdot \vec{i} \qquad (3.5)$$

where β is the forearm angle, $\vec{i}_{p/s}$ is the new rotated muscle insertion vector and $\vec{i}$ is the original muscle insertion vector.

Conversely, the Biceps muscle inserts very close to the head of the radius and requires a modified rotation calculation. Because there is a sort of self-rotation of the proximal radius during the pronation-supination movement, the rotation of the Biceps insertion vector must take place about an axis passing through the centre of the radial head. The insertion vector is redefined based on an origin at the centre of the radial head, using the following matrix operation:

$$\begin{bmatrix} i_{x1} \\ i_{y1} \\ i_{z1} \\ 1 \end{bmatrix} = \begin{bmatrix} 1 & 0 & 0 & c_x \\ 0 & 1 & 0 & c_y \\ 0 & 0 & 1 & c_z \\ 0 & 0 & 0 & 1 \end{bmatrix}^{-1} \cdot \begin{bmatrix} i_x \\ i_y \\ i_z \\ 1 \end{bmatrix} \tag{3.6a}$$

where the $\vec{c} = (c_x, c_y, c_z)$ is a vector from the origin at the centre of the trochlear sulcus to the centre of the radial head, $\vec{i}_1 = (i_{x1}, i_{y1}, i_{z1})$ is the new translated muscle insertion vector and $\vec{i} = (i_x, i_y, i_z)$ is the original muscle insertion vector. The rotation is performed on this new insertion vector using the same rotation matrix operation as for the other muscles (equation 3.5), and then the origin translated back to the centre of the trochlear sulcus, using:

$$\begin{bmatrix} i_{x3} \\ i_{y3} \\ i_{z3} \\ 1 \end{bmatrix}_{p/s} = \begin{bmatrix} 1 & 0 & 0 & -c_x \\ 0 & 1 & 0 & -c_y \\ 0 & 0 & 1 & -c_z \\ 0 & 0 & 0 & 1 \end{bmatrix}^{-1} \cdot \begin{bmatrix} i_{x2} \\ i_{y2} \\ i_{z2} \\ 1 \end{bmatrix} \tag{3.6b}$$

where $\vec{i}_{p/s} = (i_{x3}, i_{y3}, i_{z3})$ is the new muscle insertion vector and $\vec{i}_2 = (i_{x2}, i_{y2}, i_{z2})$ is the rotated translated muscle insertion vector.

The flexion-extension rotation is now performed using the resultant muscle insertion vectors from the pronation-supination. All six muscles being considered in the elbow model are affected by the flexion-extension rotation of the elbow. This is calculated with the following matrix operation:

$$\vec{i}_{f/e} = \begin{bmatrix} \cos(\gamma) & -\sin(\gamma) & 0 & 0 \\ \sin(\gamma) & \cos(\gamma) & 0 & 0 \\ 0 & 0 & 1 & 0 \\ 0 & 0 & 0 & 1 \end{bmatrix} \cdot \vec{i}_{p/s} \tag{3.7}$$

where γ is the interior elbow angle, $\vec{i}_{f/e}$ is the new rotated muscle insertion vector and $\vec{i}_{p/s}$ is the pronation-supination rotated muscle insertion vector. Special considerations were made for the Triceps Brachii muscle because it wraps around the tip of the olecranon process during the higher angles of elbow flexion. From ninety degrees to full flexion the Triceps insertion tendon comes into contact with the posterior-distal aspect of the humerus and an effective insertion point is created. Thus the Triceps muscle insertion point becomes constant over this range.

The line of action of the muscles can now be calculated from the rotated muscle insertion vectors by equation 3.4. Since the Triceps muscle insertion vector is constant from ninety degrees to maximum flexion, so is the Triceps muscle line of action. Once the line of action has been determined, its vector magnitude and unit direction vector can be computed as follows:

$$|l\vec{a}| = \sqrt{la_x^{\,2} + la_y^{\,2} + la_z^{\,2}} \tag{3.8a}$$

and

$$l\hat{a} = \frac{l\vec{a}}{|l\vec{a}|} \tag{3.8b}$$

where $|l\vec{a}|$ is the vector magnitude and $l\hat{a}$ is the unit direction vector of the individual muscle line of action. The magnitude of the muscle line of action vector is equivalent to

the basic muscle length used in the muscle mechanical energy calculations, while the unit direction vector of the muscle line of action is utilized as the unit direction vector of the individual muscle force.

Knowing the muscle line of action, along with the origin and insertion vectors, a mathematical relationship to compute the three-dimensional muscle moment arms can be established. The schematic for the moment arm calculations is presented in Figure 3.12.

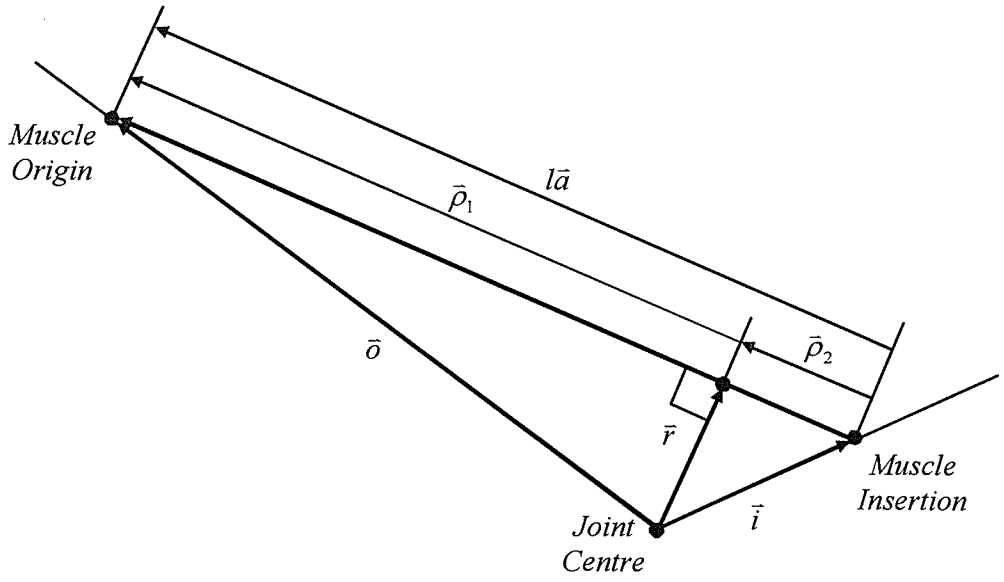

Figure 3.12 Moment Arm Schematic

where $\bar{o}$ is the origin vector, $\bar{i}$ is the insertion vector, $\bar{r}$ is the moment arm, $\bar{\rho}_1$ is the reflection of the origin vector, $\bar{\rho}_2$ is the reflection of the insertion vector, and $l\bar{a}$ is the line of action vector.

The muscle origin and insertion vectors are reflected onto the muscle line of action to ensure that the resultant moment arm is indeed perpendicular to the muscle line of action. The muscle moment arm is then calculated using vector operations. If the magnitude of the muscle origin vector is larger than the magnitude of the muscle insertion vector, the reflection of the origin vector is used to determine the moment arm as follows:

$$\vec{\rho}_1 = \left|\vec{o} \bullet l\hat{a}\right| \cdot l\hat{a} \tag{3.9a}$$

$$\vec{r} = \vec{o} - \vec{\rho}_1 \tag{3.9b}$$

where $\vec{r}$ is the moment arm, $\vec{\rho}_1$ is the reflection of the origin vector, $\vec{o}$ is the origin vector, and $l\hat{a}$ is the line of action unit direction vector. Similarly, if the insertion vector is the larger of the two, the equations become:

$$\vec{\rho}_2 = \left|\vec{i} \bullet l\hat{a}\right| \cdot l\hat{a} \tag{3.10a}$$

$$\vec{r} = \vec{i} + \vec{\rho}_2 \tag{3.10b}$$

where $\vec{r}$ is the moment arm, $\vec{\rho}_2$ is the reflection of the insertion vector, $\vec{i}$ is the insertion vector, and $l\hat{a}$ is the line of action unit direction vector.

3.6 Individual Muscle Force Determination

The rotation of a body segment about a joint is the result of moments generated by the muscles that cross the joint. The muscles produce reactions on the bones during

contractions and are converted into moments via the muscle moment arms. Unfortunately, the calculation of the individual muscle forces is an indeterminate problem due to the redundant nature of the human anatomical structures. This redundancy arises because multiple muscles are positioned to produce moments about the same joints. In order to resolve the indeterminate problem and find a solution an additional constraint equation must be developed.

3.6.1 Muscle Cross-Sectional Area

The capacity of a muscle to generate force is proportional to its physiological cross-sectional area. The individual physiological cross-sectional area of a muscle varies widely between individuals, thus a ratio of the individual muscle physiological cross-sectional area ($PCSA_i$) to the total physiological cross-sectional area of the muscles in the functional group ($PCSA_T$) will be used. This ratio, known as the relative physiological cross-sectional area of a muscle is presented as follows:

$$\alpha_i = \frac{PCSA_i}{PCSA_T} \tag{3.11}$$

The physiological cross-sectional area data being used in the elbow muscle model is from the study published by An et al. (1981). Collected from six upper limb specimens, the physiological cross-sectional area was calculated by dividing the muscle volume by the mean muscle fibre length. The individual muscle data along with the totals for the functional groups can be found in Table 3.1. The analysis of the elbow model is based on the moment about the joint and thus only the muscles found to have significant potential

for moment production are included in the functional group totals. It is important to note that the values for both Biceps and Triceps muscles are the totals for all the muscle heads.

Table 3.1 Muscle Physiological Cross-Sectional Area

MUSCLE	PHYSIOLOGICAL CROSS SECTIONAL AREA (cm^2)
Biceps Brachii	4.6
Brachialis	7.0
Brachioradialis	1.5
Extensor Carpi Radialis Longus	2.4
Pronator Teres	3.4
Total Flexors	18.9
Triceps Brachii	18.8
Total Extensors	18.8

3.6.2 Agonist and Antagonist Muscle Activity

Antagonist muscle activity is not well reported in the literature and as such an assumption had to made to allow its inclusion in the muscle force calculation. In the simulations that are presented in section 4.4 of the results, two values were implemented to show that different activation strategies could be used due to the nature of the vector formulation. As an initial approximation the activation was chosen to remain constant throughout the

activity, however, activation strategies in which the level varied as a function of the elbow joint position could easily be implemented instead.

To calculate the individual muscle forces for a set movement, it is necessary to make a distinction between the muscles which are acting as agonists and those that are acting as antagonists. There are two general methods of stopping a motion: relax the agonist muscles and allow the movement to stop on its own or if the movement must terminate within a given space or time, activate the antagonist muscles (Basmajian and DeLuca, 1985; Waters and Strick, 1981). By decelerating rapid movements initiated by the agonist muscles, antagonist muscle activity serves to protect the joint structures, such as bone surfaces, cartilage, and ligaments, from injuries that could occur should they be required to rapidly stop motion.

To produce motion without antagonist muscle activity, the agonist muscles would have to generate a certain amount of force. It is assumed for the elbow model that the antagonist muscles are activated to create 20% of the force of the agonist muscles. Hence, the agonist muscle moment level must increase 20% from its previous non-antagonist level to 120% in order to overcome the antagonistic moment effects. These values will be incorporated into the individual muscle force calculations as agonistic and antagonistic muscle activation factors.

3.6.3 Joint Moments and Muscle Forces

The particular formulations of the moment equations and the methodology to determine the individual muscle forces are once again an original development of the author. The net moment is described as the moment required to produce the desired joint motion while overcoming the moment produced by the antagonist muscles. Thus, if a level of antagonist muscle activity exists, the agonist muscle activity must increase to compensate and the net moment will remain constant. This relationship is represented in the following equation:

$$\bar{M}_{net} = \bar{M}_{agonist} - \bar{M}_{antagonist} \tag{3.12}$$

where $\bar{M}_{net}$ is the net moment about the joint rotational axis as predicted by the dynamic equations also known as $\bar{M}_{dynamic}$, $\bar{M}_{agonist}$ is the moment produced by the agonistic muscles, and $\bar{M}_{antagonist}$ is the moment produced by the antagonistic muscles.

The moment components produced by the dynamic model are equivalent to the net moment required to generate the prescribed joint motion from agonist muscle activity without any antagonist muscle action, about the joint rotational axis. The relationship between the total moment produced by the dynamic model, $\bar{M}_{dynamic}$, and the forces in the individual muscles over the full joint range of motion can be formulated as:

$$\bar{M}_{dynamic} = \left(\sum_{i=1}^{n} \bar{M}_i \right)_{agonist} = \left(\sum_{i=1}^{n} \bar{r}_i \times \bar{F}_i \right)_{agonist} \tag{3.13}$$

for $\bar{M}_{antagonist} = 0$, where n is the total number muscles in the muscle group, $\bar{M}_i$ is the individual muscle moment contribution, $\bar{r}_i$ is the individual muscle moment arm, and $\bar{F}_i$ is the individual muscle force.

It is important to note that the dynamic model moments are calculated in a coordinate system where the axes lie parallel (y and z axes) and perpendicular (x-axis) to the ground, rather than about the anatomical joint rotation axes. Therefore, before proceeding with the muscle force calculations, the component of the dynamic moment about the axis of elbow flexion-extension must be determined. This is accomplished by performing a vector dot product between the three-dimensional dynamic moment and the unit direction vector of the axis of rotation as follows:

$$M_{f/e} = \bar{M}_{dynamic} \bullet \hat{e}_{f/e} \tag{3.14}$$

where $M_{f/e}$ is the magnitude of the flexion-extension moment, and $\hat{e}_{f/e}$ is the unit direction vector of the flexion-extension axis of rotation. The three-dimensional dynamic moment about the individual joint axis of rotation is then the product of the magnitude of the moment about the rotational axis and the unit direction vector describing the axis. This is represented by:

$$\bar{M}_{f/e} = M_{f/e} \cdot \hat{e}_{f/e} \tag{3.15}$$

where $\bar{M}_{f/e}$ is the three-dimensional flexion-extension moment.

The force produced in the individual muscles is proportional to the relative physiological cross-sectional area of that muscle and the total force of the muscles crossing the joint. This can be written as:

$$\vec{F}_i \propto \alpha_i \cdot F_T \hat{f}_i \tag{3.16}$$

where α_i is the relative cross-sectional area of the muscle, F_T is the total force of all agonist muscles, and $\hat{f}_i$ is the unit direction vector of the individual muscle force or the line of action of the individual muscle force.

Combining equations 3.13 and 3.16, a general relation between the moment from the dynamic model and the total muscle force can be formulated as:

$$\vec{M}_{dynamic} = F_T \cdot \left(\sum_{i=1}^{n} \left(\vec{r}_i \times \alpha_i \hat{f}_i \right) \right)_{agonist} \tag{3.17}$$

for zero antagonist activity. The dynamic model defines elbow flexion as a positive moment and extension as a negative moment, both about the medial-lateral joint z-axis. Since the calculation of the total muscle force is based on the agonist muscle group, the muscles included in the $\left(\sum_{i=1}^{n} \left(\vec{r}_i \times \alpha_i \hat{f}_i \right) \right)$ term will change dependent on the sign of the total moment. In addition, the moment about the appropriate joint rotational axis is used and for flexion Equation 3.17 becomes:

$$\vec{M}_{f/e} = F_T \cdot \left[\begin{array}{l} \left(\vec{r}_{bic} \times \alpha_{bic} \hat{f}_{bic} \right) + \left(\vec{r}_{brach} \times \alpha_{brach} \hat{f}_{brach} \right) + \left(\vec{r}_{brad} \times \alpha_{brad} \hat{f}_{brad} \right) \\ + \left(\vec{r}_{ecrl} \times \alpha_{ecrl} \hat{f}_{ecrl} \right) + \left(\vec{r}_{pt} \times \alpha_{pt} \hat{f}_{pt} \right) \end{array} \right] \tag{3.18a}$$

For extension:

$$\bar{M}_{f/e} = F_T \cdot \left(\bar{r}_{tri} \times \alpha_{tri} \hat{f}_{tri}\right) \tag{3.18b}$$

where the subscripts used to indicate the individual muscle variables are *bic* for the Biceps Brachii, *brach* for the Brachialis, *brad* for the Brachioradialis, *ecrl* for the Extensor Carpi Radialis Longus, *pt* for the Pronator Teres, and *tri* for the Triceps Brachii.

During elbow flexion with the forearm in a pronated position, the Biceps Brachii muscle is considered to be inactive and as such it will not be included in the formulation for flexion and Equation 3.17 then becomes:

$$\bar{M}_{f/e} = F_T \cdot \left[\begin{array}{l} \left(\bar{r}_{brach} \times \alpha_{brach} \hat{f}_{brach}\right) + \left(\bar{r}_{brad} \times \alpha_{brad} \hat{f}_{brad}\right) \\ + \left(\bar{r}_{ecrl} \times \alpha_{ecrl} \hat{f}_{ecrl}\right) + \left(\bar{r}_{pt} \times \alpha_{pt} \hat{f}_{pt}\right) \end{array}\right] \tag{3.18c}$$

where the subscripts used to indicate the individual muscle variables are as described above. It should be remembered for the above formula that the relative physiological cross-sectional area, α, of each muscle is calculated as a ratio to the total cross-sectional area of the active functional group. Therefore, since the Biceps Brachii muscle is no longer active in this joint configuration, the total cross-section of the functional group is altered and the relative physiological cross-sectional areas must be recalculated for the four remaining muscles.

Once the total muscle force has been calculated from the appropriate version of equation 3.17, the individual muscle forces can be resolved. For a more accurate prediction of the

individual muscle forces, the activation levels of the muscles are incorporated into the calculations. To simplify the muscle activation, the hypothesis that all muscle fibres, and hence all muscles, in a functional group are activated to the same level will be used. This assumption is reasonable, as evolution has optimized the size of a muscle based on its function. Thus a muscle that is routinely required to produce large amounts of force would tend to be larger in size than a muscle contributing less force. Dependent on the movement of the joint, the muscle groups can have either an agonistic or antagonistic function. The individual muscle forces are formulated as:

$$F_{i,agonist} = F_T \alpha_i b_{agonist} \tag{3.19a}$$

and

$$F_{i,antagonist} = F_T \alpha_i b_{antagonist} \tag{3.19b}$$

where $b_{agonist}$ is the muscle activation level for the agonist muscle group, and $b_{antagonist}$ is the muscle activation level for the antagonist muscle group. In situations where the arm undergoes both flexion-extension and pronation-supination movements, the individual muscle forces determined from the two movements are summed together to arrive at the total force for the individual muscles.

3.7 Muscle Energy Determination

Energy represents the capacity of a system to do work on another system. In the case of this muscle model, energy is the capacity of a system of muscles to do work on the limb segments. During a movement, the muscular work done by the muscles consists of both

biological energy and mechanical energy. Thus, the total energy used by a muscle is equal to the sum of the biological energy it consumes and the mechanical energy exerted.

3.7.1 Biological Energy

Muscles use biological energy to maintain muscle contractions, and thus muscle forces, over a period of time. The muscles consume biological energy even if no physical movement is produced or no change in muscle length is evident, as in an isometric contraction. As a muscle burns biological energy, carbohydrates and sugars are broken down by chemical reactions within the muscle fibres. One of the by-products of these chemical reactions is lactic acid, which is thought to be one of the main causes of muscle fatigue. The biological energy, E_{bio}, is proportional to the integral of the force in the muscle, F_{muscle}, and the time duration of the force, represented in general form by:

$$E_{bio} = c \cdot \int_{t_1}^{t_2} F_{muscle} \cdot dt \tag{3.20}$$

where t_1 is the initial time point, t_2 is the final time point, and c is a biological constant needed to account for the oxygen consumption in the chemical reactions within the muscle to maintain a force. The ideal mechanical Carnot cycle has an efficiency of no better than 0.4 and the human body can be assumed to have a slightly higher efficiency, thus a value of 0.5 is assigned to the constant. To calculate the biological energy used by a muscle over a full task cycle, the individual increments are summed as follows:

$$E_{bio} = c \cdot \sum_{j=1}^{j=m} F_{i,avg} \cdot \Delta t \tag{3.21}$$

where $F_{i,avg}$ is the average individual muscle force over the time interval, Δt is the change in time, j is the variable representing the task cycle data point with m as the final data point. The average individual muscle force is given by:

$$F_{i,avg} = \left(\frac{F_{j-1} + F_j}{2} \right)_i \tag{3.22}$$

and the change in time is calculated as follows:

$$\Delta t = t_j - t_{j-1} \tag{3.23}$$

3.7.2 Muscle Length

During movements of the limb, the joints undergo various rotations and cause the length of the individual muscles to change. This change in the length of a muscle is directly related to the amount of mechanical energy it can produce. To determine the change in muscle length over a given time interval, the total length of the muscle at the two interval end points must first be established. The total length of the muscles being studied was calculated based on the line of action of each muscle. Because a straight line of action was assumed, the length of the muscle is simply the magnitude of its line of action vector (see Equation 3.8a).

However, due to the wrapping of the Triceps Brachii muscle around the tip of the olecranon process of the ulna at flexion angles greater than ninety degrees, special consideration was required. The method to determine the muscle length of the Triceps Brachii muscle was developed by the author. Once the insertion tendon of Triceps begins wrapping, the full muscle length is calculated as the sum of the muscle length at the ninety-degree position and the arc length of the insertion point displacement about the joint center, as seen in Figure 3.13. The distance of the insertion point from the joint center of rotation in the y-direction represents the arc radius of the Triceps insertion path. The arc length of the muscle is then calculated as follows:

$$arc\ length = arc\ radius \cdot \Delta\alpha \tag{3.24}$$

where $\Delta\alpha$ is the change in elbow angle, in radians, from the ninety-degree position.

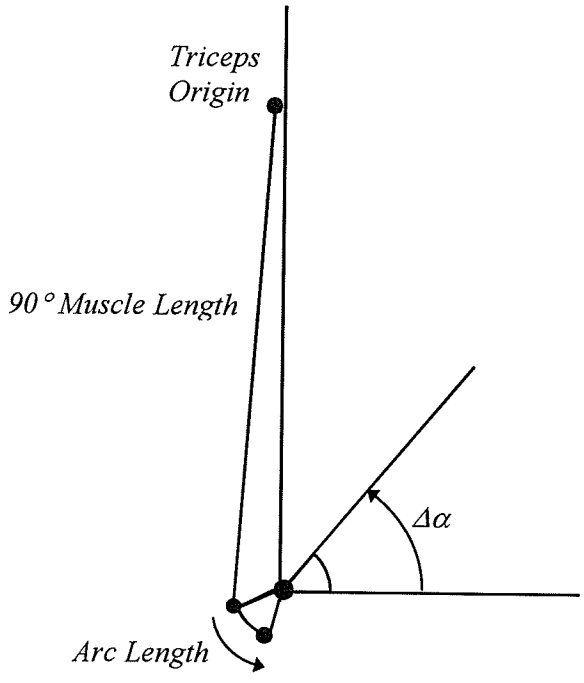

Figure 3.13 Triceps Brachii Muscle Length Schematic

3.7.3 Mechanical Energy

Mechanical energy is generally defined as the product of a force acting over a distance. It represents the actual physical work being done by the muscle to rotate the joint through a given angle. The mechanical energy, E_{mech}, is proportional to the integral of the force in the muscle, F_{muscle}, and the distance travelled, accordingly the general equation takes the following form:

$$E_{mech} = \int_{x_1}^{x_2} F_{muscle} \cdot dx \tag{3.25}$$

where x_1 is the initial position, and x_2 is the final position. In the case of the musculoskeletal system, the distance travelled by the applied force is the change in length of the muscle between consecutive joint positions. The total mechanical energy expended by a muscle over a full task cycle is thus determined by summing the individual increments as follows:

$$E_{mech} = \sum_{j=1}^{j=m} F_{i,avg} \cdot \Delta l \tag{3.26}$$

where $F_{i,avg}$ is the average individual muscle force over the time interval, Δl is the incremental change in the individual muscle length, j is the variable representing the task cycle data point with m as the final data point. The change in muscle length is calculated as follows:

$$\Delta l = l_j - l_{j-1} \tag{3.27}$$

3.8 Model Assumptions and Limitations

Any model of the musculoskeletal system must contain some simplifications of the actual system. This section will outline the various assumptions employed during the development of the elbow model along with any limitations they impose.

Muscle fibres are composed of multiple sarcomeres connected in series; these sarcomeres are not all activated at the same instant in time during a muscle contraction. This aspect of the microscopic muscle structure is not currently accounted for in the assumption that the activation within a given muscle is constant for all the fibres. The exclusion of this property of muscle structure has not been previously shown to have any significant effect on the overall force production of the muscle, and was thus taken as not relevant for this work.

Skeletal muscle undergoes dimensional changes during contractions by becoming shorter and thicker. This changes the orientation of the muscle fibres and the moment arm of the muscle. The muscle mass is also redistributed during contractions, which results in a change in the mass moment of inertia of the limb segment as a whole. However, the dimensional changes have yet to be quantified in such a way that they can be included in the current elbow model.

A key assumption in the development of this anatomical model is that electromyographic muscle signals can be used to predict muscle activation patterns. The inclusion and

exclusion of muscles in this elbow model were based on the results of electromyography studies such as Basmajian and DeLuca (1985). It was also assumed that the activation of all muscles in a functional group is uniform. In addition, the concept that the three heads of the Triceps Brachii and two heads of Biceps Brachii are not activated independently of one another was used herein.

Further simplifying assumptions were made for the calculations used in the anatomical model. The human elbow joint was considered to be a frictionless joint, thus no muscle moment production was used overcoming the friction between the joint surfaces. Force produced by an individual muscle crossing the joint is proportional to its physiological cross-sectional area. Furthermore, only the muscles with significant potential to produce moment about the joint are included in the muscle functional groups for the determination of the total physiological cross-sectional areas. Finally, a straight-line vector approximates the line of action of the muscle force from the muscle insertion to its origin.

The work of this thesis was done to determine the muscle forces associated with joint moments. Thus, muscles that are not generating moment are beyond the scope of this work. As not all muscles crossing the joint were included, any estimation of the joint contact forces using the elbow model results will be underestimated even though the net moment is not affected. This occurs because forearm muscles that are significantly active during gripping of a heavy load in the hand will cause large joint reaction forces at the elbow are not included.

Due to the assumptions used in the elbow model, the predicted values of the individual muscle forces should not be interpreted as anything more than a first approximation. As better anatomical data becomes available the elbow model can be modified to include more muscles and additional physiological parameters and relations, improving the accuracy of the force predictions.

CHAPTER 4

RESULTS AND DISCUSSION

4.1 Introduction

This thesis is focused on assessing the three-dimensional vector approach, as outlined in Chapter 3, developed for the calculation of the individual muscle forces acting across a joint. The results of the anatomical elbow model are compared to past qualitative studies, where available, to determine the extent of the validity of the techniques and assumptions employed in this work. In this chapter, the results of the dynamic simulation computations performed to generate moments for the anatomical elbow model are presented. Those moments are used as inputs to the elbow model and are taken as the most accurate data available.

The validation of the elbow model involves three parts. The first part, presented in Section 4.2, is the verification of the scaling methods used to determine the anatomical parameters for subjects of varying sizes. The second part, in Section 4.3, consists of the confirmation of the muscle moment arms. Section 4.4 presents the final aspect of the verification of the individual muscle forces by using energy balances. Following the validation of the elbow model, the results from the simulation of two industrial tasks are given in Section 4.5. These are included only to demonstrate the fact that the simulation is not limited in any way. Both the static and dynamic moments are calculated.

4.2 Anatomical Scaling Results

The validation of the moment arms, forces, and energies predicted by the anatomical elbow model are dependent on comparisons to data presented in the literature. Unfortunately, the studies in the literature have used many different and/or unspecified subject sizes. Therefore, the confirmation of the three-dimensional vector approach used in this thesis is reliant on the ability to relate the various sizes of specimens to one another. That is to say, a method of scaling the bone anatomy is needed. Once the method for the anatomical scaling has been established, we can assess our method in detail relative to the results of the elbow model presented in the literature.

As established in Section 3.4 of the methodology, the body segment parameters are calculated by using a set of correlation equations and other mathematical relations based on the subject's height and weight. It should be noted that the author, using data from other sources, developed these correlations and relations specifically for this thesis. The subject's weight is then used as an indicator of body type based on their body mass index and used to adjust the appropriate body parameters. From the body segment parameters, the dimensions of the upper limb bones (humerus, radius, ulna) and the three-dimensional points of muscle origin and insertion are calculated with a set of mathematical equations based on correlations (see Appendix B). The scaled muscle parameters are then used to determine the lines of action and moment arms of the muscles crossing the elbow joint. The scaling of the muscle points of origin and insertion to subject size also permits a

more realistic calculation of the muscle length, which is essential to the determination of muscle energies.

To examine the anatomical scaling used in the elbow model, a dynamic motion of the elbow joint was simulated and the muscle forces determined for two subjects of quite different size. Two motions were selected for the simulations. Both movements consist of the rotation of the forearm about the elbow joint through the full range of flexion-extension with the forearm in full supination.

The three-dimensional simulation program being used was developed for the Workers Compensation Board of the province of Manitoba by Chan, Thornton-Trump and Weiss-Bundy in the Biomechanics Laboratory at the University of Manitoba. The motions were simulated in the model using indirect dynamics. The model utilizes small increments in the relative positions of the upper arm and forearm, and a predetermined path in space for the hand including a prescribed acceleration profile of the hand along that path. The program is capable of simulations in three-dimensions, but the simulations here were done for special two-dimensional cases where the moments from gravitational forces were easily calculated. Details of this program are presented in a technical report by Thornton-Trump, A.B. (2002) and in several research publications currently in preparation.

In the first simulation the shoulder joint was rotated in such a way that the motion about the elbow joint would occur solely in the coronal anatomical plane, with the upper arm

maintained in a position horizontal to the ground, as seen in Figure 4.1. The second simulation has the shoulder joint positioned such that the upper arm lies along the side of the torso, allowing the rotation about the elbow joint to occur completely in the sagittal anatomical plane, pictured in Figure 4.2.

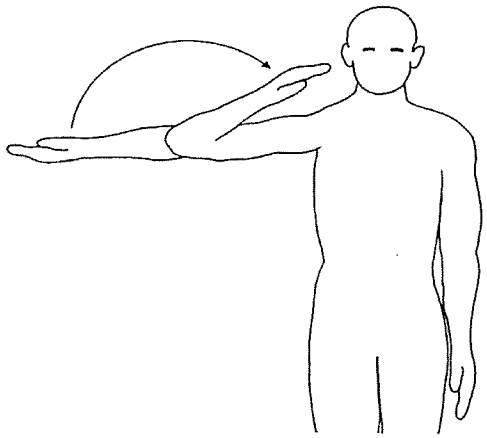

Figure 4.1 Elbow Flexion-Extension in the Coronal Plane

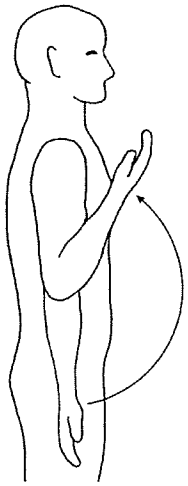

Figure 4.2 Elbow Flexion-Extension in the Sagittal Plane

The two dynamic simulations were run with a task cycle time of 0.5 seconds for a complete flexion-extension rotation about the elbow joint, with the acceleration profile defined as 50% acceleration and 50% deceleration. The two subjects used in the simulations are both female with differing heights and weights. The large subject has a height of 1.676 meters (5ft-6in) and a weight of 63.50 kilograms (140 lbs), while the small subject's height and weight are 1.524 meters (5 ft) and 49.90 kilograms (110 lbs), respectively. If the scaling methods are to be considered valid, it is expected that the relative pattern of the muscle forces, not their magnitudes, will be of the same general form for the two subjects even though their sizes are different.

The simulation results for the individual muscle forces over the task cycle time in the coronal plane are shown in Figure 4.3 (page 76) for the large subject and Figure 4.4 (page 77) for the small subject. Figures 4.5 and 4.6, on pages 78 and 79 respectively, show the individual muscle forces for the elbow joint rotation in the sagittal plane for the same large and small subjects, respectively. From these figures one can easily observe that the patterns of both the individual muscle forces and energies are of the same general form regardless of the subject height and weight. It is important to note that as not all the scaling equations are linear it is not expected that the shape of the muscle force curves should be identical in subjects of different size, rather the same general forms should be seen. The muscle forces are identified in the same manner in the figures for both the large and small subjects, and for both elbow joint motions: the upper plot shows the curves for the Biceps Brachii (solid blue line), Brachialis (dot-dash green line), and Triceps Brachii (dot red line) muscles, while the lower plot contains the curves for the

Brachioradialis (solid blue line), Extensor Carpi Radialis Longus (dot-dash green line), and Pronator Teres (dot red line) muscles. Despite the scaling of the muscle origin and insertion coordinates to the subject size, the individual muscle forces retain the same relative positions and relative magnitudes. The Brachialis muscle is shown to be the main force producing muscle of the flexor functional group during the acceleration phase of the flexion motion and the deceleration phase of the extension movement, for both subjects and during both movements. The Biceps Brachii and Pronator Teres muscles are found to be the next largest force generating muscles of the flexor group during these movements, followed by the Extensor Carpi Radialis Longus and Brachioradialis muscles. The relatively small contribution to the flexor muscle group made by the Brachioradialis in these two simulations can be attributed in part to the supinated position of the forearm, a position that does not yield a favourable moment arm for the Brachioradialis. During the deceleration phase of flexion and the acceleration phase of extension, the Triceps Brachii, being the only muscle examined from the extensor muscle group, produces the force required for joint motion. In addition, the muscle forces do not cross paths with one another during the flexion-extension movement of the elbow joint. The muscle with the lowest muscle force remains the lowest, the muscle with the largest muscle force remains the largest, and so on.

The simulation results for the muscle mechanical energies in the coronal plane motion are shown in Figure 4.7(a) for the large subject and Figure 4.7(b) for the small subject, on page 80. The same colour of line is used in both figures to identify the mechanical energy of each muscle. The mechanical energy of each muscle is based on the force in

the muscle, the change in muscle length and the change in time. Thus, the muscles can change order with respect to their relative magnitudes from the individual forces to the mechanical energies. However, as with the individual muscle forces, the muscle mechanical energies maintain their relative positions when scaled to different subject sizes. The Brachialis and Biceps Brachii muscles have the highest mechanical energies of the flexor group; while the remaining three flexor muscles Brachioradialis, Extensor Carpi Radialis Longus, and Pronator Teres have much lower mechanical energies. The Triceps Brachii has a much larger mechanical energy than the individual flexor muscles, as it is the only muscle of the extensor group being examined in the model and had a very high muscle force when active. In addition, it can be seen in Figure 4.7 that the mechanical energy balance between the flexor muscle group and the extensor muscle group remains consistent for both subjects.

Also of note in Figures 4.3 to 4.7 (pages 76 through 80) is that the 0.5 seconds task cycle time represents a full flexion-extension cycle of the elbow joint. This means that during the first half (0.0 to 0.25 seconds), or flexion stage, the elbow joint is going from a fully extended position (0 degrees) to full flexion at 150 degrees. From 0.25 to 0.5 seconds, the elbow is undergoing extension from the fully flexed position to full extension. Due to the high speed with which this motion is being simulated, the first half of the elbow flexion stage is dominated by activity of the flexor muscle group as the movement is initiated from a rest position and accelerated to the halfway point. During the second portion, however, the flexor activity can be seen to drop off and the extensor muscles (in this case the Triceps Brachii) are now fully active to control the deceleration of the

forearm about the elbow joint to a resting position. The reverse pattern can be observed during the extension of the elbow joint as the extensors dominate the first half of the movement for initiation and acceleration and the flexors dominate for the deceleration to a stop.

The sets of curves for the two subject sizes do not change shape or order with respect to one another, indicating that the equations developed for the scaling of the anatomical parameters are reasonably applicable. However, if the curves did exhibit a noticeable change between subject sizes it would indicate that there were large anatomical errors in the scaling method. The results also suggest that despite the limited data available to formulate the anatomical scaling equations, they are adequate initial approximations of the scaling relationships. Although there was insufficient data to find correlation equations for all the bone parameters and muscle origin and insertion locations, in consideration of the simulation results it now seems to be a reasonable assumption that these anatomical correlations are present. However, the accuracy of the correlations cannot be quantified using the very small anatomical data set contained in Murray (1997). The errors in the correlations are masked by the inter-subject variations present in the anatomical specimen variations.

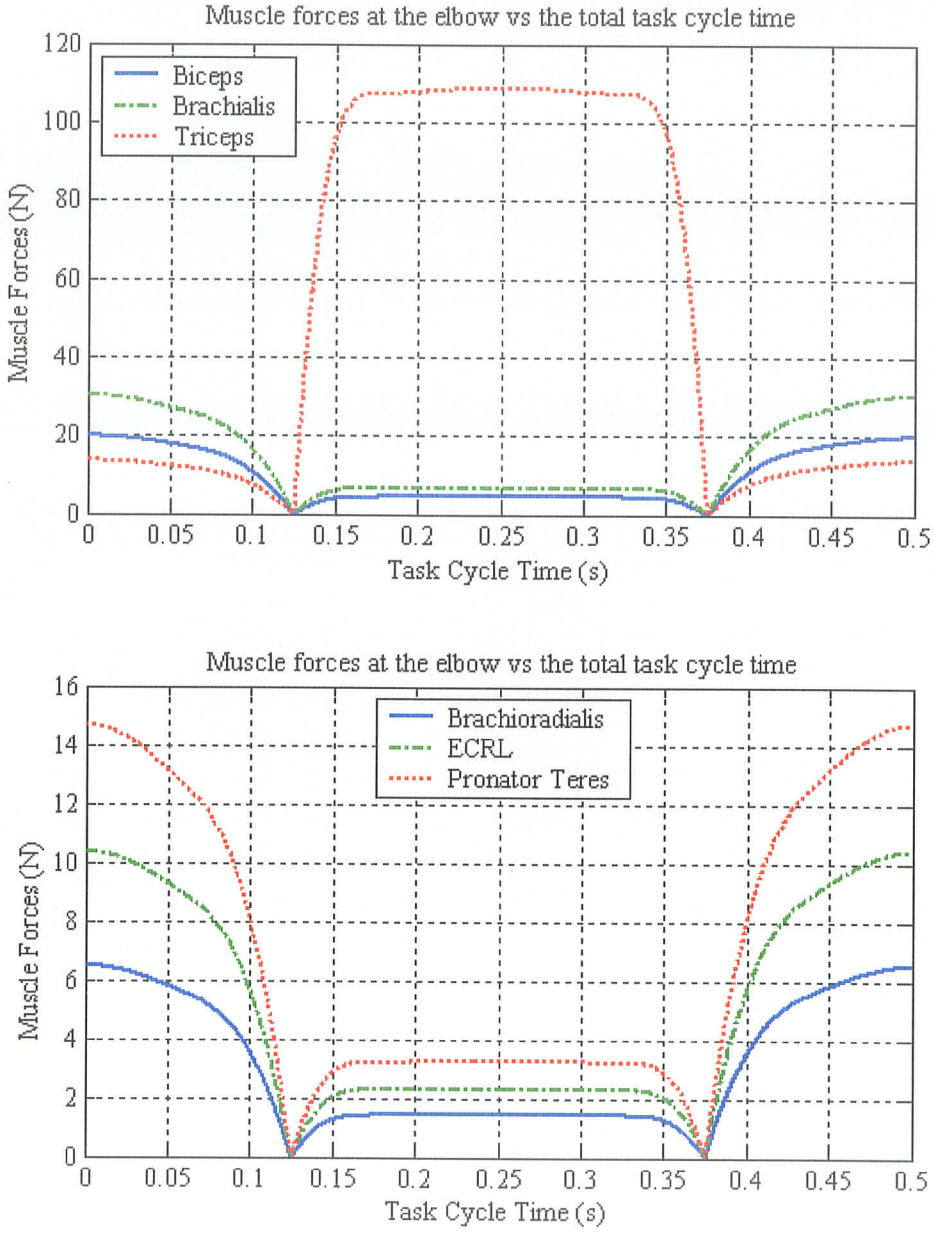

Figure 4.3 Individual Muscle Forces for Large Subject, Coronal Plane
(Female: 1.676 meters, 49.90 kilograms)

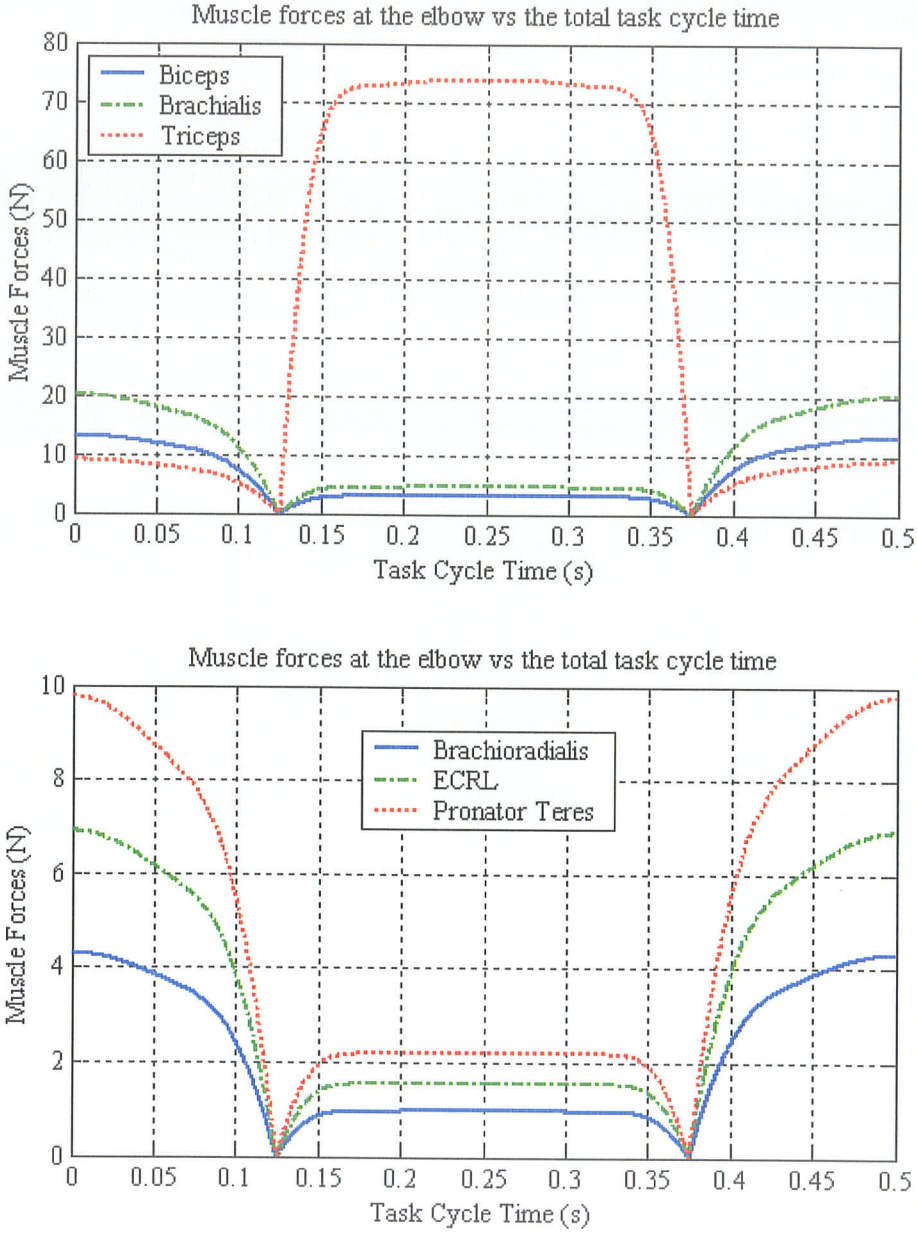

Figure 4.4 Individual Muscle Forces for Small Subject, Coronal Plane
(Female: 1.524 meters, 49.90 kilograms)

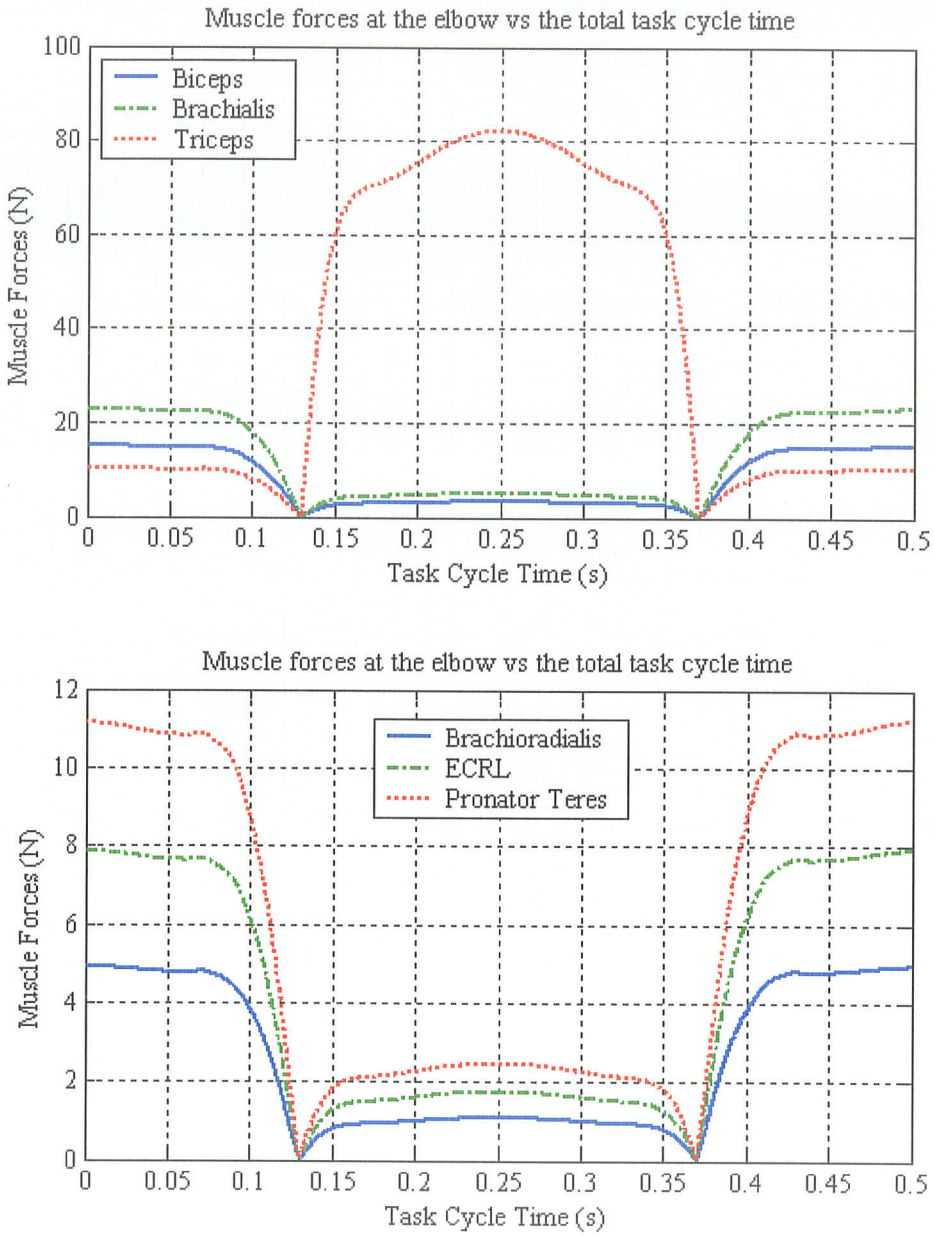

Figure 4.5 Individual Muscle Forces for Large Subject, Sagittal Plane
(Female: 1.676 meters, 63.50 kilograms)

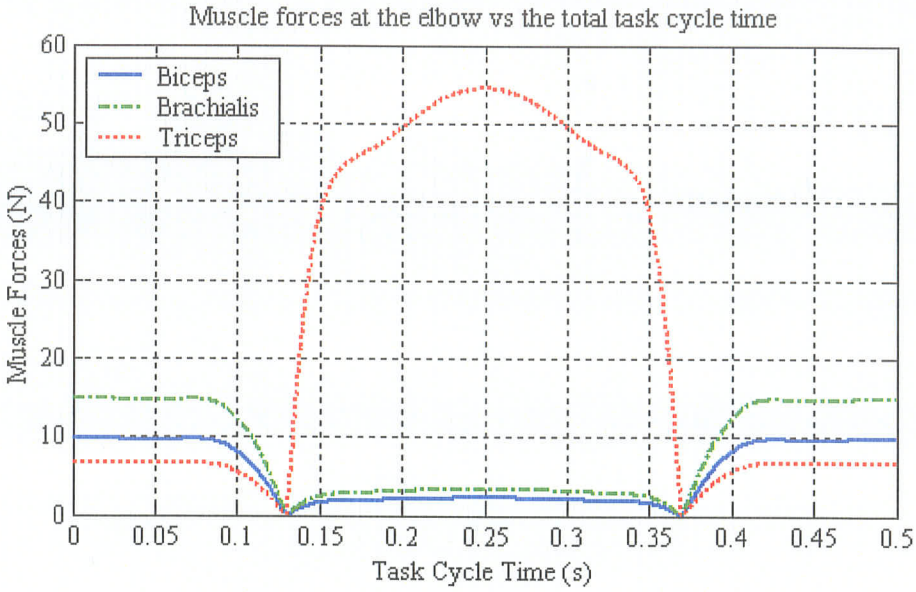

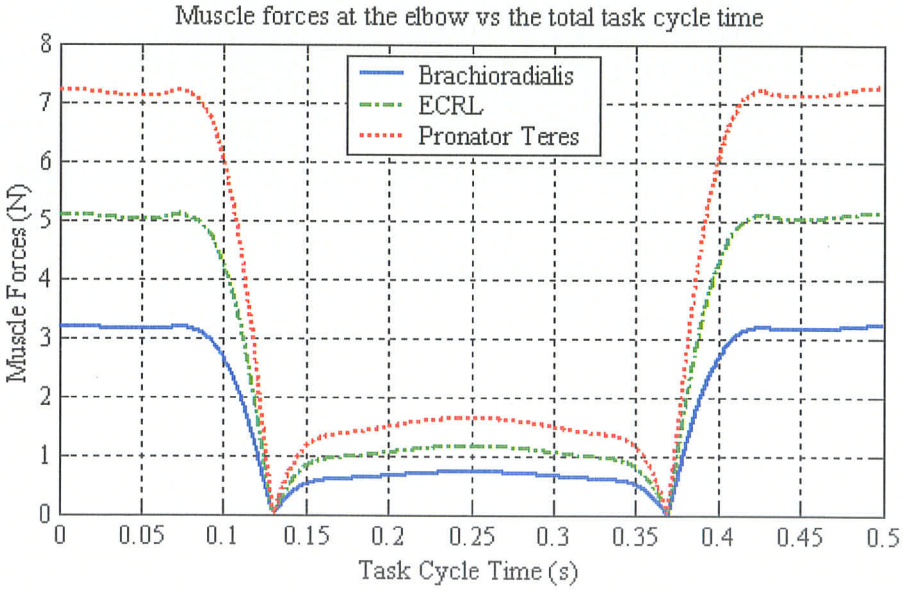

Figure 4.6 Muscle Forces for Small Subject, Sagittal Plane
(Female: 1.524 meters, 49.90 kilograms)

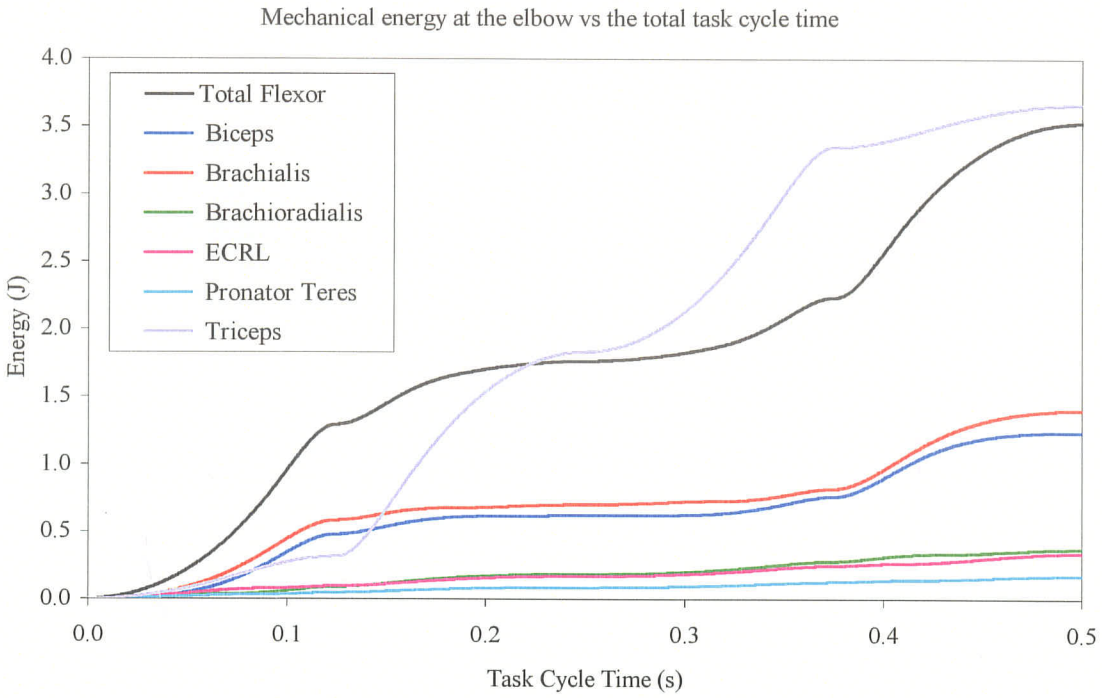

(a) Large Subject (Female: 1.676 meters, 63.50 kilograms)

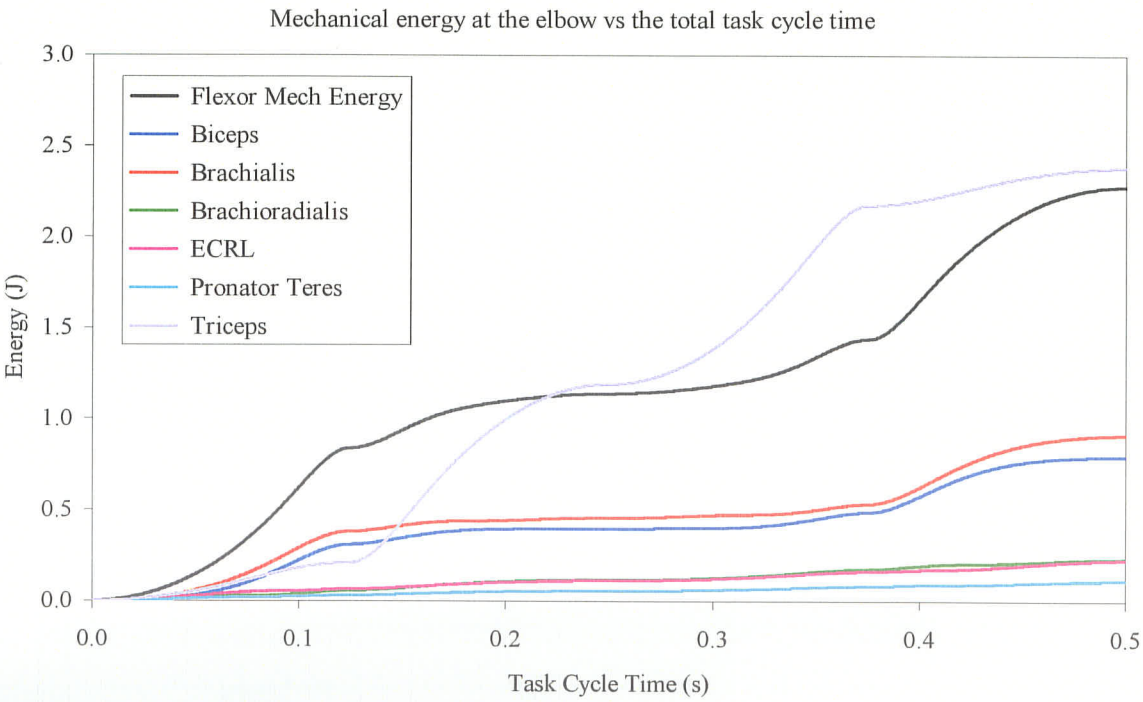

(b) Small Subject (Female: 1.524 meters, 49.90 kilograms)

Figure 4.7 Muscle Mechanical Energies, Coronal Plane

4.3 Muscle Moment Arm Analysis

The muscle moment arms are a crucial component in the prediction of the individual muscle forces. Thus, the calculation of the three-dimensional muscle moment arms must be confirmed to enable the later verification of the individual muscle forces.

The moment arms of the individual muscles crossing the elbow joint are calculated for each successive increments of elbow angle using the three-dimensional vector method developed in Chapter 3. First the muscle insertion coordinates are rotated to the desired degrees of flexion-extension and pronation-supination. As an example, for the Brachioradialis muscle at an elbow angle of forty-five degrees and the forearm in the neutral position, the origin and insertion vectors are as follows:

$$\vec{o} = 57.075_{\hat{i}} + 22.168_{\hat{j}} + 17.587_{\hat{k}}$$

$$\vec{i} = -235.13_{\hat{i}} + 41.896_{\hat{j}} + 48.00_{\hat{k}}$$

As the forearm is in the neutral position, no pronation-supination rotation of the Brachioradialis muscle insertion vector is necessary. Using equation (3.7) the insertion vector is rotated to the flexion angle as follows:

$$\vec{i}_{f/e} = \begin{bmatrix} \cos(45°) & -\sin(45°) & 0 \\ \sin(45°) & \cos(45°) & 0 \\ 0 & 0 & 1 \end{bmatrix} \cdot \left[\vec{i}\right] = -195.90_{\hat{i}} - 136.60_{\hat{j}} + 48.00_{\hat{k}}$$

The muscle lines of action are then established using the three-dimensional origin and insertion coordinates and the straight line of muscle force assumption. The mass of a

muscle changes shape during contraction and affects the line of action of the muscle force and thus the muscle moment arm. However, this characteristic of the muscle line of action was not included in this model at this point. For the example situation with Brachioradialis, the line of action is calculated from equation (3.4) as:

$$\vec{la} = \vec{o} - \vec{i}_{f/e} = 252.975_{\hat{i}} + 158.768_{\hat{j}} - 30.413_{\hat{k}}$$

The magnitude and unit direction vector of the line of action are then calculated by equations (3.8a) and (3.8b):

$$\left|\vec{la}\right| = \sqrt{\left(252.975_{\hat{i}}\right)^2 + \left(158.768_{\hat{j}}\right)^2 + \left(-30.413_{\hat{k}}\right)^2} = 300.214 \ mm$$

$$\hat{la} = \frac{\vec{la}}{\left|\vec{la}\right|} = 0.8426_{\hat{i}} + 0.5288_{\hat{j}} - 0.1013_{\hat{k}}$$

Finally, the muscle moment arms are determined using the reflection of the origin or insertion vector onto the muscle line of action. For Brachioradialis, using equations (3.10a) and (3.10b) the moment arm is calculated as:

$$\vec{\rho}_2 = \left|\vec{i} \bullet \hat{la}\right| \cdot \hat{la} = 204.046_{\hat{i}} + 128.055_{\hat{j}} - 24.531_{\hat{k}}$$

$$\vec{r} = \vec{i} + \vec{\rho}_1 = \left(8.146_{\hat{i}} - 8.545_{\hat{j}} + 23.469_{\hat{k}}\right)$$

The magnitude of this three-dimensional moment arm vector is calculated as follows:

$$\left|\vec{r}\right| = \sqrt{\left(8.146_{\hat{i}}\right)^2 + \left(-8.545_{\hat{j}}\right)^2 + \left(23.469_{\hat{k}}\right)^2} = 26.271 \ mm$$

Extending the calculations over the full range of elbow joint flexion-extension for the six muscles crossing the elbow joint, the three-dimensional muscle moment arms are produced. Figure 4.8 shows the muscle moment arms for flexion-extension with the forearm in the neutral position for a male subject with a height of 1.78 meters (5ft-10in) and a weight of 72.57 kilograms (160 lbs), while Figures 4.9 and 4.10 display curves for the fully pronated and supinated forearm, respectively. The same mathematical procedure can be employed to determine the three-dimensional muscle moment arms of the flexor muscles as they vary over the full range of forearm pronation-supination. It should be noted that for ease of comparison, the individual muscle forces are identified using the same colour lines in Figures 4.8 through 4.10.

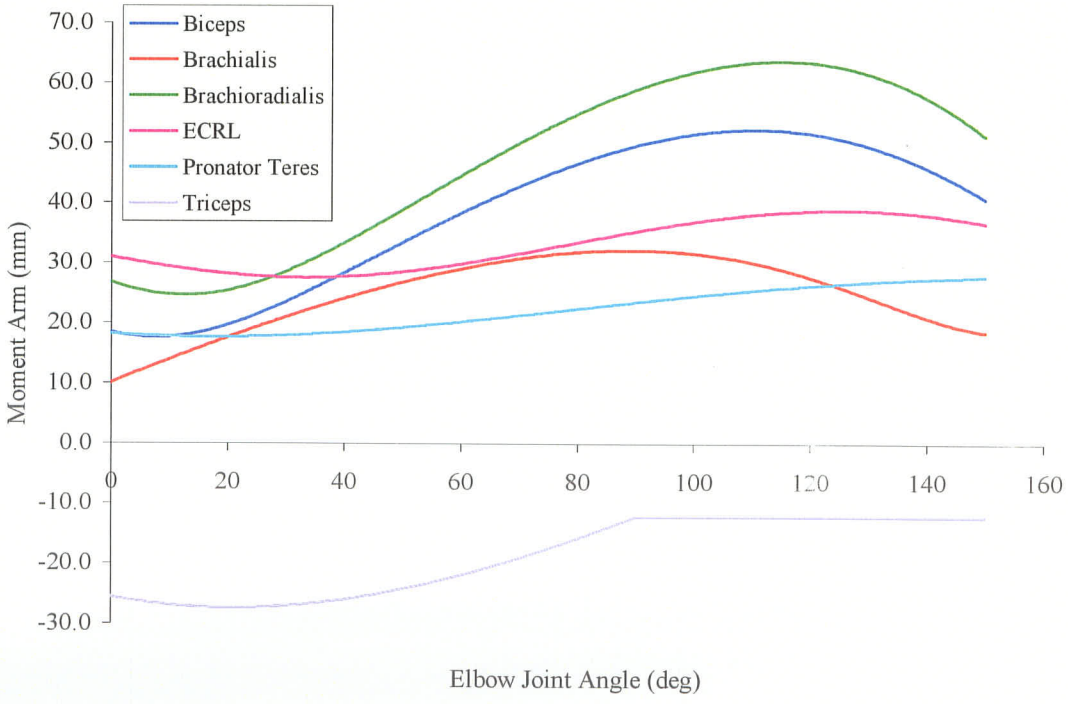

Figure 4.8 Muscle Moment Arms with Neutral Forearm

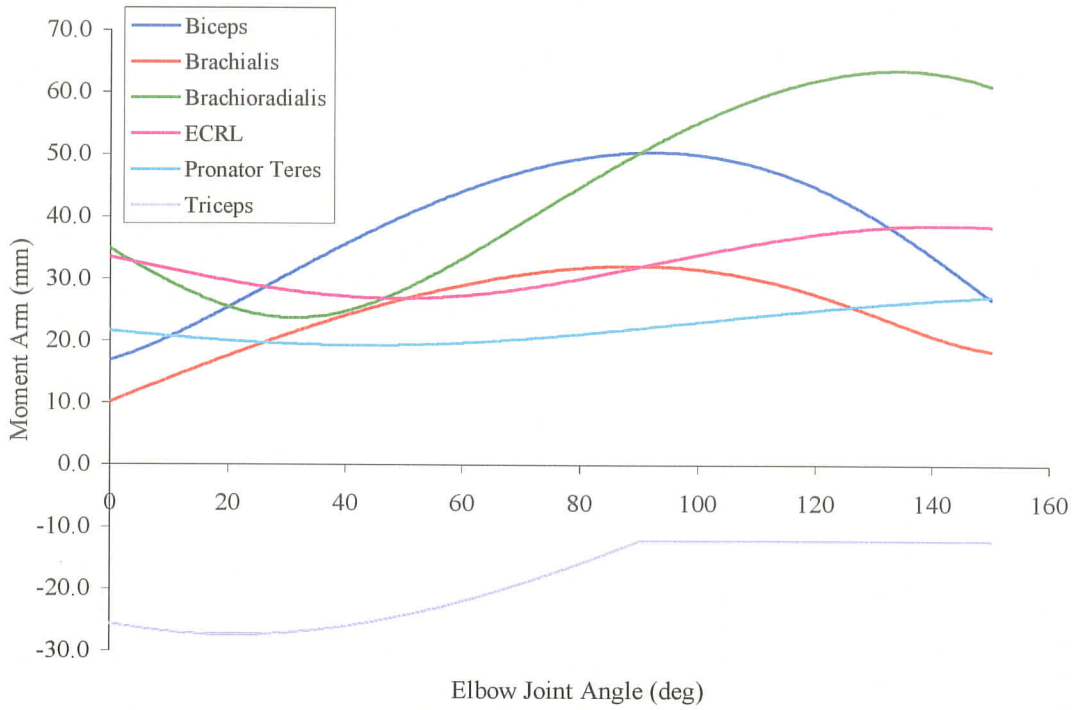

Figure 4.9 Muscle Moment Arms in Full Pronation

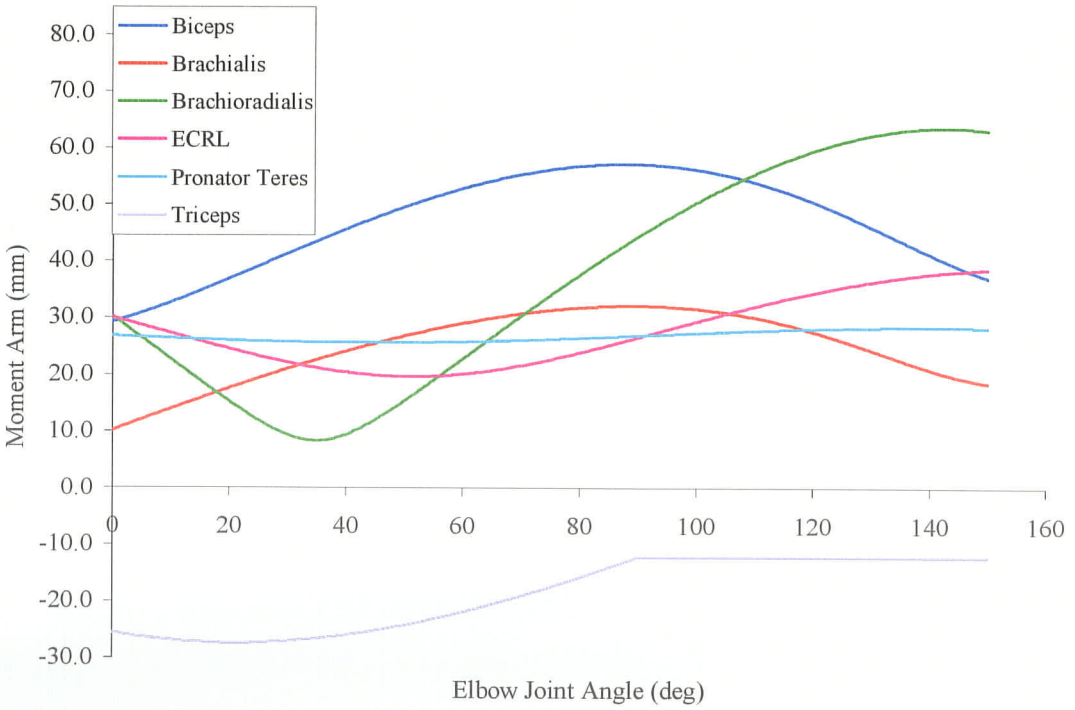

Figure 4.10 Muscle Moment Arms in Full Supination

The three-dimensional vector analysis method used in the current model is a new approach, and for validation, requires comparison with the previous findings in the literature. Preceding studies, as detailed in section 2.4.2 of the literature review, have reported both two- and three-dimensional muscle moment arms in static positions and over the full elbow joint range of flexion-extension. Some of these studies have also included the effects of forearm self-rotation. The anatomical study conducted by Amis et al. (1979) determined the two-dimensional muscle moment arms from the digitization of the muscles in a single configuration of the elbow joint and then estimated the moment arms at other joint positions. An et al. (1981) calculate the moment arms, again in two-dimensions, from the geometry of the muscles crossing the joint in fixed flexion-extension and pronation-supination positions of the elbow joint. These and other elbow muscle models in two-dimensions do not represent a full vector method. In a two-dimensional analysis the muscle lines of force, and thus moment arms, are only correctly represented if they lie in one of the coordinate planes. Otherwise, they are simply projections of a three-dimensional vector quantity onto a coordinate plane, in most cases neglecting the medial-lateral component. Without this component of the moment arm, the magnitudes will not be equivalent.

One of the few three-dimensional studies found in the literature was conducted by Murray et al. (1995), in which a three-dimensional anatomical computer model was created and used to calculate the moment arms of the muscles over the ranges of motion of both the forearm and elbow. Despite the construction of the model in three-dimensions, the direct evaluation of the muscle moment arms found in the research of

Murray et al. (1995) and those found using the vector method of this thesis remains very difficult. This is due to the omission of certain anthropometric dimensions of the subject, which would permit the scaling relationships to be applied and thus the direct comparison of the results is not possible. In consequence, the moment arms calculated with the current three-dimensional vector analysis are compared in only a qualitative manner to the prior findings reported in the literature.

The results of the moment arms over the full range of joint flexion-extension compare well qualitatively with the observations reported in previous investigations. Amis et al. (1979), Murray et al. (1995), and Murray (1997) established in their work that the muscle moment arm magnitudes vary substantially with the angle of elbow flexion-extension, as do those reported herein. When the forearm is in the neutral position, as shown in Figure 4.8 (page 83), the Brachioradialis and Biceps Brachii muscles have the largest overall moment arms of the flexor group, while the moment arms of the Extensor Carpi Radialis Longus, Pronator Teres, and Brachialis muscles are relatively lower in magnitude. However, it must be remembered that the potential moment contribution of a muscle about a given joint is dependent not only on the magnitude of its moment arm but also its physiological cross-sectional area. The pronation-supination of the forearm was found to influence the moment arms of the muscles crossing the elbow joint in a similar manner as found by Murray et al. (1995). When the forearm is in the pronated or supinated position, the magnitudes of the muscle moment arms about the flexion-extension axis of the elbow remain essentially consistent with those found when the forearm is in the neutral position. In addition, the moment arms for each of the muscles crossing the

elbow joint maintain the same general form relative to one another when the forearm is rotated as when it is in a neutral position. However, the moment arm curves in pronation become shallower, while those in supination become more exaggerated. The main effect of the pronation and supination of the forearm on the individual muscle moment arms is to shift the moment arm curves in relation to the elbow joint angle, as seen in Figure 4.9 (page 84) for pronation and Figure 4.10 (page 84) for supination. The Brachioradialis and Biceps Brachii muscles still have the largest moment arms overall of the flexor muscle group. In particular, the Biceps Brachii moment arm is more affected by the rotation of the forearm than the other muscles due to its insertion on the medial aspect of the radius. The peak flexion-extension moment arm of the Biceps Brachii muscle occurs at a lesser degree of elbow flexion as the forearm is supinated and at a more flexed elbow position in full pronation. Thus, the relative contribution of the Biceps Brachii muscle to the force production across the elbow joint is influenced by the position of the forearm. This illustrates the importance of considering both the flexion-extension of the elbow joint and the pronation-supination of the forearm when approximating the moment arms in flexion-extension of the muscles crossing the joint.

Anatomical data have indicated that the maximum moment arms of the flexor muscles occur at an angle of elbow flexion greater than 75°. The anatomical elbow model calculates the maximum moment arms of the Biceps, Brachialis, Brachioradialis, Extensor Carpi Radialis Longus, and Pronator Teres muscles to occur at or beyond 85° of flexion in all positions of the forearm (Table 4.1). The maximum moment arm of the Triceps Brachii muscle occurs at an elbow flexion angle of 21° (Table 4.1). It should be

noted from Figures 4.8 to 4.10 (pages 83-84) that the moment arm of Brachioradialis undergoes a decrease in the early stages of flexion; this decrease is more prominent when the forearm is fully supinated. The drop in the moment arm could be corrected by adding an anatomical wrapping point to the model as the elbow nears the latter stages of extension. In addition, further wrapping points can be used to improve the estimation of the Triceps Brachii muscle moment arm past 90° of elbow flexion, a section which is currently estimated to remain at a constant value. Unfortunately, the anatomical coordinate point data were not available to allow the inclusion of these wrapping points in the current model.

Table 4.1 Locations of Maximum Muscle Moment Arms in Flexion-Extension

	Neutral Forearm	Full Pronation	Full Supination
Biceps Brachii	92.0° - 93.0°	110.0° - 111.5°	87.0° - 89.0°
Brachialis	88.5° - 89.5°	88.5° - 89.5°	88.5° - 89.5°
Brachioradialis	133.0° - 135.0°	114.0° - 116.0°	142° - 143.5°
ECRL	150°	124.0° - 126.5°	150°
Pronator Teres	150°	150°	136.5° - 142.5°
Triceps	21.0°	21.0°	21.0°

In addition to the variation of the muscle moment arms with the angle of elbow flexion-extension, the moment arms will vary with the size of the subject. Figure 4.11 shows a range of three-dimensional moment arms for the muscles over the full range of elbow joint flexion-extension with the forearm maintained in the neutral position, as calculated

by the anatomical elbow model. The shaded area represents the range of magnitudes produced by the elbow model. This area is bordered on the lower end by the moment arm curve for a female subject with a height of 1.47 meters (4ft-10in) and a weight of 48.8 kilograms (107.5 lbs). The upper border is the moment arm magnitudes calculated for a male subject with a height and weight of 1.93 meters (6ft-4in) and 84.0 kilograms (185 lbs), respectively. The variation of the moment arm magnitudes according to subject size is not constant due to the non-linearity of some of the equations used in the scaling of the subjects.

Murray (1997) determined the lengths of the muscle moment arms for ten subjects, both male and female, of varying sizes as depicted in Figure 4.12. The moment arms were found using the tendon displacement method and moving the forearm through its range of rotation about the elbow joint. The muscle tendons were constrained to follow their anatomical paths and the forearm was maintained in the neutral position during the measurement process. Due to the lack of subject height and weight data for the ten subjects supplied by Murray (1997), it is not possible, and would also be misleading, to directly compare the curves found in Figures 4.11 and 4.12. However, despite the differences between the muscle moment arms calculated by the anatomical elbow model and those determined by Murray (1997) in terms of magnitude, the same general trends can be observed in both sets of curves.

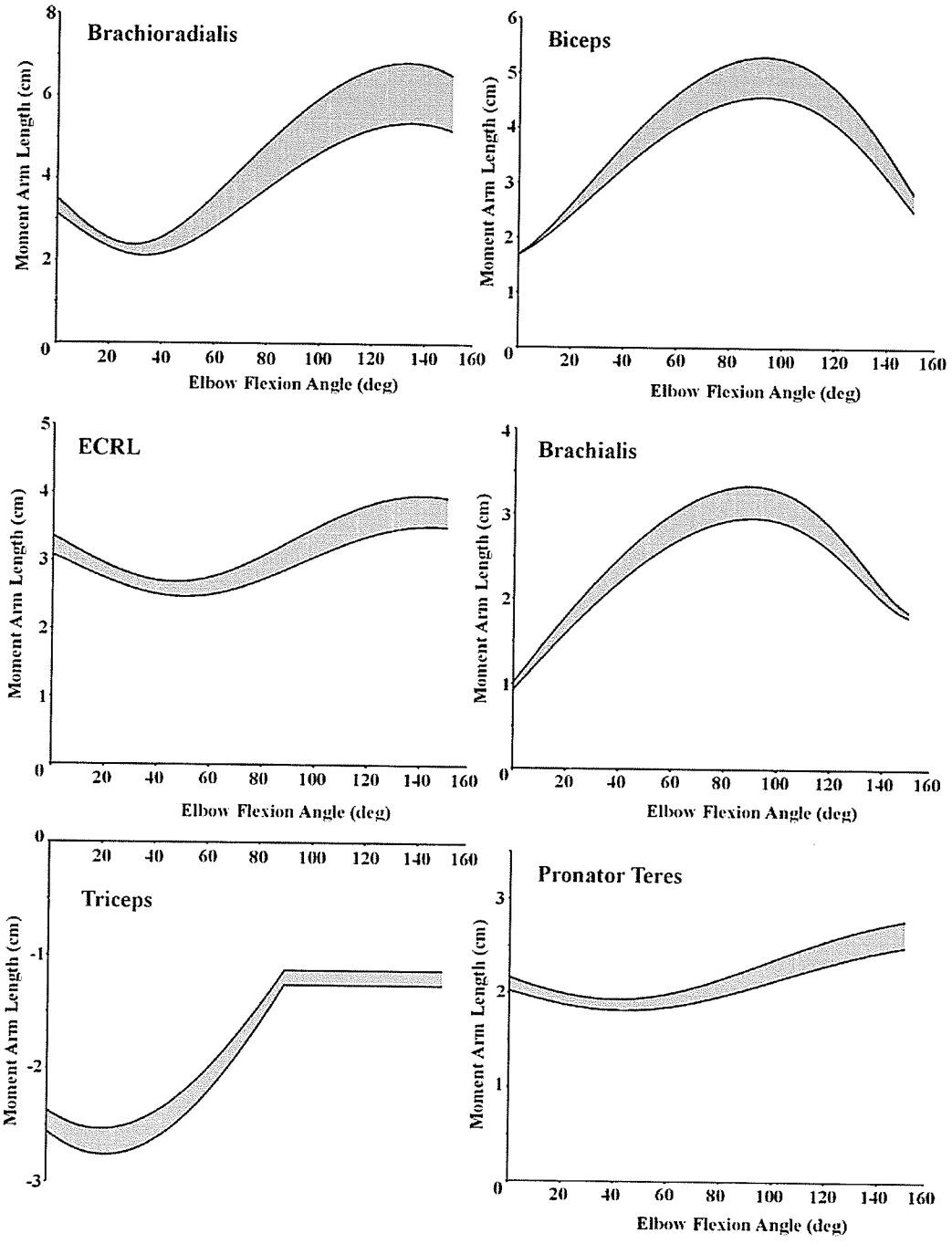

Figure 4.11 Muscle Moment Arms for Subject Size Range
(Upper Border: Male, 1.93 meters, 84.0 kilograms
Lower Border: Female, 1.47 meters, 48.8 kilograms)

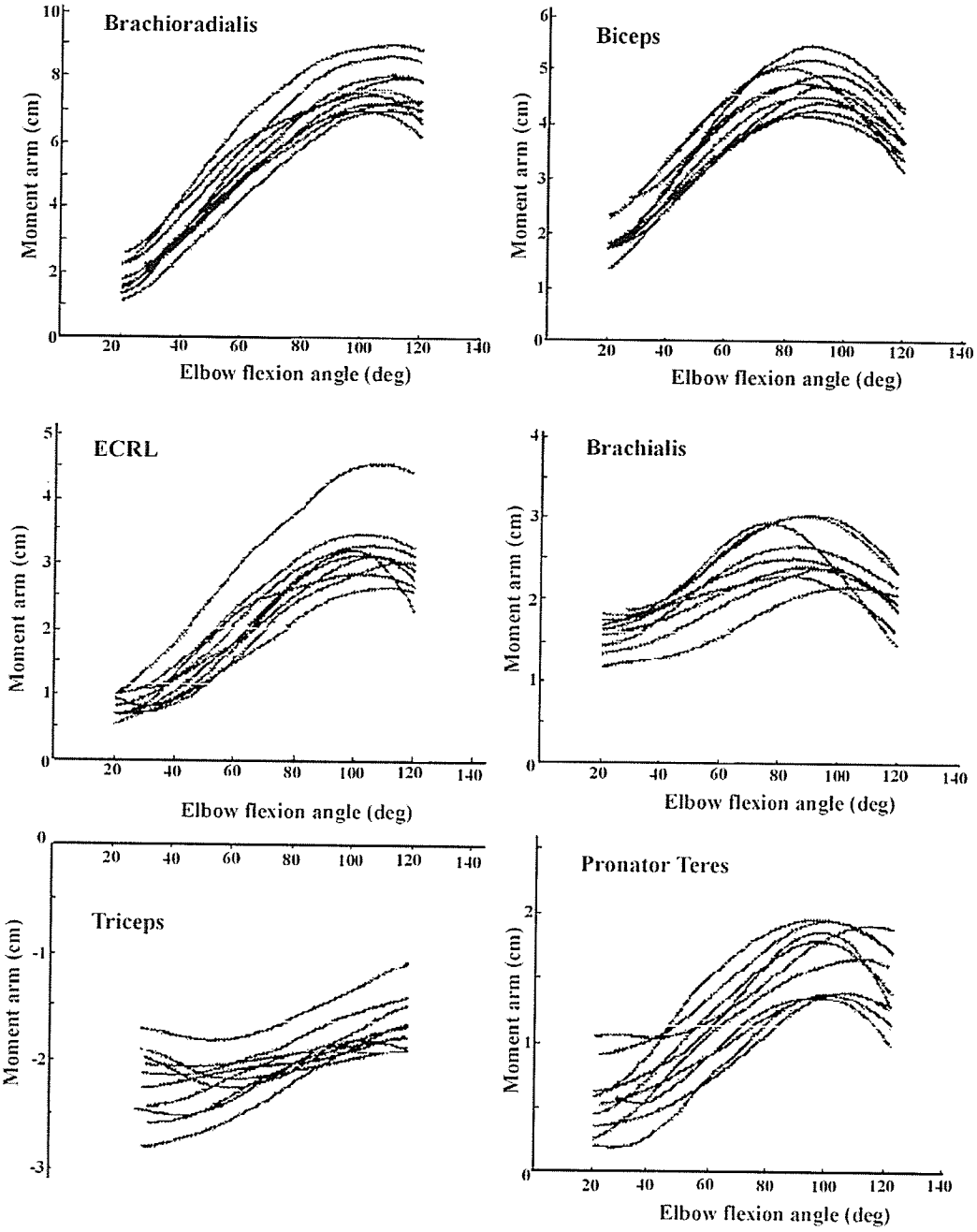

Figure 4.12 Muscle Moment Arms for Ten Subjects
(adapted from Murray, 1997)

4.4 Validation of Muscle Forces

From the literature survey, it has been found that a method for the quantitative prediction of individual muscle forces crossing a given joint had not previously been established. Having shown that the moment arms of the muscles can be calculated from appropriately scaled anatomical data for any given elbow joint configuration, the calculation of the individual muscle forces is now possible given a muscle activation strategy.

As detailed in the methodology in (Chapter 3), the activation strategy being used is based on the premise that all the fibres of the muscles in a functional group are activated to a common level. Due to the mathematical formulation of the moments generated, the muscle activation strategy allowed the development of force for each muscle as it relates to the total force, F_T, developed by all the muscles of the functional group. As a result of this formulation, it is possible to extract the total functional group muscle force from the individual muscle moment equations, which are equated to the net moment produced by the dynamic model. An alternate muscle activation strategy, in which levels of activation differed for each of the muscles in the functional group, would lead to different forces in each muscle. An example of which was shown in the electromyographic research done by Basmajian and Latif (1957), with the Biceps Brachii being mostly inactive in elbow movements with the forearm in pronation. However, a relationship between the total force, F_T, and each individual muscle would still have to be formulated in order to make use of the method presented here.

The antagonist muscles are incorporated in the mathematical model for net moment. The activation of the muscles in the antagonist functional group can be set to any desired level relative to the agonist muscle group. The result of including the antagonistic muscles is to increase the total joint dynamic muscle force, F_T, for the agonist muscles. This increase compensates for the antagonist moment and thus leads to the identical required net moment at the elbow joint for the dynamics of the movement. For the simulations presented in this thesis, the antagonistic muscles are activated to produce 20% of the force generated by the agonist muscles. However, data to determine actual activation levels in the elbow musculature was not experimentally undertaken in this thesis, as it is beyond the scope.

The individual muscle forces determined with antagonist muscle activity of 5% and 20% are shown in Figure 4.13. It is important to note that the muscle forces predicted for 5% antagonist muscle activity are lower than the forces for 20% antagonist activity. This confirms that the calculated muscle forces do, indeed, change appropriately when the antagonist muscle activity is applied. It should also be noted that the force curves are related to the same net joint moment.

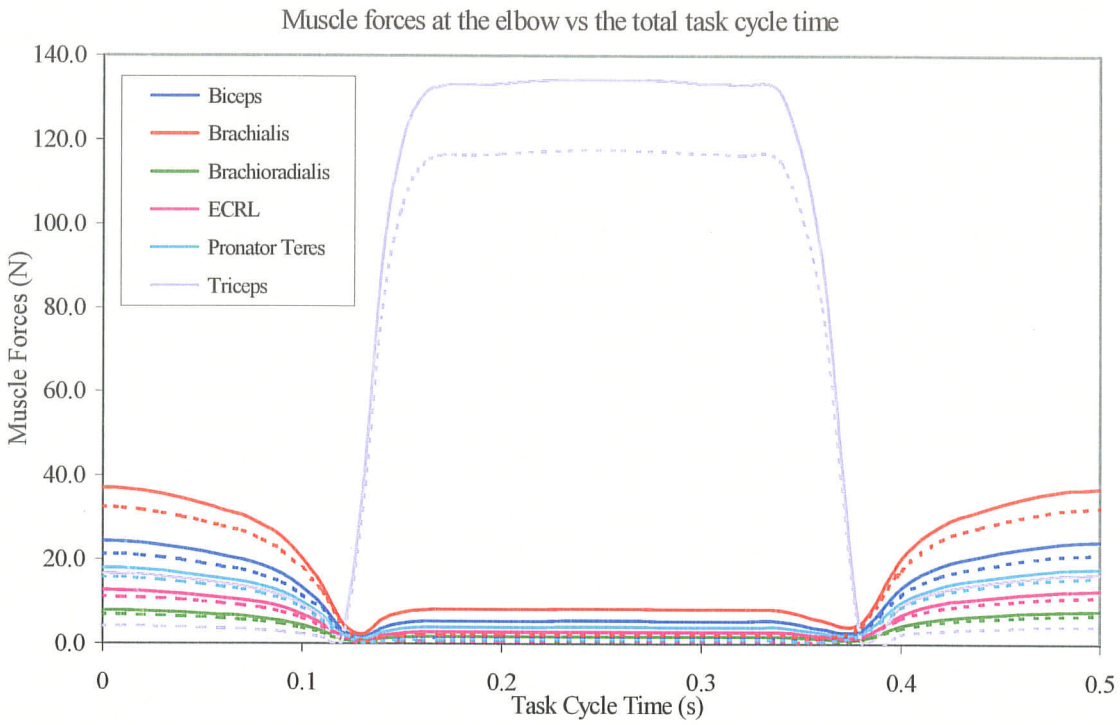

Figure 4.13 Individual Forces for Two Muscle Activation Levels
——— 20% activation ------- 5% activation

An example of the use of muscle activation strategy for the calculation of muscle forces is presented here. The uniform muscle activation strategy allows muscle force to be related to the ratio of the physiological cross-sectional area of the individual muscle to the total physiological cross-sectional area of the functional group. Thus, the force generating capacity of a muscle is assumed to be proportional to its relative physiological cross-sectional area. Continuing the example calculation begun in the previous section, the relative physiological cross-sectional area ratio, α_1 is calculated as follows for the Brachioradialis muscle:

$$\alpha_1 = \frac{PCSA_i}{PCSA_T} = \frac{1.5cm^2}{18.9cm^2} = 0.07937$$

From the dynamic simulation, the net moment produced at the elbow joint for any elbow flexion angle in a prescribed movement is determined based solely on the activity of the agonist muscles. Due to the use of a non-anatomical based axis system in the dynamic model, the component of the dynamic moment about the flexion-extension axis of the elbow must be calculated using equation (3.13) as follows:

$$M_{f/e} = \bar{M}_{dynamic} \bullet \hat{e}_{f/e} = [0 \quad 0 \quad 0.2288] \bullet [0.0442 \quad 0.0294 \quad 0.9986] = 0.2285N \cdot m$$

The three-dimensional dynamic moment about the elbow joint axis of rotation is then calculated from equation (3.14) as follows:

$$\bar{M}_{f/e} = M_{f/e} \cdot \hat{e}_{f/e} = [1.010x10^{-2} \quad 6.717x10^{-3} \quad 0.2282]N \cdot m$$

Now, from the dynamic moment, the total muscle force can be determined using the appropriate version of equation (3.16). In the case of our example calculation, the elbow is undergoing a flexion movement, thus the agonist muscle group will be the flexor muscles and the total muscle force is calculated as follows:

$$F_T = \frac{\bar{M}_{f/e}}{\left(\sum \left(\vec{r}_i \times \alpha_i \hat{f}_i\right)\right)_{agonist}} = 9.811N$$

Now that the total muscle force required to produce the net moment across the elbow joint, assuming there is no antagonist muscle activity, has been determined; the minimum force produced in the individual muscles can be calculated. If there is antagonist muscle activity, then a relative activation level can be applied to the antagonistic muscle group. This antagonist activation increases the agonist muscle forces. Making use of the relative

physiological cross-sectional areas of the muscles and their activation level according to their function as either agonists or antagonists, the individual muscle force, is then calculated using equation (3.17) as:

$$F_{bic,agonist} = F_T \alpha_{bic} b_{agonist} = (9.811N)(0.24339)(1.2) = 2.865N$$

$$F_{brach,agonist} = F_T \alpha_{brach} b_{agonist} = (9.811N)(0.37037)(1.2) = 4.360N$$

$$F_{brad,agonist} = F_T \alpha_{brad} b_{agonist} = (9.811N)(0.07937)(1.2) = 0.9344N$$

$$F_{ecrl,agonist} = F_T \alpha_{ecrl} b_{agonist} = (9.811N)(0.12698)(1.2) = 1.495N$$

$$F_{pt,agonist} = F_T \alpha_{pt} b_{agonist} = (9.811N)(0.17989)(1.2) = 2.118N$$

The lack of literature data available for comparison of the muscle force curves required that another method for the validation of the individual muscle forces be established. It is extremely difficult and invasive to measure the individual muscle forces in vivo, and would also require qualified medical personnel to perform the required surgical implantation of force transducers within the muscle tissue. It is also doubtful that ethical approval could be obtained to perform the experiments on human subjects. Therefore, dynamic motions in which geometries were controlled have been used in this thesis as a means of evaluation.

The energy consumed by the muscles during the performance of a movement is directly related to the force produced by the muscle group of concern. As a way of checking the validity of the individual muscle force calculations, the dynamic model simulated a movement geometry, which possessed an energy balance between the flexors and extensors. The geometry was chosen such that both the dynamic and static moments

could be easily calculated. From the known behaviour of the dynamic and static moments, the mechanical energy of the flexor muscle group would have to be equal to the mechanical energy of the extensor muscles. If the energies of the flexors and extensors were not equal, then the method of computation of the individual muscle forces from which the energies could be questioned. Given the nature of anatomical scaling, some small error (±10%) would be expected. The mechanical energies were calculated by applying the individual muscle forces, in the direction of the muscle, over small increments in the joint angle to the change in length of the muscle. These elements of the mechanical energy were summed over the full movement and for all muscles of the functional group.

The geometry used for the balanced energy situation was one in which the forearm, in the neutral position, rotates about the elbow joint purely in the coronal anatomical plane, as shown previously in Figure 4.1 (page 71). Angular displacement of the elbow joint was incremented through a complete cycle of flexion and extension; that is, from full extension to full flexion and then back to full extension. In addition, the upper arm was positioned parallel to the ground so that the gravitational effects would be equal during both the flexion and extension portions of the movement. It must also be confirmed that the elbow model is capable of handling both static and dynamic situations properly. Hence, the same simulation was run first with a task cycle time of 10 seconds (approximately a quasi-static situation) and then with a task cycle time of 0.5 seconds.

The cyclic motion being simulated can be divided into four distinct sections, each comprising 25% of the task cycle time. The first quarter of the movement consists of the flexion of the elbow from full extension to the 90° flexed position, during which the movement is initiated and accelerated by the flexor muscle group. This is followed by the second portion of the flexion from 90° to the fully flexed position, when the movement is decelerated and brought to a stop by the extensor muscles. The third portion involves the extension of the elbow from full flexion back to the 90° position, a movement initiated and accelerated by the extensor muscle group. The final phase of the movement ranges from 90° of flexion to full extension, during which the rotation of the elbow is decelerated and brought to a stop by the flexor muscles. The simulations were run using a male subject, with a height of 1.78 meters (5ft–10in) and a weight of 72.57 kilograms (160 lbs).

The individual muscle force curves are shown in Figure 4.14 (page 101) for a task cycle time of 10 seconds and in Figure 4.15 (page 102) for a task cycle time of 0.5 seconds. It can be seen that the forces in each muscle are of the same general form and maintain the same magnitude order regardless of the task cycle time. The more squared-off shape of the force curves in the 0.5 second simulation are due to the increased acceleration effects in the dynamic component of the model. The other effect of the faster task cycle time is to increase the magnitude of the muscle forces by approximately 400%. This increase in muscle force is necessary to produce the higher moments required by the elevated rate of angular acceleration for completing the full movement cycle in such a short time period.

In addition, the high rate of acceleration demands a large force production to produce the rapid deceleration of the movement.

The individual muscle force curves for the same subject and elbow joint motion simulation, with a task cycle time of 10 seconds, are shown in Figure 4.16 (page 103) with the forearm in a supinated position and in Figure 4.17 (page 104) in pronation. In comparison to the muscle force curves displayed in Figure 4.14 (page 101), those predicted with the forearm in supination, Figure 4.16, are of the same form and retain the same relative order. However, the magnitude of the individual muscle forces decreases when the forearm is supinated compared to the neutral position, due to the change in the muscle moment arms caused by the changed forearm geometry. When examining the individual muscle force curves with the forearm in pronation, Figure 4.17, the most notable change is the lack of force in the Biceps Brachii muscle. It would be expected that the magnitude of the muscle forces would again be lower than those in the neutral position, however because there is one less active flexor muscle, the Biceps Brachii, the remaining four muscles must compensate. The slight change in the shape of the force curves of the flexors can once again be attributed to the change in the moment arms as a result of the pronation of the forearm. The results of further simulations in the coronal plane, along with additional plots from the four simulations already presented can be found in Appendix D.

As found by Basmajian (1969), Basmajian and DeLuca (1985), Basmajian and Latif (1957), de Sousa et al. (1961), and Pauly et al. (1967) and displayed in Figures 4.14

through 4.16, on pages 101 through 103, the Biceps Brachii, Brachialis, and Brachioradialis muscles are the primary flexors of the elbow joint. In addition, the Brachialis muscle is found to produce the highest force of the flexor muscle group regardless of the forearm position and speed of the movement, reconfirming previous findings that it is the "workhorse" of the elbow flexors. As noted in the discussion in the previous chapter, the Biceps Brachii is inactive during movements wherein the forearm is pronated due to its insertion position on the radius. From Figure 4.17, on page 104, it can be seen that the Biceps Brachii is properly activated based on the rotation of the forearm in the anatomical elbow model to be inactive when the forearm is pronated. The Pronator Teres and Extensor Carpi Radialis Longus muscles have the lowest force production of the flexor muscle group, but combined they produce more force than the Brachioradialis muscle. In Figures 4.14 through 4.17 the Triceps Brachii dominates the force production of the extensor muscle group, being the sole extensor muscle included in the model. Further force curves for the motion in the coronal plane can be found in Appendix D.

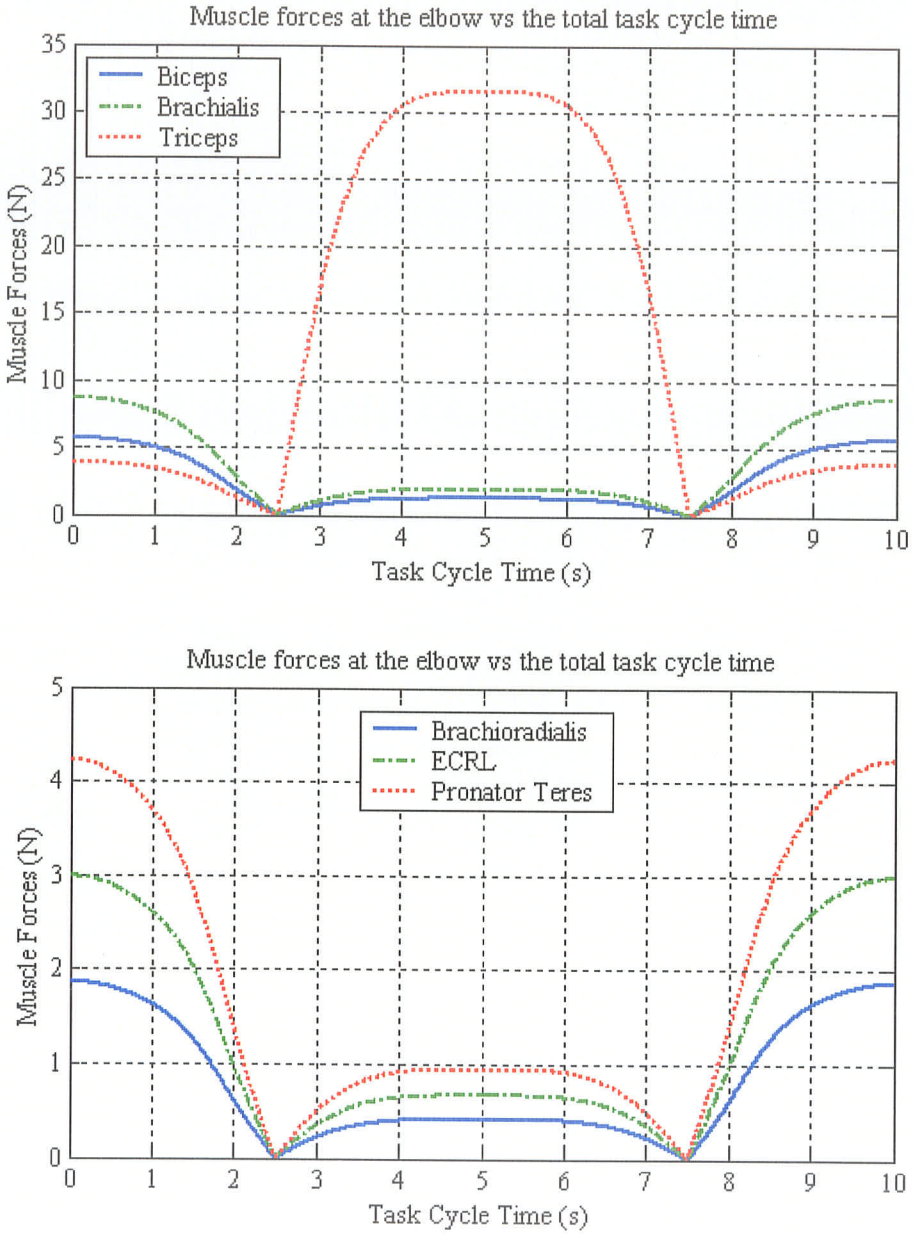

Figure 4.14 Individual Muscle Forces in Coronal Plane with Neutral Forearm, 10s Task Cycle

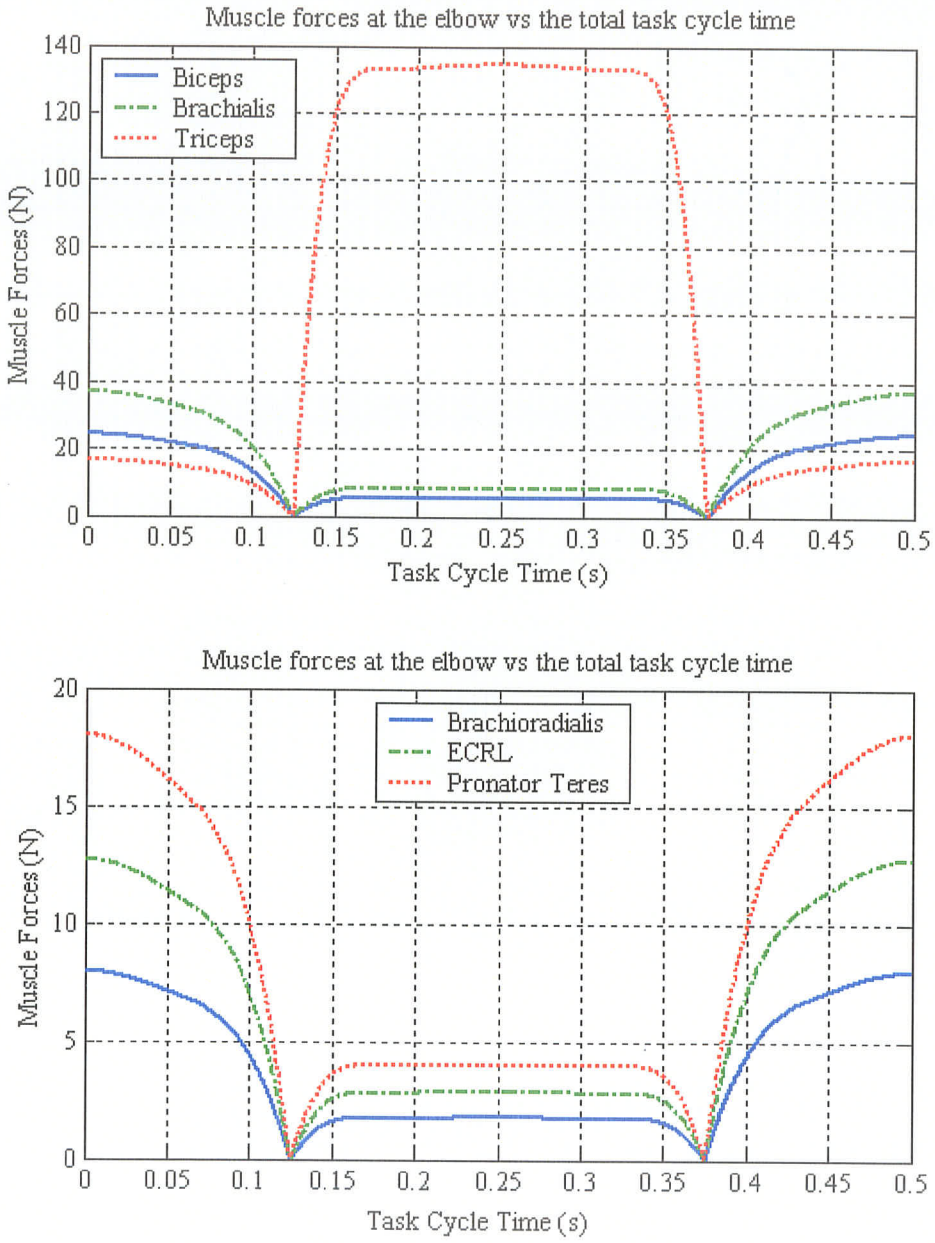

Figure 4.15 Individual Muscle Forces in Coronal Plane with Neutral Forearm, 0.5s Task Cycle

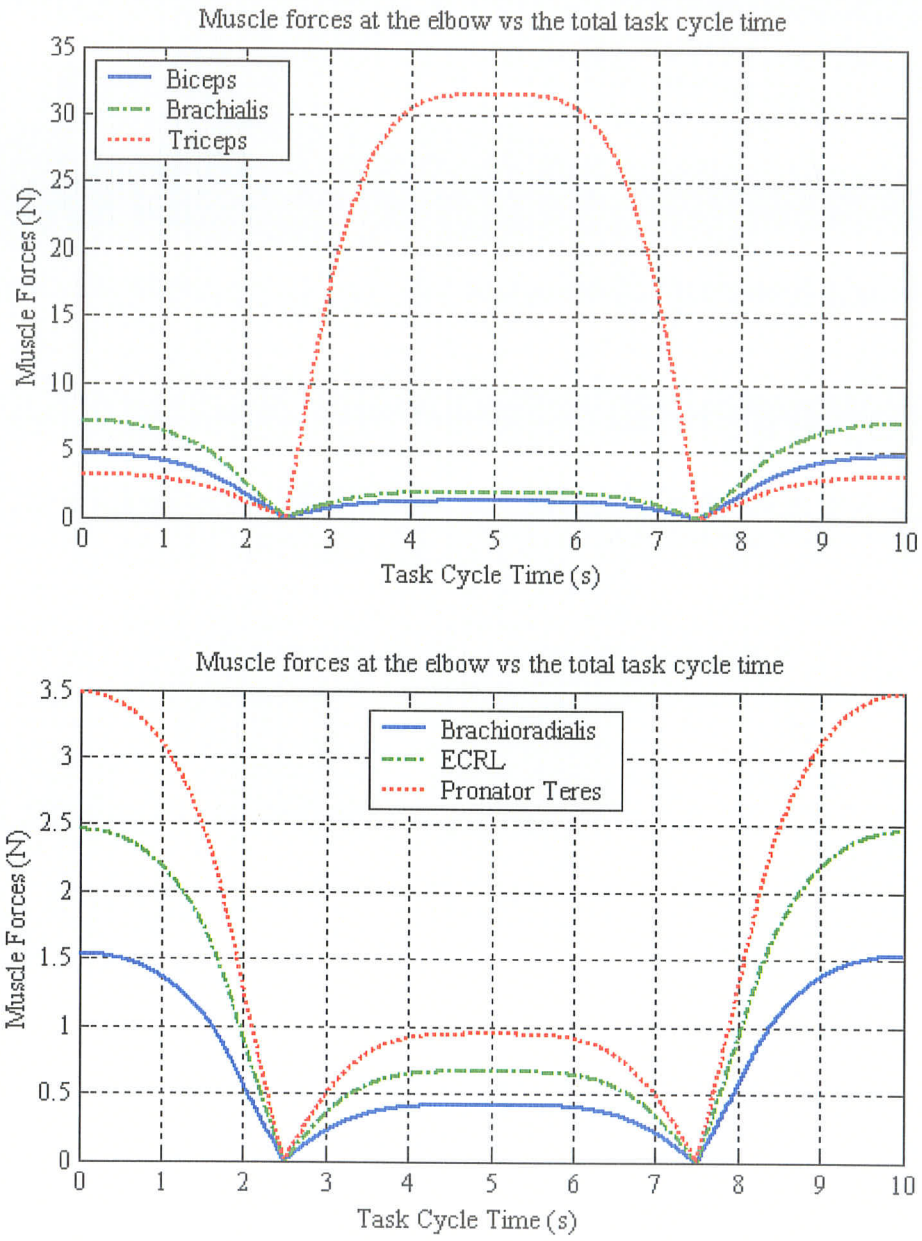

Figure 4.16 Individual Muscle Forces in Coronal Plane with Supination, 10s Task Cycle

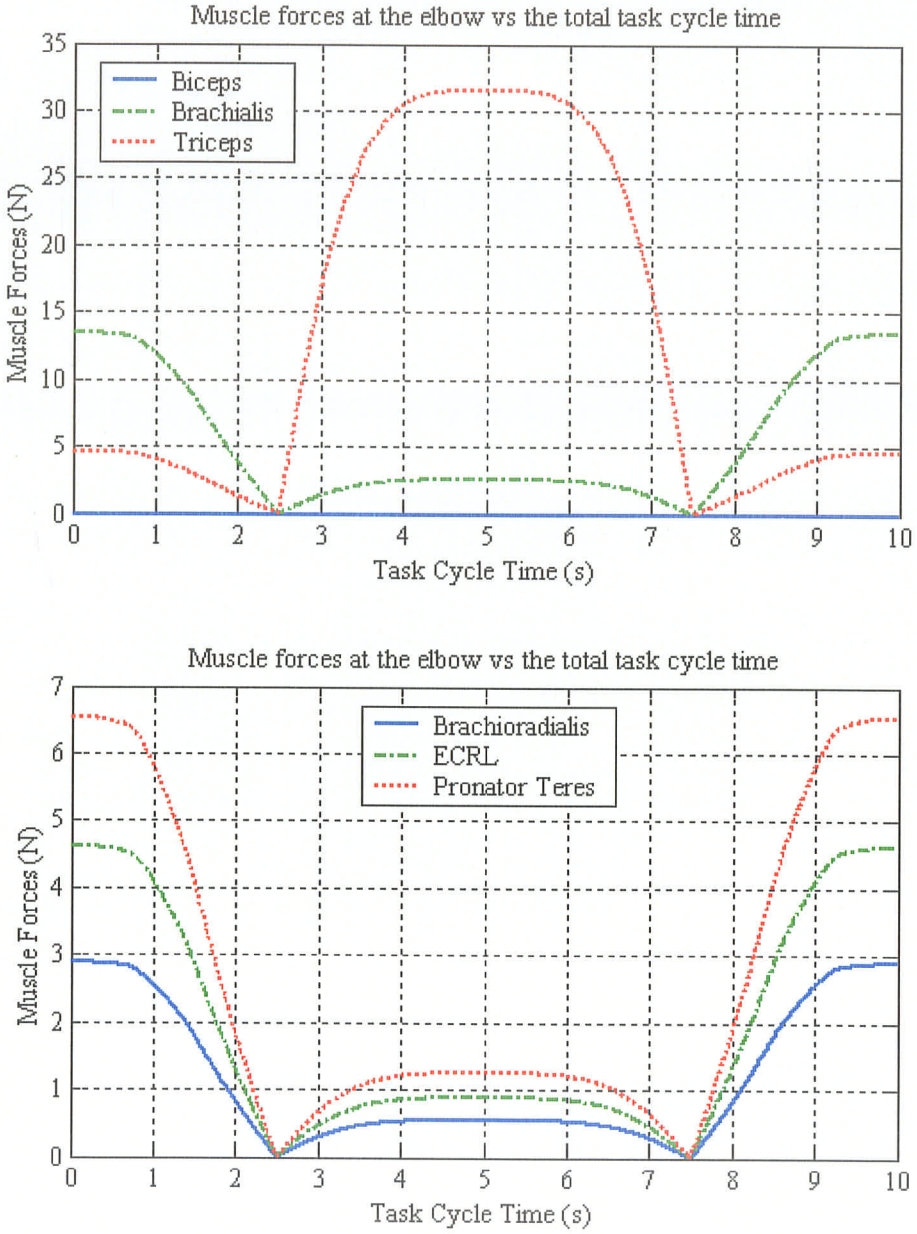

Figure 4.17 Individual Muscle Forces in Coronal Plane with Pronation, 10s Task Cycle

The mechanical energy produced by a muscle during the rotation of the joint through a small increment in angle is proportional to the force in the muscle and its change in length over the change in angle. The total mechanical energy expended by a muscle during a full movement cycle is then determined by summing the small energy increments through the cycle. Figure 4.18, on page 108, shows the mechanical energy produced by the muscles of the anatomical elbow model during the coronal plane motion with the forearm in the neutral position for the 10 second task cycle time and Figure 4.19, on page 109, for the 0.5 second task cycle time. The Brachialis and Biceps Brachii have the largest mechanical energy production of the flexor muscles, while the mechanical energies of the Brachioradialis, Pronator Teres and Extensor Carpi Radialis Longus are very close to one another in magnitude. The similar mechanical energies of the Biceps Brachii and Brachialis despite the relatively large difference in their individual muscle forces can be attributed to the larger change in length of the Biceps Brachii during the flexion and extension of the elbow joint.

The total mechanical energy of the flexor muscle group is compared to the total mechanical energy of the extensor muscle group to see if the expected balance has indeed occurred. As a result of the variation in the muscle moment arms a straight-line relationship for the mechanical energies is not expected, rather a complex curve is expected, as seen in Figures 4.18 and 4.19 (pages 108 and 109). In addition, the curves for the total flexor and extensor mechanical energies are not superimposed upon one another as could possibly be expected. However, due to the opposing functions of the two muscle groups during the simulated movement as alternating between agonist and

antagonist behaviours, the forces in the two functional groups also alternate dominance and thus their mechanical energies do as well. The flexors have a much higher mechanical energy during the first phase of the movement while acting as the agonist muscles and then the extensors catch-up during the second phase when they are the agonists. The same activation pattern occurs in the second half of the movement with the extensor muscle group having the larger increase in mechanical energy to be followed by the increase in flexor mechanical energy for the deceleration phase.

The mechanical energies produced by the flexor and extensor muscle groups over the two halves of the movement, flexion from full extension to full flexion (0° to 180°) and extension from full flexion to full extension (180° to 0°) are displayed in Table 4.2. Calculating the percent difference in the energies of the two muscle groups for each half of the movement, we find that there is a 7.91% and 7.69% variation in the energies with the 10 second task cycle time and differences of 3.42% and 2.99% for the 0.5 second cycle. The higher divergence in the energy balance during the slower simulation can be attributed to the fact that the energies of the muscle groups are much lower (0.396 to 0.430 joules) than those for the fast simulation (2.26 to 2.34 joules) and thus the percent energy differences are magnified. Nevertheless, the energy balance between the muscle groups is remarkably small, since the balance is being determined between five flexor muscles as compared to a single extensor. In addition, the change in muscle length used to determine the mechanical energies is based on a straight-line assumption for the muscle line of action and minimal wrapping of the muscles around bony structures was considered to take place.

The energy balance curves for the motion in the coronal plane with the forearm in pronation and supination can be found in Appendix D. In supination, the percent differences in the energies of the two muscle groups are found to be 3.49% and 3.06% with a task cycle time of 0.5 seconds, and 7.16% and 7.38% for a 10 second cycle. When the forearm is pronated the energy differences for the 0.5 second task time are 13.03% and 13.39%, while the 10 second task cycle time produces variations of 18.22% and 18.45%. The larger error in pronation can be attributed to the difference in the muscle activation strategy in this situation. It was assumed that the Biceps Brachii muscle is completely inactive when the forearm is pronated. However, there may be some small activity of the Biceps Brachii that is being neglected. If there is indeed activity of the Biceps Brachii in elbow motion with pronation, because the Biceps also functions as a supinator of the forearm, increased activity in the Pronator Teres muscle would be required to counteract the Biceps force in the direction of supination. Since, the possible activity in the Biceps Brachii and the increase in activity of the Pronator Teres during pronation have been neglected in the current model, it could account for the increased percent energy difference seen when the forearm is pronated.

Table 4.2 Mechanical Energy Balance, Coronal Plane Motion with Neutral Forearm

	10s Task Cycle Time		0.5s Task Cycle Time	
	Flexor Group	Extensor Group	Flexor Group	Extensor Group
0° to 180°	0.396 Joules	0.430 Joules	2.26 Joules	2.34 Joules
180° to 0°	0.396 Joules	0.429 Joules	2.27 Joules	2.34 Joules

Based on the mechanical energy balances between the flexor and extensor muscle groups it can be concluded that the techniques developed to determine the individual muscle forces are reasonably accurate. If the model was theoretically flawed or incorrect methodology had been utilized there would be a large discrepancy in the mechanical energy balances.

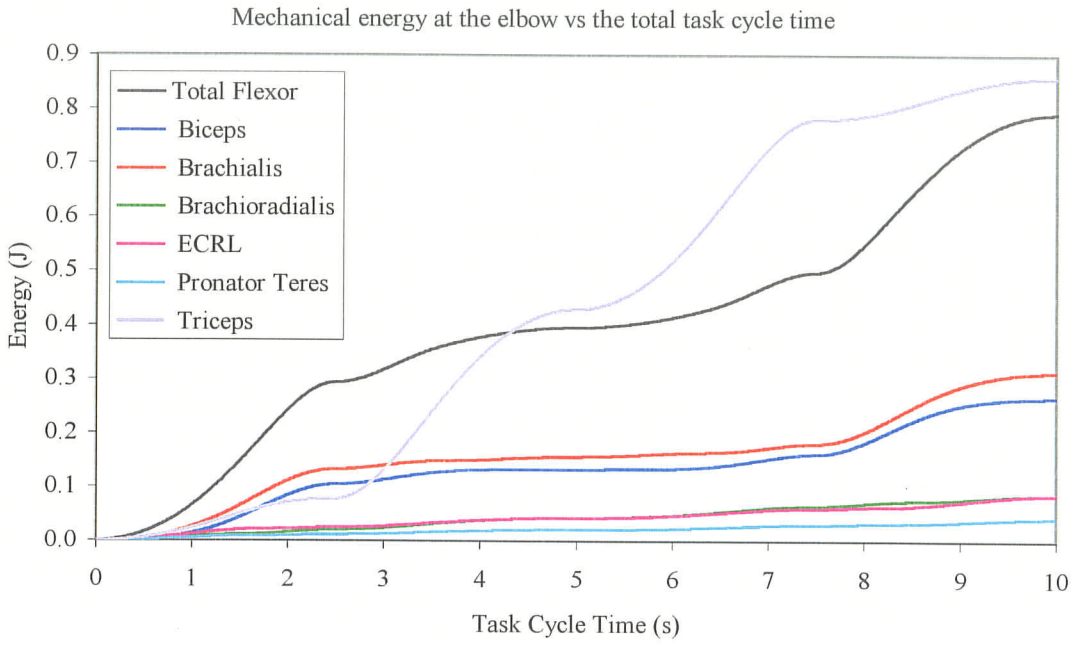

Figure 4.18 Mechanical Energies in Coronal Plane with Neutral Forearm, 10s Task Cycle

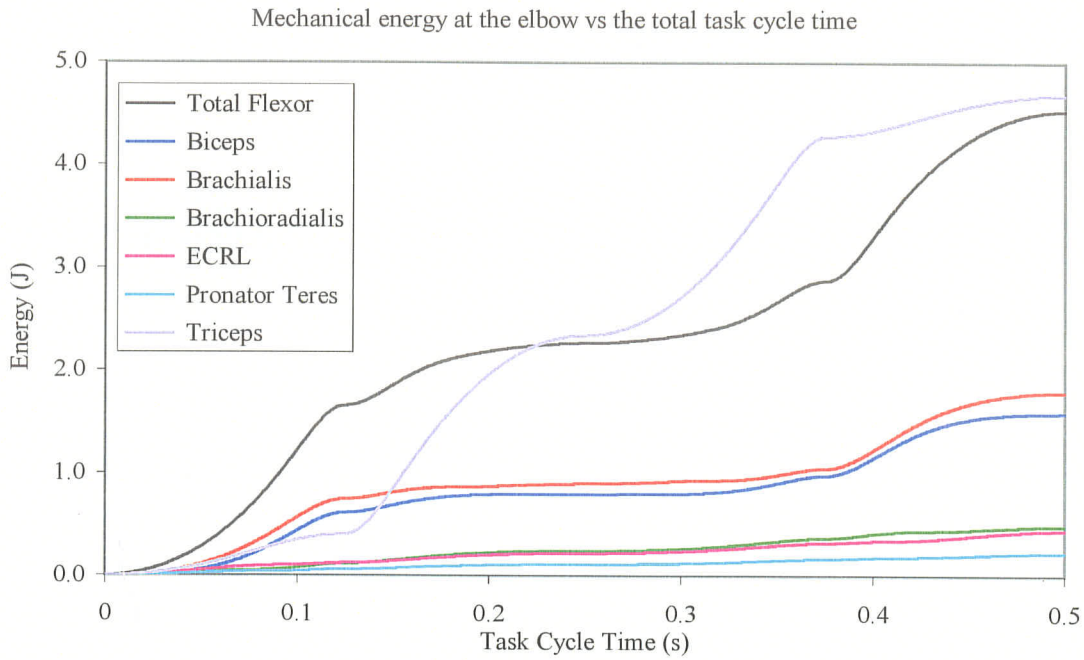

Figure 4.19 Mechanical Energies in Coronal Plane with Neutral Forearm, 0.5s Task Cycle

A second situation using a controlled geometry with known behaviour was simulated using the dynamic model to investigate the response of the model to gravitational effects. Once again the geometry was chosen such that the static and dynamic moments could be calculated easily. However in this case an energy balance is not expected to occur between the flexor and extensor muscle groups. The geometry used in this case was one in which the forearm, in the neutral position, rotates about the elbow joint within the sagittal anatomical plane, as shown in Figure 4.2 (page 71). The upper arm was positioned to lie along the side of the trunk, so that in the fully extended position of the elbow, the fingers point towards the ground. This geometry provides a situation in which gravity will influence the flexion and extension portions of the action differently.

The elbow joint was rotated through a complete cycle from full extension to full flexion and back to full extension. The simulation was run with task cycle times of 10 and 0.5 seconds, to examine the effects of both quasi-static and dynamic motion on the model. The cyclic motion is divided into four distinct sections covering 25% of the task cycle time each. In the first section the elbow joint is flexed from the fully extended position to 90° of flexion, the second segment of the flexion from 90° to full flexion. This is then followed by the extension of the elbow joint from full flexion to 90°, finally the fourth section ranges from the 90° flexed position to full extension. The simulations were performed using a male subject with a height of 1.78 meters (5ft-10in) and a weight of 72.57 kilograms (160lbs).

The individual muscle force curves are shown in Figure 4.20 (page 112) for the task cycle time of 10 seconds and in Figure 4.21 (page 113) for the 0.5 second task cycle. From Figure 4.20, on page 112, it can be observed that the flexor muscle group dominates all phases of the flexion and extension motion when the task cycle time is slow. The flexor muscle group acts in opposition to gravity during the flexion of the elbow joint to accelerate the movement to the 90° position and then continues to be active at a decreasing magnitude to maintain the motion. Due to the geometry of the simulation motion, the moment produced by the gravitational effects is sufficient to control the deceleration of the flexion until the motion comes to a stopped position. The gravitational effects are also sufficient to initiate and produce the required acceleration for the extension of the elbow joint. The flexor muscle group now serves to control the rate of extension and decelerates the motion to a stop at full extension. A small burst of

Triceps Brachii activity is seen in Figure 4.20 at the end of the flexion phase as the movement comes to a stop. This Triceps muscle force serves to reverse the moments at the elbow and bring the movement to a complete stop while protecting the bony structures from coming into contact with one another. The muscle forces for the fast task cycle, Figure 4.21 (page 113) are of the same general pattern and in the same order with respect to their magnitudes, as the individual forces found for the balanced simulations in the coronal plane. This is an expected result due to the speed of the task cycle. The extensor muscles are activated to decelerate the rapid flexion motion because the moment due to gravity is insufficient to counter the flexor moment in the same manner as in the slow task cycle. In addition, the extensor muscle group activation is needed to achieve the quick acceleration to complete the extension of the elbow joint within the required task time.

The anatomical elbow model simulations in the sagittal plane do not produce an energy balance, as did the coronal plane motions. That is to say that an energy balance based only on the muscle forces is not possible. In order to achieve an energy balance the potential energy created by the gravitational effects would have to be included. However, with the faster task cycle time, the energy created by gravity on the forearm becomes smaller when compared to the dynamic component. In general, the simulations in the sagittal plane have confirmed that the anatomical elbow model, along with the dynamic simulation, are able to appropriately account for the effects of gravity on the motion of the elbow joint. The results of simulations in the sagittal plane with the forearm in both pronation and supination are shown in Appendix E.

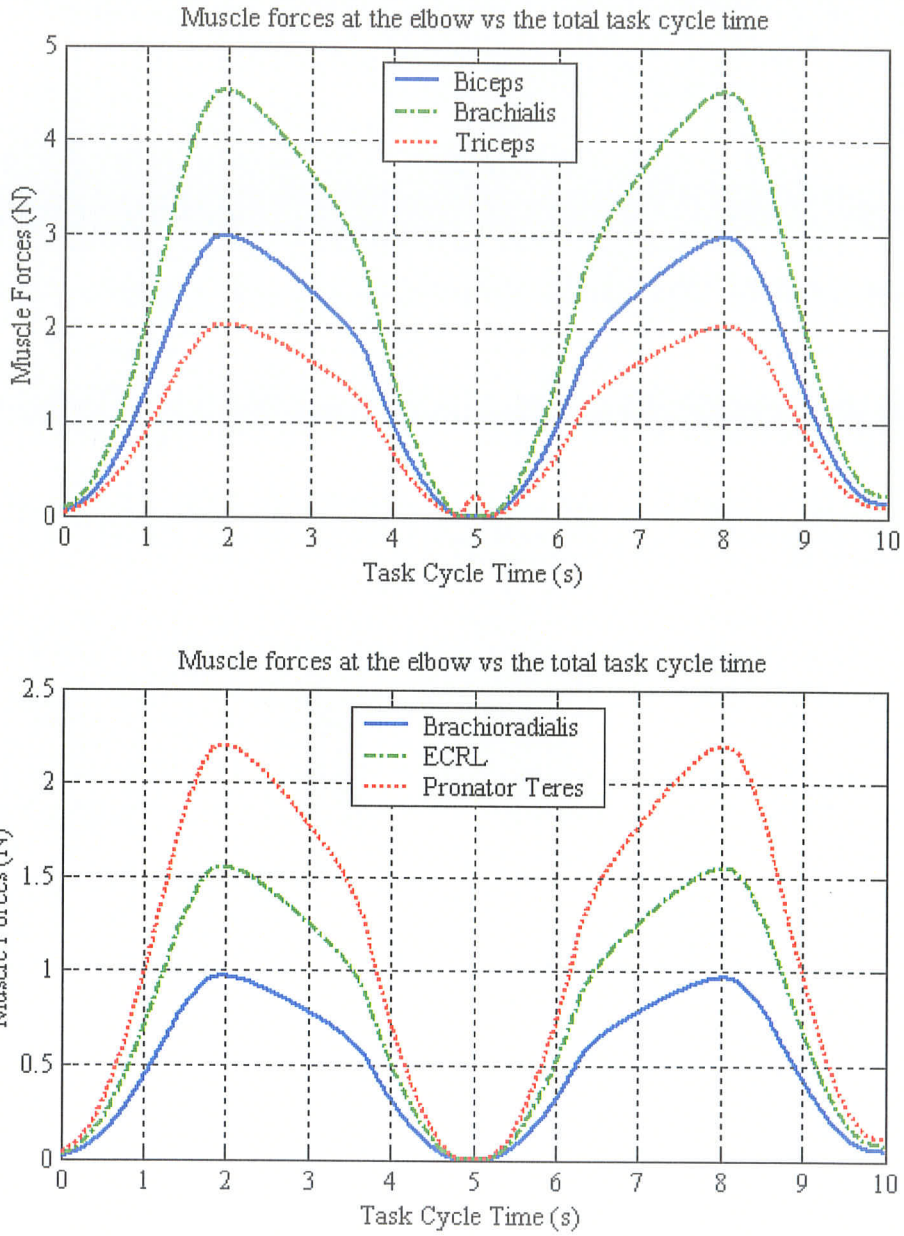

Figure 4.20 Individual Muscle Forces in Sagittal Plane with Neutral Forearm 10s Task Cycle

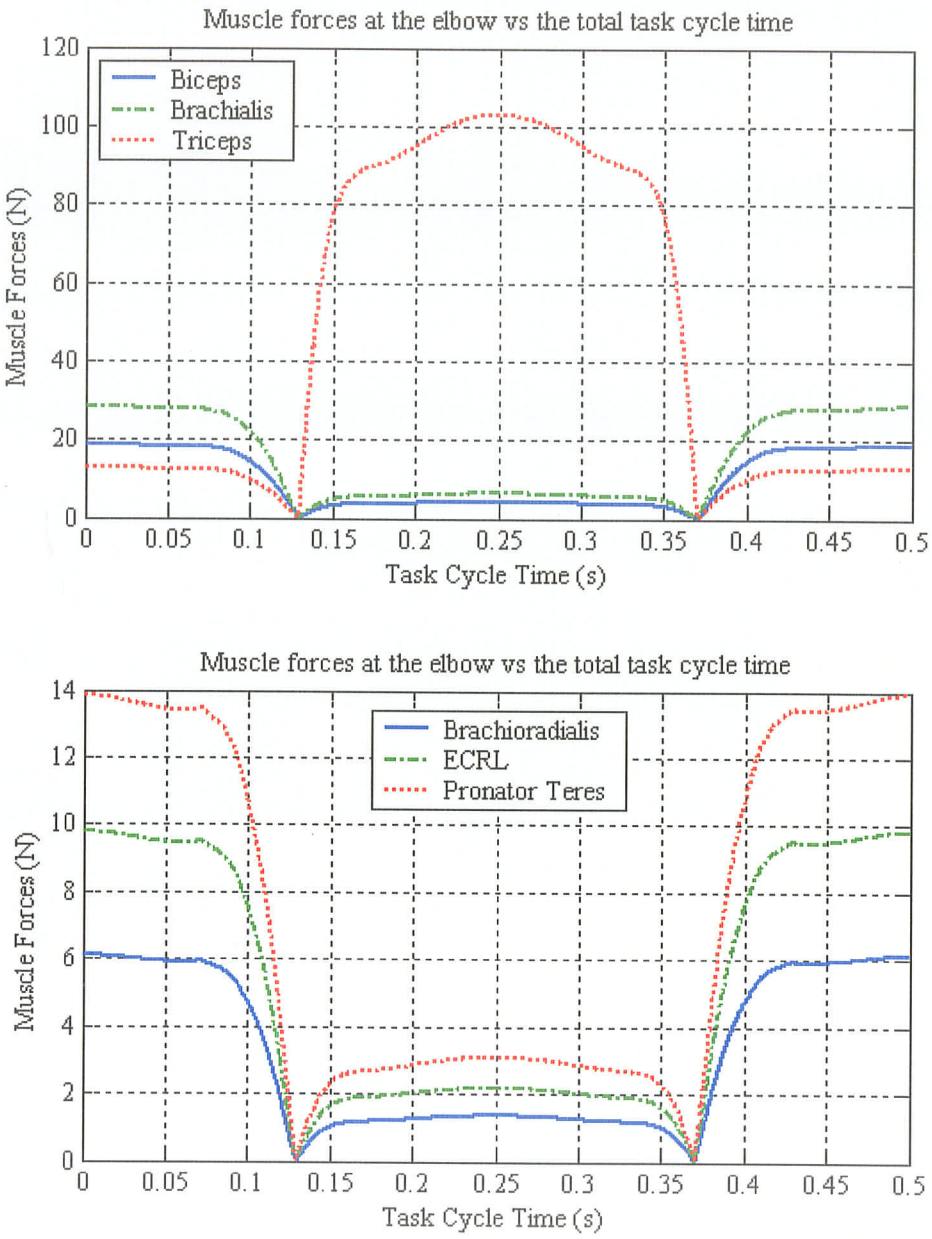

Figure 4.21 Individual Muscle Forces in Sagittal Plane with Neutral Forearm 0.5s Task Cycle

The mechanical energy determined by the anatomical elbow model is produced by the muscles during the rotation of a joint. There is also biological energy being consumed by the muscles during the movement and when maintaining an active muscle contraction even when there is no change in muscle length. It is believed that the utilization of biological energy is one of the principle factors in the development of repetitive strain injuries. The biological energy is proportional to the force in the muscle and the incremental time duration of the muscle activity. In addition, a biological constant representing the oxygen consumption within the muscle fibres needed to maintain force production must be included in the total energy calculation. The biological constant, c, is assumed based on the efficiency of the human body to be 0.5. By summing the individual increments over the full task cycle, the total biological energy is determined. The total energy for the task cycle is calculated as the sum of the mechanical and biological energies.

When calculating the mechanical energy produced during the execution of a task only the muscles considered to be active are included. The remaining muscles of the functional group are not included in the determination of the mechanical energy because they are relatively inactive in the creation of joint movement; however, these muscles may be active in stabilizing the joint structures. If these muscles don't contribute much to the moment production about the joint it is assumed that their change in length is minimal. However, these muscles would contribute to the biological energy consumption as a result of the assumption of equal force per unit area of the muscles.

Figure 4.22 shows the mechanical, biological, and total energies for the 0.5 second task cycle simulation of motion in the coronal plane with the forearm in the neutral position for the Biceps Brachii muscle. It can be seen that the biological energy is much higher than the mechanical energy throughout the task cycle. This supports the idea that it is the consumption of biological energy within the muscle during the performance of a task, which is more likely to cause a repetitive strain injury to the subject. Thus from the ability to determine the individual muscle forces and the related muscle energies for a general activation strategy, it is now possible to predict which muscles are most likely at the greatest risk of injury.

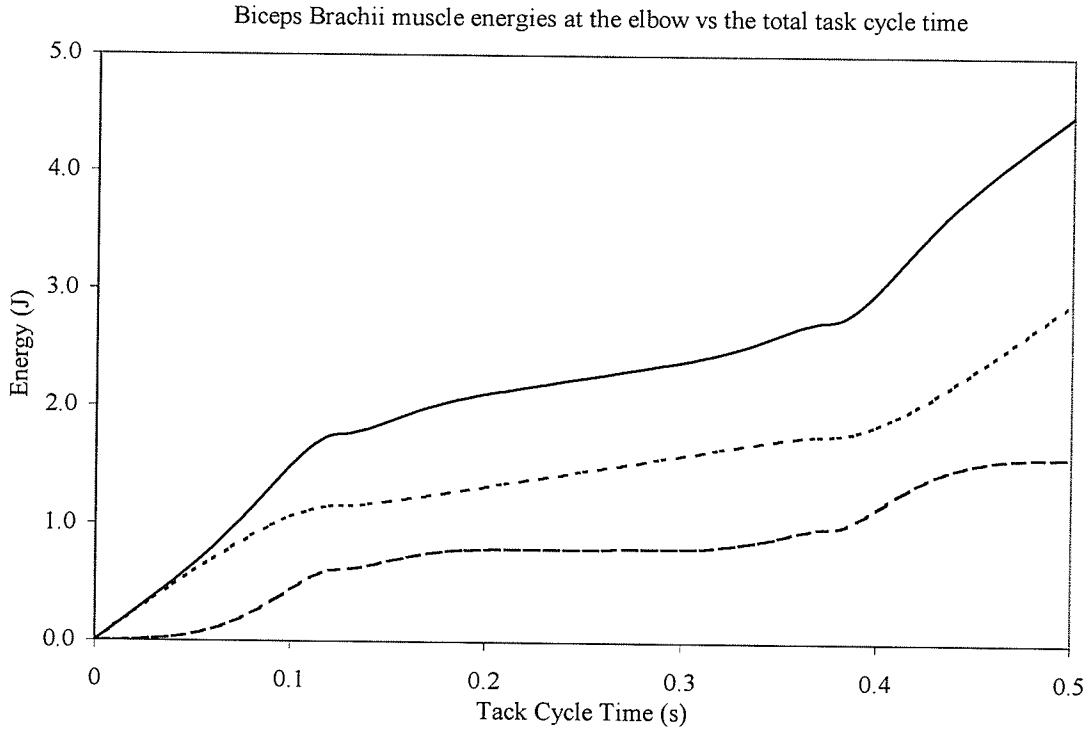

Figure 4.22 Biceps Brachii Muscle Mechanical, Biological, and Total Energies in Coronal Plane with Neutral Forearm, 0.5s Task Cycle

Total Energy ····· Biological Energy - - - - Mechanical Energy

4.5 Complex Motion Simulations

The anatomical elbow model constitutes an application that can use the moments from the dynamic simulation model. It allows the dynamic simulation to be a detailed analysis tool for industrial workstation design. In the future, additional anatomical models dealing with the shoulder joint, and back segments will be developed. However, the capacity of the current dynamic model to be a valuable tool for the prediction of repetitive strain injury risk in workstation design is already apparent. The dynamic model determines the path trajectories of the joints of the upper limb and the net dynamic moments required at each of the joints to complete the given motion. The complex three-dimensional motion that occurs in normal human movement between the joints can now be analysed using the dynamic model.

As an example of the ability of the dynamic model to analyze a complex movement and provide the information necessary to predict injury risk, two industrial scenarios were simulated. The first simulation involves picking an object up off the surface of a table and placing it in a box, which is sitting on top of the table. The second situation is picking up the same object and placing it in a box where the top edge of the box is level with the tabletop. The subject being used in these simulations is a female with a height of 1.4732 meters (4ft-10in) and weight of 55 kilograms (121.3lbs). The object weighs 1.0 kilogram (2.2lbs), the table is 1 meter (39in) long by 0.5 meters (20in) wide by 0.864 meters (34in) high, and the box is 0.251 meters (10in) high.

The three-dimensional elbow and shoulder moments are made available for analysis by the dynamic simulation. From Figures 4.23 and 4.24, both on page 118, it is apparent that the most dramatic change related to the lowering of the position of the box occurs in the decrease of the shoulder and elbow moments. As demonstrated in the preceding section of the discussion, the anatomical elbow model can be used to determine the individual muscle forces from the dynamic joint moment. Figure 4.25 (page 119) shows the individual forces calculated for the elbow muscles when placing the object in the box sitting on the surface of the table. The individual muscle forces across the elbow joint are displayed in Figure 4.26 (page 120) for the simulation of putting the object in the box when it is level with the tabletop. From these two figures, it can be seen that the muscle forces, like the joint moment, decrease dramatically when the box is lowered. Thus the risk of repetitive strain injuries to the muscles and joint structures of the elbow are reduced by an improved workstation design. When the vector approach is developed for the musculature of the shoulder and individual muscle forces are predicted, the reduction in muscle forces can then be associated with proper workstation design.

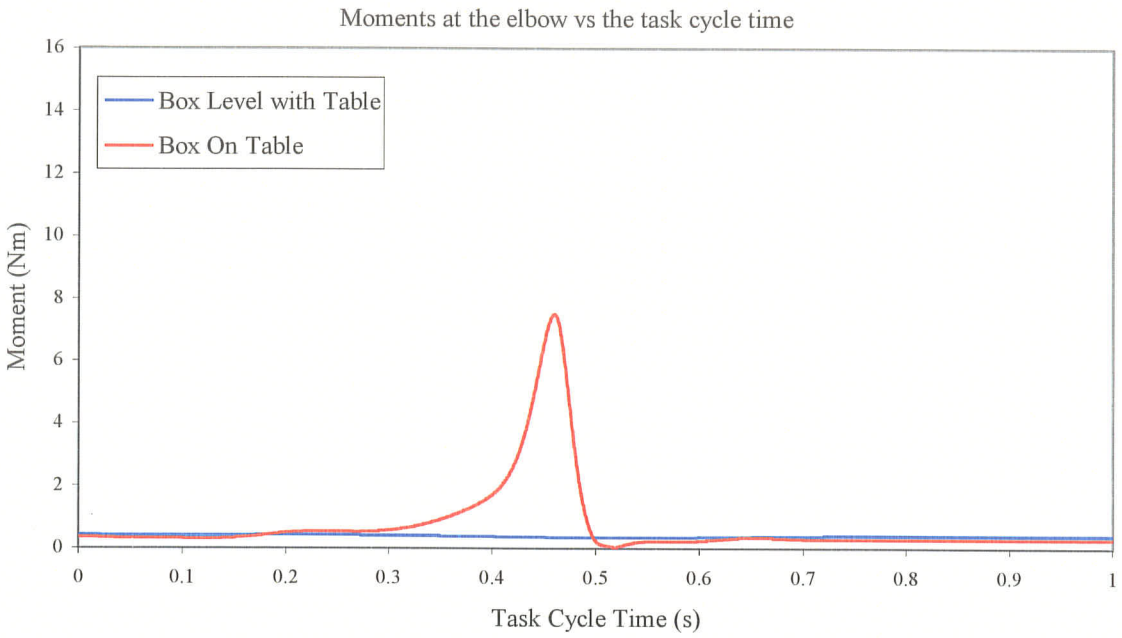

Figure 4.23 Elbow Joint Moments, Object in Box Simulations

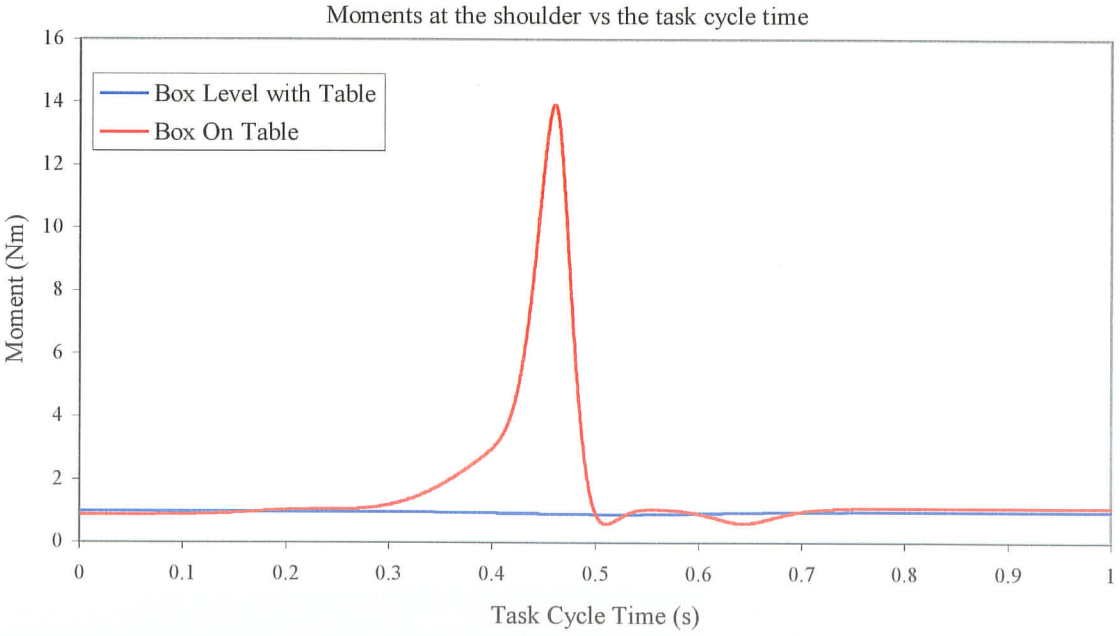

Figure 4.24 Shoulder Joint Moments, Object in Box Simulations

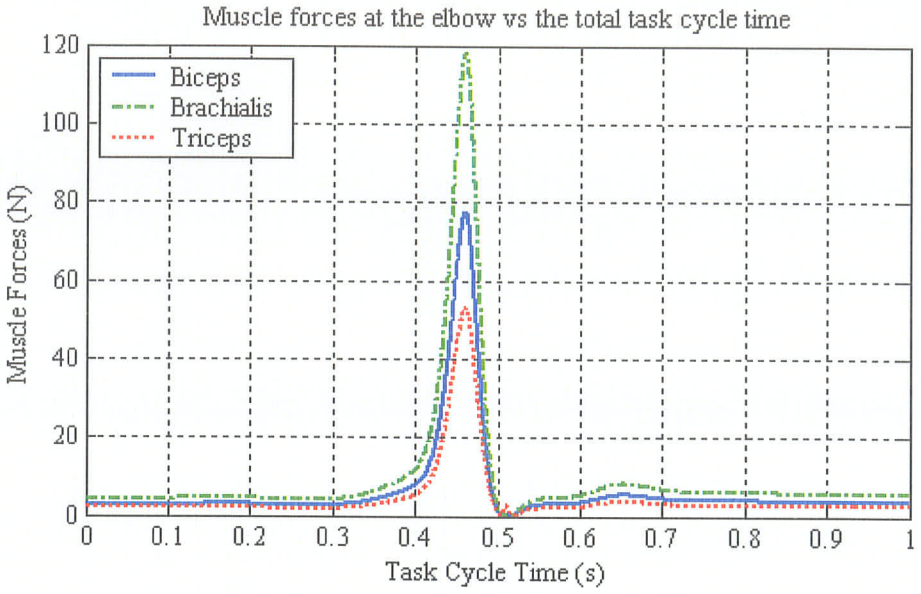

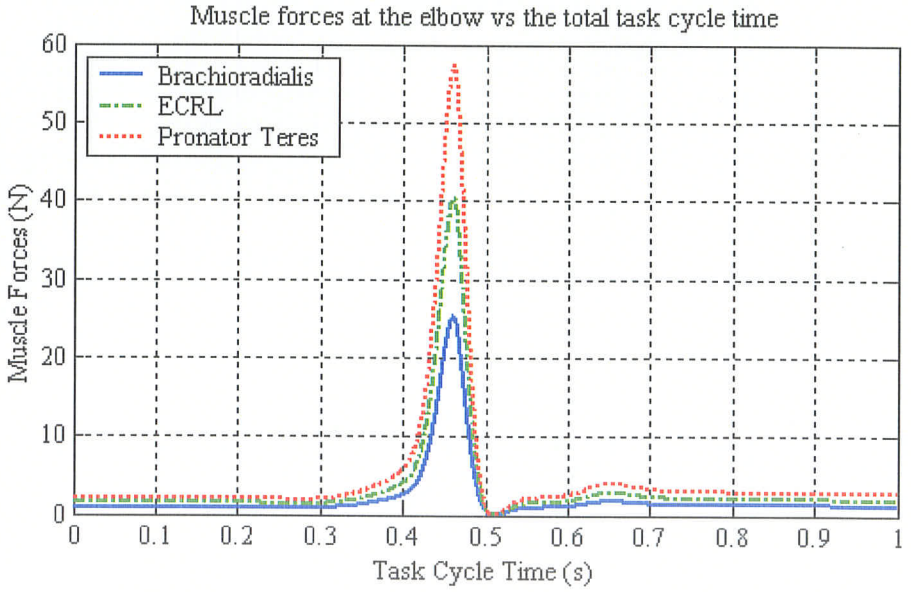

Figure 4.25 Individual Muscle Forces at Elbow,
Object in Box On Table Simulation

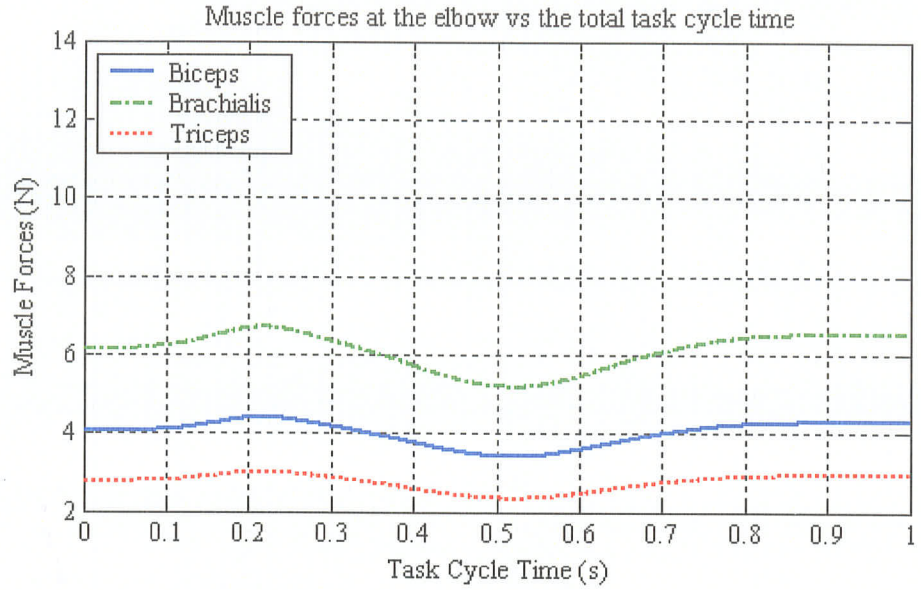

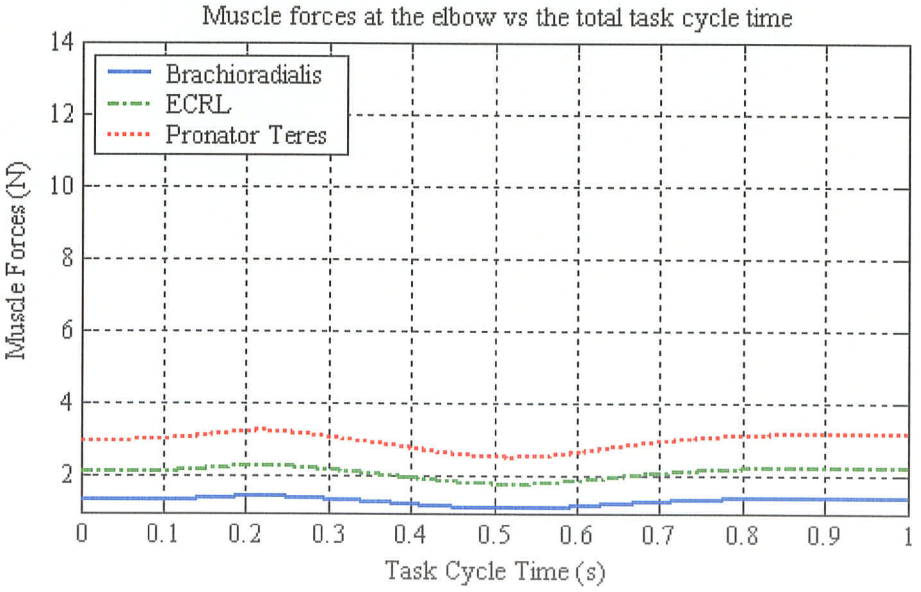

Figure 4.26 Individual Muscle Forces at the Elbow
Object in Box Level With Table Simulation

4.6 Summary

To develop successful anatomical correlations for the scaling of bone anatomy it was necessary to have anatomical specimen data that were related to the standard population height and weight distribution. Very few anatomical studies found in the literature had been related in such a way. Using limited data and a best curve fit analysis, scaling correlations of several types were found. Some correlations were linear and some curvilinear, while others were exponential or logarithmic. The correlations developed here were shown to be valid by using a small subject and comparing the model results to those of a much larger subject. The results showed that the correlations were indeed valid in that the relative values of the individual forces in the muscles remained constant under scaling and the general shape of the force curves remained the same.

Essential to the calculation of individual muscle forces is the determination of the moment arms of each of the muscle over the full range of joint motion. It was shown here, through the use of a three-dimensional vector formulation, that the three-dimensional moment arms could be approximated once the muscle line of action and the vector positions of the origin and insertion points of the muscle relative to the joint centre of rotation were known. These computed three-dimensional moment arms were compared to the moment arms calculated for the same muscles in the literature. The comparison showed that the vector determination of muscle moment arms displayed the same general behaviour as the moment arms found in the literature. Differences between those found in the literature and those calculated here can be attributed to the fact that a

multiplicity of different techniques was used in the literature studies. By virtue of being predominantly two-dimensional studies, many of the moment arms reported in the literature would be expected to differ slightly from those reported here.

Having the three-dimensional vector technique properly developed for the calculation of moments and moment arms, through the use of vector dot and cross products, the total force, F_T, of the muscle group considered could be obtained from the moment equations. To perform these calculations, an activation strategy was selected. The activation strategy gives an equation showing the relationship between the total force and the degree of activation of each muscle in the group. Different activation strategies would yield different individual muscle forces. The selection of the constant activation level per unit cross-sectional area of all muscles in the functional group was chosen. Force curves were generated from dynamic joint moment data supplied by the dynamic simulation program. The relative position of muscle forces computed was found to be consistent with early electromyography studies by Basmajian and Latif (1957) and other research groups. It was thus shown that the three-dimensional vector model and the activation strategy were valid as the results were consistent with the experiments in the literature. Simulations with pronation and supination of the forearm as well as for the neutral position also showed changes in individual muscle forces consistent with the literature.

The general shapes of the moment arm and force curves were consistent with the results reported in the literature. However, if any methodological errors were made the flexor and extensor mechanical energies were likely to differ under circumstances where they

should not. A situation in which quasi-static and dynamic moments in flexion and extension should exhibit the same mechanical energy over a task cycle were indeed similar. The energy balance was shown to occur to within 2.99% for the best cases in the neutral and supinated forearm positions to within 13.03% in the best case with the forearm pronated. It was determined that even though there must be some errors in the anatomical scaling and moment arm calculations, and that these errors would differ between the extensor and flexor muscle groups, the energy balance error of 2.99% indicates that the three-dimensional vector approach is quite acceptable as a method of determining muscle forces.

By determining the individual muscle forces and their changes in length during a task cycle, the energy throughput for each muscle during the task could also be calculated. Once the force in the muscle was calculated for each incremental position and because the time increments were known, it was possible to approximate the biological energy consumption required to accomplish a task. Since the biological efficiency is not generally known, a factor of 0.5 was used to demonstrate the calculation methodology. The biological consumption of energy would seem to be greater than the mechanical work done. Therefore, the total energy consumed during a task would be the sum of the mechanical work done performing the task plus the biological energy consumed in maintaining the forces within the muscles. Finally, the application of the vector joint model to a specific task was included to demonstrate the usefulness and importance of the techniques developed here.

A review of this chapter demonstrates that contributions in the development of theory and application were made in four key areas. In the first area, scaling, new correlations were developed to relate bone and muscle anatomy with human subject height and weight. In the area of functional anatomy, three-dimensional vector models of joints and muscles were developed to determine muscle moment arms. For the calculation of individual muscle forces, a vector model utilizing the net dynamic joint moments was developed. Finally, a muscle activation strategy was proposed, thus allowing the individual muscle forces to be resolved.

The work done in this thesis allows the determination of individual muscle forces during an activity. The muscle forces are dependent on the motion of the arm segments in space. Since the path and geometric arrangement of the limb segments is constrained by the arrangement of a workstation, the muscle forces for a task will change with the workstation layout and design. As the workstation design is changed, the forces in the muscles crossing the elbow joint will change due to the new limb segment geometries necessary to pick-up and move objects without contacting other objects. The workstation geometry that minimizes muscle force will be least likely to result in repetitive strain injuries to the joint structures and muscles. Iterations in workstation designs and individual muscle forces required to use the designs can therefore reduce risk of injury.

The results also show that if the forearm is required to be in the fully pronated position, only four of the five main flexors are active. Thus, the organization of work tasks should avoid the pronated position as it causes higher forces in the remaining four flexors for the

same task performed with the forearm in the neutral or supinated position. In addition, when the net moments entered into the anatomical elbow model are such that the dynamic effects are included, the speed of work is related to the individual muscle forces. These dynamic components of the joint moments result in high accelerations of the limb segments for shortened task cycle times and thus generating high muscle forces.

CHAPTER 5

CONCLUSIONS

5.1 Conclusions

In this thesis, a three-dimensional vector model to predict the individual muscle forces across the elbow joint was developed. To apply the model to various subjects it became apparent that there were four necessary theoretical developments. First, correlations had to be developed to associate the bone and muscle anatomy to the height and weight of a human subject. These correlations had to be shown to be valid, which is to say large differences in the form of the muscle force curves were not introduced by scaling. Three-dimensional muscle moment arms had to be determined over the full range of elbow joint motion. The moment arms had to be shown to behave in a manner similar to the results of previous studies in the literature. Given the three-dimensional moment arms, a suitable muscle activation strategy had to be developed. The activation strategy is then used to allow the total force to be apportioned properly to the individual muscles. Finally, the individual muscle forces had to be resolved from the net dynamic joint moments. A method to determine the energy associated with each muscle was then developed. This energy is used to confirm that the general form of the muscle force calculation was appropriate for the simulated tasks. Overall, the anatomical elbow model developed in this thesis has the potential to allow for better diagnostics as to the relative risk of repetitive strain injuries.

From the detailed analysis of the four main advancements outlined above, we can draw the following conclusions:

- The scaling correlations for bone anatomy and muscle origins and insertions have been developed. They have been shown to be essential in allowing the three-dimensional vector method to be applied over all subject sizes for muscle force predictions.
- The various scaling correlations shown in Appendix B, were found to be linear, curvilinear, and non-linear in nature, depending on the bone anatomical parameter being scaled.
- Having developed the scaling correlations from a small set of literature data, more extensive data is needed to further confirm their validity. We do know, however, that the scaling functions presented here maintain the usual functionality of the individual muscles.
- Three-dimensional vector models can be used to calculate the moment arms for the flexor and extensor muscles crossing the elbow joint.
- The moment arms of the muscles crossing the elbow joint must take into consideration the self-rotation of the forearm.
- The muscle moment arms determined using the three-dimensional vector method were consistent with the general two-dimensional patterns of moment arms found in the literature.
- The vector model of the moments about the elbow joint when used with a muscle activation strategy, allow the resolution of individual muscle forces. If the activation strategy is changed, the individual muscle forces will also change.

- The forces in the individual muscles of the flexor and extensor functional groups can be mathematically calculated when the dynamic moment about the elbow joint and muscle moment arms are known.
- The vector model was demonstrated to be capable of including the effects of pronation and supination of the forearm and showed the appropriate changes in the individual muscle forces.
- The muscle forces were found to be consistent with the patterns established using electromyographic studies.
- The individual muscle forces determined with a large dynamic moment component were found to be approximately four times the muscle forces for the quasi-static situation.
- The relationship between the agonist and antagonist muscle forces are found to be related properly to muscle forces by verifying the presence of a mechanical energy balance. The mechanical energy balance was found to range from a difference of 2.99% in the best case for supination and neutral forearm positions to 13.03% in the best case for pronation.
- The mechanical energy balance further validates the methodology behind the individual muscle force and change in muscle length calculations.
- The three-dimensional vector model developed is valid in both quasi-static and dynamic situations.
- Knowing the individual muscle force pattern for the general activation strategy, the muscles at greatest risk for repetitive strain injuries can be predicted. The energy per unit cross-section put through a muscle has been associated with fatigue and is

therefore also an indicator of repetitive strain injury risk level and can thus be computed.

5.2 Recommendations for Future Work

The results of this thesis represent an important initial step in the development of anatomical models for the prediction of individual muscle forces and assessing the risk of repetitive strain injuries. The findings also indicate that there are several areas in which future work should continue. Further anatomical studies need to be carried out to improve the accuracy of the current scaling correlations. These new anatomical studies must relate the data collected to the height and weight of the individual subject to be of any use in a vector model such as the one presented here. Different muscle activation strategies should be investigated using the current model. A strategy wherein the fatigue of the prime mover occurs and the other muscles of the functional group are forced to compensate would be a very valuable addition with respect the estimation of repetitive strain injuries. In addition, the interplay between the muscles both within a functional group and between the agonist and antagonist groups needs to be examined further. Finally, a full analysis of the musculature of the shoulder, including the scapular stabilizing muscles, and the back muscles should be undertaken using the theory developed in this thesis. By including these anatomical models with the current dynamic simulation, the strength of this tool in the prediction of repetitive strain injury risk associated with workstation design will greatly increase.

BIBLIOGRAPHY

Ait-Haddou, R., Binding, P., and Herzog, W. (2000). **Theoretical Considerations on Cocontraction of Sets of Agonistic and Antagonistic Muscles.** *Journal of Biomechanics, 33,* p. 1105-1111.

Amis, A.A., Dowson, D., and Wright, V. (1979). **Muscle Strengths and Musculo-Skeletal Geometry of the Upper Limb.** *Engineering In Medicine, 8(1),* p. 41-48.

Amis, A.A., Dowson, D., and Wright, V. (1980). **Elbow Joint Force Predictions For Some Strenuous Isometric Actions.** *Journal of Biomechanics, 13,* p. 765-775.

An, K.N., Chao, E.Y., Cooney, W.P., and Linscheid, R.L. (1985). **Forces in the Normal and Abnormal Hand.** *Journal of Orthopaedic Research, 3,* p. 202-211.

An, K.N., Hui, B.F., Morrey, R.L., Linscheid, R.L., and Chao, E.Y. (1981). **Muscles Across the Elbow Joint: A Biomechanical Analysis.** *Journal of Biomechanics, 14(10),* p.659-669.

An, K.N., Kaufman, K.R., and Chao, E.Y.S. (1989). **Physiological Considerations of Muscle Force Through the Elbow Joint.** *Journal of Biomechanics, 22(11/12),* p. 1249-1256.

An, K.N., Kwak, B.M., Chao, E.Y., and Morrey, B.F. (1984a). **Determination of Muscle and Joint Forces: A New Technique to Solve the Indeterminate Problem.** *Journal of Biomechanical Engineering, 106(4),* p. 364-367.

An, K.N., Morrey, B.F., and Chao, E.Y. (1985). **Kinematics of the Elbow.** In *Biomechanics IX-A* (Edited by Winter, D.A., Norman, R.W., Wells, R.P., Hayes, K.C., and Patla, A.E.) p. 154-159. Human Kinetics Publishers, Illinois.

An, K.N., Takahashi, K., Harrigan, T.P., and Chao, E.Y. (1984b). **Determination of Muscle Orientations and Moment Arms.** *Journal of Biomechanical Engineering, 106,* p. 280-282.

Andrews, J.G., and Hay, J.G. (1983). **Biomechanical Considerations in the Modeling of Muscle Function.** *Acta-Morphol-Neerl-Scand, 21(3),* p. 199-223.

Basmajian, J.V. (1969). **Recent Advances in the Functional Anatomy of the Upper Limb.** *American Journal of Physical Medicine, 48(4),* p. 165-177.

Basmajian, J.V., and DeLuca, C.J. (1985). **Muscles Alive, Their Functions Revealed by Electromyography, 5th ed.** Williams and Williams, Baltimore.

Basmajian, J.V., and Griffin, W.R. (1972). **Function of Anconeus Muscle: An Elecromyographic Study.** *Journal of Bone and Joint Surgery, 54A,* p. 1712-1714.

Basmajian, J.V., and Latif, A. (1957). **Integrated Actions and Functions of the Chief Flexors of the Elbow: A Detailed Electromyographic Analysis.** *Journal of Bone and Joint Surgery, 39A,* p. 1106-1118.

Basmijian, J.V., and Travill, A. (1961). **Electromyography of the Pronator Muscles in the Forearm.** *The Anatomical Record, 139,* p. 45-49.

Bilodeau, M., Arsenault, A.B., Gravel, D., and Bourbonnais, D. (1994). **EMG Power Spectrum of Elbow Extensors: A Reliability Study**. *Electromyography and Clinical Neurophysiology, 34,* p. 149-158.

Brand, R.A., Pedersen, D.R., and Friederich, J.A. (1986). **The Sensitivity of Muscle Force Predictions to Changes in Physiologic Cross-Sectional Area**. *Journal of Biomechanics, 19(8),* p.589-596.

Chandler, R.F., Clauser, C.E., McConville, J.T., Reynolds, H.M., and Young, J.W. (1975). **Investigation of Inertial Properties of the Human Body.** *Aerospace Medical Research Laboratory, Wright-Patterson Air Force Base, AMRL-TR-74-137.*

Chang, Y.W., Su, F.C., Wu, H.W., and An, K.N. (1999). **Optimum Length of Muscle Contraction.** *Clinical Biomechanics, 14,* p. 537-542.

Chao, E.Y. and Morrey, B.F. (1978). **Three-Dimensional Rotation of the Elbow**. *Journal of Biomechanics, 11,* p. 57-73.

Charlton, I.W., and Johnson, G.R. (2001). **Application of Spherical and Cylindrical Wrapping Algorithms in a Musculoskeletal Model of the Upper Limb.** *Journal of Biomechanics, 34,* p. 1209-1216.

Clauser, C.E., McConville, J.T., and Young, J.W. (1969). **Weight, Volume, and Center of Mass of Segments of the Human Body.** *Aerospace Medical Research Laboratory, Wright-Patterson Air Force Base, AMRL-TR-69-70.*

Cnockaert, J.C., Lensel, G., and Pertuzon, E. (1976). **Les synergies musculaires dans la flexion isométrique du coude.** *Seances de la Société de Biologie de Lille, 170(3),* p. 606-614.

Crowninshield, R.D., and Brand, R.A. (1981). **A Physiologically Based Criterion of Muscle Force Prediction in Locomotion.** *Journal of Biomechanics, 14(11),* p. 793-801.

Cutts, A. and Seedholm, B.B. (1993). **Validity of Cadaveric Data for Muscle Physiological Cross-Sectional Area Ratios: A Comparative Study of Cadaveric and In-Vivo Data in Human Thigh Muscles.** *Clinical Biomechanics, 8,* p. 156-162.

de Leva, P. (1996). **Adjustments to Zatsiorsky – Seluyanov's Segment Inertia Parameters.** *Journal of Biomechanics, 29(9),* p. 1223-1230.

de Leva, P. (1996). **Joint Center Longitudinal Positions Computed From A Selected Subset of Chandler's Data.** *Journal of Biomechanics, 29(9),* p. 1231-1233.

de Sousa, O.M., de Moraes, J.L., and de Morais Vieira, F.L. (1961). **Electromyographic Study of the Brachialis Muscle.** *The Anatomic Record, 139,* p. 125-131.

Delp, S.L., Grierson, A.E., and Buchanan, T.S. (1996). **Maximum Isometric Moments Generated by the Wrist Muscles in Flexion-Extension and Radial-Ulnar Deviation.** *Journal of Biomechanics, 29(10),* p. 1371-1375.

Dhaher, Y.Y., Delp, S.L., and Rymer, W.Z. (2000). **The Use of Basis Functions in Modelling Joint Articular Surfaces: Application to the Knee Joint.** *Journal of Biomechanics, 33,* p. 901-907.

Diffrient, N., Tilley, A.R., and Bardagjy, J.C. (1974). **Humanscale 1/2/3.** The MIT Press, Cambridge, MA.

Dowling, J.J. (1987). **The Prediction of Force in Individual Muscles Crossing the Human Elbow Joint.** Ph.D. Thesis, Dept. of Kinesiology, University of Waterloo.

Dowling, J.J., and Cardone, N. (1994). **Relative Cross-Sectional Areas of Upper and Lower Extremity Muscles and Implications for Force Prediction.** *International Journal of Sports Medicine, 15(8),* p. 453-459.

Dul, J., Johnson, G.E., Shiavi, R., and Townsend, M.A. (1984a). **Muscular Synergism – II. A Minimum-Fatigue Criterion for Load Sharing Between Synergistic Muscles.** *Journal of Biomechanics, 17(9),* p. 675-684.

Dul, J., Townsend, M.A., Shiavi, R., and Johnson, G.E. (1984b). **Muscular Synergism – I. On Criteria for Load Sharing Between Synergistic Muscles.** *Journal of Biomechanics, 17(9),* p. 663-673.

Edgerton, V.R., Roy, R.R., and Apor, P. (1986). **Specific Tension of Human Elbow Flexor Muscles.** *Biochemistry of Exercise VI, 16,* p. 487-500.

Ettema, G.J.C., Styles, G., and Kippers, V. (1998). **The Moment Arms of 23 Muscle Segments of the Upper Limb with Varying Elbow and Forearm Positions: Implications for Motor Control.** *Human Movement Science, 17(2),* p. 201-220.

Forwood, M.R., Neal, R.J., and Wilson, B.D. (1985). **Scaling Segmental Moments of Inertia for Individual Subjects.** *Journal of Biomechanics, 18(10),* p. 755-761.

Freund, J., and Takala, E.-P. (2001). **A Dynamic Model of the Forearm Including Fatigue.** *Journal of Biomechanics, 34(5),* p. 597-605.

Frigo, C., and Pedotti, A. (1978). **Determination of Muscle Length During Locomotion.** In *Biomechanics VI-A* (Edited by Asmussen, E., and Jorgensen, K.) p. 355-360. University Park Press, Baltimore.

Funk, D.A., An, K.N., Morrey, B.F., and Daube, J.R. (1987). **Electromyographic Analysis of Muscles Across the Elbow Joint.** *Journal of Orthopaedic Research, 5(4),* p. 529-538.

Gerbeaux, M., Turpin, E., and Lensel-Corbeil, G. (1996). **Musculo-Articular Modelling of the Triceps Brachii.** *Journal of Biomechanics, 29,* p. 171-180.

Gonzalez, R.V., Buchanan, T.S., and Delp, S.L. (1997). **How Muscle Architecture and Moment Arms Affect Wrist Flexion-Extension Moments.** *Journal of Biomechanics, 30(7),* p. 705-712.

Gonzalez, R.V., Hutchins, E.L., Barr, R.E., and Abraham, L.D. (1996). **Development and Evaluation of a Musculoskeletal Model of the Elbow Joint Complex.** *Journal of Biomechanical Engineering, 118(1),* p. 32-40.

Hayes, K.C., and Hatze, H. (1977). **Passive Visco-Elastic Properties of the Structure Spanning the Human Elbow Joint.** *European Journal of Applied Physiology and Occupational Physiology, 37,* p. 265-274.

Herzog, W. (1996). **Force-Sharing Among Synergistic Muscles: Theoretical Considerations and Experimental Approaches.** *Exercise Sport Sciences Reviews, 24,* p. 173-203.

Hof, A.L. (2001). **The Force Resulting From the Action of Mono- and Biarticular Muscles in a Limb.** *Journal of Biomechanics, 34,* p. 1085-1089.

Högfors, C., Sigholm, G., and Herberts, P. (1987). **Biomechanical Model of the Human Shoulder – I. Elements.** *Journal of Biomechanics, 20(2),* p. 157-166.

Hutchins, E.L., Gonzalez, R.V., and Barr, R.E. (1993). **Comparison of Experimental and Analytical Torque-Angle Relationships of the Human Elbow Joint Complex.** *Biomedical Science Instrumentation, 29,* p. 17-24.

Ishizuki, M. (1979). **Functional Anatomy of the Elbow Joint and Three-Dimensional Quantitative Motion Analysis of the Elbow Joint.** *Journal of the Japanese Orthopaedic Association, 53(8),* p. 989-996.

Jensen, R.H., and Davy, D.T. (1975). **An Investigation of Muscle Lines of Action About the Hip: A Centroid Line Approach vs. the Straight Line Approach.** *Journal of Biomechanics, 8,* p. 103-110.

Kaleps, I., Clauser, C.E., Young, J.W., Chandler, R.F., Zehner, G.F., and McConville, J.T. (1984). **Investigation into the Mass Distribution Properties of the Human Body and its Segments.** *Ergonomics, 27(12),* p. 1225-1237.

Karlsson, D. and Peterson, B. (1992). **Towards a Model for Force Predictions in the Human Shoulder.** *Journal of Biomechanics, 25(2),* p.189-199.

Kaufman, K.R., An, K.N., and Chao, E.Y.S. (1989). **Incorporation of Muscle Architecture into the Muscle Length-Tension Relationship**. *Journal of Biomechanics, 22(8/9)*, p. 943-948.

Kaufman, K.R., An, K.N., Litchy, W.J., and Chao, E.Y.S. (1991a). **Physiological Prediction of Muscle Forces – I. Theoretical Formulation.** *Neuroscience, 40(3)*, p. 781-792.

Kaufman, K.R., An, K.N., Litchy, W.J., and Chao, E.Y.S. (1991b). **Physiological Prediction of Muscle Forces – II. Application to Isokinetic Exercise**. *Neuroscience, 40(3)*, p. 793-804.

Kawakami, Y., Nakazawa, K., Fujimoto, T., Nozaki, D., Miyashita, M., and Fukunaga, T. (1994). **Specific Tension of Elbow Flexor and Extensor Muscles Based on Magnetic Resonance Imaging.** *European Journal of Applied Physiology and Occupational Physiology, 68*, p. 139-147.

Koolstra, J.H., van Eijden, T.M.G.J., and Weijs, W.A. (1989). **An Iterative Procedure to Estimate Muscle Lines of Action *In Vivo***. *Journal of Biomechanics, 22(8/9)*, p. 911-920.

Leiber, R.L., Jacobson, M.D., Fazeli, B.M., Abrams, R.A., and Botte, M.J. (1992). **Architecture of Selected Muscles of the Arm and Forearm: Anatomy and Implications for Tendon Transfer**. *The Journal of Hand Surgery (American Volume), 17A(5)*, p. 787-798.

London, J.T. (1981). **Kinematics of the Elbow**. *Journal of Bone and Joint Surgery, 63A(4)*, p.529-535.

Maurel, W., Thalmann, D., Hoffmeyer, P., Beylot, P., Gingins, P., Kalra, P., and Magnenat Thalmann, N. (1996). **A Biomechanical Musculoskeletal Model of Human Upper Limb For Dynamic Simulation**. *7th Eurographics International Workshop on Computer Animation and Simulation*, p. 121-136.

Maurel, W., and Thalmann, D. (1999). **A Case Study on Human Upper Limb Modelling for Dynamic Simulation.** *Computer Methods in Biomechanics and Biomedical Engineering, 1(2)*, p. 1-17.

Moore, K.L. and Dalley, A.F. (1999). **Clinically Oriented Anatomy, 4th ed.** Lippincott, Williams & Wilkins, Baltimore.

Morrey, B.F. and Chao, E.Y.S. (1976). **Passive Motion of the Elbow Joint: A Biomechanical Analysis**. *Journal of Bone and Joint Surgery, 58A(4)*, p. 501-508.

Murray, W.M. (1997). **The Functional Capacity of the Elbow Muscles: Anatomical Measurements, Computer Modeling, and Anthropometric Scaling.** Ph.D. Thesis, Dept. of Biomedical Engineering, Northwestern University.

Murray, W.M., Buchanan, T.S., and Delp, S.L. (2000). **The Isometric Functional Capacity of Muscles That Cross the Elbow.** *Journal of Biomechanics, 33,* p. 943-952.

Murray, W.M., Delp, S.L., and Buchanan, T.S. (1995). **Variation of Muscle Moment Arms With Elbow and Forearm Position.** *Journal of Biomechanics, 28(5),* p. 513-525.

Norkin, C.C. and Levangie, P.K. (1992). **Joint Structure & Function: A Comprehensive Analysis, 2nd ed.** F.A. Davis Company, Philadelphia.

Pauly, J.E., Rushing, J.L., and Scheving, L.E. (1967). **An Electromyographic Study of Some Muscles Crossing the Elbow Joint.** *The Anatomical Record, 159(1),* p. 47-53.

Pearsall, D.J., and Reid, J.G. (1994). **The Study of Human Body Segment Parameters in Biomechanics**. *Sports Medicine, 18(2),* p. 126-140.

Pertuzon, E., and Lestienne, F. (1973). **Détermination dynamique de la position d'équilibre d'une articulation.** *Int. Z. angew. Physiol., 31,* p. 315-325.

Pigeon, P., Yahia, L., and Feldman, A.G. (1996). **Moment Arms and Lengths of Human Upper Limb Muscles as Functions of Joint Angles**. *Journal of Biomechanics, 29(10),* p. 1365-1370.

Raikova, R. (1992). **A General Approach for Modelling and Mathematical Investigation of the Human Upper Limb**. *Journal of Biomechanics, 25(8),* p. 857-867.

Raikova, R. (1996). **A Model of the Flexion-Extension Motion in the Elbow Joint – Some Problems Concerning Muscle Forces Modelling and Computation.** *Journal of Biomechanics, 29(6),* p. 763-772.

Raikova, R. (1999). **About Weight Factors in the Non-Linear Objective Functions Used for Solving Indeterminate Problems in Biomechanics.** *Journal of Biomechanics, 32,* p. 689-694.

Rasmussen, J., Damsgaard, M., and Voight, M. (2001). **Muscle Recruitment by the Min/Max Criterion – A Comparative Numerical Study.** *Journal of Biomechanics, 34,* p. 409-415.

Seireg, A., and Arvikar, R. (1989). **Biomechanical Analysis of the Musculoskeletal Structure for Medicine and Sports.** Hemisphere Publishing Corporation, New York.

Sergio, L.E. and Ostry, D.J. (1995). **Coordination of Multiple Muscles in Two Degree of Freedom Elbow Movements.** *Experimental Brain Research, 105,* p. 123-137.

Soechting, J.F., and Flanders, M. (1997). **Evaluating an Integrated Musculoskeletal Model of the Human Arm.** *Journal of Biomechanical Engineering, 119,* p. 93-102.

Solomonow, M., Baratta, R., Zhou, B.H., and D'Ambrosia, R. (1988). **Electromyogram Coactivation Patterns of the Elbow Antagonist Muscles During Slow Isokinetic Movement.** *Experimental Neurology, 100,* p. 470-477.

Sommer, H.J., Miller, N.R., and Pijanowski, G.J. (1982). **Three-Dimensional Osteometric Scaling and Normative Modelling of Skeletal Segments.** *Journal of Biomechanics, 15(3),* p. 171-180.

Teitz, C., and Graney, D. **Musculoskeletal Atlas: A Musculoskeletal Atlas of the Human Body.** University of Washington – Seattle, School of Medicine. *http://eduserv.hscer.washington.edu/hubio553/atlas/index.html.*

Thornton-Trump, A.B. (2002). **Reduction of Repetitive Strain Injuries Using Computer Simulation.** Biomechanics Research Laboratory Report, Dept. of Mechanical and Industrial Engineering, University of Manitoba.

Travill, A.A. (1962). **Electromyogrphic Study of the Extensor Apparatus of the Forearm.** *The Anatomical Record, 144,* p. 373-376.

van der Helm, F.C.T. (1994). **A Finite Element Musculoskeletal Model of the Shoulder Mechanism.** *Journal of Biomechanics, 27(5),* p.551-569.

van Zuylen, E.J., van Velzen, A., and Denier van der Gon, J.J. (1988). **A Biomechanical Model for Flexion Torques of Human Arm Muscles as a Function of Elbow Angle.** *Journal of Biomechanics, 21(3),* p. 183-190.

Veeger, H.E.J., and Yu, B. (1996). **Orientation of Axes in the Elbow and Forearm for Biomechanical Modelling.** In *XVth Biomedical Engineering Society Conference* (Edited by Bajpai, J.), p. 377-380. Dayton, Ohio.

Veeger, H.E.J., Yu, B., and An, K.N. (1997a). **Orientation of Axes in the Elbow and Forearm for Biomechanical Modelling.** In *First Conference of the International Shoulder Group* (Edited by Veeger, H.E.J., van der Helm, F.C.T., and Rozing, P.M.), p. 83-88. Delft: Shaker Publishers, Maastricht.

Veeger, H.E.J., Yu, B., An, K.N., and Rozendal, R.H. (1997b). **Parameters for Modeling the Upper Extremity**. *Journal of Biomechanics, 30(6),* p. 647-652.

Waters, P. and Strick, P.L. (1981). **Influence of "Strategy" on Muscle Activity During Ballistic Movements.** *Brain Research, 207,* p. 189-194.

Winters, J.M, and Kleweno, D.G., (1993). **Effect of Inertial Upper-Limb Alignment on Muscle Contributions to Isometric Strength Curves.** *Journal of Biomechanics, 26(2),* p. 143-153.

Winters, J.M., and Woo, S.L.-Y. (1990). **Multiple Muscle Systems: Biomechanics and Movement Organization.** Springer-Verlag, New York.

Wood, J.E., Meek, S.G., and Jacobsen, S.C. (1989). **Quantitation of Human Shoulder Anatomy for Prosthertic Arm Control – I. Surface Modelling.** *Journal of Biomechanics, 22(3),* p. 273-292.

Wood, J.E., Meek, S.G., and Jacobsen, S.C. (1989). **Quantitation of Human Shoulder Anatomy for Prosthetic Arm Control – II. Anatomy Matrices.** *Journal of Biomechanics, 22(4),* p. 309-325.

Yeo, B.P. (1976). **Investigations Concerning the Principle of Minimal Total Muscular Force.** *Journal of Biomechanics, 9,* p. 413-416.

Youm, Y., Dryer, R.F., Thambyrajah, K., Flatt, A.E., and Sprague, B.L. (1979). **Biomechanical Analyses of Forearm Pronation-Supination and Elbow Flexion-Extension**. *Journal of Biomechanics, 12,* p. 245-255.

Zajac, F.E. (1989). **Muscle and Tendon: Properties, Models, Scaling, and Application to Biomechanics and Motor Control.** *Critical Reviews in Biomedical Engineering, 17(4),* p. 359-411.

Zatsiorsky, V., and Seluyanov, V. (1983). **The Mass and Inertia Characteristics of the Main Segments of the Human Body**. In *Biomechanics VIII-B* (Edited by Matsui, H., and Kobayashi, K.) p. 1152-1159. Human Kinetics Publishers, Illinois.

Zatsiorsky, V., and Seluyanov, V. (1985). **Estimation of the Mass and Inertia Characteristics of the Human Body by Means of the Best Predictive Regression Equations**. In *Biomechanics IX-B* (Edited by Winter, D.A., Norman, R.W., Wells, R.P., Hayes, K.C., and Patla, A.E.) p. 233-239. Human Kinetics Publishers, Illinois.

APPENDIX A

ANATOMICAL ELBOW MODEL

Appendix A contains a listing of the anatomical elbow model program code written in MatLab, version 6.0.0.88, release 12. The percent symbol, %, preceding a line denotes a comment line, any following text is ignored.

```
% Sub - program to determine the individual muscle moment arms, forces and energies.

function elbow_mforce_right

% Read elbow angle and moment into the variable m_elbow.

fid = fopen('moment_elbow_right.txt','r');
[elbow_moment,count] = fscanf(fid,'%g %e %e %e %e %e',[6 inf]);
elbow_moment = elbow_moment';
m = count / 6;

% Create files for storing data.

fid = fopen('e_momentarm_right.txt','w+');
fid = fopen('e_force_right.txt','w+');
fid = fopen('e_mechenergy_right.txt','w+');
fid = fopen('e_bioenergy_right.txt','w+');
fid = fopen('e_totalenergy_right.txt','w+');

% Initialize variables for energy calculations.

time_old = 0;
f_bic2 = 0;
f_brach2 = 0;
f_brad2 = 0;
f_ecrl2 = 0;
f_pt2 = 0;
f_tri2 = 0;
bic_mech_nrg = 0;
brach_mech_nrg = 0;
brad_mech_nrg = 0;
ecrl_mech_nrg = 0;
pt_mech_nrg = 0;
tri_mech_nrg = 0;
bic_bio_nrg = 0;
brach_bio_nrg = 0;
brad_bio_nrg = 0;
ecrl_bio_nrg = 0;
pt_bio_nrg = 0;
tri_bio_nrg = 0;
bic_tot_nrg = 0;
brach_tot_nrg = 0;
brad_tot_nrg = 0;
ecrl_tot_nrg = 0;
pt_tot_nrg = 0;
tri_tot_nrg = 0;

% Muscle coordinate input variables.

global BIC_O BIC_I BRACH_O BRACH_I BRAD_O BRAD_I ECRL_O ECRL_I PT_O PT_I
TRI_O TRI_I TROCH_CENTER CAPI_CENTER RAD_CENTER DIST_ULNA
```

```
bic_origin = BIC_O;
bic_insert = BIC_I;
brach_origin = BRACH_O;
brach_insert = BRACH_I;
brad_origin = BRAD_O;
brad_insert = BRAD_I;
ecrl_origin = ECRL_O;
ecrl_insert = ECRL_I;
pt_origin = PT_O;
pt_insert = PT_I;
tri_origin = TRI_O;
tri_insert = TRI_I;
center_trochlea = TROCH_CENTER;
center_capitulum = CAPI_CENTER;
center_rad_head = RAD_CENTER;
center_dist_ulna = DIST_ULNA;

% Calculate the muscle origin vector magnitudes and muscle insertion vector magnitudes.

mag_bic_origin = ((bic_origin(1)^2 + bic_origin(2)^2 + bic_origin(3)^2)^0.5);
mag_brach_origin = ((brach_origin(1)^2 + brach_origin(2)^2 + brach_origin(3)^2)^0.5);
mag_brad_origin = ((brad_origin(1)^2 + brad_origin(2)^2 + brad_origin(3)^2)^0.5);
mag_ecrl_origin = ((ecrl_origin(1)^2 + ecrl_origin(2)^2 + ecrl_origin(3)^2)^0.5);
mag_pt_origin = ((pt_origin(1)^2 + pt_origin(2)^2 + pt_origin(3)^2)^0.5);
mag_tri_origin = ((tri_origin(1)^2 + tri_origin(2)^2 + tri_origin(3)^2)^0.5);

mag_bic_insert = ((bic_insert(1)^2 + bic_insert(2)^2 + bic_insert(3)^2)^0.5);
mag_brad_insert = ((brad_insert(1)^2 + brad_insert(2)^2 + brad_insert(3)^2)^0.5);
mag_brach_insert = ((brach_insert(1)^2 + brach_insert(2)^2 + brach_insert(3)^2)^0.5);
mag_ecrl_insert = ((ecrl_insert(1)^2 + ecrl_insert(2)^2 + ecrl_insert(3)^2)^0.5);
mag_pt_insert = ((pt_insert(1)^2 + pt_insert(2)^2 + pt_insert(3)^2)^0.5);
mag_tri_insert = ((tri_insert(1)^2 + tri_insert(2)^2 + tri_insert(3)^2)^0.5);

% Calculate the axes of rotation for flexion-extension.

fe_axis(1:3) = centre_capitulum(1:3) - centre_trochlea(1:3);

mag_fe_axis = ((fe_axis(1)^2 + fe_axis(2)^2 + fe_axis(3)^2)^0.5);

uv_fe_axis = (fe_axis / mag_fe_axis);

% Calculate the arc length parameter for triceps muscle length.

rot_z_tri = [0 1 0 0
             1 0 0 0
             0 0 1 0
             0 0 0 1];

tri_insert2(1:3) = rot_z_tri(1:3,1) * tri_insert(1) + rot_z_tri(1:3,2) * tri_insert(2) +
                   rot_z_tri(1:3,3) * tri_insert(3) + rot_z_tri(1:3,4);
```

```
tri_la(1:3) = tri_origin(1:3)  -  tri_insert2(1:3);
tri_length_90 = ((tri_la(1)^2 + tri_la(2)^2 + tri_la(3)^2)^0.5);
arc_rad = tri_insert2(2);

% Begin loop.

for i = 1:m

% Calculation of the muscle moment arms about the elbow joint for the given joint position.

  time = elbow_moment(i,1);
  elbow_angle = elbow_moment(i,2);
  forearm_angle = elbow_moment(i,3) - 80*(pi / 180);

  % Rotate the affected insertion vectors to the desired forearm self-rotation angle.

  rot_x = [1 0 0 0
           0 cos(forearm_angle) -sin(forearm_angle) 0
           0 sin(forearm_angle) cos(forearm_angle) 0
           0 0 0 1];

  brach_insert1(1:3) = brach_insert(1:3);
  brad_insert1(1:3) = rot_x(1:3,1)*brad_insert(1) + rot_x(1:3,2)*brad_insert(2) +
                      rot_x(1:3,3)*brad_insert(3) + rot_x(1:3,4);
  ecrl_insert1(1:3) = rot_x(1:3,1)*ecrl_insert(1) + rot_x(1:3,2)*ecrl_insert(2) +
                      rot_x(1:3,3)*ecrl_insert(3) + rot_x(1:3,4);
  pt_insert1(1:3) = rot_x(1:3,1)*pt_insert(1) + rot_x(1:3,2)*pt_insert(2) +
                      rot_x(1:3,3)*pt_insert(3) + rot_x(1:3,4);
  tri_insert1(1:3) = tri_insert(1:3);

  T1 = [1 0 0 centre_rad_head(1)
        0 1 0 centre_rad_head(2)
        0 0 1 centre_rad_head(3)
        0 0 0 1];

  T2 = [1 0 0  -centre_rad_head(1)
        0 1 0  -centre_rad_head(2)
        0 0 1  -centre_rad_head(3)
        0 0 0 1];

  invT1 = inv(T1);
  invT2 = inv(T2);

  bic_insert_trans(1:3) = invT1(1:3,1)*bic_insert(1) + invT1(1:3,2)*bic_insert(2) +
                          invT1(1:3,3)*bic_insert(3) + invT1(1:3,4);
  bic_insert_rot(1:3)= rot_x(1:3,1)*bic_insert_trans(1) + rot_x(1:3,2)*bic_insert_trans(2) +
                       rot_x(1:3,3)*bic_insert_trans(3) + rot_x(1:3,4);
  bic_insert1(1:3) = invT2(1:3,1)*bic_insert_rot(1) + invT2(1:3,2)*bic_insert_rot(2) +
                     invT2(1:3,3)*bic_insert_rot(3) + invT2(1:3,4);
```

```
% Rotate the insertion vectors to the desired elbow joint angle.

  rot_z = [cos(elbow_angle)  -sin(elbow_angle) 0 0
           sin(elbow_angle) cos(elbow_angle) 0 0
           0 0 1 0
           0 0 0 1];

  bic_insert2(1:3) = rot_z(1:3,1)*bic_insert1(1) + rot_z(1:3,2)*bic_insert1(2) +
                     rot_z(1:3,3)*bic_insert1(3) + rot_z(1:3,4);
  brad_insert2(1:3) = rot_z(1:3,1)*brad_insert1(1) + rot_z(1:3,2)*brad_insert1(2) +
                      rot_z(1:3,3)*brad_insert1(3) + rot_z(1:3,4);
  brach_insert2(1:3) = rot_z(1:3,1)*brach_insert1(1) + rot_z(1:3,2)*brach_insert1(2) +
                       rot_z(1:3,3)*brach_insert1(3) + rot_z(1:3,4);
  ecrl_insert2(1:3) = rot_z(1:3,1)*ecrl_insert1(1) + rot_z(1:3,2)*ecrl_insert1(2) +
                      rot_z(1:3,3)*ecrl_insert1(3) + rot_z(1:3,4);
  pt_insert2(1:3) = rot_z(1:3,1)*pt_insert1(1) + rot_z(1:3,2)*pt_insert1(2) +
                    rot_z(1:3,3)*pt_insert1(3) + rot_z(1:3,4);

  if elbow_angle <= 90*(pi / 180)
     tri_insert2(1:3) = rot_z(1:3,1)*tri_insert1(1) + rot_z(1:3,2)*tri_insert1(2) +
                        rot_z(1:3,3)*tri_insert1(3) + rot_z(1:3,4);
  else
     tri_insert2(1:3) = tri_insert2(1:3);
  end

  % Calculate the muscle line of action vectors.

  bic_la(1:3) = bic_origin(1:3) - bic_insert2(1:3);
  brach_la(1:3) = brach_origin(1:3) - brach_insert2(1:3);
  brad_la(1:3) = brad_origin(1:3) - brad_insert2(1:3);
  ecrl_la(1:3) = ecrl_origin(1:3) - ecrl_insert2(1:3);
  pt_la(1:3) = pt_origin(1:3) - pt_insert2(1:3);
  tri_la(1:3) = tri_origin(1:3) - tri_insert2(1:3);

  % Decompose the muscle line of action vector into magnitude and unit vector.

  mag_bic_la = ((bic_la(1)^2 + bic_la(2)^2 + bic_la(3)^2)^0.5);
  mag_brach_la = ((brach_la(1)^2 + brach_la(2)^2 + brach_la(3)^2)^0.5);
  mag_brad_la = ((brad_la(1)^2 + brad_la(2)^2 + brad_la(3)^2)^0.5);
  mag_ecrl_la = ((ecrl_la(1)^2 + ecrl_la(2)^2 + ecrl_la(3)^2)^0.5);
  mag_pt_la = ((pt_la(1)^2 + pt_la(2)^2 + pt_la(3)^2)^0.5);
  mag_tri_la = ((tri_la(1)^2 + tri_la(2)^2 + tri_la(3)^2)^0.5);

  uv_bic_la = (bic_la / mag_bic_la);
  uv_brach_la = (brach_la / mag_brach_la);
  uv_brad_la = (brad_la / mag_brad_la);
  uv_ecrl_la = (ecrl_la / mag_ecrl_la);
  uv_pt_la = (pt_la / mag_pt_la);
  uv_tri_la = (tri_la / mag_tri_la);
```

```
% Calculate the initial muscle length parameters.

 if i = = 1
    bic_length = mag_bic_la;
    brach_length = mag_brach_la;
    brad_length = mag_brad_la;
    ecrl_length = mag_ecrl_la;
    pt_length = mag_pt_la;
    tri_length = mag_tri_la;
 end

% Calculate the reflection of the muscle origin or insertion vector on the line of action vector,
    then calculate the muscle moment arm vector.

 if mag_bic_origin >= mag_bic_insert
    r_bic_origin = abs(dot(bic_origin,uv_bic_la))*uv_bic_la;
    bic_ma = bic_origin - r_bic_origin;
 else
    r_bic_insert = abs(dot(bic_insert2,uv_bic_la))*uv_bic_la;
    bic_ma = bic_insert2 + r_bic_insert;
 end

 if mag_brach_origin >= mag_brach_insert
    r_brach_origin = abs(dot(brach_origin,uv_brach_la))*uv_brach_la;
    brach_ma = brach_origin - r_brach_origin;
 else
    r_brach_insert = abs(dot(brach_insert2,uv_brach_la))*uv_brach_la;
    brach_ma = brach_insert2 + r_brach_insert;
 end

 if mag_brad_origin >= mag_brad_insert
    r_brad_origin = abs(dot(brad_origin,uv_brad_la))*uv_brad_la;
    brad_ma = brad_origin - r_brad_origin;
 else
    r_brad_insert = abs(dot(brad_insert2,uv_brad_la))*uv_brad_la;
    brad_ma = brad_insert2 + r_brad_insert;
 end

 if mag_ecrl_origin >= mag_ecrl_insert
    r_ecrl_origin = abs(dot(ecrl_origin,uv_ecrl_la))*uv_ecrl_la;
    ecrl_ma = ecrl_origin - r_ecrl_origin;
 else
    r_ecrl_insert = abs(dot(ecrl_insert2,uv_ecrl_la))*uv_ecrl_la;
    ecrl_ma = ecrl_insert2 + r_ecrl_insert;
 end

 if mag_pt_origin >= mag_pt_insert
    r_pt_origin = abs(dot(pt_origin,uv_pt_la))*uv_pt_la;
    pt_ma = pt_origin - r_pt_origin;
 else
    r_pt_insert = abs(dot(pt_insert2,uv_pt_la))*uv_pt_la;
```

```
    pt_ma = pt_insert2 + r_pt_insert;
  end

  if mag_tri_origin >= mag_tri_insert
    r_tri_origin = abs(dot(tri_origin,uv_tri_la))*uv_tri_la;
    tri_ma = tri_origin - r_tri_origin;
  else
    r_tri_insert = abs(dot(tri_insert2,uv_tri_la))*uv_tri_la;
    tri_ma = tri_insert2 + r_tri_insert;
  end

  mag_bic_ma = ((bic_ma(1)^2 + bic_ma(2)^2 + bic_ma(3)^2)^0.5);
  mag_brach_ma = ((brach_ma(1)^2 + brach_ma(2)^2 + brach_ma(3)^2)^0.5);
  mag_brad_ma = ((brad_ma(1)^2 + brad_ma(2)^2 + brad_ma(3)^2)^0.5);
  mag_ecrl_ma = ((ecrl_ma(1)^2 + ecrl_ma(2)^2 + ecrl_ma(3)^2)^0.5);
  mag_pt_ma = ((pt_ma(1)^2 + pt_ma(2)^2 + pt_ma(3)^2)^0.5);
  mag_tri_ma = ((tri_ma(1)^2 + tri_ma(2)^2 + tri_ma(3)^2)^0.5)*-1;

  uv_bic_ma = (bic_ma / mag_bic_ma);
  uv_brach_ma = (brach_ma / mag_brach_ma);
  uv_brad_ma = (brad_ma / mag_brad_ma);
  uv_ecrl_ma = (ecrl_ma / mag_ecrl_ma);
  uv_pt_ma = (pt_ma / mag_pt_ma);
  uv_tri_ma = (tri_ma / mag_tri_ma);

% Calculate the individual muscle forces.

  m_elbow = [elbow_moment(i,4) elbow_moment(i,5) elbow_moment(i,6)];

  % Calculate the component of the dynamic moment about the joint axis of rotation.

  m_elbowfe = dot(m_elbow,uv_fe_axis)*uv_fe_axis;

  m_elbowfe_mag = ((m_elbowfe(1)^2 + m_elbowfe(2)^2 + m_elbowfe(3)^2)^0.5);

% Subject muscle physiological cross-sectional areas (cm^2).
% The physiological cross-sectional areas of biceps and triceps include all muscle heads.
% The total flexor and extensor physiological cross-sectional areas include all muscles in the
    functional group.
% In pronation the Biceps Brachii is inactive; therefore the total flexor cross-section does not
    include Biceps.

  pcsa_bic = 4.6;
  pcsa_brach = 7.0;
  pcsa_brad = 1.5;
  pcsa_ecrl = 2.4;
  pcsa_pt = 3.4;
  pcsa_tri = 18.8;

  pcsa_flexpro = 14.3;
  pcsa_flex = 18.9;
```

```
pcsa_ext = 18.8;

% Calculate the relative physiological cross-sectional areas of the muscles.

rpcsa_bic = pcsa_bic / pcsa_flex;
rpcsa_brach = pcsa_brach / pcsa_flex;
rpcsa_brad = pcsa_brad / pcsa_flex;
rpcsa_ecrl = pcsa_ecrl / pcsa_flex;
rpcsa_pt = pcsa_pt / pcsa_flex;
rpcsa_tri = pcsa_tri / pcsa_ext;
rpcsapro_brach = pcsa_brach / pcsa_flexpro;
rpcsapro_brad = pcsa_brad / pcsa_flexpro;
rpcsapro_ecrl = pcsa_ecrl / pcsa_flexpro;
rpcsapro_pt = pcsa_pt / pcsa_flexpro;

% Calculate the total elbow force.

bic = rpcsa_bic*uv_bic_la;
brach = rpcsa_brach*uv_brach_la;
brad = rpcsa_brad*uv_brad_la;
ecrl = rpcsa_ecrl*uv_ecrl_la;
pt = rpcsa_pt*uv_pt_la;
tri = rpcsa_tri*uv_tri_la;
brachpro = rpcsapro_brach*uv_brach_la;
bradpro = rpcsapro_brad*uv_brad_la;
ecrlpro = rpcsapro_ecrl*uv_ecrl_la;
ptpro = rpcsapro_pt*uv_pt_la;

muscle_flex = abs(cross(bic_ma,bic)) + abs(cross(brach_ma,brach)) +
              abs(cross(brad_ma,brad)) + abs(cross(ecrl_ma,ecrl)) + abs(cross(pt_ma,pt));
muscle_flexpro = abs(cross(brach_ma,brachpro)) + abs(cross(brad_ma,bradpro)) +
                 abs(cross(ecrl_ma,ecrlpro)) + abs(cross(pt_ma,ptpro));
muscle_ext = abs(cross(tri_ma,tri));

% Calculate the flexion / extension total muscle force.

if elbow_moment(i,6) >= 0
   if forearm_angle <= 1.0
      muscle_totalfe = muscle_flex;
   else
      muscle_totalfe = muscle_flexpro;
   end
   muscle_totalfe_mag = ((muscle_totalfe(1)^2 + muscle_totalfe(2)^2 +
                          muscle_totalfe(3)^2)^0.5);
else
   muscle_totalfe = muscle_ext;
   muscle_totalfe_mag = ((muscle_totalfe(1)^2 + muscle_totalfe(2)^2 +
                          muscle_totalfe(3)^2)^0.5);
end

f_elbowfe = abs(m_elbowfe_mag / muscle_totalfe_mag);
```

```
% Set the muscle activation levels for flexion / extension.
% Biceps muscle is inactive when the forearm is pronated in both flexion and extension.

  if elbow_moment(i,6) >= 0
     brach_activefe = 1.2;
     brad_activefe = 1.2;
     ecrl_activefe = 1.2;
     pt_activefe = 1.2;
     tri_activefe = 0.2;
     if forearm_angle <= 1.0
        bic_activefe = 1.2;
     else
        bic_activefe = 0;
     end
  else
     brach_activefe = 0.2;
     brad_activefe = 0.2;
     ecrl_activefe = 0.2;
     pt_activefe = 0.2;
     tri_activefe = 1.2;
     if forearm_angle <= 1.0
        bic_activefe = 0.2;
     else
        bic_activefe = 0;
     end
  end

  % Calculate the individual muscle forces.

  f_bic = (rpcsa_bic*f_elbowfe*bic_activefe);
  f_tri = (rpcsa_tri*f_elbowfe*tri_activefe);
  if forearm_angle <= 1.0
     f_brach = (rpcsa_brach*f_elbowfe*brach_activefe);
     f_brad = (rpcsa_brad*f_elbowfe*brad_activefe);
     f_ecrl = (rpcsa_ecrl*f_elbowfe*ecrl_activefe);
     f_pt = (rpcsa_pt*f_elbowfe*pt_activefe);
  else
     f_brach = (rpcsapro_brach*f_elbowfe*brach_activefe);
     f_brad = (rpcsapro_brad*f_elbowfe*brad_activefe);
     f_ecrl = (rpcsapro_ecrl*f_elbowfe*ecrl_activefe);
     f_pt = (rpcsapro_pt*f_elbowfe*pt_activefe);
  end
  f_flex = f_bic + f_brach + f_brad + f_ecrl + f_pt;


% Calculate individual muscle energies.

  bio_const = 0.5;
```

```
% Calculate the change in time and length over the interval.

  delta_time = time - time_old;

  delta_bic = mag_bic_la - bic_length;
  delta_brach = mag_brach_la - brach_length;
  delta_brad = mag_brad_la - brad_length;
  delta_ecrl = mag_ecrl_la - ecrl_length;
  delta_pt = mag_pt_la - pt_length;

  if elbow_angle <= (pi / 2)
     tri_length2 = mag_tri_la;
  else
     arc_length = arc_rad*(elbow_angle - (pi / 2));
     tri_length2 = tri_length_90 + arc_length;
  end

  delta_tri = tri_length2 - tri_length;

  % Calculate the average muscle force for each interval.

  avg_bic_f = (f_bic + f_bic2) / 2;
  avg_brach_f = (f_brach + f_brach2) / 2;
  avg_brad_f = (f_brad + f_brad2) / 2;
  avg_ecrl_f = (f_ecrl + f_ecrl2) / 2;
  avg_pt_f = (f_pt + f_pt2) / 2;
  avg_tri_f = (f_tri + f_tri2) / 2;

  % Calculate the individual mechanical energy for each muscle.

  bic_mech_nrg = bic_mech_nrg + abs(avg_bic_f*delta_bic);
  brach_mech_nrg = brach_mech_nrg + abs(avg_brach_f*delta_brach);
  brad_mech_nrg = brad_mech_nrg + abs(avg_brad_f*delta_brad);
  ecrl_mech_nrg = ecrl_mech_nrg + abs(avg_ecrl_f*delta_ecrl);
  pt_mech_nrg = pt_mech_nrg + abs(avg_pt_f*delta_pt);
  tri_mech_nrg = tri_mech_nrg + abs(avg_tri_f*delta_tri);

  tot_flex_mech_nrg = bic_mech_nrg + brach_mech_nrg + brad_mech_nrg + ecrl_mech_nrg +
                      pt_mech_nrg;
  tot_mech_nrg = bic_mech_nrg + brach_mech_nrg + brad_mech_nrg + ecrl_mech_nrg +
                 pt_mech_nrg + tri_mech_nrg;

  % Calculate the individual biological energy for each muscle.

  bic_bio_nrg = bic_bio_nrg + abs(avg_bic_f*delta_time*bio_const);
  brach_bio_nrg = brach_bio_nrg + abs(avg_brach_f*delta_time*bio_const);
  brad_bio_nrg = brad_bio_nrg + abs(avg_brad_f*delta_time*bio_const);
  ecrl_bio_nrg = ecrl_bio_nrg + abs(avg_ecrl_f*delta_time*bio_const);
  pt_bio_nrg = pt_bio_nrg + abs(avg_pt_f*delta_time*bio_const);
  tri_bio_nrg = tri_bio_nrg + abs(avg_tri_f*delta_time*bio_const);
```

```
tot_flex_bio_nrg = bic_bio_nrg + brach_bio_nrg + brad_bio_nrg + ecrl_bio_nrg + pt_bio_nrg;
tot_bio_nrg = bic_bio_nrg + brach_bio_nrg + brad_bio_nrg + ecrl_bio_nrg + pt_bio_nrg +
              tri_bio_nrg;

% Calculate the total individual muscle energy.

bic_tot_nrg = bic_mech_nrg + bic_bio_nrg;
brach_tot_nrg = brach_mech_nrg + brach_bio_nrg;
brad_tot_nrg = brad_mech_nrg + brad_bio_nrg;
ecrl_tot_nrg = ecrl_mech_nrg + ecrl_bio_nrg;
pt_tot_nrg = pt_mech_nrg + pt_bio_nrg;
tri_tot_nrg = tri_mech_nrg + tri_bio_nrg;

flex_tot_nrg = bic_tot_nrg + brach_tot_nrg + brad_tot_nrg + ecrl_tot_nrg + pt_tot_nrg;
tot_nrg = bic_tot_nrg + brach_tot_nrg + brad_tot_nrg + ecrl_tot_nrg + pt_tot_nrg + tri_tot_nrg;

% Create variable for muscle energy data storage.

mech_energy = [time elbow_angle forearm_angle tot_mech_nrg tot_flex_mech_nrg
               bic_mech_nrg brach_mech_nrg brad_mech_nrg ecrl_mech_nrg pt_mech_nrg
               tri_mech_nrg];
bio_energy = [time elbow_angle forearm_angle tot_bio_nrg tot_flex_bio_nrg bic_bio_nrg
              brach_bio_nrg brad_bio_nrg ecrl_bio_nrg pt_bio_nrg tri_bio_nrg];
energy = [time elbow_angle forearm_angle tot_nrg flex_tot_nrg bic_tot_nrg brach_tot_nrg
          brad_tot_nrg ecrl_tot_nrg pt_tot_nrg tri_tot_nrg];

% Print muscle energy data to file.

fid = fopen('e_mechenergy_right.txt','a');
fprintf(fid,'%-7.4f %+5.3e %+5.3e %+5.3e %+5.3e %+5.3e %+5.3e %+5.3e
        %+5.3e %+5.3e\n',mech_energy);
fid = fopen('e_bioenergy_right.txt','a');
fprintf(fid,'%-7.4f %+5.3e %+5.3e %+5.3e %+5.3e %+5.3e %+5.3e %+5.3e
        %+5.3e %+5.3e\n',bio_energy);
fid = fopen('e_totalenergy_right.txt','a');
fprintf(fid,'%-7.4f %+5.3e %+5.3e %+5.3e %+5.3e %+5.3e %+5.3e %+5.3e
        %+5.3e %+5.3e\n',energy);

% Create variables for muscle moment arm and force data storage.

moment = [time elbow_angle forearm_angle mag_bic_ma mag_brach_ma mag_brad_ma
          mag_ecrl_ma mag_pt_ma mag_tri_ma];
force = [time elbow_angle forearm_angle f_elbowfe f_flex f_bic f_brach f_brad f_ecrl f_pt
         f_tri];

% Print muscle moment arm and force data to file.

fid = fopen('e_momentarm_right.txt','a');
fprintf(fid,'%-7.4f %+5.3e %+5.3e %+5.3e %+5.3e %+5.3e %+5.3e
        %+5.3e\n',moment);
fid = fopen('e_force_right.txt','a');
```

```
    fprintf(fid,'%-7.4f %+5.3e %+5.3e %+5.3e %+5.3e %+5.3e %+5.3e %+5.3e %+5.3e
            %+5.3e %+5.3e\n',force);

    % Reset variables for first interval point.

    time_old = time;
    bic_length = mag_bic_la;
    brach_length = mag_brach_la;
    brad_length = mag_brad_la;
    ecrl_length = mag_ecrl_la;
    pt_length = mag_pt_la;
    tri_length = tri_length2;
    f_bic2 = f_bic;
    f_brach2 = f_brach;
    f_brad2 = f_brad;
    f_ecrl2 = f_ecrl;
    f_pt2 = f_pt;
    f_tri2 = f_tri;

end

status = fclose('all');
```

APPENDIX B

SCALING FORMULATIONS

Appendix B details the correlation equations developed for the anatomical scaling. Using the data sets from Murray (1997) and HumanScale (1974), correlation equations for the body segment parameters and bone and muscle parameters were developed using a best fit statistical analysis whenever possible. The scaling correlations take the form of linear, curvilinear, exponential, and logarithmic equations. When a correlation equation for the given parameter was determined, the statistical correlation coefficient, r, is also reported.

Table B.1 Body Segment Parameters

Body Segment Parameter y	**Mathematical Relation**			**Correlation Coefficient** r
Head Width	$y = 0.142$			
	$y = 0.145$			
	$y = 1.22571 \times 10^{-2} + (8.19417 \times 10^{-2}) \cdot height$			0.9963
Head Length	Male	$height < 1.4732$ m	$y = 0.211$	
		$1.4732 \text{ m} \le height < 1.6002 \text{ m}$	$y = 0.213$	
		$1.66002 \text{ m} \le height$	$y = 0.105983 \cdot e^{(4.293126 \cdot \text{height})}$	0.9541
	Female	$y = 0.013 \cdot male\ head\ length$		
Shoulder to Crown Length	$y = 7.6123 \times 10^{-2} + 0.166185 \cdot height$			0.9997
Chest Width	$y = (6.58907 \times 10^{-2}) \cdot e^{(0.850877 \cdot height)}$			0.9985
Chest Depth	Male	$height < 1.615$ m	$y = 0.196$	
		$1.615 \text{ m} \le height < 1.880 \text{ m}$	$y = 0.229$	
		$1.880 \text{ m} \le height$	$y = 0.272$	
	Female	$height < 1.491$ m	$y = 0.198$	
		$1.491 \text{ m} \le height < 1.740 \text{ m}$	$y = 0.231$	
		$1.740 \text{ m} \le height$	$y = 0.277$	
Full Torso Length	$y = 4.02057 \times 10^{-2} + 0.238075 \cdot height$			0.9999

Table B.1 Body Segment Parameters

Body Segment Parameter y	**Mathematical Relation**			**Correlation Coefficient** r
Upper Torso Length	Male	$y = 0.3209 \cdot$ *full torso length*		
	Female	$y = 0.2692 \cdot$ *full torso length*		
Mid Torso Length	Male	$y = 0.4052 \cdot$ *full torso length*		
	Female	$y = 0.3879 \cdot$ *full torso length*		
Lower Torso Length	Male	$y = 0.2739 \cdot$ *full torso length*		
	Female	$y = 0.3429 \cdot$ *full torso length*		
Lower Body Length	Male	$y = (7.74767 \times 10^{-2}) \cdot e^{(0.83898 \cdot height)}$		0.9987
	Female	$y = (5.357718 \times 10^{-2}) \cdot e^{(1.164551 \cdot height)}$		0.9876
Hip Depth	Male	*height* < 1.615 m	y = 0.188	
		1.615 m ≤ *height* < 1.880 m	y = 0.224	
		1.880 m ≤ *height*	y = 0.269	
	Female	*height* < 1.491 m	y = 0.173	
		1.491 m ≤ *height* < 1.740 m	y = 0.208	
		1.740 m ≤ *height*	y = 0.249	
Lower Body Length	$y = -0.11551 + 0.59529 \cdot height$			

Table B.1 Body Segment Parameters

Body Segment Parameter y		**Mathematical Relation**	**Correlation Coefficient** r
Shoulder Pivot Width		$y = (8.38014 \times 10^{-2}) \cdot e^{(0.811558 \cdot height)}$	0.9986
Upper Arm Length		$y = 1.9274 \times 10^{-3} + 0.1516 \cdot height$	0.9972
Forearm Length		$y = -1.01591 \times 10^{-2} + 0.15307 \cdot height$	0.9959
Hand Length		$y = (5.92602 \times 10^{-2}) \cdot e^{(0.67137 \cdot height)}$	0.9979
Upper Torso Centre of Mass	Male	$y = 0.4934 \cdot upper\ torso\ length$	
	Female	$y = 0.4950 \cdot upper\ torso\ length$	
Mid Torso Centre of Mass	Male	$y = 0.5498 \cdot mid\ torso\ length$	
	Female	$y = 0.5488 \cdot mid\ torso\ length$	
Lower Torso Centre of Mass	Male	$y = 0.3885 \cdot lower\ torso\ length$	
	Female	$y = 0.5080 \cdot lower\ torso\ length$	
Upper Arm Centre of Mass	Male	$y = 0.5772 \cdot upper\ arm\ length$	
	Female	$y = 0.5754 \cdot upper\ arm\ length$	
Forearm Centre of Mass	Male	$y = 0.4574 \cdot forearm\ length$	
	Female	$y = 0.4559 \cdot forearm\ length$	
Hand Centre of Mass	Male	$y = 0.3624 \cdot hand\ length$	
	Female	$y = 0.3427 \cdot hand\ length$	

Table B.1 Body Segment Parameters

Subject Gender	Limiting Condition	Body Segment Parameter, y	Mathematical Relation
Male	*height* < 1.615 m	Head Circumference	$y=0.541$
		Chest Circumference	$y=0.889$
		Waist Circumference	$y=0.754$
		Pelvis Circumference	$y=0.886$
		Upper Arm Circumference	$y=0.284$
		Elbow Circumference	$y=0.284$
		Forearm Circumference	$y=0.267$
		Wrist Circumference	$y=0.155$
		Hand Circumference	$y=0.198$
	1.615 m ≤ *height* < 1.880 m	Head Circumference	$y=0.564$
		Chest Circumference	$y=0.983$
		Waist Circumference	$y=0.869$
		Pelvis Circumference	$y=0.978$
		Upper Arm Circumference	$y=0.323$
		Elbow Circumference	$y=0.312$
		Forearm Circumference	$y=0.292$
		Wrist Circumference	$y=0.168$
		Hand Circumference	$y=0.216$
	1.880 m ≤ *height*	Head Circumference	$y=0.587$
		Chest Circumference	$y=1.087$
		Waist Circumference	$y=1.003$
		Pelvis Circumference	$y=1.074$
		Upper Arm Circumference	$y=0.358$
		Elbow Circumference	$y=0.348$
		Forearm Circumference	$y=0.320$
		Wrist Circumference	$y=0.185$
		Hand Circumference	$y=0.234$

Table B.1 Body Segment Parameters

Subject Gender	Limiting Condition	Body Segment Parameter, y	Mathematical Relation
Female	*height* < 1.491 m	Head Circumference	$y=0.518$
		Chest Circumference	$y=0.848$
		Waist Circumference	$y=0.724$
		Pelvis Circumference	$y=0.932$
		Upper Arm Circumference	$y=0.269$
		Elbow Circumference	$y=0.257$
		Forearm Circumference	$y=0.244$
		Wrist Circumference	$y=0.145$
		Hand Circumference	$y=0.170$
	1.491 m ≤ *height* < 1.740 m	Head Circumference	$y=0.549$
		Chest Circumference	$y=0.892$
		Waist Circumference	$y=0.742$
		Pelvis Circumference	$y=1.008$
		Upper Arm Circumference	$y=0.290$
		Elbow Circumference	$y=0.282$
		Forearm Circumference	$y=0.262$
		Wrist Circumference	$y=0.155$
		Hand Circumference	$y=0.188$
	1.740 m ≤ *height*	Head Circumference	$y=0.579$
		Chest Circumference	$y=0.945$
		Waist Circumference	$y=0.803$
		Pelvis Circumference	$y=1.059$
		Upper Arm Circumference	$y=0.307$
		Elbow Circumference	$y=0.312$
		Forearm Circumference	$y=0.277$
		Wrist Circumference	$y=0.163$
		Hand Circumference	$y=0.203$

Table B.2 Bone Parameters

Bone Parameter y	**Body Parameter** x	**Mathematical Relation**		**Correlation Coefficient** r
Humerus Length	Upper Arm Length	$y = 0.520784 + 0.94734 \cdot ln(x)$		0.8825
Radius Length	Forearm Hand Length	$y = 0.150896 + 0.224922 \cdot x$		0.8111
Ulna Length	Forearm Hand Length	$y = 0.148817 + 0.275298 \cdot x$		0.8725
Humeral Head Radius		Male	$y = 0.0243$	
		Female	$y = 0.0215$	
Transepicondylar Width	Elbow Circumference	$y = 4.13254 \times 10^{-2} + (9.718394 \times 10^{-2}) \cdot x$		0.8205
Humeral Shaft Radius	Transepicondylar Width	$y = x/6$		
Distal Radial-Ulna Width	Wrist Circumference	$y = 0.32762 \cdot x$		
Centre of Capitulum, x	Humerus Length	$y = 0.00473 \cdot x$		
Centre of Capitulum, y	Elbow Circumference	$y = 0.00282 \cdot x$		
Centre of Capitulum, z	Elbow Circumference	$y = 095848 \cdot x$		
Centre of Radial Head, x	Radius Length	$y = 0.0506 \cdot x$		
Centre of Radial Head, y	Forearm Circumference	$y = 0.0045 \cdot x$		
Centre of Radial Head, z	Forearm Circumference	$y = 0.0988 \cdot x$		
Centre of Distal Ulna, x	Ulna Length	$y = 0.535772 + 0.223601 \cdot ln(x)$		0.95923
Centre of Distal Ulna, y	Wrist Circumference	$y = 0.27824 \cdot x$		
Centre of Distal Ulna, z	Wrist Circumference	$y = 0.13623 \cdot x$		

Table B.3 Muscle Parameters

Bone Parameter y	**Body Parameter** x	**Mathematical Relation**	**Correlation Coefficient** r
Biceps Origin, x	Humerus Length	$y = 0.645314 + 0.312888 \cdot ln(x)$	0.9700
Biceps Origin, y	Humeral Ball Radius	$y = 0.863943 \cdot x$	
Biceps Origin, z	Humeral Ball Radius	$y = 0.43659 \cdot x$	
Biceps Insertion, x	Radius Length	$y = -2.163901 \times 10^{-2} + 0.223601 \cdot x$	0.8396
Biceps Insertion, y	Center of Radial Head, y	$y = 3.018911 \times 10^{-3} + 1.091462 \cdot x$	0.9958
Biceps Insertion, z	Center of Radial Head, y	$y = 1.616645 \times 10^{-2} + 0.226601 \cdot x$	0.7354
Brachialis Origin, x	Humerus Length	$y = x/3$	
Brachialis Origin, y	Humeral Shaft Radius	$y = 0.3383 \cdot x$	
Brachialis Origin, z	Humeral Shaft Radius	$y = 1.5231 \cdot x$	
Brachialis Insertion, x	Ulna Length	$y = .01064 \cdot x$	
Brachialis Insertion, y	Transepicondylar Width	$y = 0.169295 \cdot x$	
Brachialis Insertion, z	Transepicondylar Width	$y = 0.08907 \cdot x$	

Table B.3 Muscle Parameters

Bone Parameter y	**Body Parameter** x	**Mathematical Relation**	**Correlation Coefficient** r
Brachialis Origin, x	Humerus Length	$y = (1.343071 \times 10^{-2}) \cdot e^{(5.417023 \cdot x)}$	0.7394
Brachialis Origin, y	Humeral Shaft Radius	$y = 1.856473 \cdot x$	
Brachialis Origin, z	Humeral Shaft Radius	$y = 1.472820 \cdot x$	
Brachialis Insertion, x	Radius Length	$y = -8.567392 \times 10^{-3} + 0.963827 \cdot x$	0.9599
Brachialis Insertion, y	Distal Radial-Ulna Width	$y = 0.78454 \cdot x$	
Brachialis Insertion, z	Distal Radial-Ulna Width	$y = 0.898832 \cdot x$	
ECRL Origin, x	Humerus Length	$y = 0.084596 \cdot x$	
ECRL Origin, y	Humeral Shaft Radius	$y = 1.591899 \cdot x$	
ECRL Origin, z	Humeral Shaft Radius	$y = 2.112148 \cdot x$	
ECRL Insertion, x	Radius Length	$y = -6.566875 \times 10^{-3} + 1.046475 \cdot x$	0.9657
ECRL Insertion, y	Distal Radial-Ulna Width	$y = 0.737915 \cdot x$	
ECRL Insertion, z	Distal Radial-Ulna Width	$y = 0.78172 \cdot x$	

Table B.3 Muscle Parameters

Bone Parameter y	**Body Parameter** x	**Mathematical Relation**	**Correlation Coefficient** r
Pronator Teres Origin, x	Humerus Length	$y = 0.041256 \cdot x$	
Pronator Teres Origin, y	Humeral Shaft Radius	$y = 0.469679 \cdot x$	
Pronator Teres Origin, z	Transepicondylar Width	$y = 0.357365 \cdot x$	
Pronator Teres Insertion, x	Radius Length	$y = 0.488758 \cdot x$	
Pronator Teres Insertion, y	Distal Radial-Ulna Width	$y = 0.643778 \cdot x$	
Pronator Teres Insertion, z	Distal Radial-Ulna Width	$y = 0.556456 \cdot x$	
Triceps Origin, x	Humerus Length	$y = 0.707286 \cdot x$	
Triceps Origin, y	Humeral Shaft Radius	$y = 1.583216 \cdot x$	
Triceps Origin, z	Humeral Shaft Radius	$y = 2.453401 \cdot x$	
Triceps Insertion, x	Ulna Length	$y = 0.041103 \cdot x$	
Triceps Insertion, y	Transepicondylar Width	$y = 0.347264 \cdot x$	
Triceps Insertion, z	Transepicondylar Width	$y = 0.031214 \cdot x$	

APPENDIX C

ANATOMICAL SCALING MODEL

Appendix C contains a listing of the anatomical scaling program code written in MatLab, version 6.0.0.88, release 12. The percent symbol, %, preceding a line denotes a comment line, any following text is ignored.

```
% Sub-program to determine the subject segment, bone, and muscle parameters.

function anatomical_scale

% Subject input variables.
% If OPERATOR = 1 subject is male, if OPERATOR = 2 subject is female.

global OPERATOR OPERATORH OPERATORW

height = OPERATORH;
weight = OPERATORW;

% Subject output variables.
% Segment widths and depths.

global HEAD_W SHOULDER_W CHEST_W CHEST_D PELVIS_W PELVIS_D

% Segment circumferences.

global HEAD_CIR CHEST_CIR WAIST_CIR PELVIS_CIR UPPERARM_CIR ELBOW_CIR
FOREARM_CIR WRIST_CIR HAND_CIR

% Segment lengths.

global CROWN_L HEAD_L NECK_L FULLTORSO_L UPTORSO_L MIDTORSO_L
LOWTORSO_L LOWERBODY_L UPPERARM_L FOREARM_L HAND_L

% Segment centres of mass.

global UPTORSO_CM MIDTORSO_CM LOWTORSO_CM UPPERARM_CM
FOREARM_CM HAND_CM

% Muscle coordinate output variables.

global BIC_O BIC_I BRACH_O BRACH_I BRAD_O BRAD_I ECRL_O ECRL_I PT_O PT_I
TRI_O TRI_I TROCH_CENTER CAPI_CENTER RAD_CENTER DIST_ULNA

% Calculate the segment circumferences based on the subject's gender and height.

if OPERATOR == 1
  if height <= 1.615
     HEAD_CIR = 0.541;
     CHEST_CIR = 0.889;
     WAIST_CIR = 0.754;
     PELVIS_CIR = 0.886;
     UPPERARM_CIR = 0.284;
     ELBOW_CIR = 0.284;
     FOREARM_CIR = 0.267;
     WRIST_CIR = 0.155;
     HAND_CIR = 0.198;
  elseif height >= 1.88
```

```
        HEAD_CIR = 0.587;
        CHEST_CIR = 1.087;
        WAIST_CIR = 1.003;
        PELVIS_CIR = 1.074;
        UPPERARM_CIR = 0.358;
        ELBOW_CIR = 0.348;
        FOREARM_CIR = 0.320;
        WRIST_CIR = 0.185;
        HAND_CIR = 0.234;
    else
        HEAD_CIR = 0.564;
        CHEST_CIR = 0.983;
        WAIST_CIR = 0.869;
        PELVIS_CIR = 0.978;
        UPPERARM_CIR = 0.323;
        ELBOW_CIR = 0.312;
        FOREARM_CIR = 0.292;
        WRIST_CIR = 0.168;
        HAND_CIR = 0.216;
    end
end

if OPERATOR == 2
    if height <= 1.491
        HEAD_CIR = 0.518;
        CHEST_CIR = 0.848;
        WAIST_CIR = 0.724;
        PELVIS_CIR = 0.932;
        UPPERARM_CIR = 0.269;
        ELBOW_CIR = 0.257;
        FOREARM_CIR = 0.244;
        WRIST_CIR = 0.145;
        HAND_CIR = 0.170;
    elseif height >= 1.74
        HEAD_CIR = 0.579;
        CHEST_CIR = 0.945;
        WAIST_CIR = 0.803;
        PELVIS_CIR = 1.059;
        UPPERARM_CIR = 0.307;
        ELBOW_CIR = 0.312;
        FOREARM_CIR = 0.277;
        WRIST_CIR = 0.163;
        HAND_CIR = 0.203;
    else
        HEAD_CIR = 0.549;
        CHEST_CIR = 0.892;
        WAIST_CIR = 0.742;
        PELVIS_CIR = 1.008;
        UPPERARM_CIR = 0.290;
        ELBOW_CIR = 0.282;
        FOREARM_CIR = 0.262;
```

```
      WRIST_CIR = 0.155;
      HAND_CIR = 0.188;
    end
end

% Calculate the subject's Body Mass Index (BMI).
% BMI < 20 indicates an ectomorphic body type.
% BMI >= 20 and <=25 indicates a standard body type.
% BMI > 25 and <=27 indicates a slightly endomorphic body type.
% BMI > 27 indicates an endomorphic body type.

bmi = weight/(height^2);

% Adjust the segment circumferences based on the subject's body mass index.

if bmi < 20
   CHEST_CIR = CHEST_CIR*0.90;
   WAIST_CIR = WAIST_CIR*0.90;
   PELVIS_CIR = PELVIS_CIR*0.90;
   UPPERARM_CIR = UPPERARM_CIR*0.90;
   FOREARM_CIR = FOREARM_CIR*0.90;
elseif bmi >=20 & bmi <=25
   CHEST_CIR = CHEST_CIR;
   WAIST_CIR = WAIST_CIR;
   PELVIS_CIR = PELVIS_CIR;
   UPPERARM_CIR = UPPERARM_CIR;
   FOREARM_CIR = FOREARM_CIR;
elseif bmi > 25 & bmi <=27
   CHEST_CIR = CHEST_CIR*1.1;
   WAIST_CIR = WAIST_CIR*1.1;
   PELVIS_CIR = PELVIS_CIR*1.1;
   UPPERARM_CIR = UPPERARM_CIR*1.1;
   FOREARM_CIR = FOREARM_CIR*1.1;
else
   CHEST_CIR = CHEST_CIR*1.2;
   WAIST_CIR = WAIST_CIR*1.2;
   PELVIS_CIR = PELVIS_CIR*1.2;
   UPPERARM_CIR = UPPERARM_CIR*1.2;
   FOREARM_CIR = FOREARM_CIR*1.2;
end

% Calculate the head width and length (from crown to chin).

if height < 1.3716
   HEAD_W = 0.142;
elseif height >= 1.3716 & height < 1.6510
   HEAD_W = 0.145;
else
   HEAD_W = 1.22571e-2 + (8.19417e-2*height);
end
```

```
if height < 1.4732
   HEAD_L = 0.211;
elseif height >= 1.4732 & height < 1.6002
   HEAD_L = 0.213;
else
   HEAD_L = 0.105983*(exp(0.4293126*height));
end

if OPERATOR == 2
   HEAD_L = HEAD_L - 0.013;
end

% Calculate the length from the shoulder joint to crown of the head.

CROWN_L = 7.6123e-2 + (1.66185e-1*height);

% Calculate the neck length (from the shoulder joint to the chin).

NECK_L = CROWN_L - HEAD_L;

% Calculate the width of the chest.

CHEST_W = 6.58907e-2*exp(0.850877*height);

% Adjust the chest width based on the subject's body mass index.

if bmi < 20
   CHEST_W = CHEST_W*0.90;
elseif bmi >=20 & bmi <=25
   CHEST_W = CHEST_W;
elseif bmi > 25 & bmi <=27
   CHEST_W = CHEST_W*1.1;
else
   CHEST_W = CHEST_W*1.2;
end

% Calculate the chest depth.

if OPERATOR == 1
   if height <= 1.615
      CHEST_D = 0.196;
   elseif height >= 1.880
      CHEST_D = 0.272;
   else
      CHEST_D = 0.229;
   end
end

if OPERATOR == 2
   if height <= 1.491
      CHEST_D = 0.198;
```

```
    elseif height >= 1.740
      CHEST_D = 0.277;
    else
      CHEST_D = 0.231;
    end
end

% Adjust the chest depth based on the subject's body mass index.

if bmi < 20
   CHEST_D = CHEST_D*0.90;
elseif bmi >=20 & bmi <=25
   CHEST_D = CHEST_D;
elseif bmi > 25 & bmi <=27
   CHEST_D = CHEST_D*1.1;
else
   CHEST_D = CHEST_D*1.2;
end

% Calculate the full length of the torso (from base of neck to hip joint).

FULLTORSO_L = 4.02057e-2 + (0.238075*height);

% Calculate the lengths of the torso segments.
% Upper torso (base of neck to level of xyphoid process).
% Mid-torso (level of xyphoid process to level of omphalion).
% Lower torso (level of omphalion to hip joint).

if OPERATOR == 1
   UPTORSO_L = 0.3209*FULLTORSO_L;
   MIDTORSO_L = 0.4052*FULLTORSO_L;
   LOWTORSO_L = 0.2739*FULLTORSO_L;
end

if OPERATOR == 2
   UPTORSO_L = 0.2692*FULLTORSO_L;
   MIDTORSO_L = 0.3879*FULLTORSO_L;
   LOWTORSO_L = 0.3429*FULLTORSO_L;
end

% Calculate the width of the pelvis.

if OPERATOR == 1
   PELVIS_W = 7.74767e-2*exp(0.83898*height);
end

if OPERATOR == 2
   PELVIS_W = 5.357718e-2*exp(1.164551*height);
end
```

```
% Adjust the pelvis width based on the subject's body mass index.

if bmi < 20
   PELVIS_W = PELVIS_W*0.90;
elseif bmi >=20 & bmi <=25
   PELVIS_W = PELVIS_W;
elseif bmi > 25 & bmi <=27
   PELVIS_W = PELVIS_W*1.1;
else
   PELVIS_W = PELVIS_W*1.2;
end

% Calculate the depth of the pelvis.

if OPERATOR == 1
   if height <= 1.615
      PELVIS_D = 0.188;
   elseif height >= 1.880
      PELVIS_D = 0.269;
   else
      PELVIS_D = 0.224;
   end
end

if OPERATOR == 2
   if height <= 1.491
      PELVIS_D = 0.173;
   elseif height >= 1.740
      PELVIS_D = 0.249;
   else
      PELVIS_D = 0.208;
   end
end

% Adjust the pelvis depth based on the subject's body mass index.

if bmi < 20
   PELVIS_D = PELVIS_D*0.90;
elseif bmi >=20 & bmi <=25
   PELVIS_D = PELVIS_D;
elseif bmi > 25 & bmi <=27
   PELVIS_D = PELVIS_D*1.1;
else
   PELVIS_D = PELVIS_D*1.2;
end

% Calculate the length of the lower body (from hip joint to floor).

LOWERBODY_L = -0.11551 + (0.59529*height);
```

```
% Calculate the width of the shoulder pivots.

SHOULDER_W = 8.38014e-2*exp(0.811558*height);

% Calculate the length of the upper arm segment (from shoulder joint to elbow joint).

UPPERARM_L = 1.9274e-3 + (0.1516*height);

% Calculate the length of the forearm segment (from elbow joint to wrist joint).

FOREARM_L = -1.01591e-2 + (0.15037*height);

% Calculate the length of the hand segment (from wrist joint to third dactylion).

HAND_L = 5.92602e-2*exp(0.67137*height);

% Calculate the segment centres of mass.
% Torso centre of mass are longitudinal from the hip joint.
% Upper arm centre of mass is longitudinal from the shoulder joint.
% Forearm centre of mass is longitudinal from the elbow joint.
% Hand centre of mass is longitudinal from the wrist joint.

if OPERATOR == 1
   UPTORSO_CM = (MIDTORSO_L + LOWTORSO_L) + 0.4934*(UPTORSO_L);
   MIDTORSO_CM = (LOWTORSO_L) + 0.5498*(MIDTORSO_L);
   LOWTORSO_CM = 0.3885*(LOWTORSO_L);
   UPPERARM_CM = 0.5772*(UPPERARM_L);
   FOREARM_CM = 0.4574*(FOREARM_L);
   HAND_CM = 0.3624*(HAND_L);
end

if OPERATOR == 2
   UPTORSO_CM = (MIDTORSO_L + LOWTORSO_L) + 0.4950*(UPTORSO_L);
   MIDTORSO_CM = (LOWTORSO_L) + 0.5488*(MIDTORSO_L);
   LOWTORSO_CM = 0.5080*(LOWTORSO_L);
   UPPERARM_CM = 0.5754*(UPPERARM_L);
   FOREARM_CM = 0.4559*(FOREARM_L);
   HAND_CM = 0.3427*(HAND_L);
end

% Calculate the length of the humerus.

humerus_l = 0.520784 + (0.194734*log(UPPERARM_L));

% Calculate the lengths of the ulna and radius.

forearmhand_l = FOREARM_L + HAND_L;

radius_l = 0.150896 + (0.224922*forearmhand_l);
ulna_l = 0.148819 + (0.275298*forearmhand_l);
```

```
% Calculate the trans-epicondylar width.

transepi_w = 4.13254e-2 + (9.718394e-2*ELBOW_CIR);

% Calculate the distal radial-ulnar width.

radiusulna_w = 0.32762*WRIST_CIR;

% Calculate the humeral shaft radius.

humerals_radius = transepi_w / 6;

% Calculate the humeral head radius.

if OPERATOR == 1
   humeralh_radius = 0.0243;
end

if OPERATOR == 2
   humeralh_radius = 0.0215;
end

% Calculate the coordinates for the centre of the trochlear sulcus.

TROCH_CENTER(1) = 0;
TROCH_CENTER(2) = 0;
TROCH_CENTER(3) = 0;

% Calculate the coordinates for the centre of the capitulum.

CAPI_CENTER(1) = 0.00473*humerus_l;
CAPI_CENTER(2) = 0.00282*ELBOW_CIR;
CAPI_CENTER(3) = 0.095848*ELBOW_CIR;

% Calculate the coordinates for the centre of the radial head.

RAD_CENTER(1) = -(0.0506*radius_l);
RAD_CENTER(2) = 0.0045*FOREARM_CIR;
RAD_CENTER(3) = 0.0988*FOREARM_CIR;

% Calculate the coordinates for the centre of the distal ulna.

DIST_ULNA(1) = -(0.535772 + (0.223601*log(ulna_l)));
DIST_ULNA(2) = 0.27824*WRIST_CIR;
DIST_ULNA(3) = 0.13623*WRIST_CIR;

% Calculate the Biceps Brachii muscle coordinates.

BIC_O(1) = 0.645314 + (0.312888*log(humerus_l));
BIC_O(2) = -(0.863943*humeralh_radius);
BIC_O(3) = 0.49659*humeralh_radius;
```

```
BIC_I(1) = -(-2.163901e-2 + (0.273615*radius_l));
BIC_I(2) = -(3.018911e-3 + (1.091462*RAD_CENTER(2)));
BIC_I(3) = 1.616645e-2 + (0.226601*RAD_CENTER(2));

% Calculate the Brachialis muscle coordinates.

BRACH_O(1) = (3^-1)*humerus_l;
BRACH_O(2) = -(0.3383*humerals_radius);
BRACH_O(3) = 1.5231*humerals_radius;
BRACH_I(1) = -0.1064*ulna_l;
BRACH_I(2) = -0.169295*transepi_w;
BRACH_I(3) = -0.08907*transepi_w;

% Calculate the Brachioradialis muscle coordinates.

BRAD_O(1) = 1.343071e-2*(exp(5.417023*humerus_l));
BRAD_O(2) = 1.856473*humerals_radius;
BRAD_O(3) = 1.472820*humerals_radius;
BRAD_I(1) = -(-8.567392e-3 + (0.963827*radius_l));
BRAD_I(2) = 0.78454*radiusulna_w;
BRAD_I(3) = 0.898832*radiusulna_w;

% Calculate the Extensor Carpi Radialis Longus muscle coordinates.

ECRL_O(1) = 0.084596*humerus_l;
ECRL_O(2) = 1.591899*humerals_radius;
ECRL_O(3) = 2.112148*humerals_radius;
ECRL_I(1) = -(-6.566875e-3 + (1.046475*radius_l));
ECRL_I(2) = 0.737915*radiusulna_w;
ECRL_I(3) = 0.78172*radiusulna_w;

% Calculate the Pronator Teres muscle coordinates.

PT_O(1) = 0.041256*humerus_l;
PT_O(2) = 0.469679*humerals_radius;
PT_O(3) = -0.357365*transepi_w;
PT_I(1) = -0.488758*radius_l;
PT_I(2) = 0.643778*radiusulna_w;
PT_I(3) = 0.556456*radiusulna_w;

% Calculate the Triceps Brachii muscle coordinates.

TRI_O(1) = 0.707286*humerus_l;
TRI_O(2) = 1.583216*humerals_radius;
TRI_O(3) = 2.453401*humerals_radius;
TRI_I(1) = 0.041103*ulna_l;
TRI_I(2) = 0.347264*transepi_w;
TRI_I(3) = -0.031214*transepi_w;
```

APPENDIX D

SIMULATION RESULTS – CORONAL PLANE MOTION

Appendix D contains the plots obtained from the model simulations for elbow joint motion in the coronal plane with the forearm in the neutral position, with pronation, and supination. These motion simulations were carried out for both a quasi-static situation (task cycle time of 10 seconds) and a dynamic situation (task cycle time of 0.5 seconds). It should be noted that the elbow joint angle curve shown in Figure D.1 is the same angle progression that occurs for all the simulations in the coronal plane.

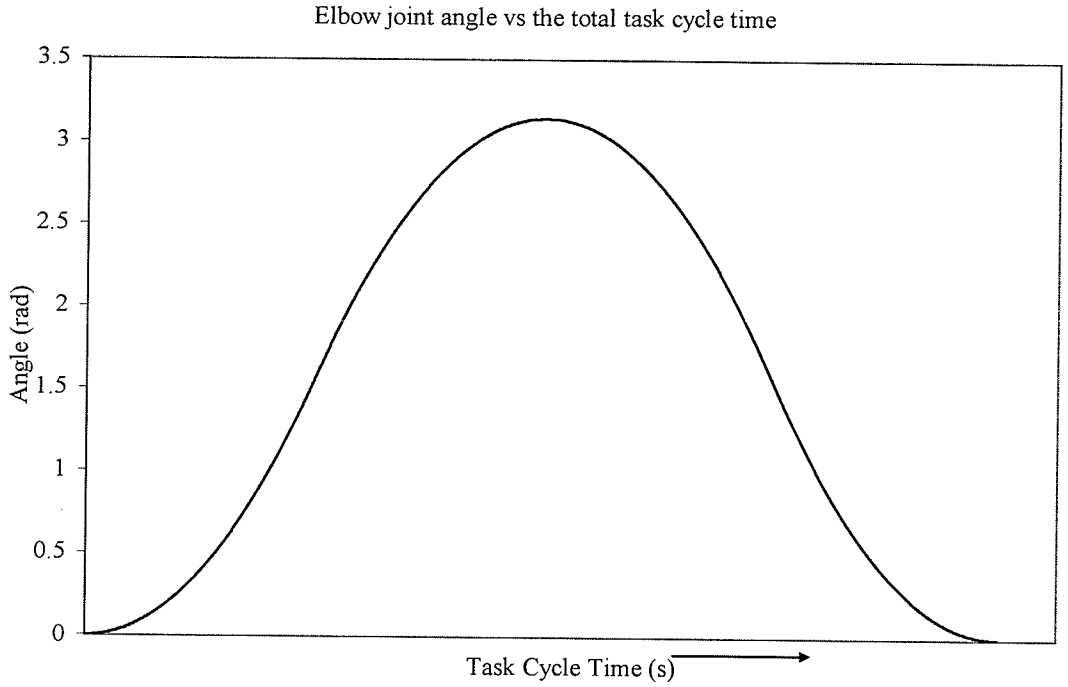

Figure D.1 Elbow Joint Angle

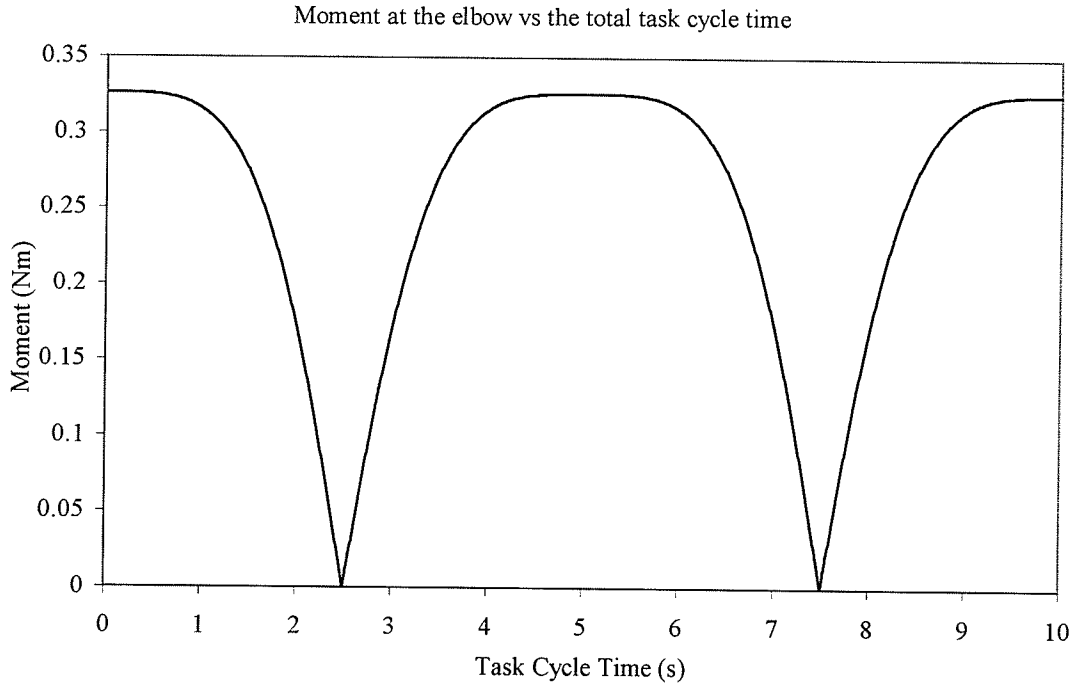

Figure D.2 Elbow Joint Moment with Neutral Forearm, 10s Task Cycle

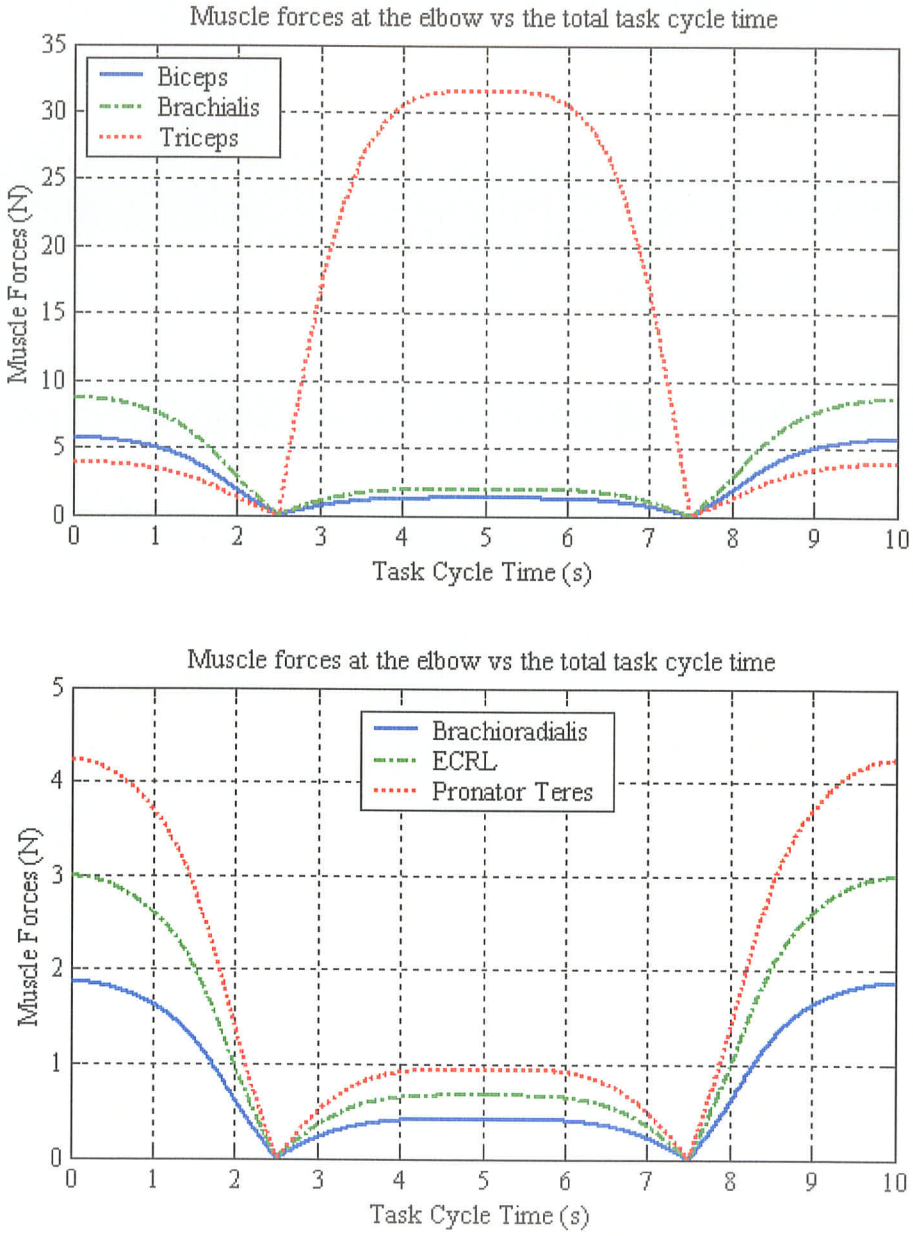

Figure D.3 Individual Muscle Forces with Neutral Forearm, 10s Task Cycle

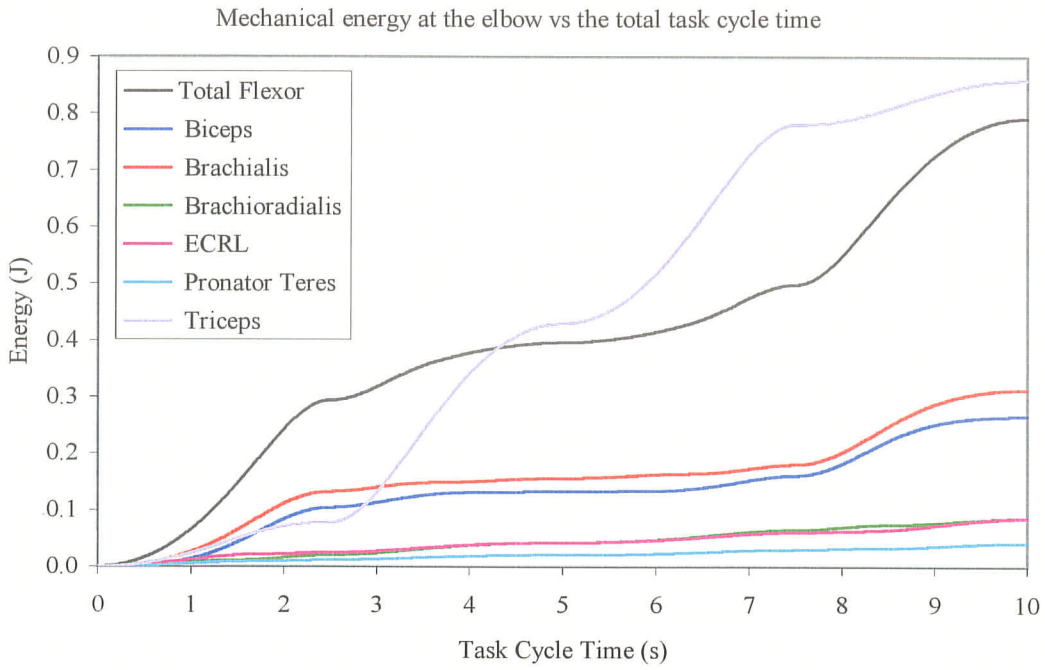

Figure D.4 Mechanical Energy with Neutral Forearm, 10s Task Cycle

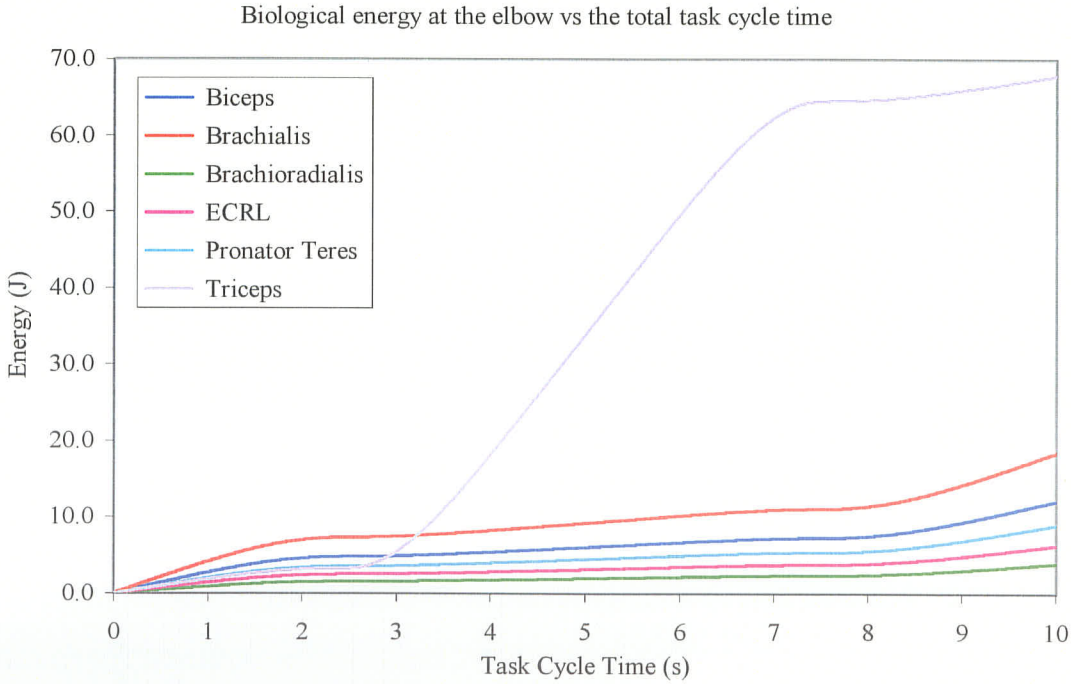

Figure D.5 Biological Energy with Neutral Forearm, 10s Task Cycle

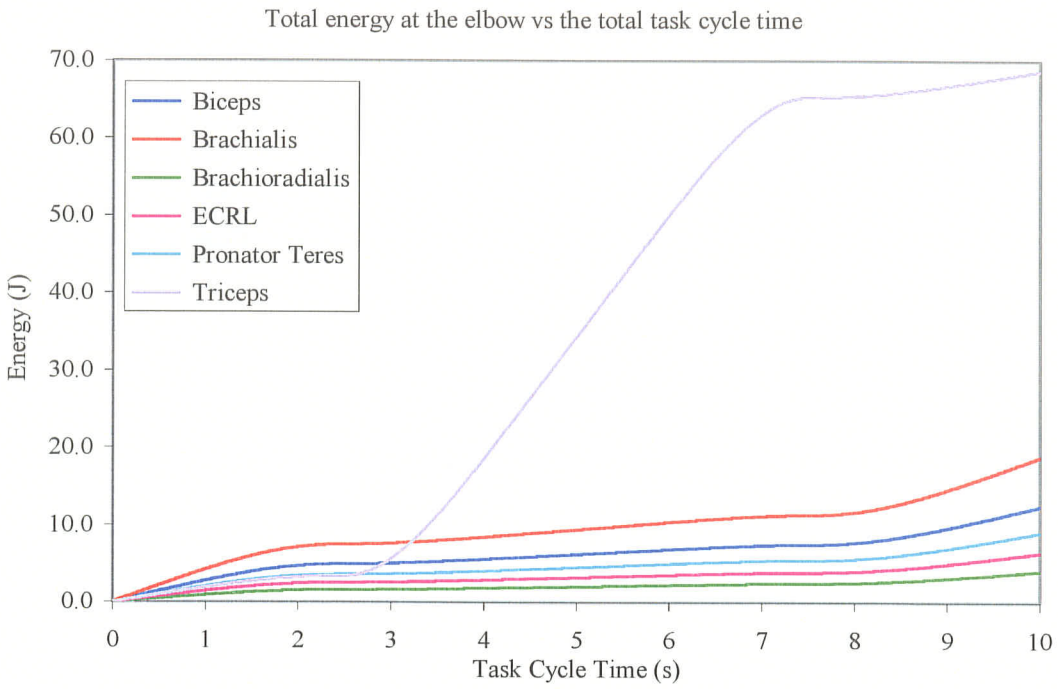

Figure D.6 Total Energy with Neutral Forearm, 10s Task Cycle

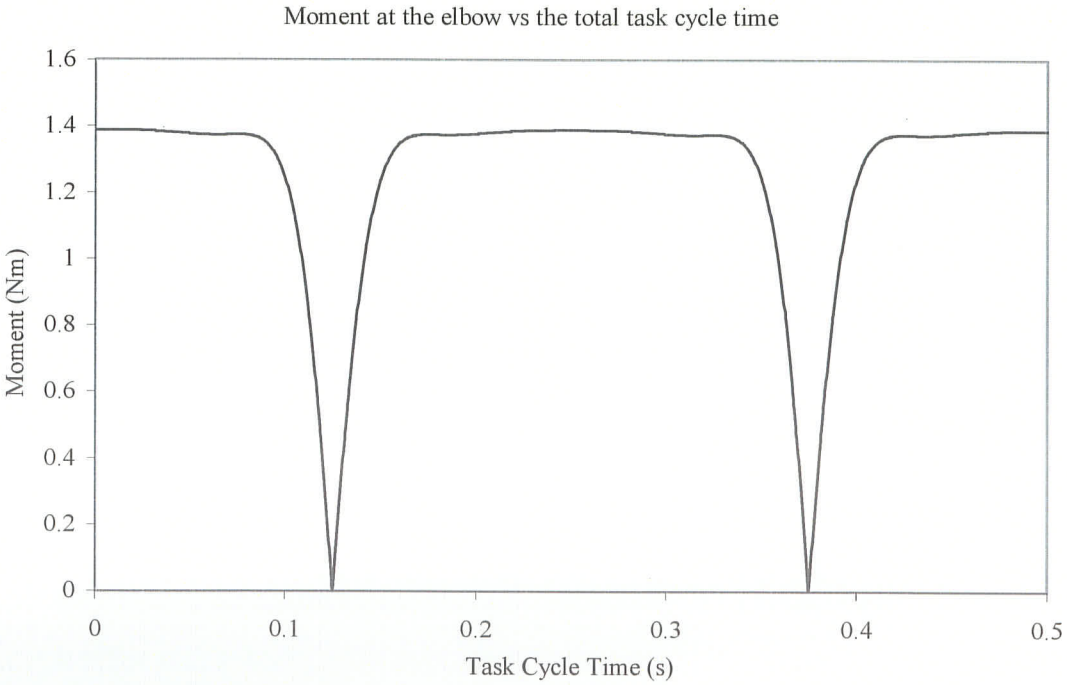

Figure D.7 Elbow Joint Moment with Neutral Forearm, 0.5s Task Cycle

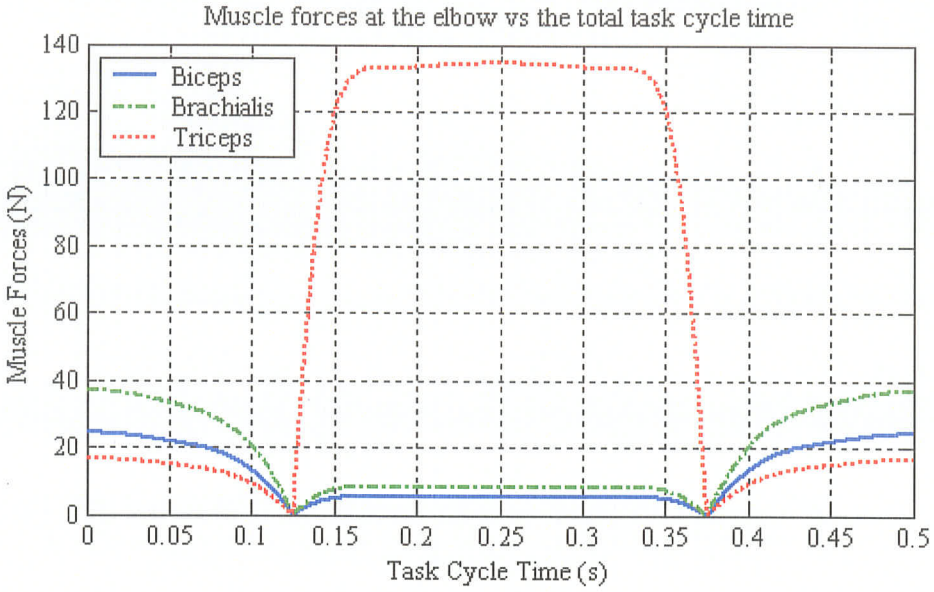

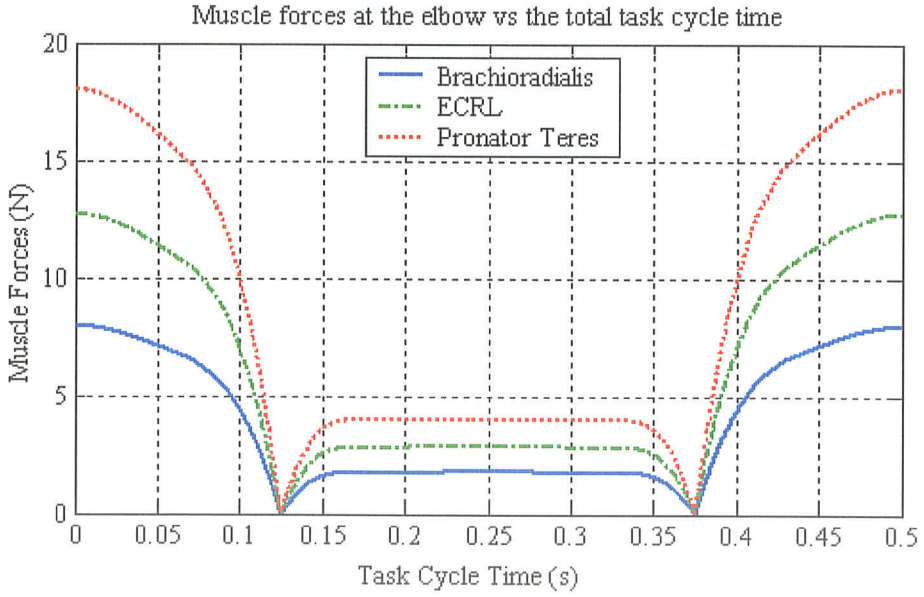

Figure D.8 Individual Muscle Forces with Neutral Forearm, 0.5s Task Cycle

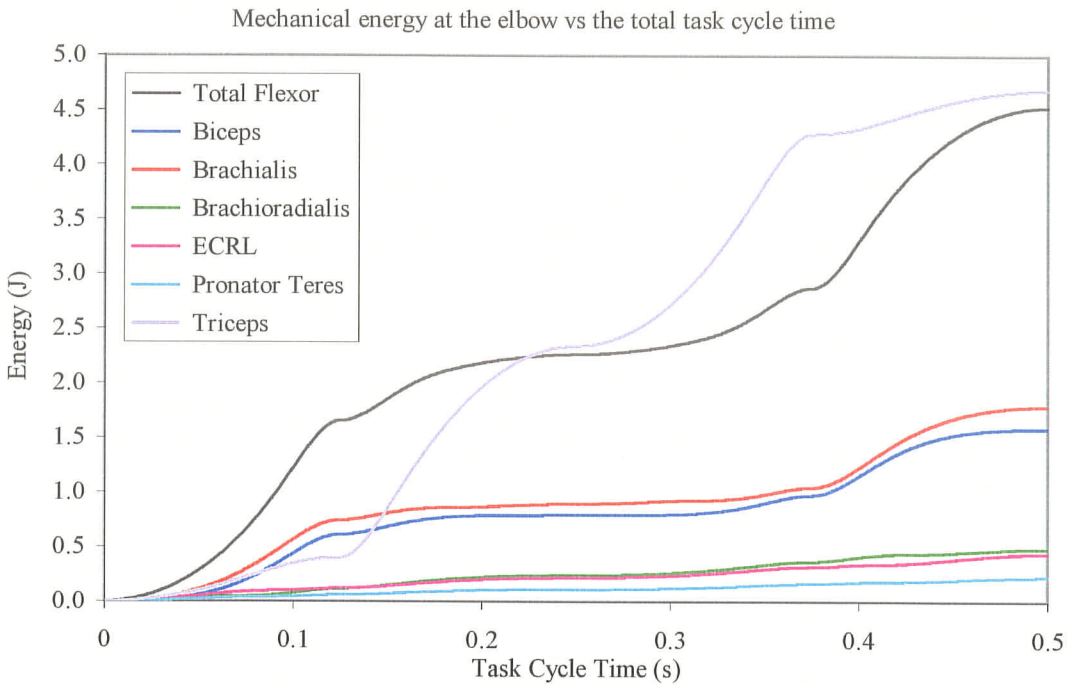

Figure D.9 Mechanical Energy with Neutral Forearm, 0.5s Task Cycle

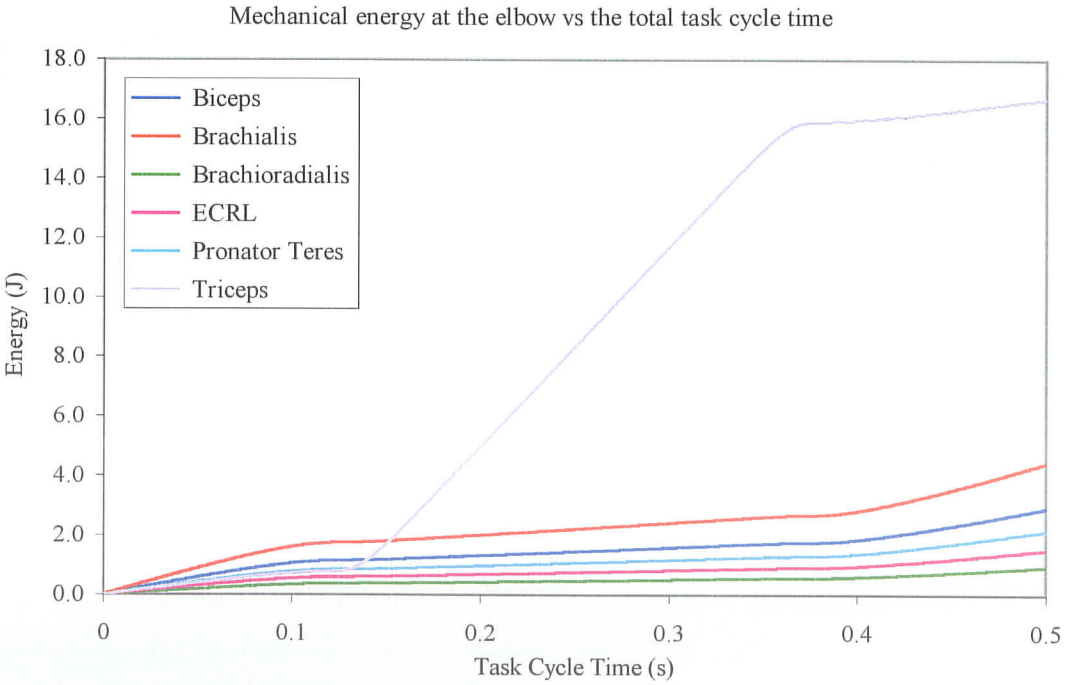

Figure D.10 Biological Energy with Neutral Forearm, 0.5s Task Cycle

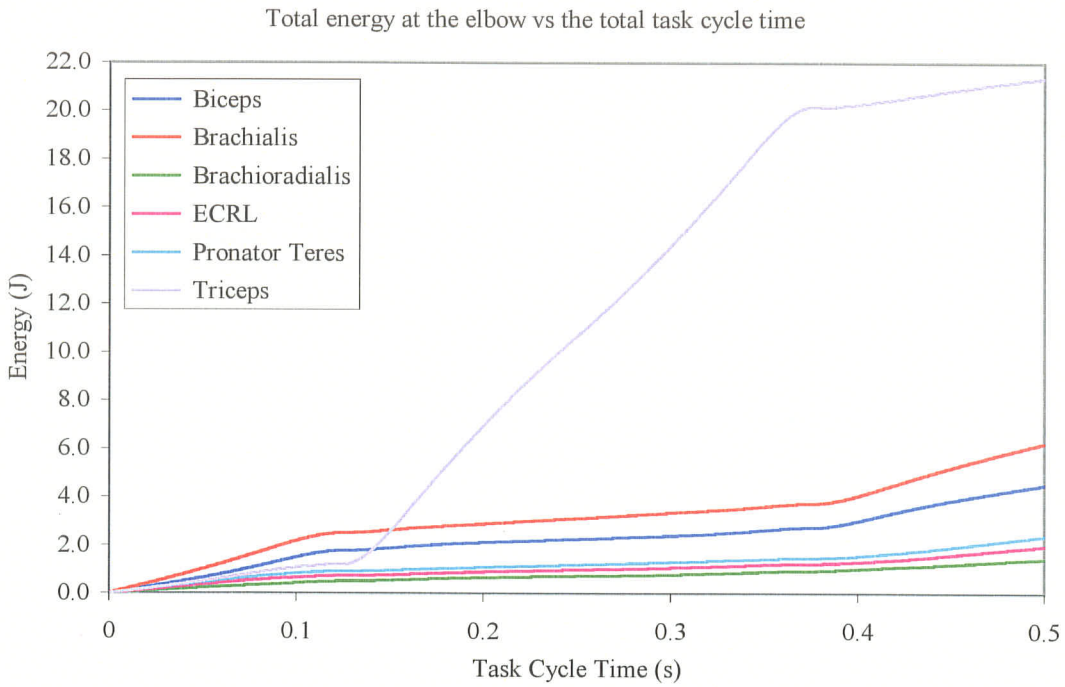

Figure D.11 Total Energy with Neutral Forearm, 0.5s Task Cycle

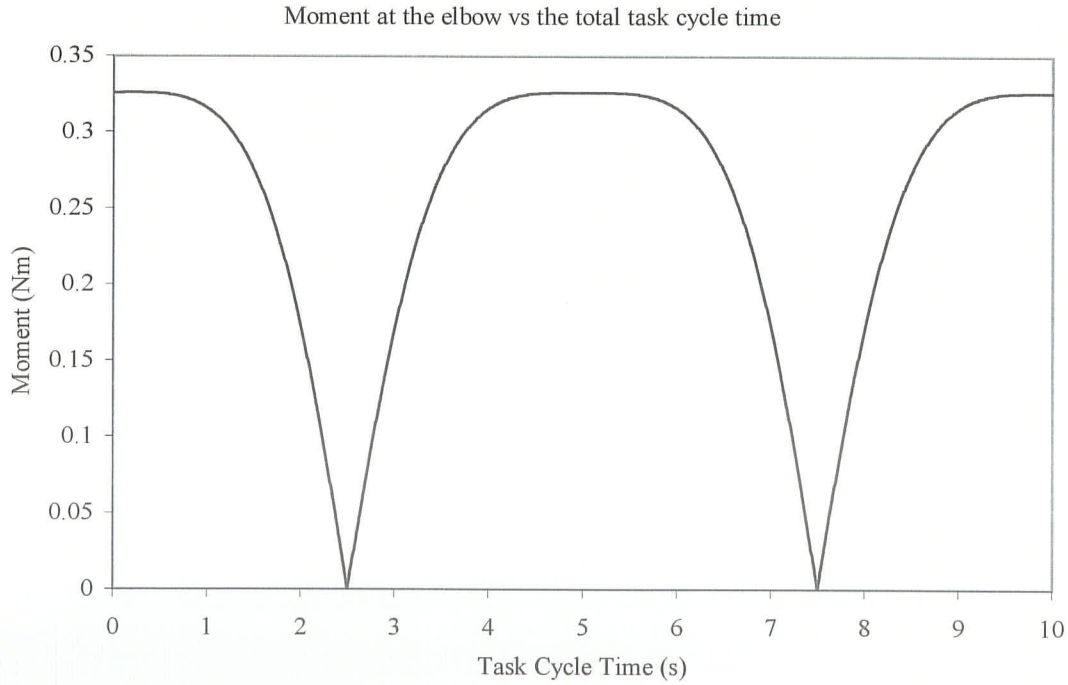

Figure D.12 Elbow Joint Moment in Pronation, 10s Task Cycle

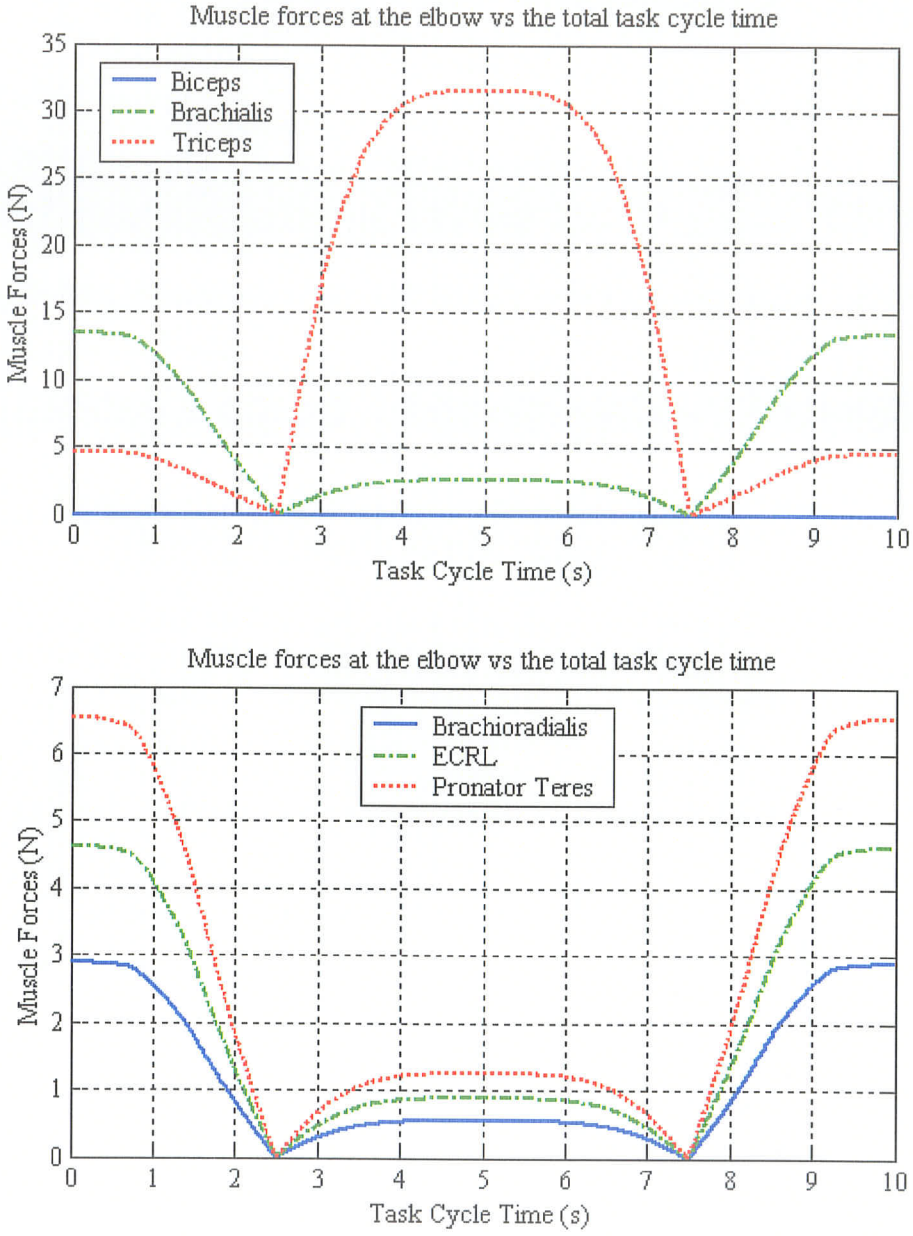

Figure D.13 Individual Muscle Forces in Pronation, 10s Task Cycle

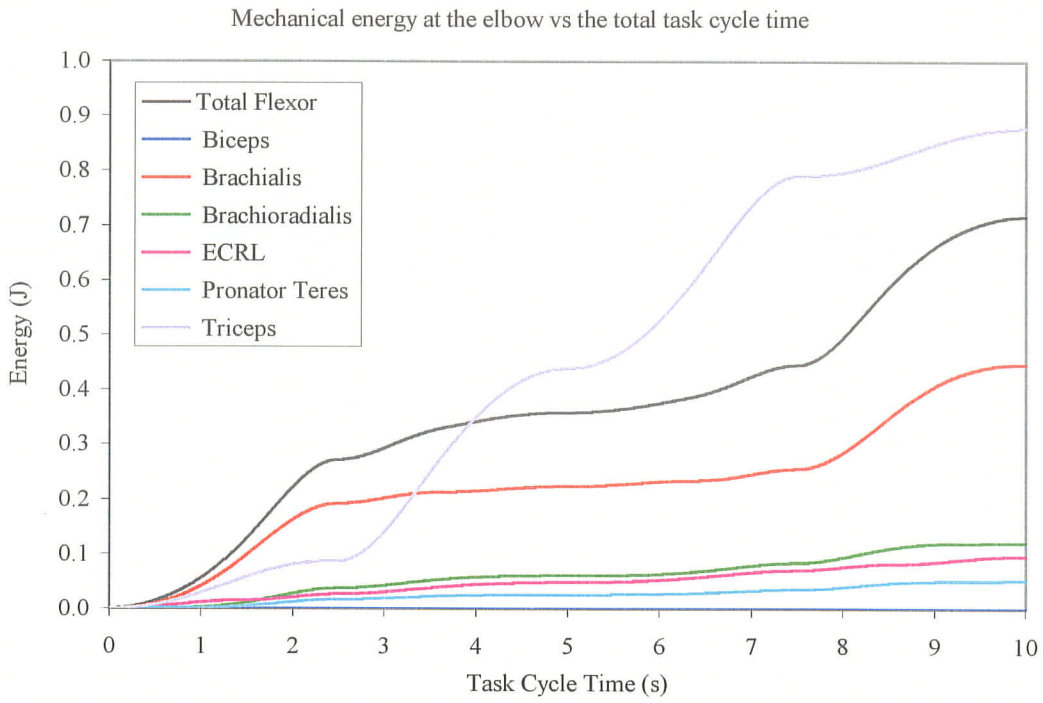

Figure D.14 Mechanical Energy in Pronation, 10s Task Cycle

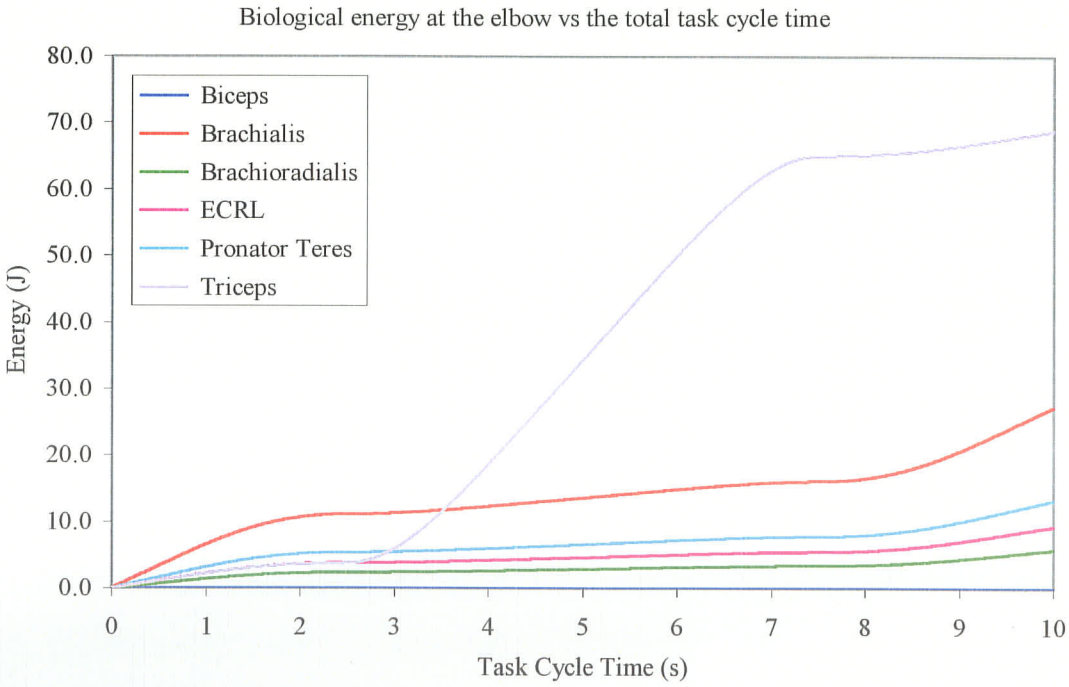

Figure D.15 Biological Energy in Pronation, 10s Task Cycle

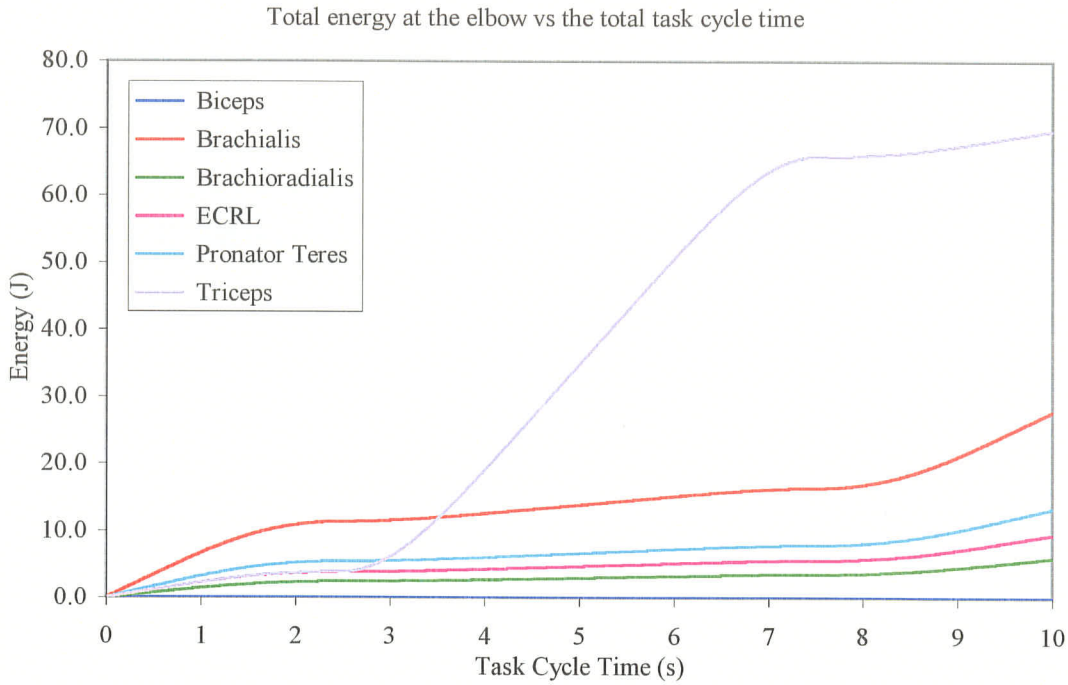

Figure D.16 Total Energy in Pronation, 10s Task Cycle

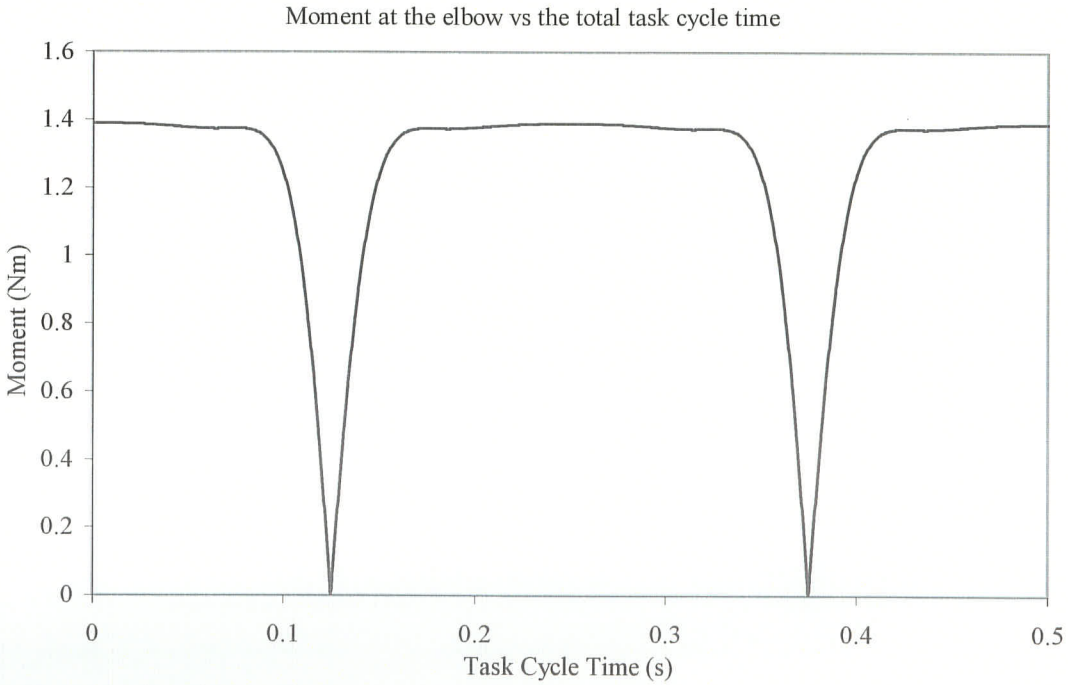

Figure D.17 Elbow Joint Moment in Pronation, 0.5s Task Cycle

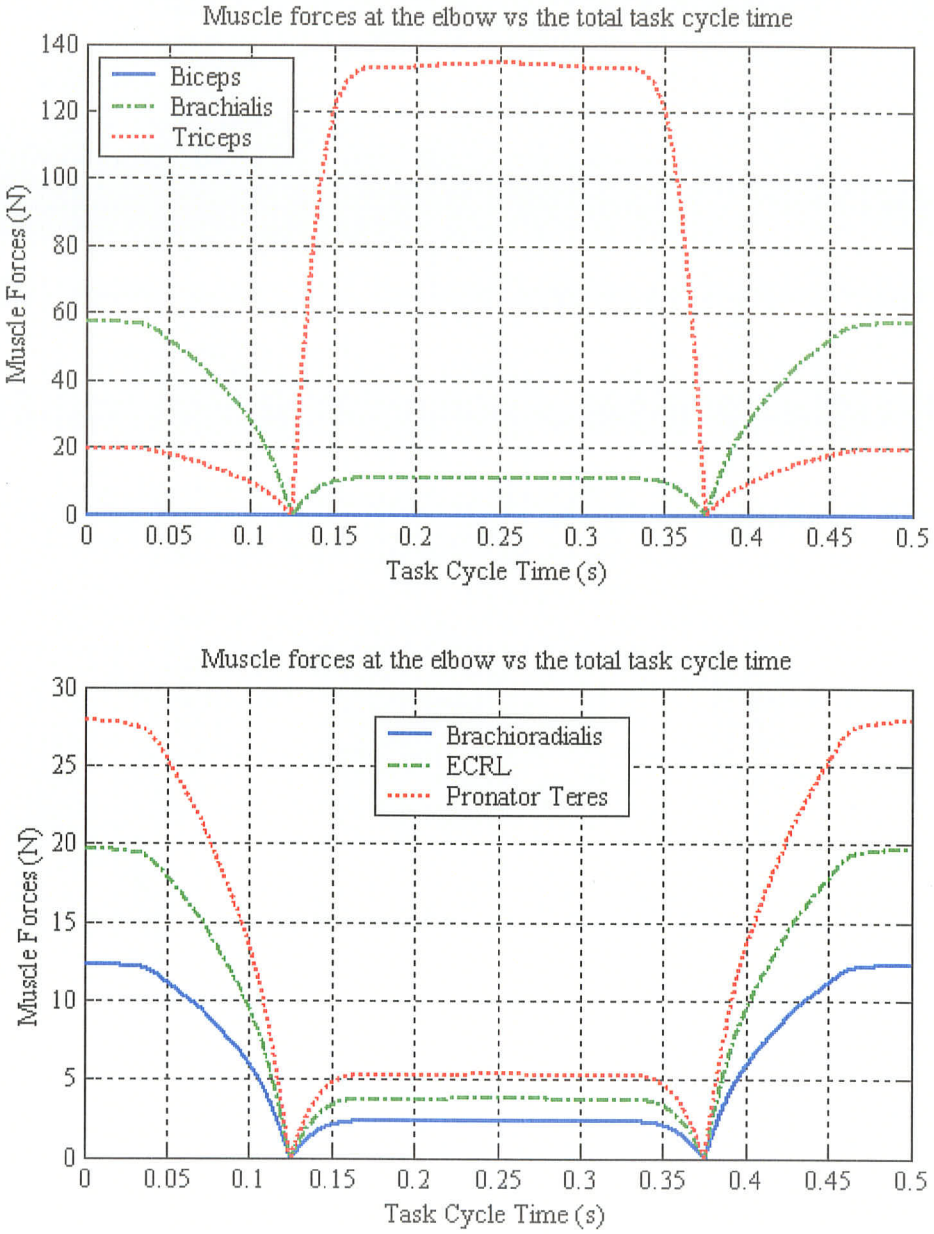

Figure D.18 Individual Muscle Forces in Pronation, 0.5s Task Cycle Time

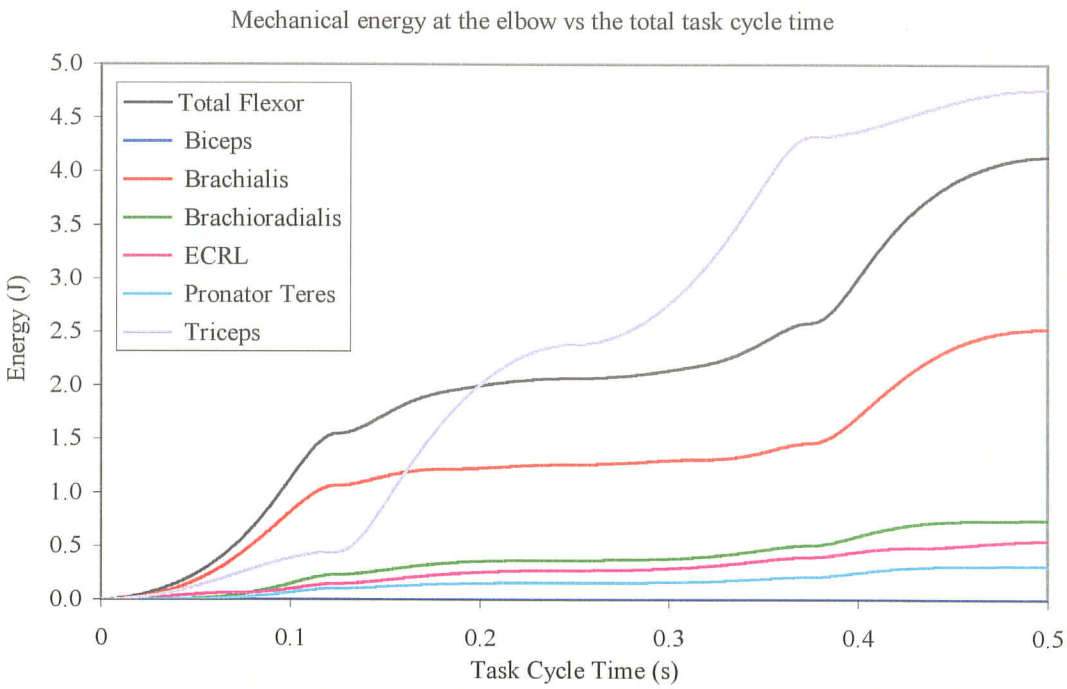

Figure D.19 Mechanical Energy in Pronation, 0.5s Task Cycle

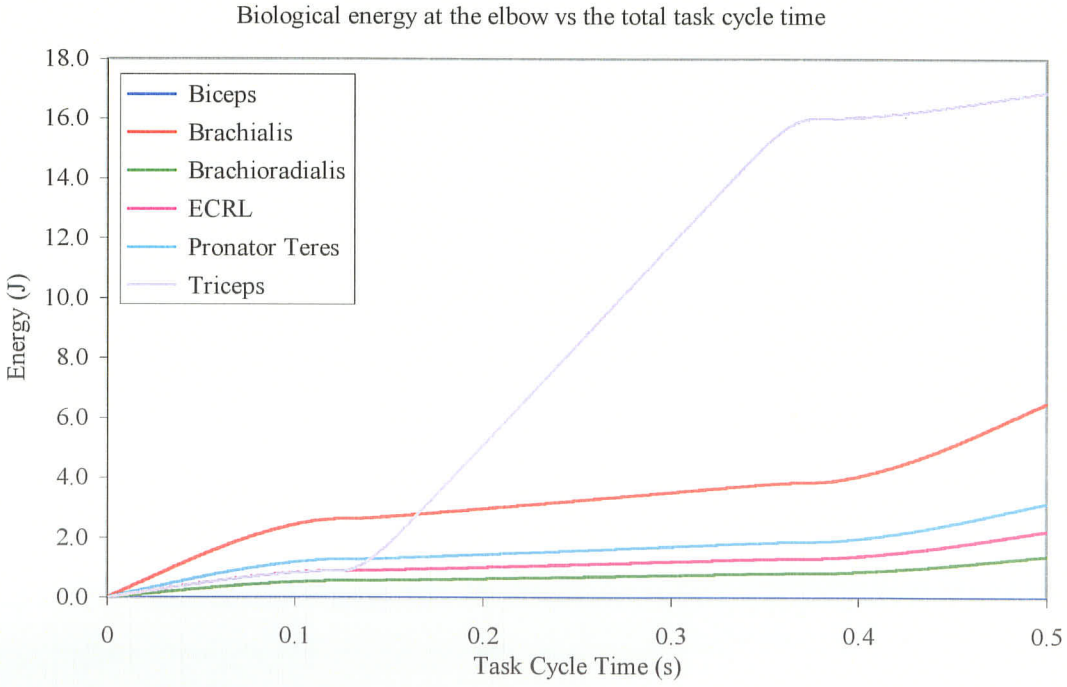

Figure D.20 Biological Energy in Pronation, 0.5s Task Cycle

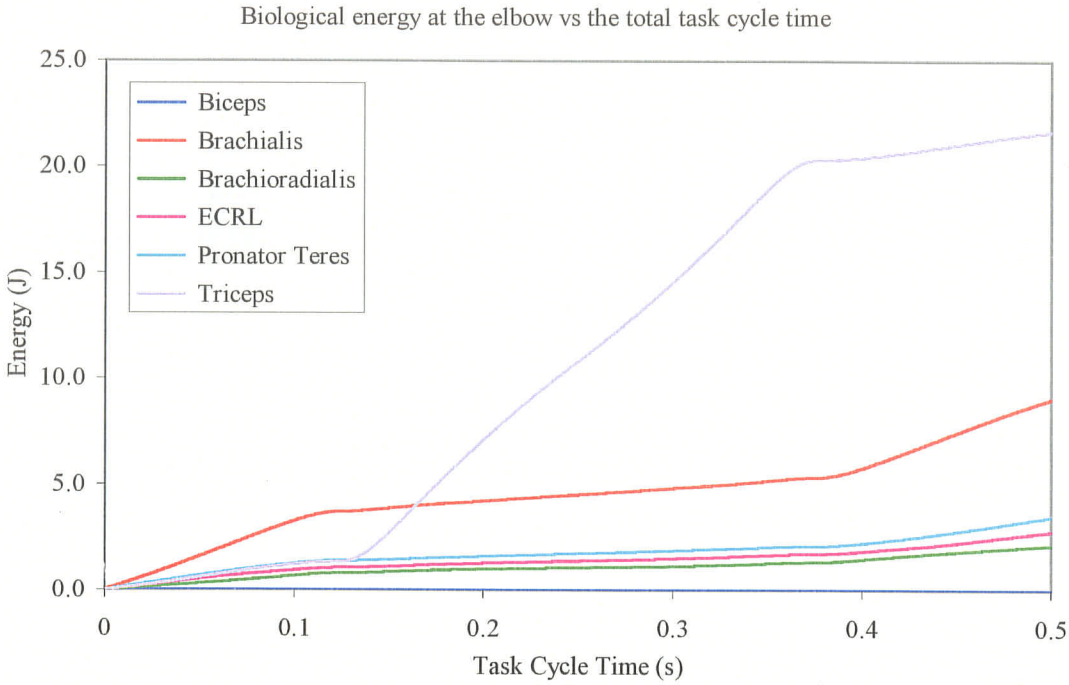

Figure D.21 Total Energy in Pronation, 0.5s Task Cycle

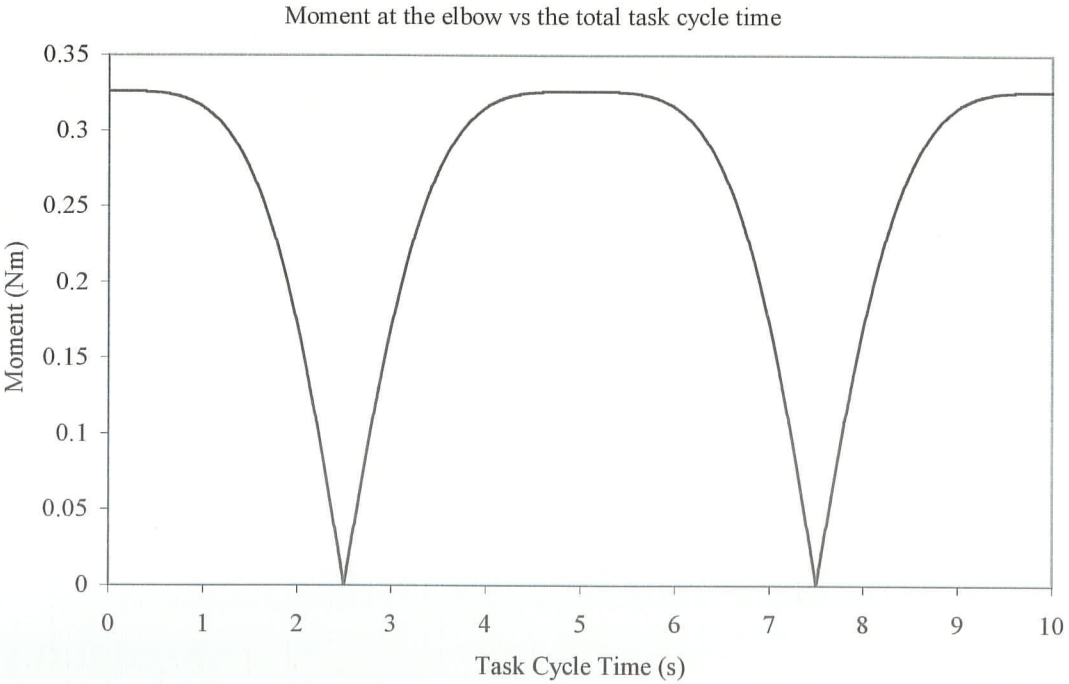

Figure D.22 Elbow Joint Moment in Supination, 10s Task Cycle

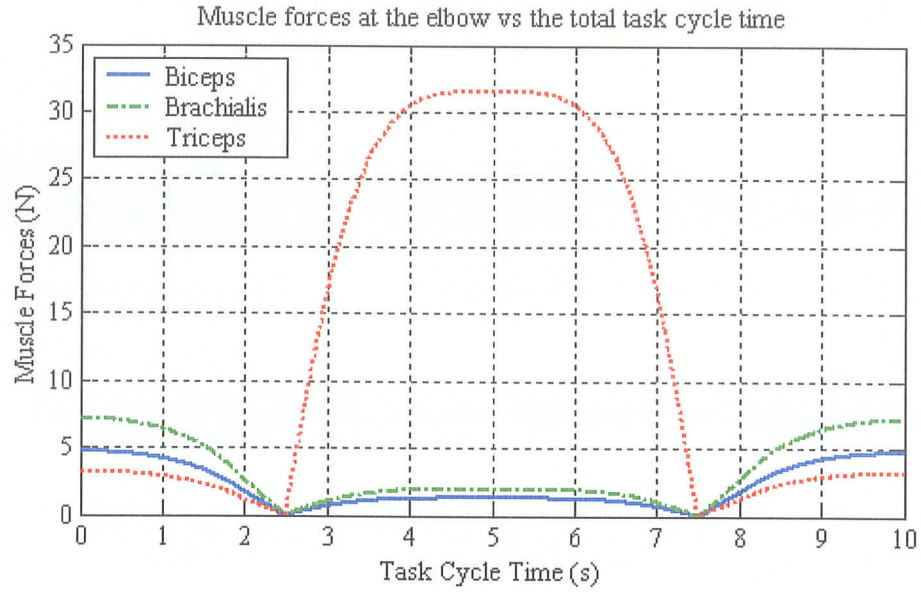

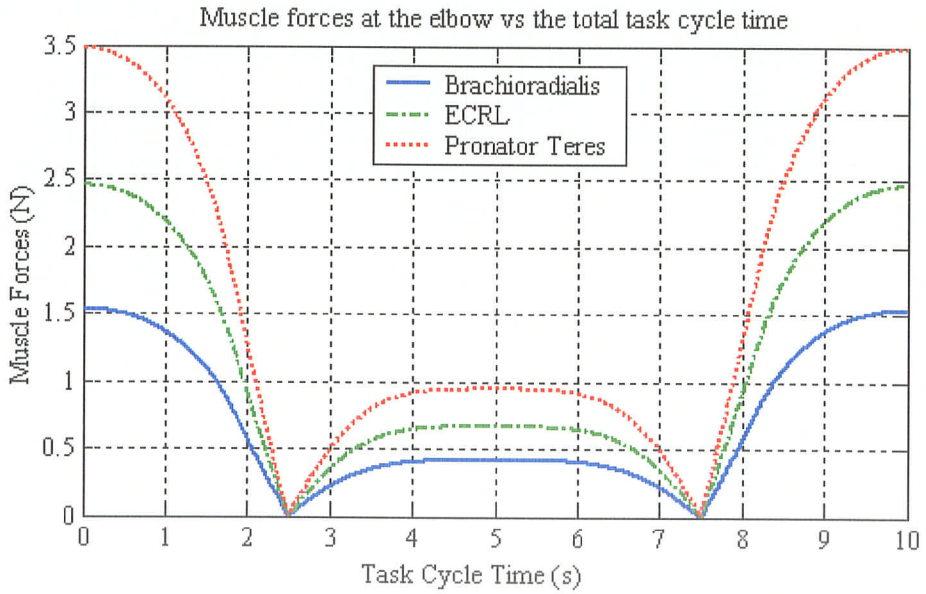

Figure D.23 Individual Muscle Forces in Supination, 10s Task Cycle

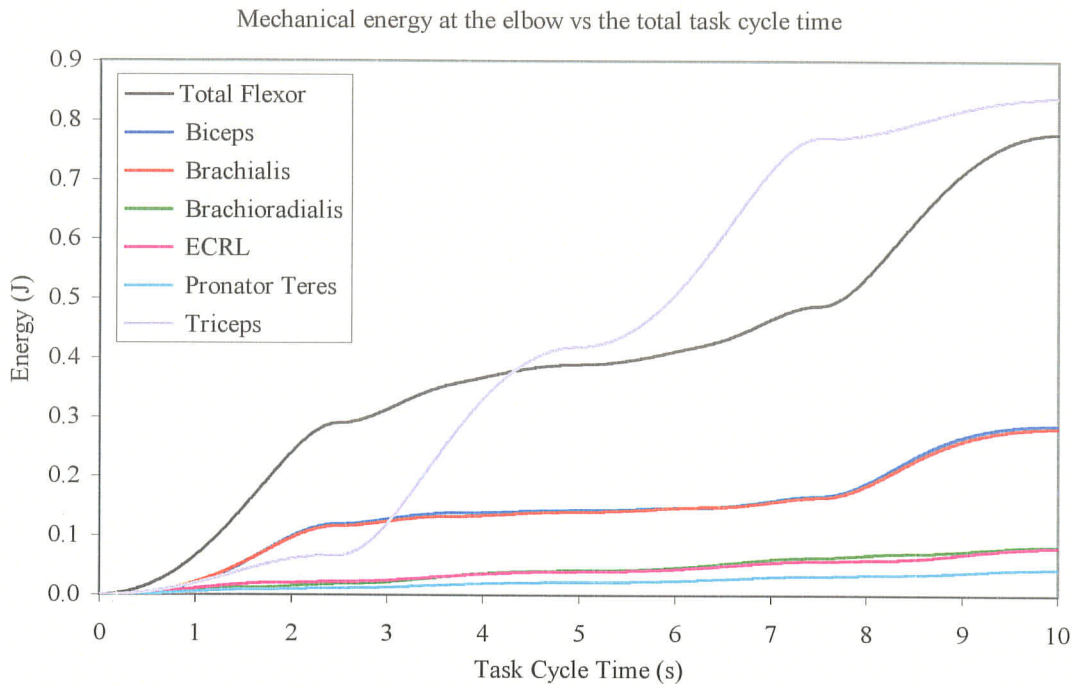

Figure D.24 Mechanical Energy in Supination, 10s Task Cycle

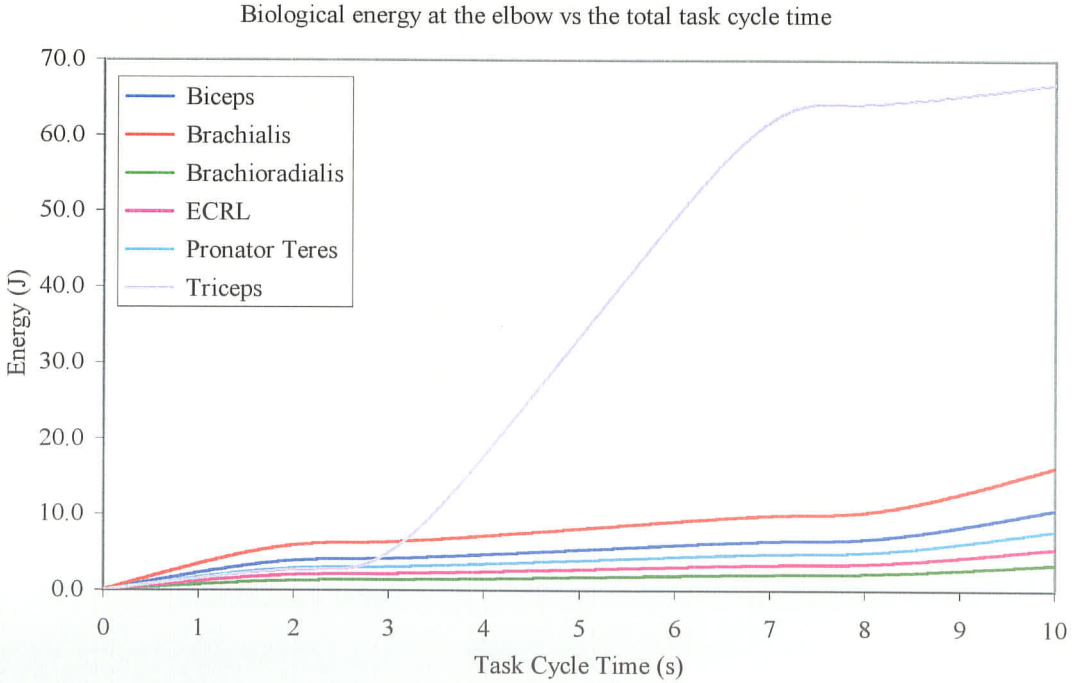

Figure D.25 Biological Energy in Supination, 10s Task Cycle

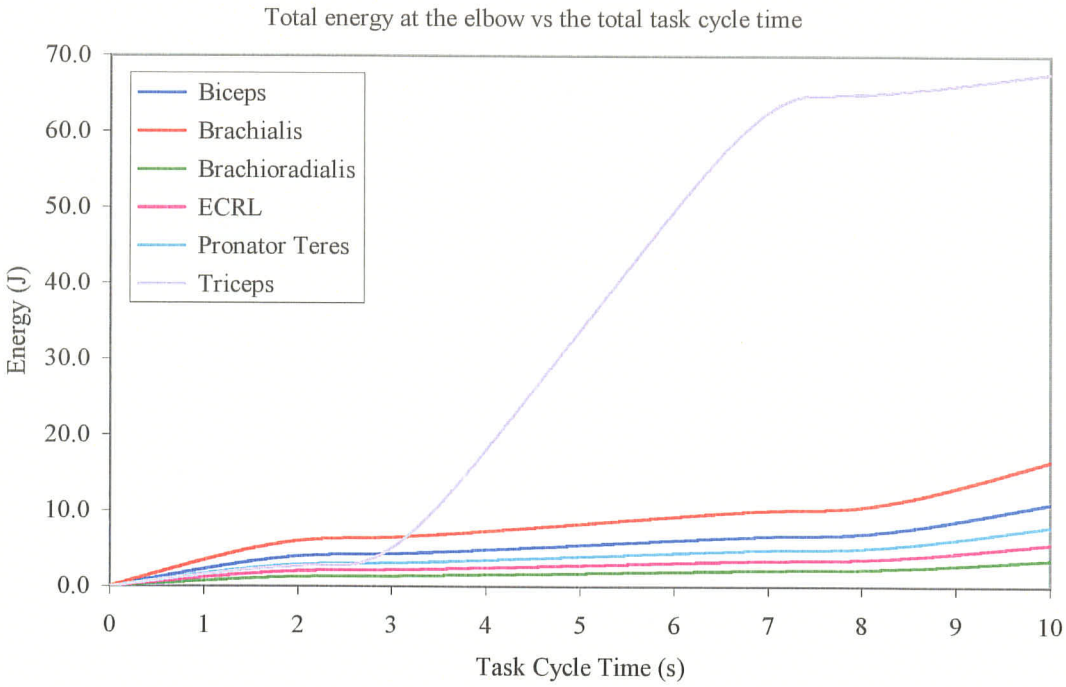

Figure D.26 Total Energy in Pronation, 10s Task Cycle

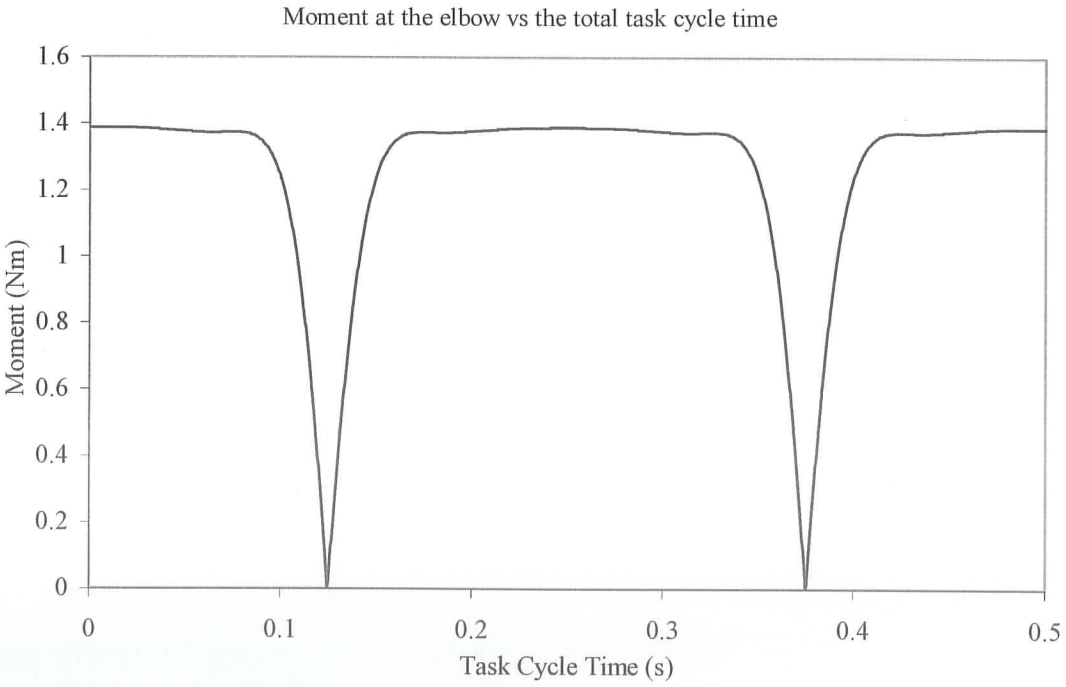

Figure D.27 Elbow Joint Moment in Supination, 0.5s

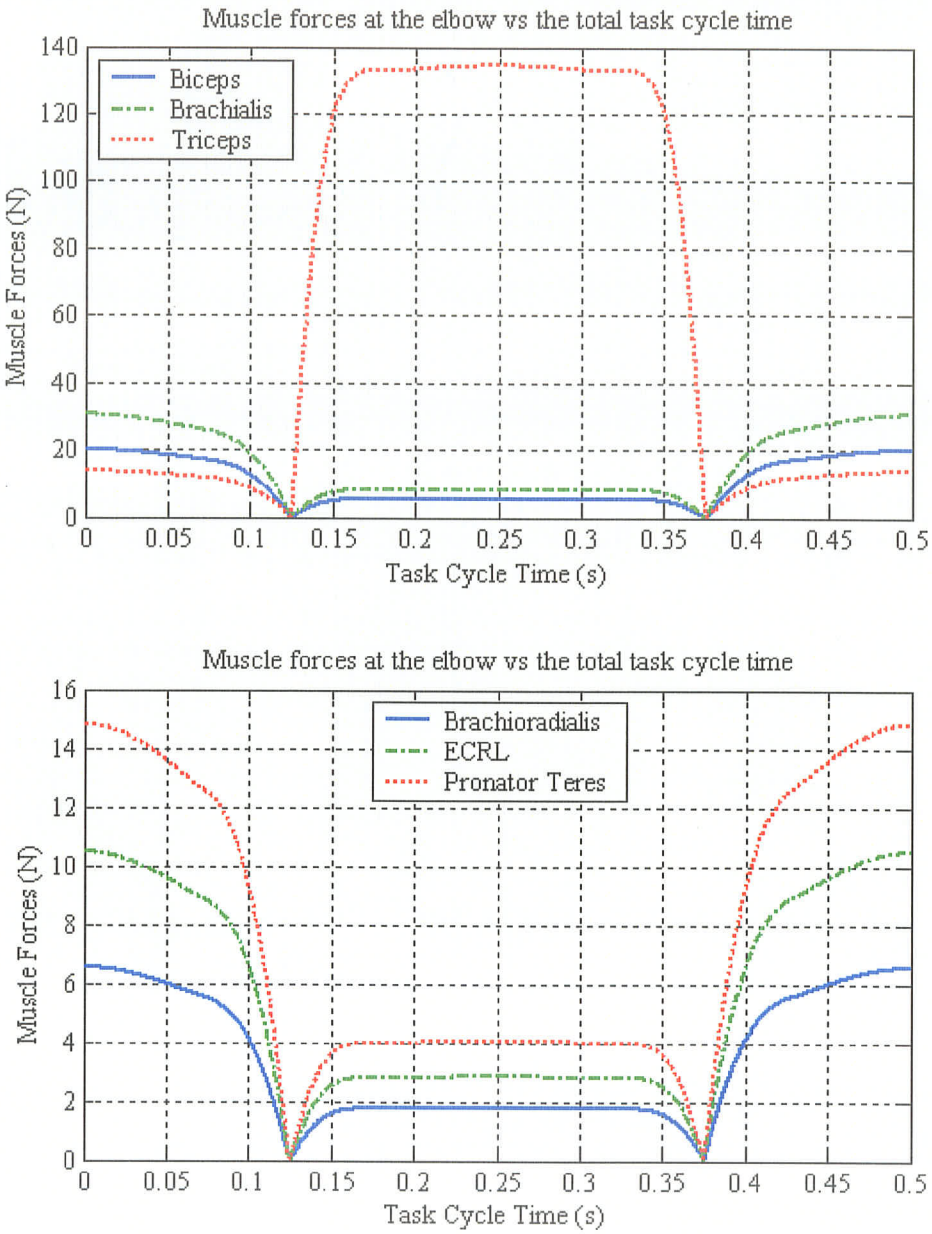

Figure D.28 Individual Muscle Forces in Supination, 0.5s Task Cycle

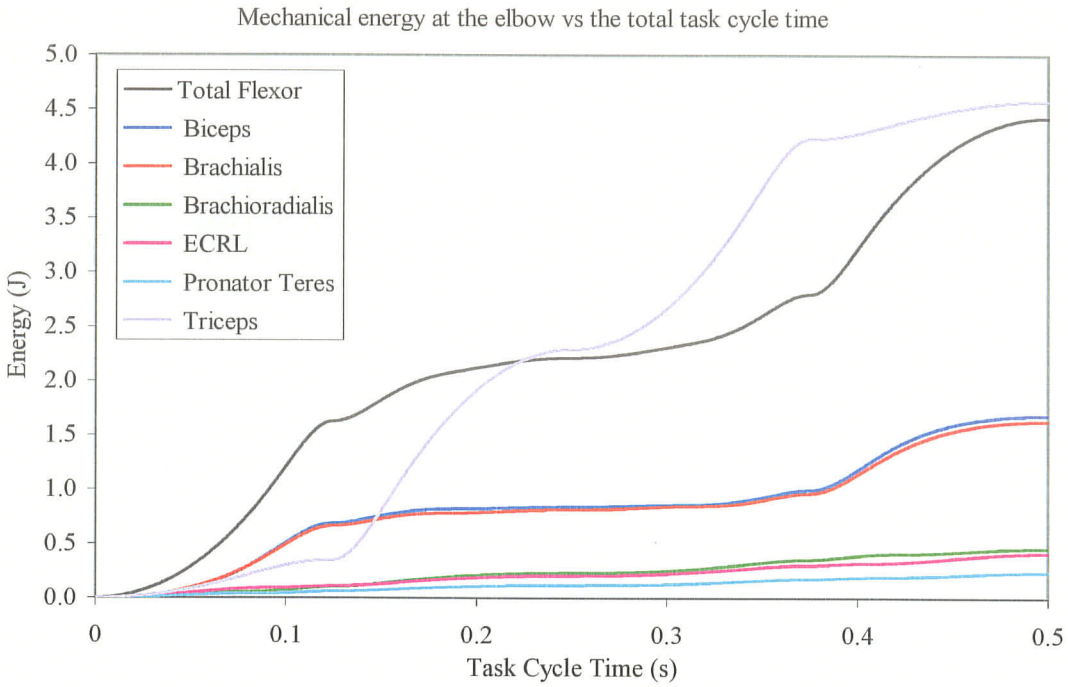

Figure D.29 Mechanical Energy in Supination, 0.5s Task Cycle

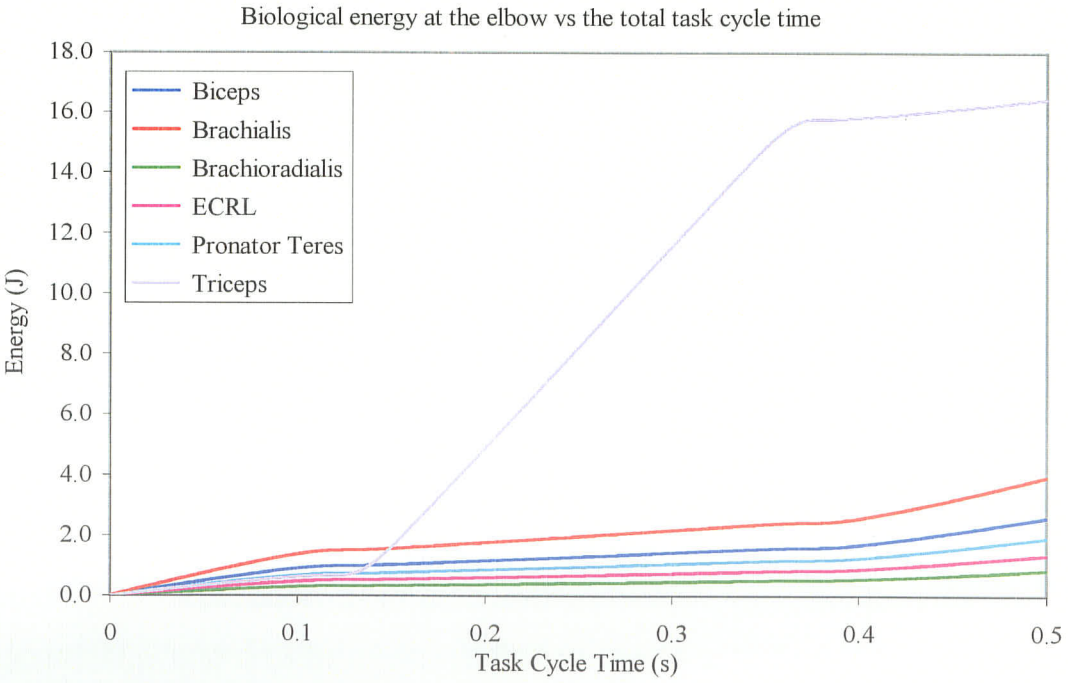

Figure D.30 Biological Energy in Supination, 0.5s Task Cycle

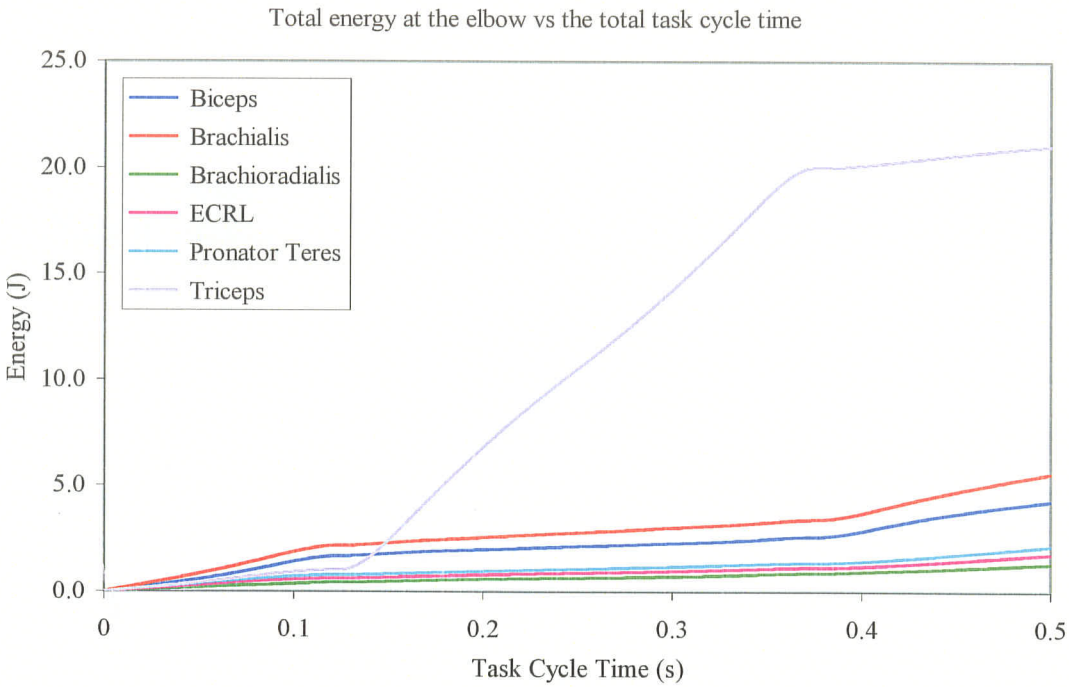

Figure D.31 Total energy in Supination, 0.5s Task Cycle

APPENDIX E

SIMULATION RESULTS – SAGITTAL PLANE MOTION

Appendix E contains the plots obtained from the model simulations for elbow joint motion in the sagittal plane with the forearm in the neutral position, in pronation, and supination. These motion simulations were carried out for both a quasi-static situation (task cycle time of 10 seconds) and a dynamic situation (task cycle time of 0.5 seconds). It should be noted that the elbow joint angle curve shown in Figure E.1 is the same angle progression that occurs for all the simulations in the sagittal plane.

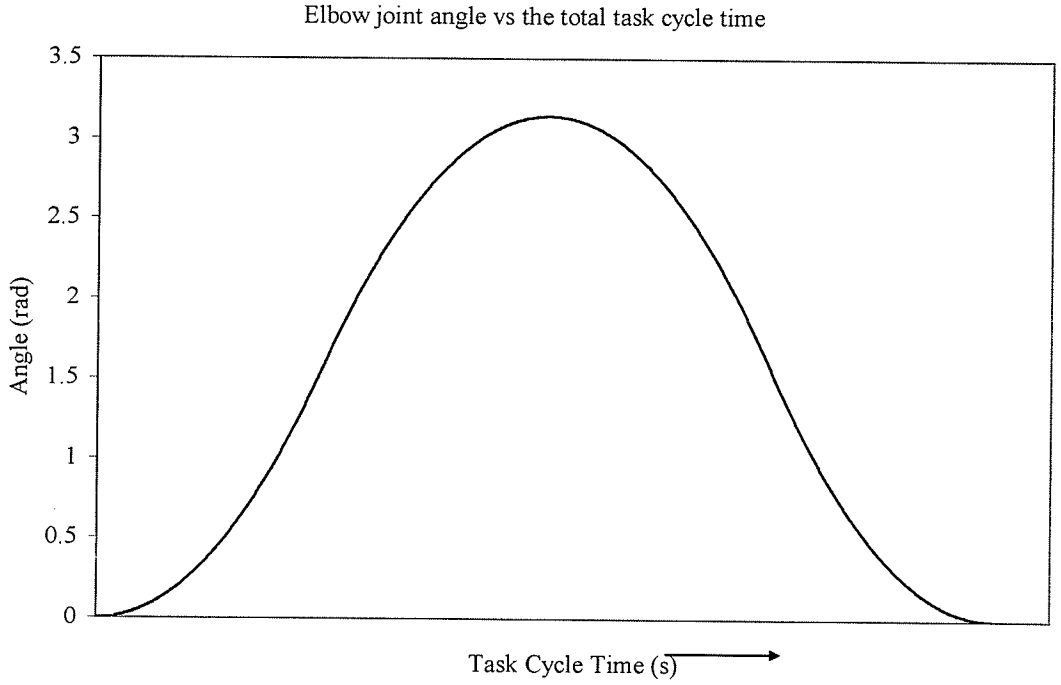

Figure E.1 Elbow Joint Angle

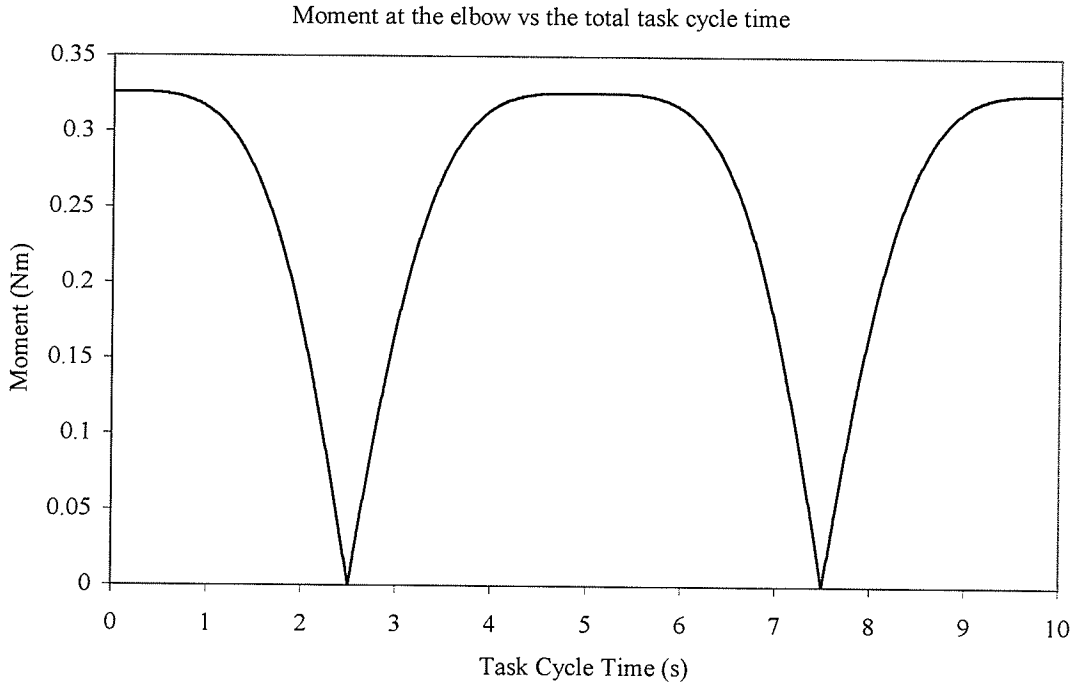

Figure E.2 Elbow Joint Moment with Neutral Forearm, 10s Task Cycle

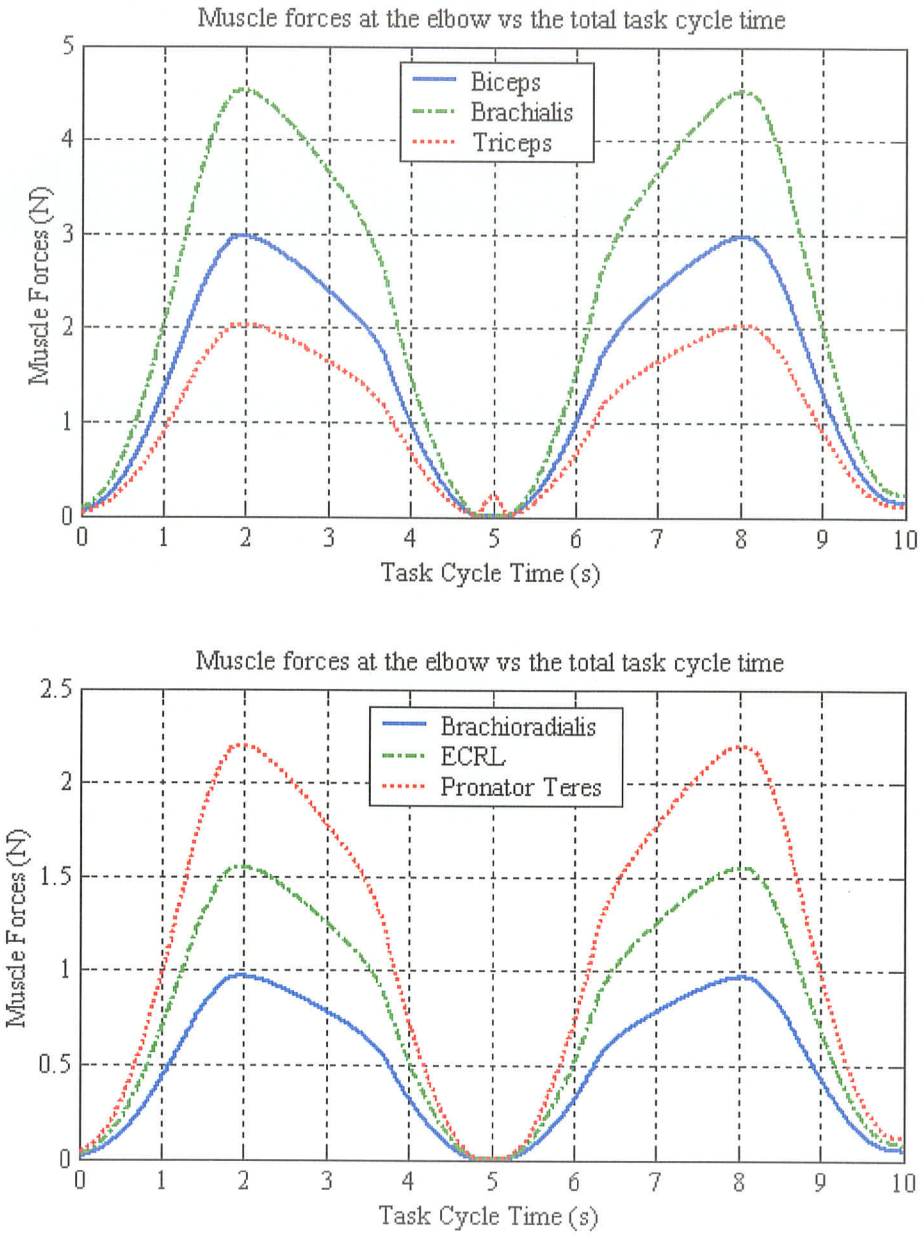

Figure E.3 Individual Muscle Forces with Neutral Forearm, 10s Task Cycle

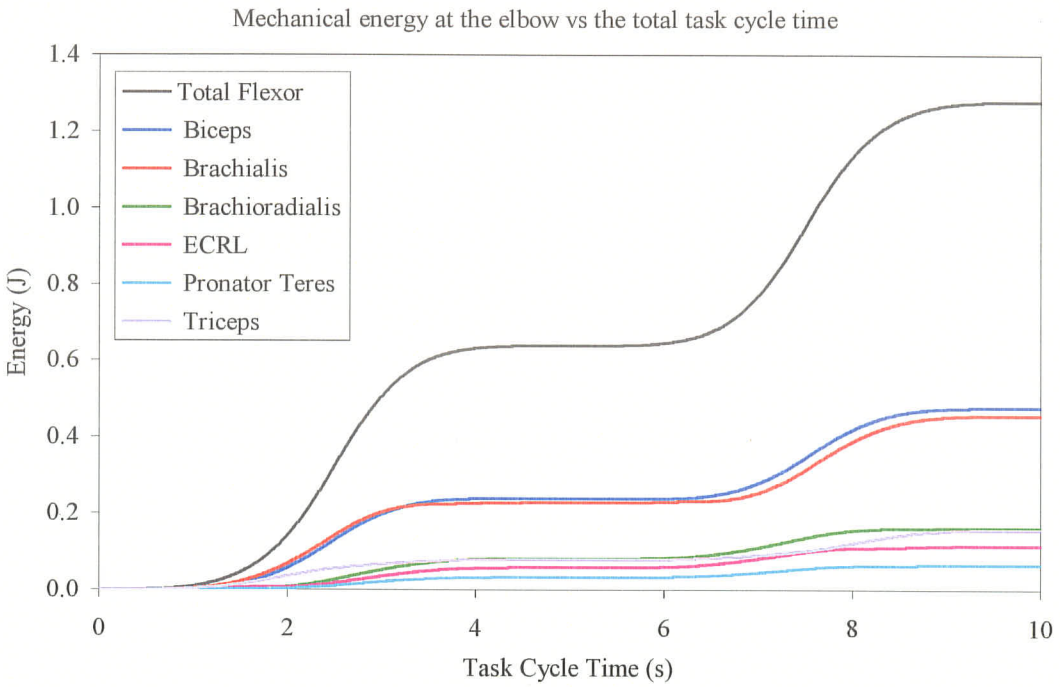

Figure E.4 Mechanical Energy with Neutral Forearm, 10s Task Cycle

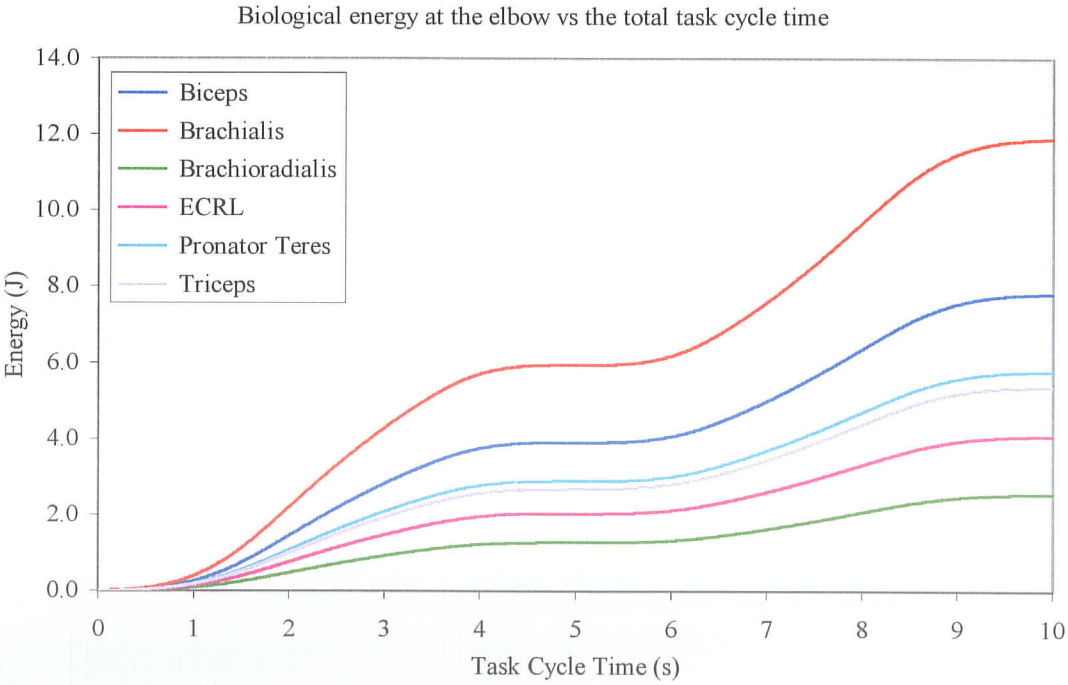

Figure E.5 Biological Energy with Neutral Forearm, 10s Task Cycle

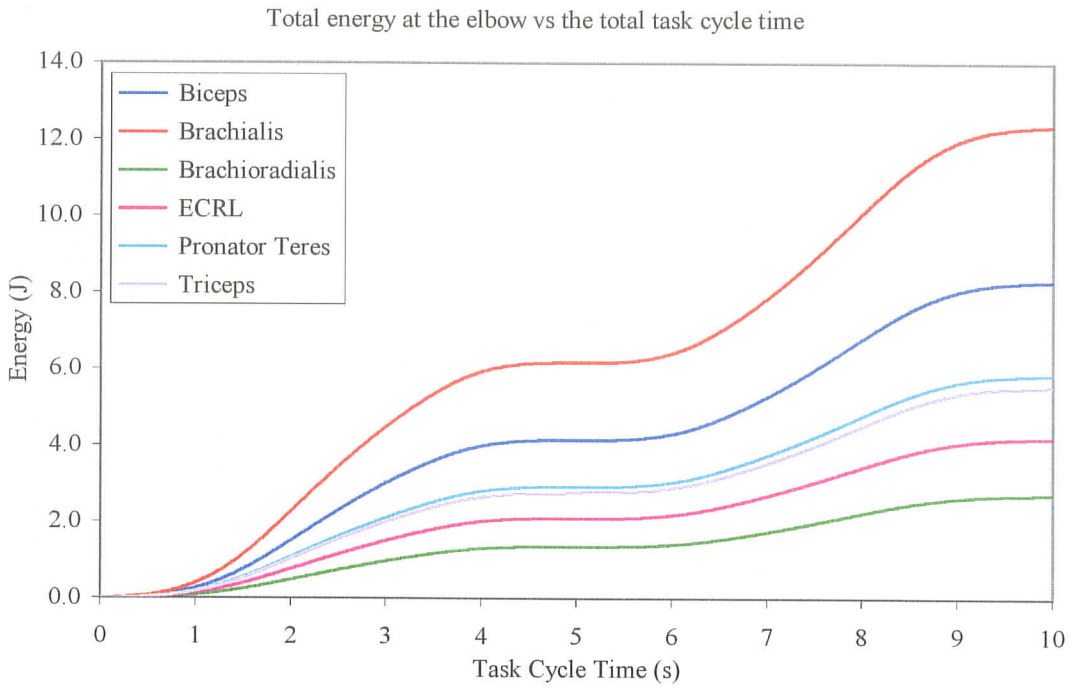

Figure E.6 Total Energy with Neutral Forearm, 10s Task Cycle

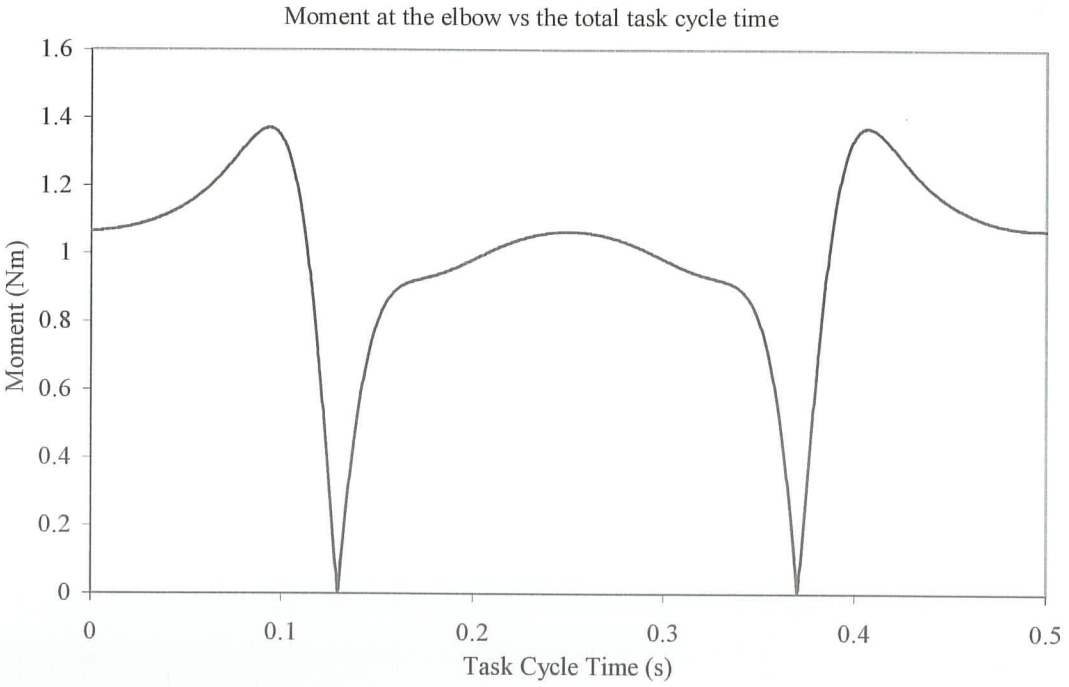

Figure E.7 Elbow Joint Moment with Neutral Forearm, 0.5s Task Cycle

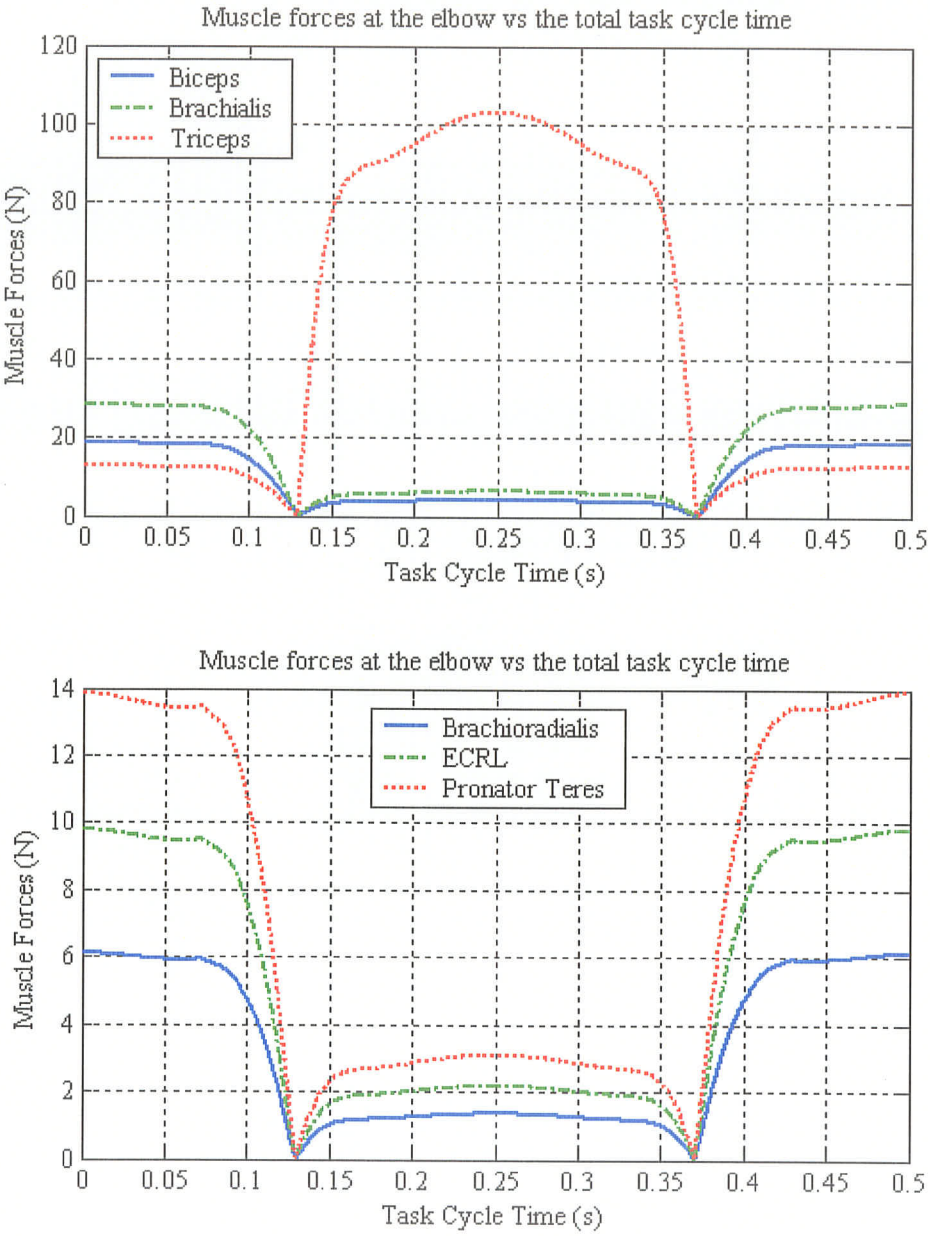

Figure E.8 Individual Muscle Forces with Neutral Forearm, 0.5s Task Cycle

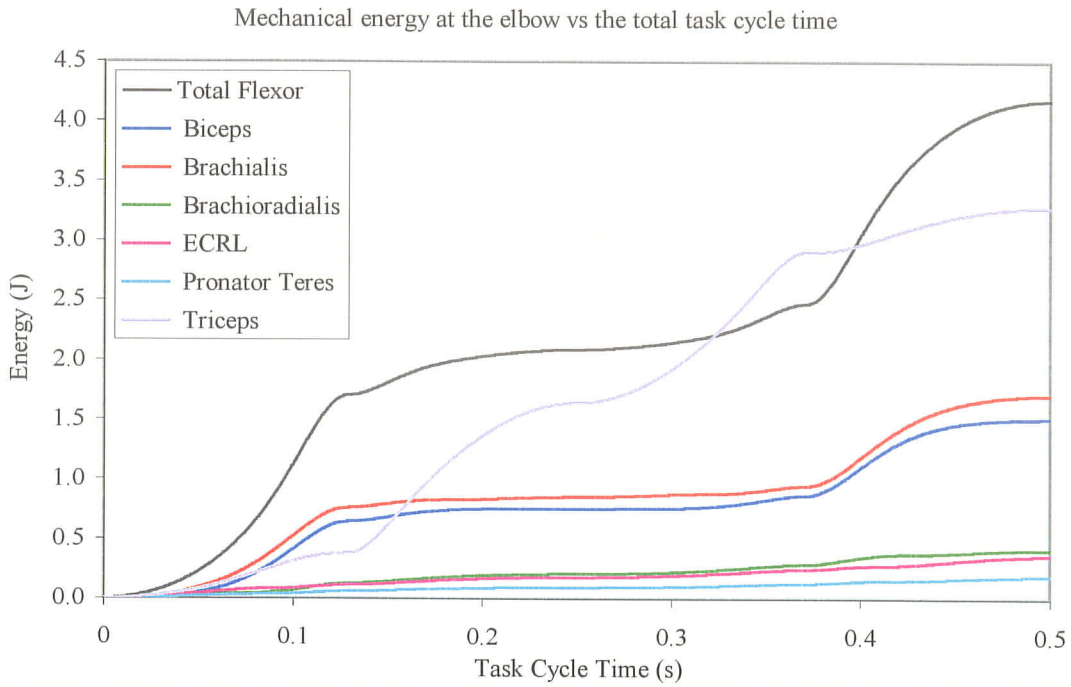

Figure E.9 Mechanical Energy with Neutral Forearm, 0.5s Task Cycle

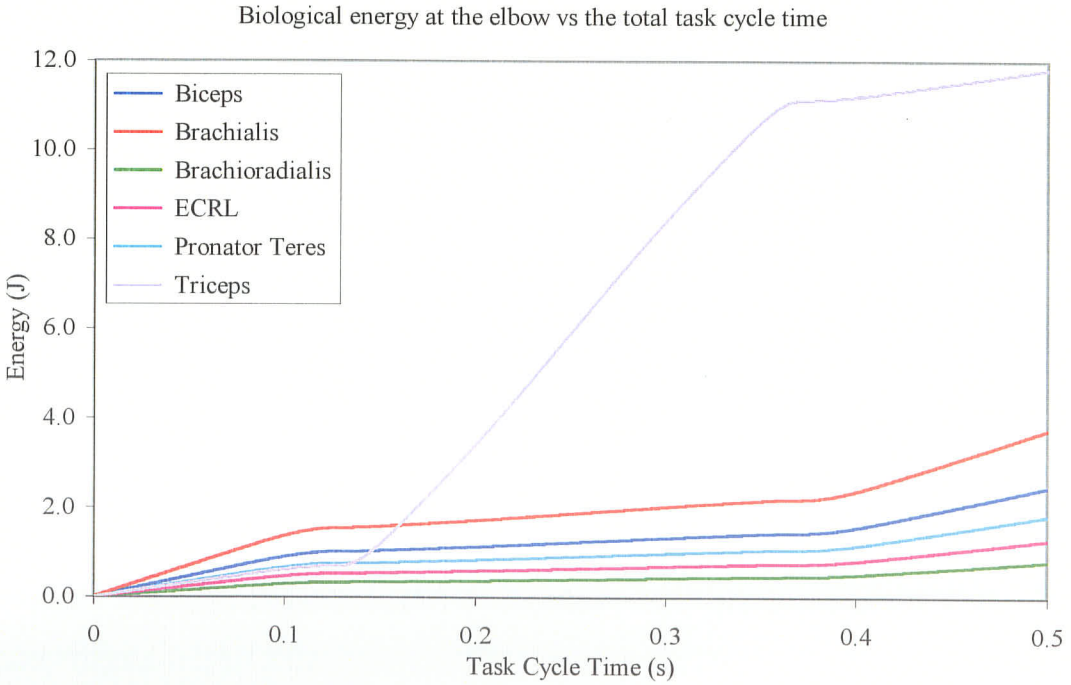

Figure E.10 Biological Energy with Neutral Forearm, 0.5s Task Cycle

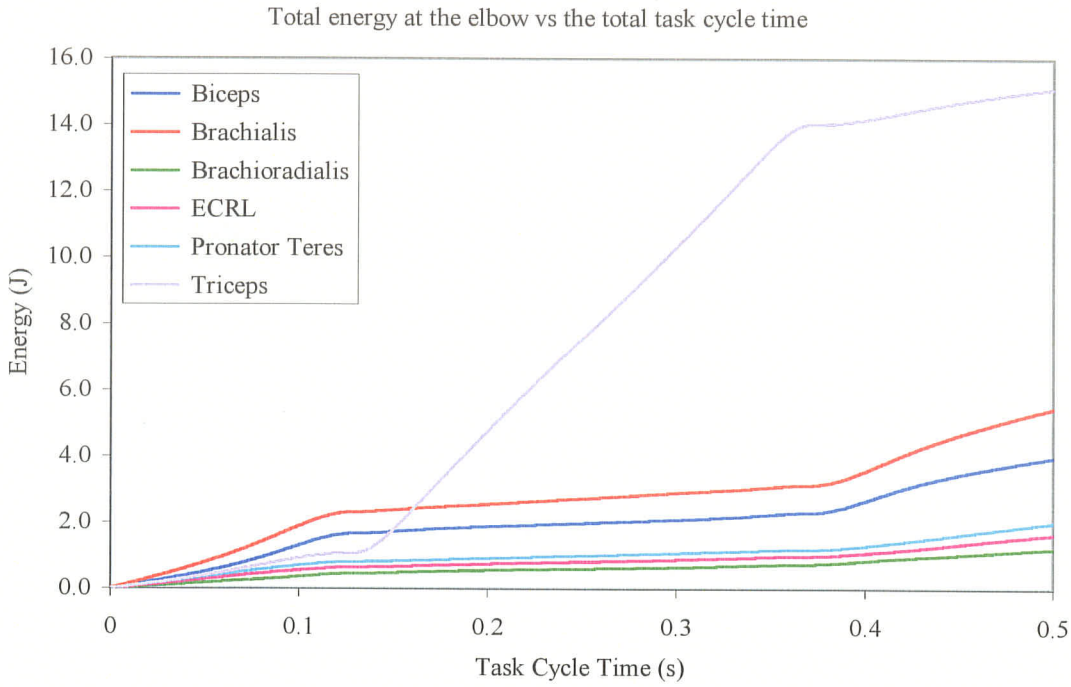

Figure E.11 Total Energy with Neutral Forearm, 0.5s Task Cycle

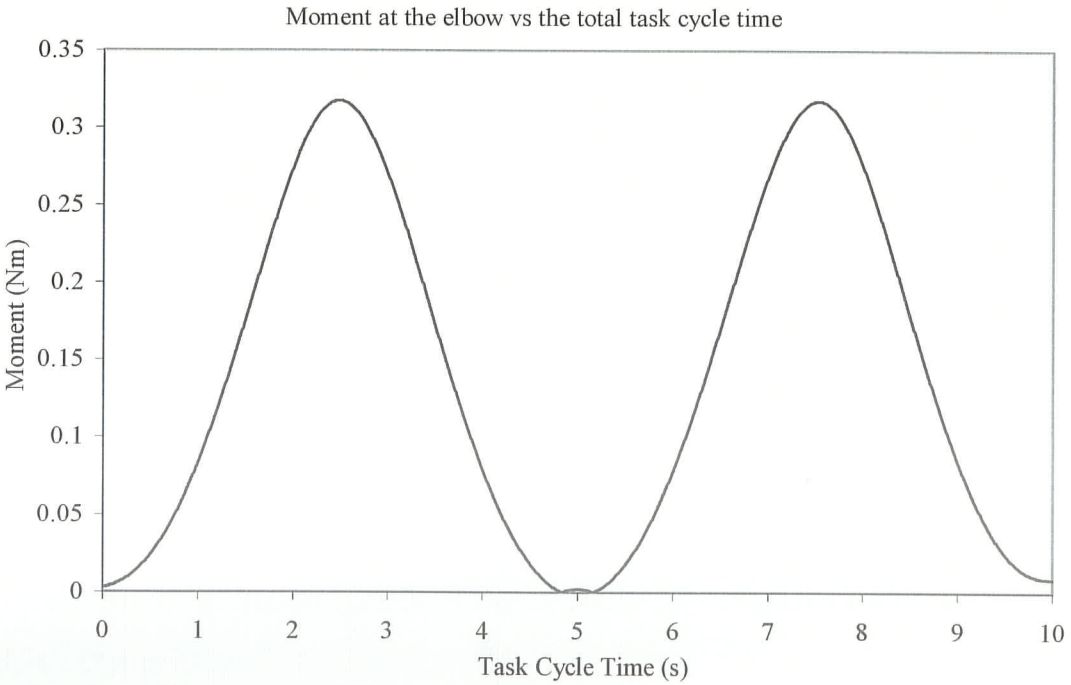

Figure E.12 Elbow Joint Moment in Pronation, 10s Task Cycle

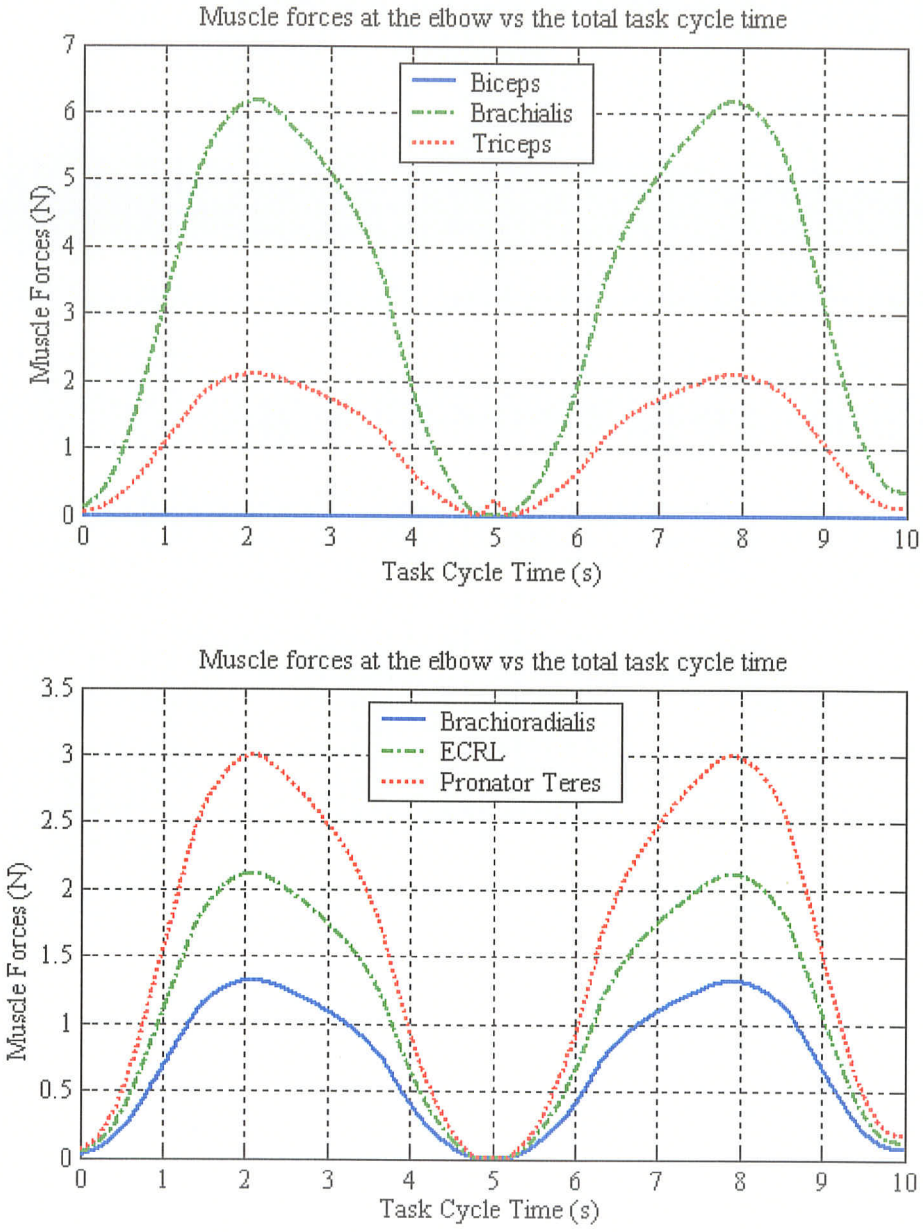

Figure E.13 Individual Muscle Forces in Pronation, 10sTask Cycle

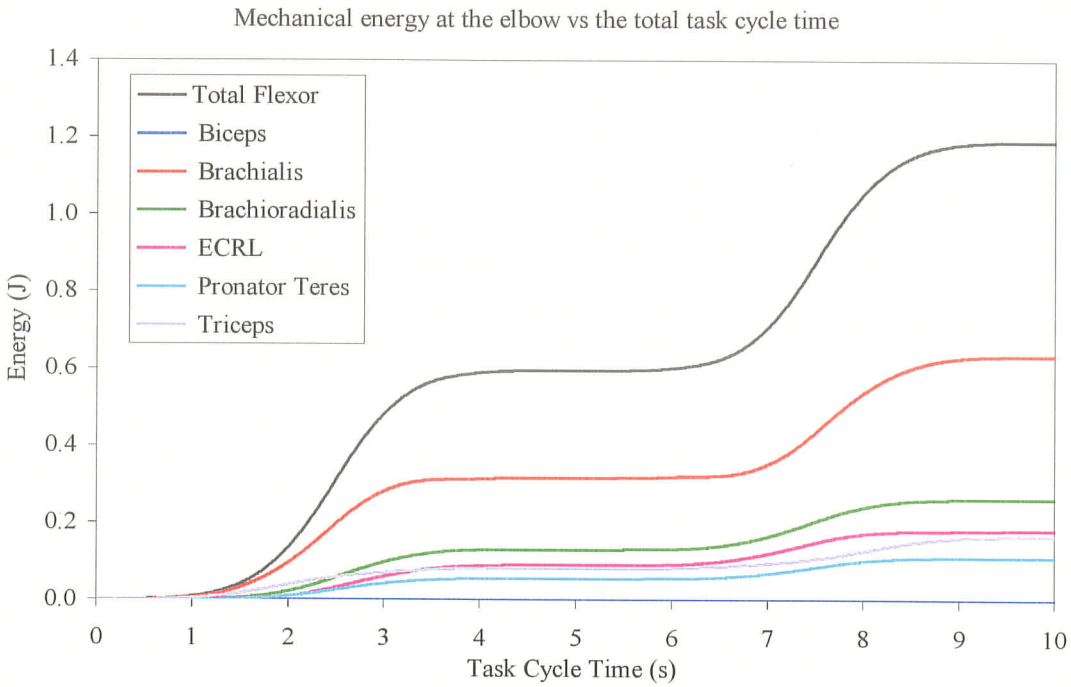

Figure E.14 Mechanical Energy in Pronation, 10s Task Cycle

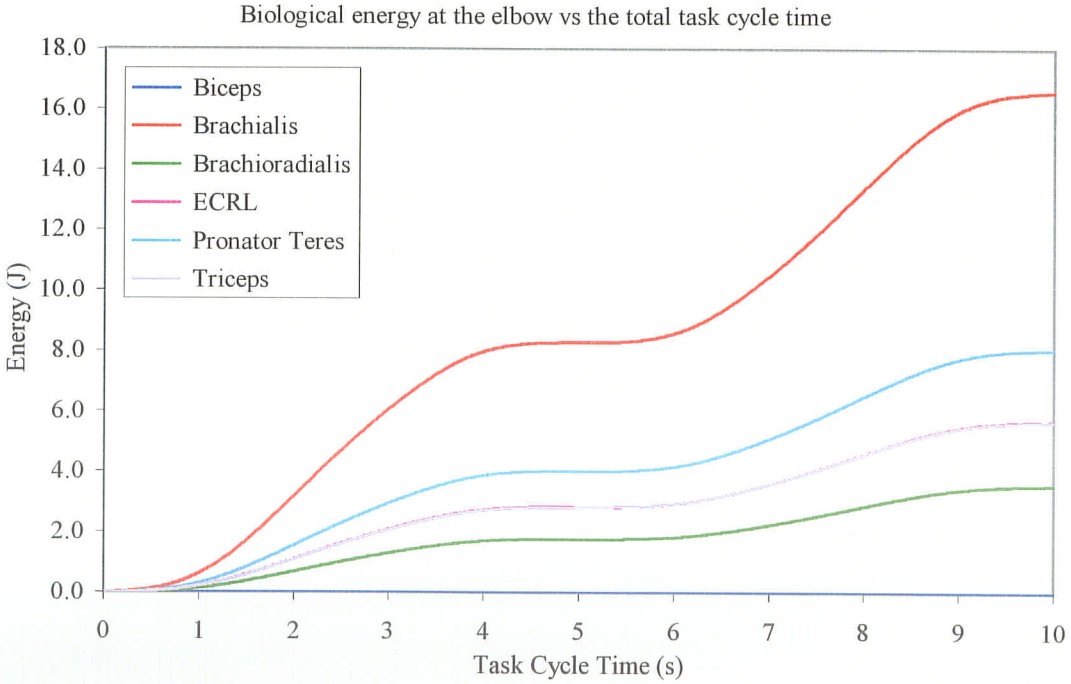

Figure E.15 Biological Energy in Pronation, 10s Task Cycle Time

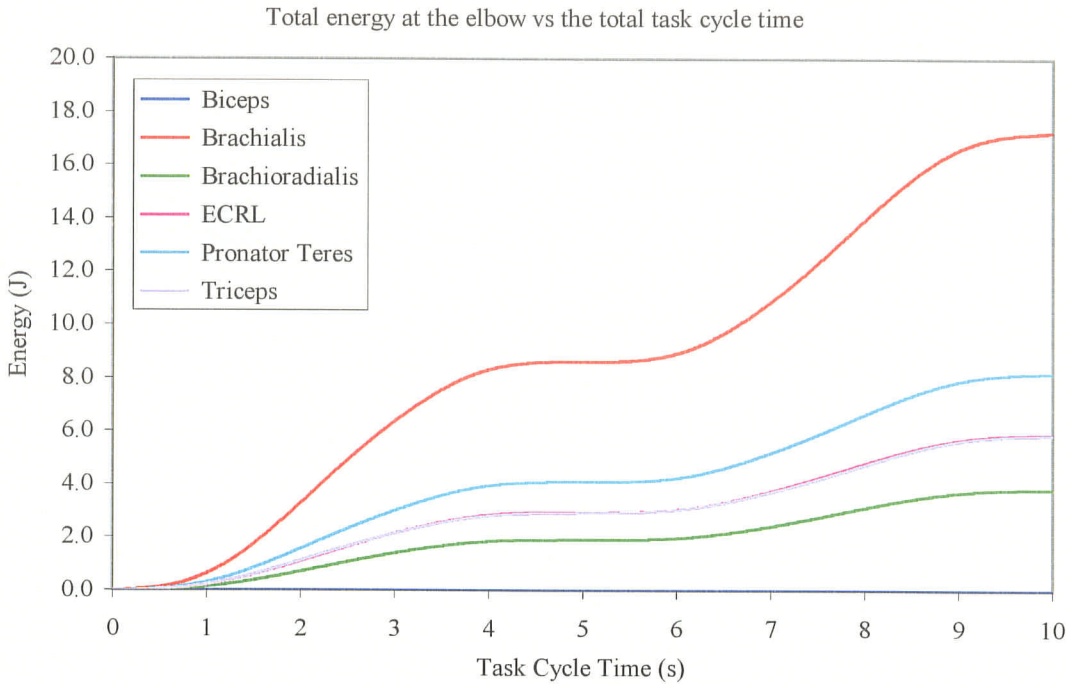

Figure E.16 Total Energy in Pronation, 10s Task Cycle

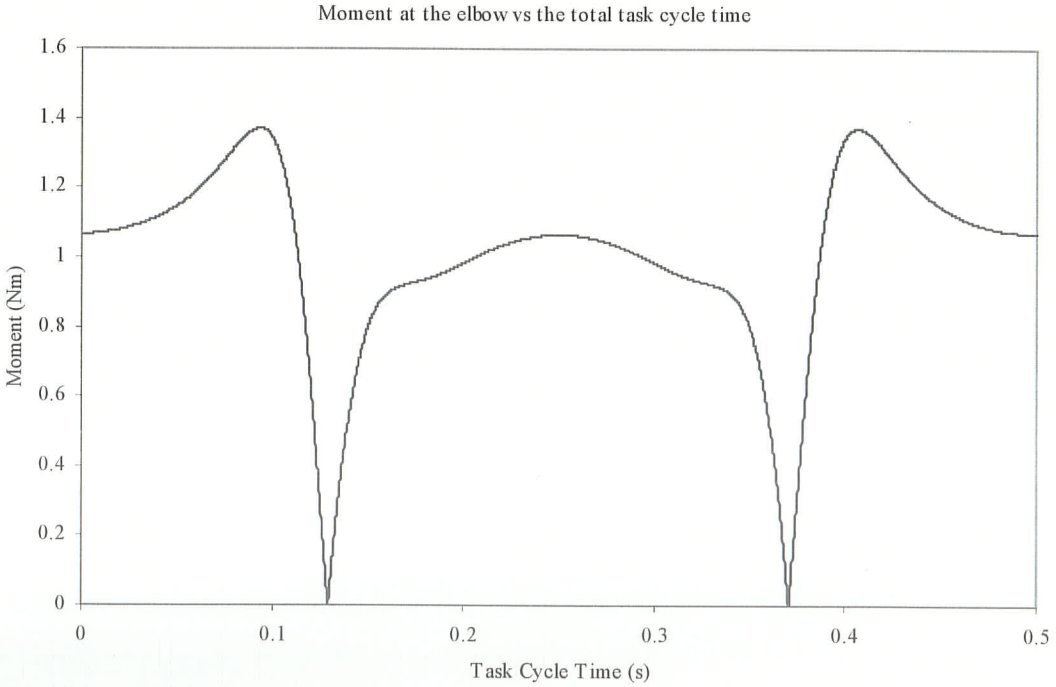

Figure E.17 Elbow Joint Moment in Pronation, 0.5s Task Cycle

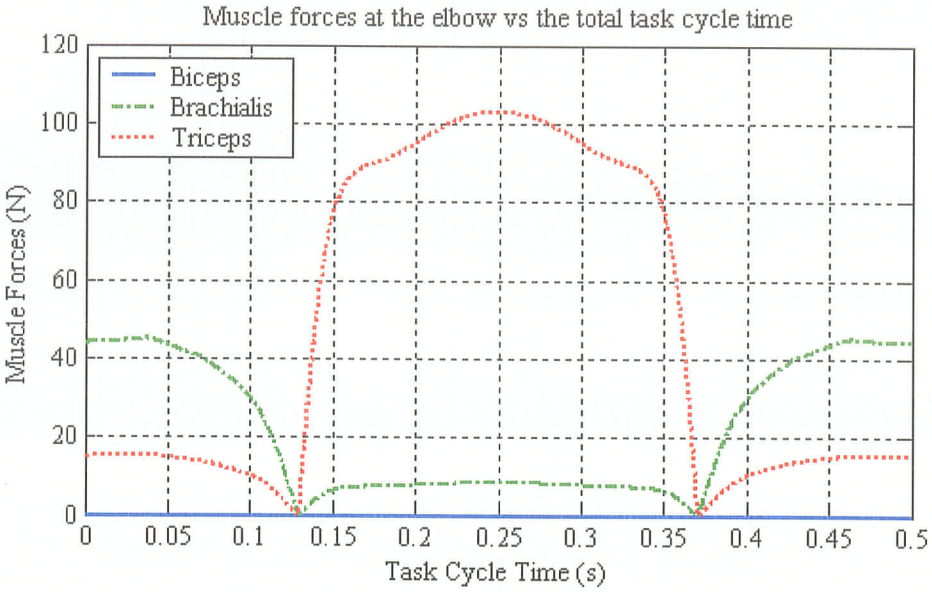

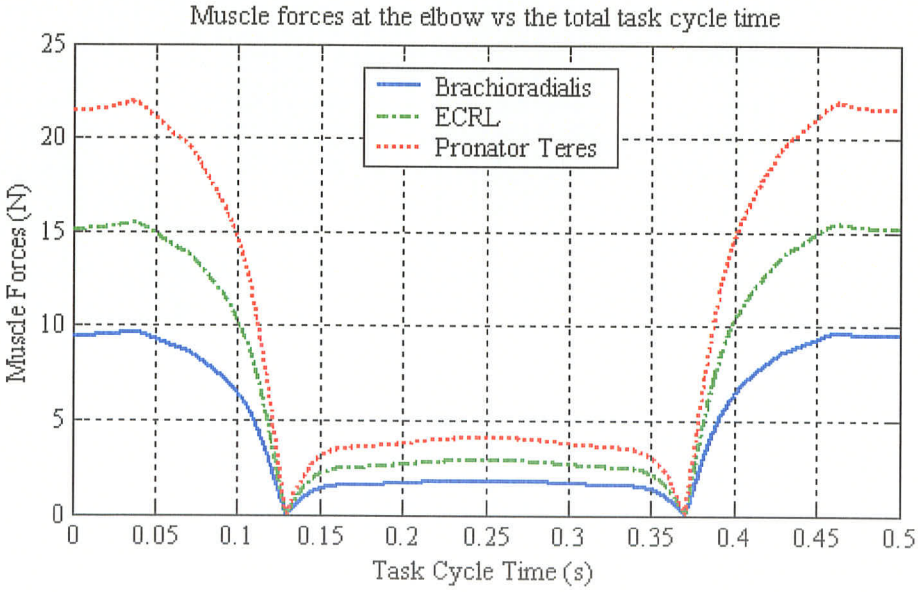

Figure E.18 Individual Muscle Forces in Pronation, 0.5s Task Cycle

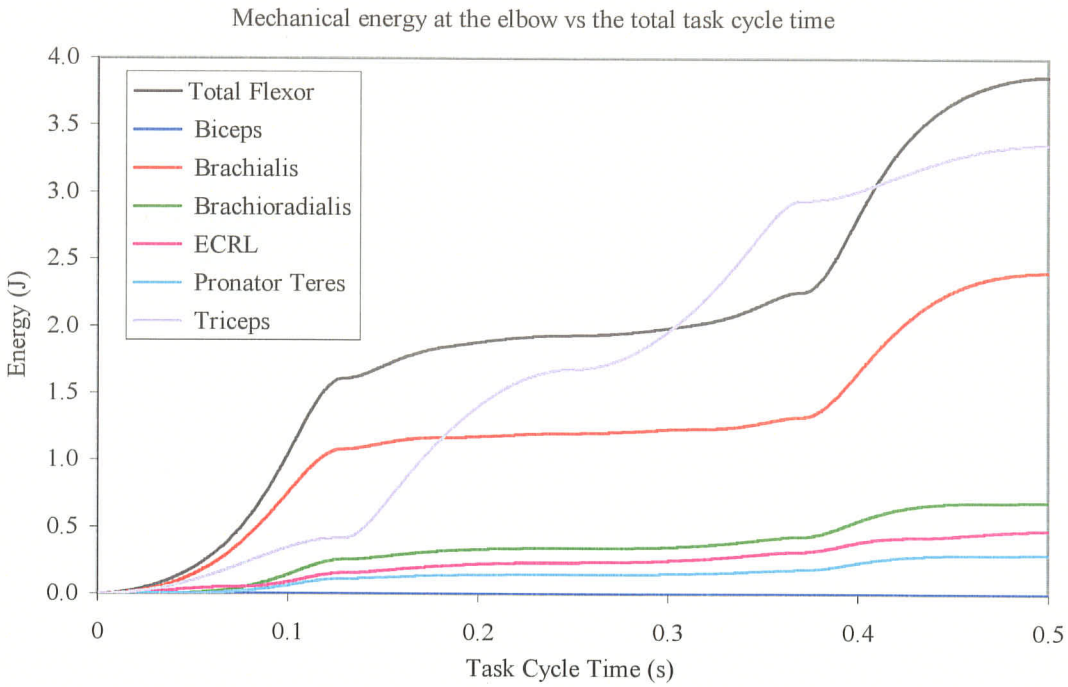

Figure E.19 Mechanical Energy in Pronation, 0.5s Task Cycle

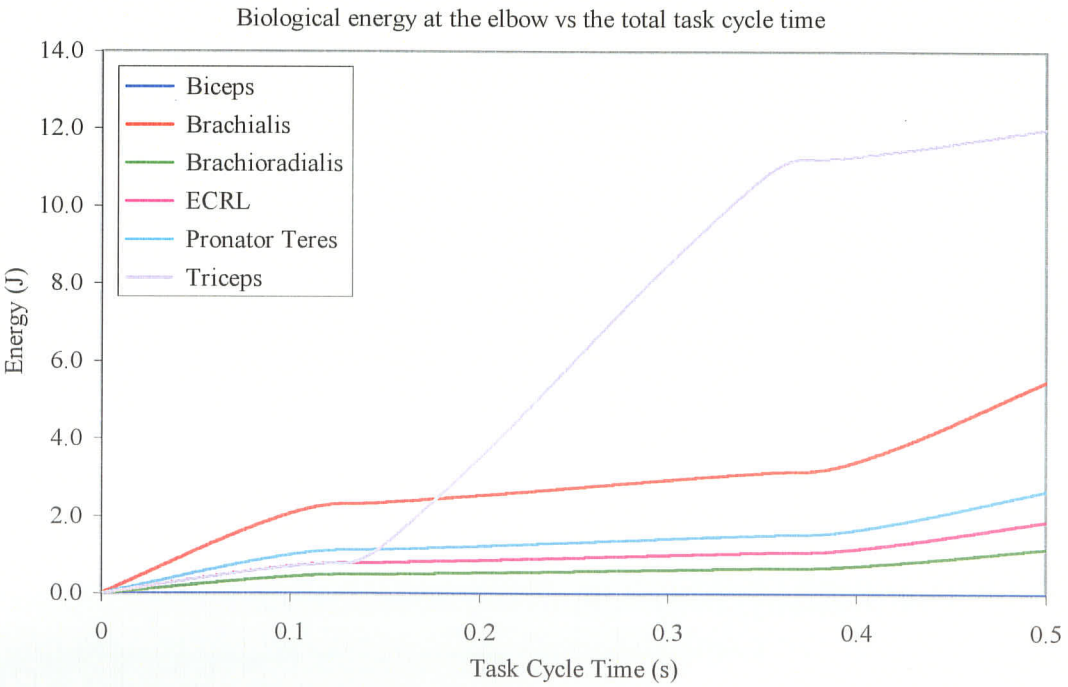

Figure E.20 Biological Energy in Pronation, 0.5s Task Cycle

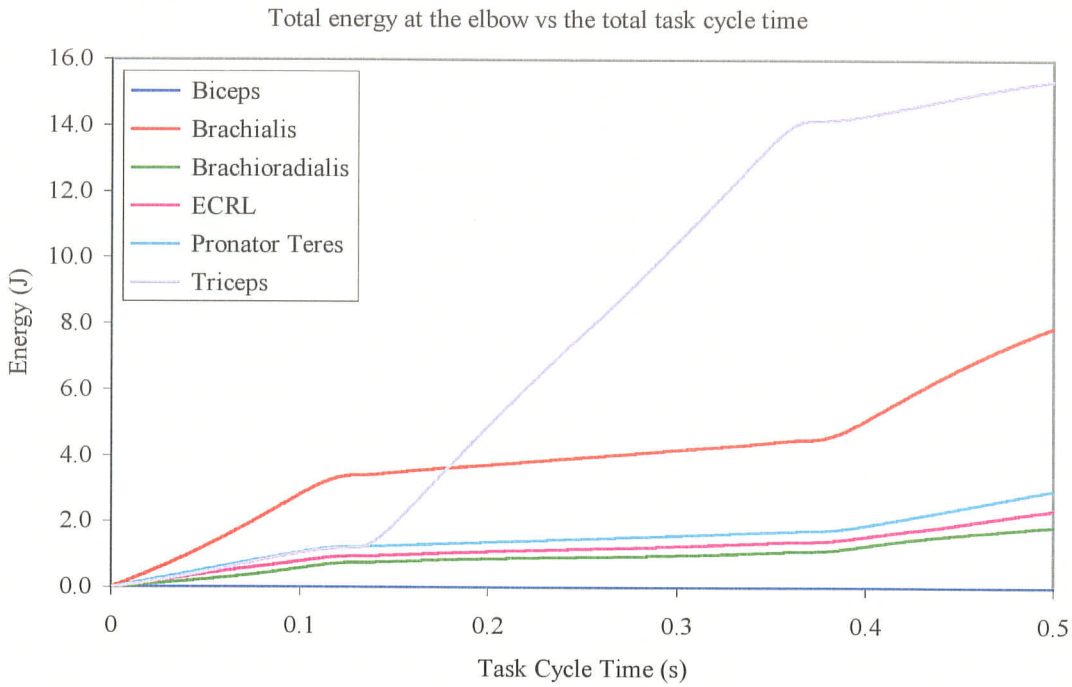

Figure E.21 Total Energy in Pronation, 0.5s Task Cycle

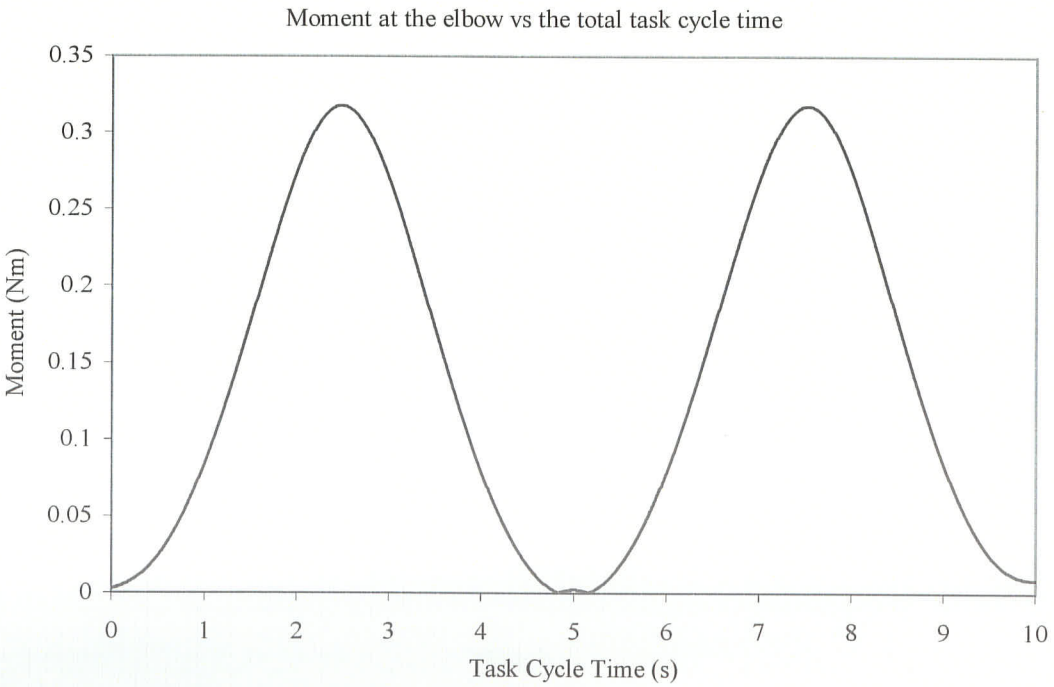

Figure E.22 Elbow Joint Moment in Supination, 10s Task Cycle

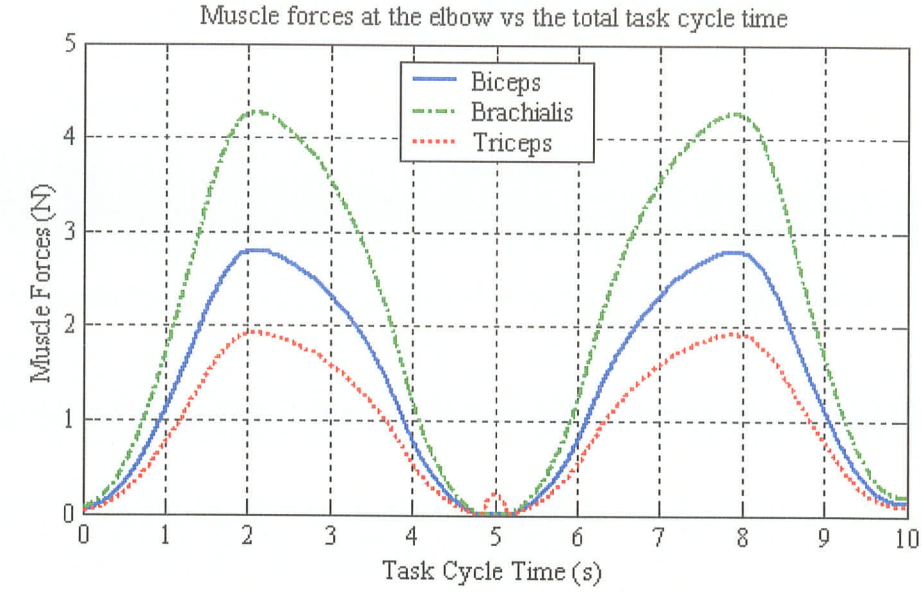

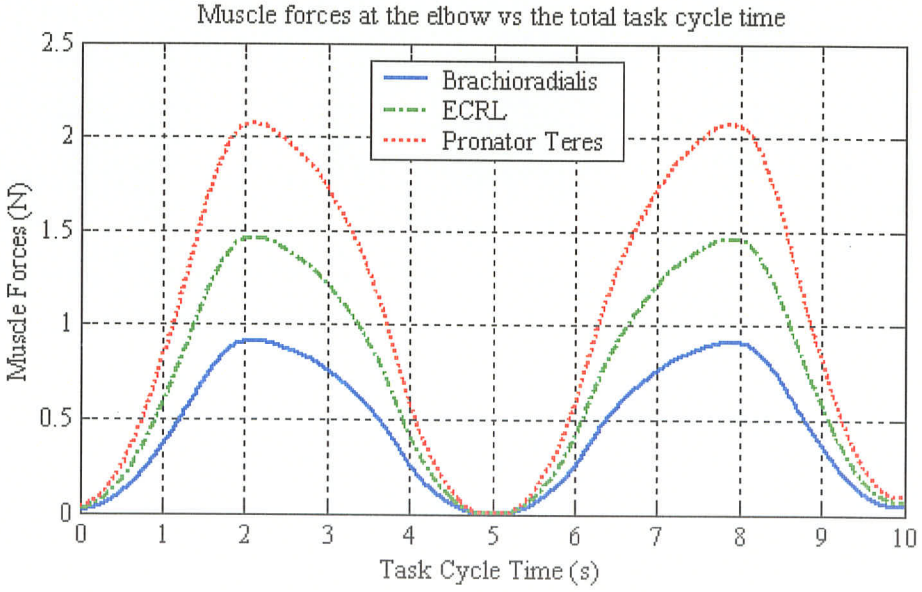

Figure E.23 Individual Muscle Forces in Supination, 10s Task Cycle

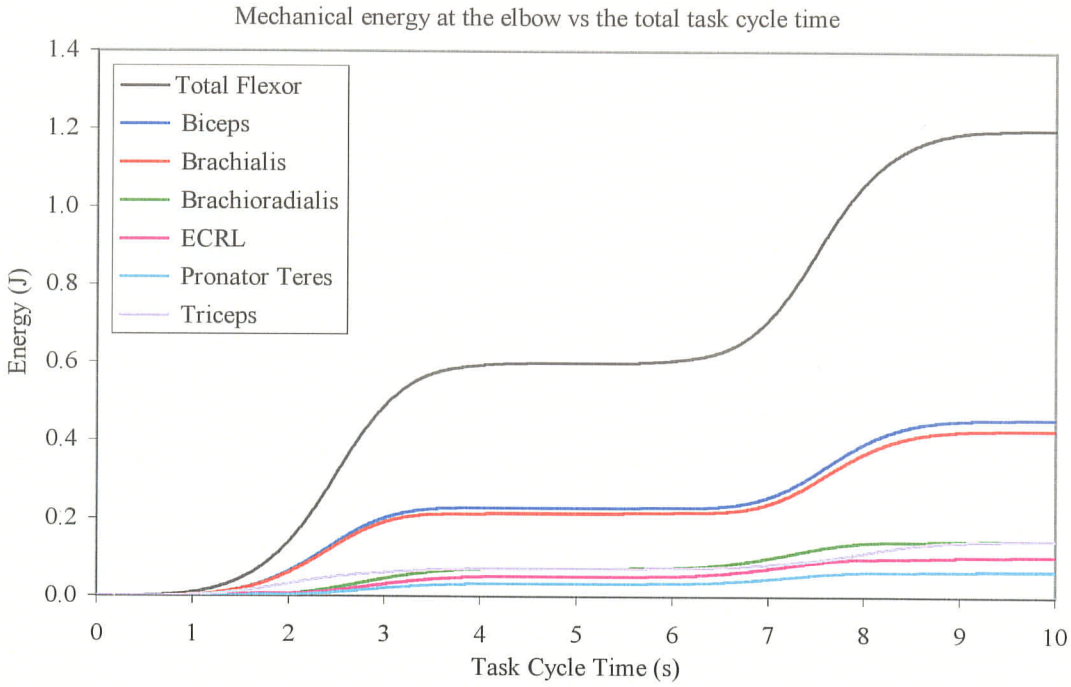

Figure E.24 Mechanical Energy in Supination, 10s Task Cycle

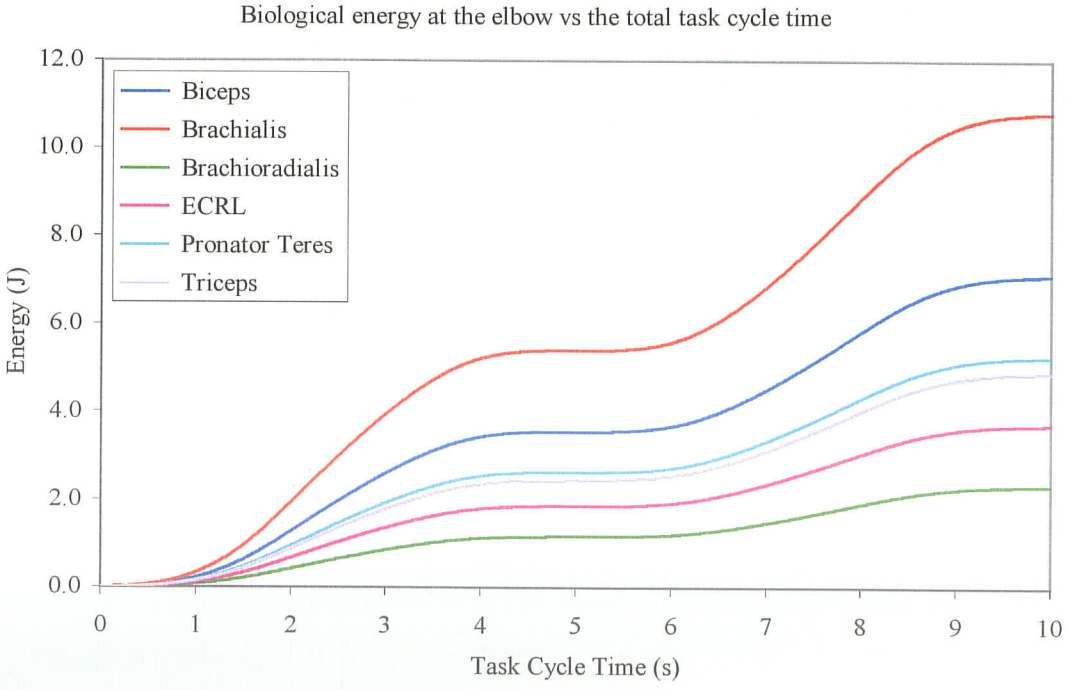

Figure E.25 Biological Energy in Supination, 10s Task Cycle

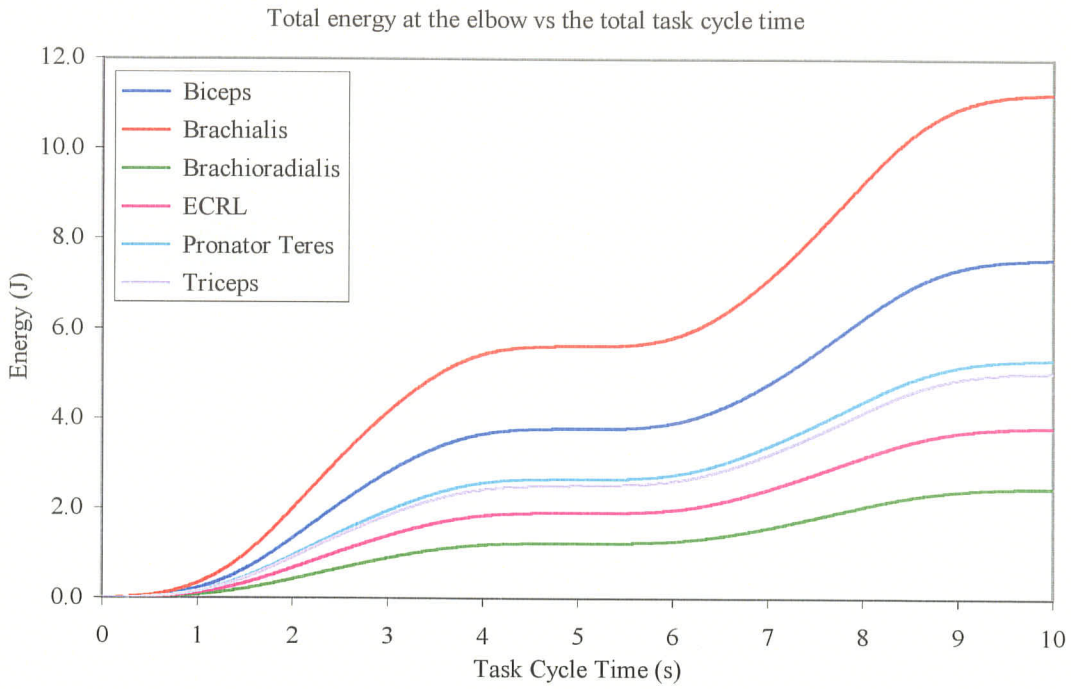

Figure E.26 Total Energy in Supination, 10s Task Cycle

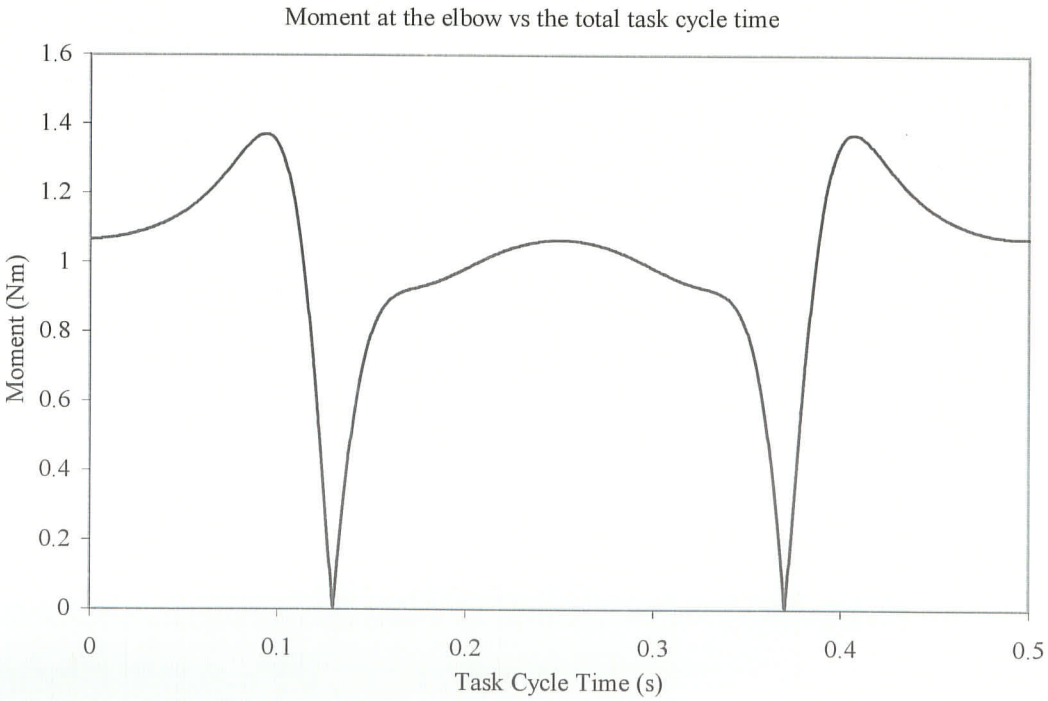

Figure E.27 Elbow Joint Moment in Supination, 0.5s Task Cycle

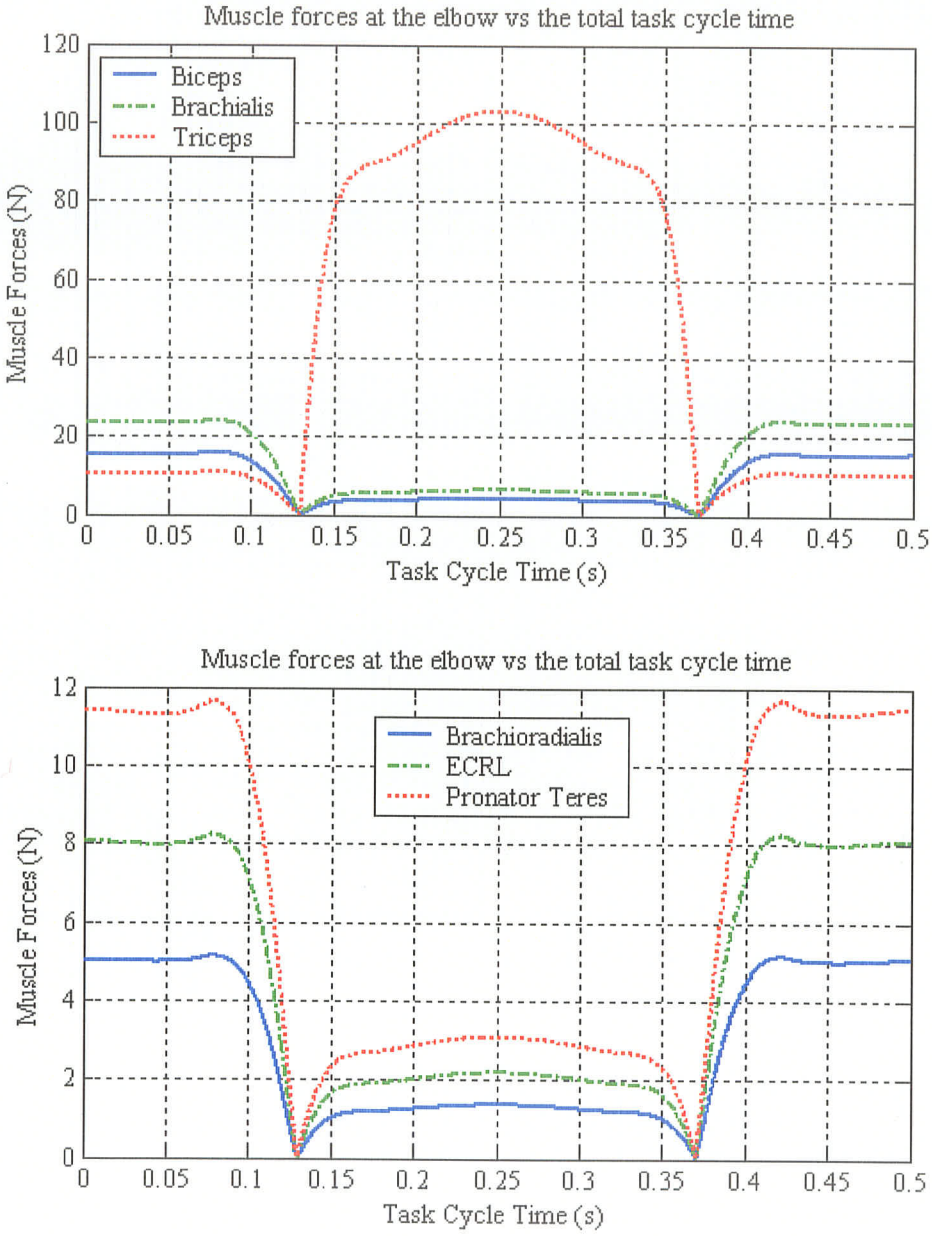

Figure E.28 Individual Muscle Forces in Supination, 0.5s Task Cycle

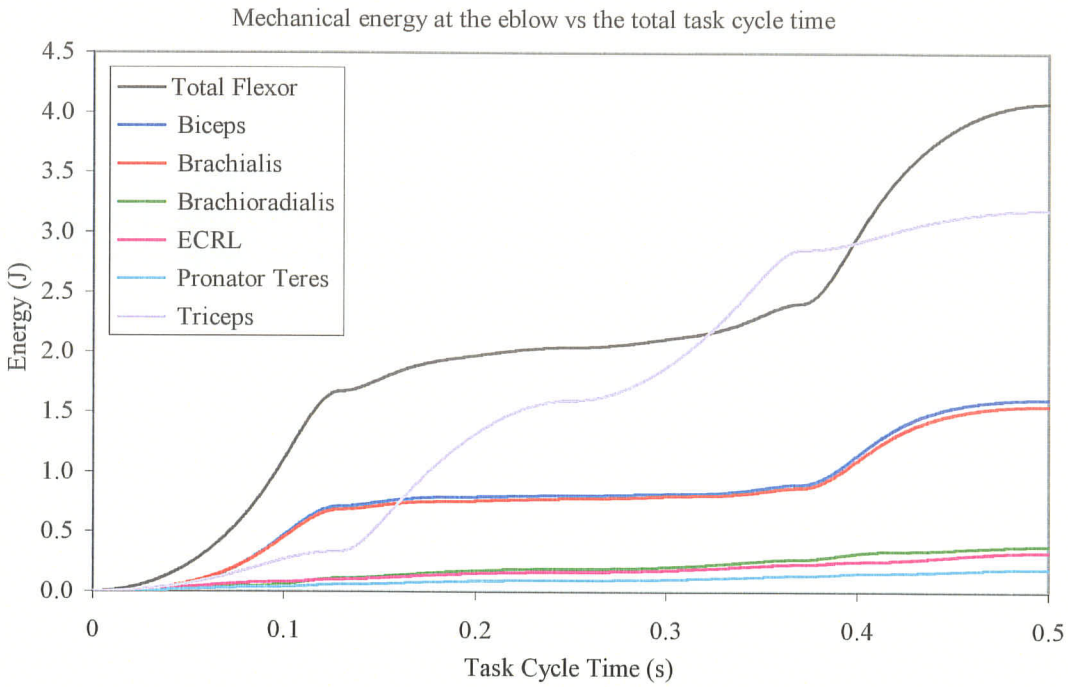

Figure E.29 Mechanical Energy in Supination, 0.5s Task Cycle

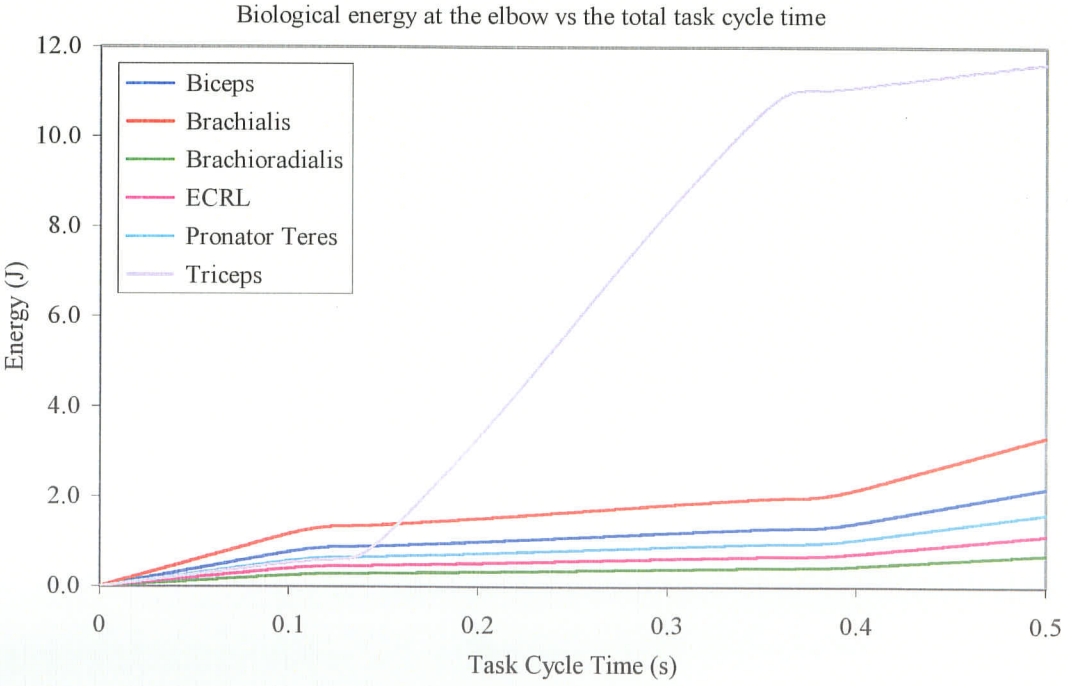

Figure E.30 Biological Energy in Supination, 0.5 s Task Cycle

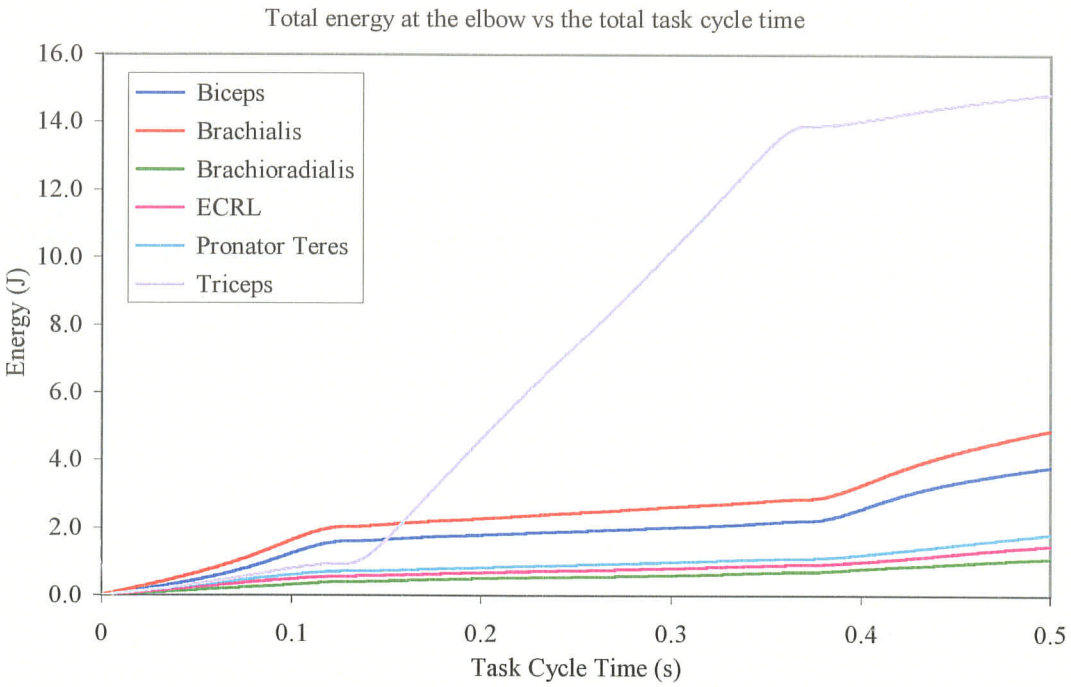

Figure E.31 Total Energy in Supination, 0.5s Task Cycle